

# 637

PIONEER VENUS 1

12 SECOND SAMPLED ENERGETIC ION (40 EV)

78-051A-11D

12 SECOND DATA 1 HOUR AROUND PERIAPSIS

78-051A-12F,13E

2 MINUTE OVERLAPPED AVG., EVERY MINUTE

78-051A-12G,13D

LOW & HIGH RESOL. NEUT. DENSITIES

78-051A-11G

HIGH RESOL-ENERGETIC ION (>40EV)

78-051A-11F

---

## Table of Contents

1. Introduction
2. Errata/Change Log
3. LINKS TO RELEVANT INFORMATION IN THE ONLINE NSSDC INFORMATION SYSTEM
4. Catalog Materials
  - a. Associated Documents
  - b. Core Catalog Materials

---

## **1. INTRODUCTION:**

The documentation for this data set was originally on paper, kept in NSSDC's Data Set Catalogs (DSCs). The paper documentation in the Data Set Catalogs have been made into digital images, and then collected into a single PDF file for each Data Set Catalog. The inventory information in these DSCs is current as of July 1, 2004. This inventory information is now no longer maintained in the DSCs, but is now managed in the inventory part of the NSSDC information system. The information existing in the DSCs is now not needed for locating the data files, but we did not remove that inventory information.

The offline tape datasets have now been migrated from the original magnetic tape to Archival Information Packages (AIP's).

A prior restoration may have been done on data sets, if a requestor of this data set has questions; they should send an inquiry to the request office to see if additional information exists.

## 2. ERRATA/CHANGE LOG:

NOTE: Changes are made in a text box, and will show up that way when displayed on screen with a PDF reader.

*When printing, special settings may be required to make the text box appear on the printed output.*

Version	Date	Person	Page	Description of Change
01				
02				

3 LINKS TO RELEVANT INFORMATION IN THE ONLINE NSSDC INFORMATION SYSTEM:

<http://nssdc.gsfc.nasa.gov/nmc/>

[NOTE: This link will take you to the main page of the NSSDC Master Catalog. There you will be able to perform searches to find additional information]

4. CATALOG MATERIALS:

- a. Associated Documents      To find associated documents you will need to know the document ID number and then click here.  
<http://nssdcftp.gsfc.nasa.gov/miscellaneous/documents/>

- b. Core Catalog Materials

REQ. AGENT

RAND NO.

ACQ. AGENT

RLR

DKB

PIONEER VENUS-1

12 SECOND SAMPLED ENERGETIC ION (40 EV) DATA

78-051A-11D PSPA-00302

This data set consists of 1 tape. The tape is 1600 bpi, 9-track, multifiled, ascii, and created on the IBM 360. The D and C numbers, time spans, and number of files are as follows:

D#	C#	FILES	TIME SPANS
D-78715	C-26834	1	12/05/78 - 01/03/89

07-MAR-90

TO: 633/P. Butterworth  
National Space Science Data Center

FROM: 615.1/W.T. Kasprzak

SUBJECT: Pioneer Venus Orbiter Neutral Mass Spectrometer  
Replacement tape for NSSDC data set 78-051A-11D  
(ASCII 12 s Energetic Ion Tape Orbits 1 to 3681)  
Replacement fiche for NSSDC data set 78-051A-11E  
(Energetic Ion Fiche Orbits 1 to 3681)

Enclosed is a replacement tape for the above data sets. The set contains 12 second sampled energetic ion data with orbital position parameters added. Since the data set was submitted in 1987 several improvements have been made in the data: a) corrections to the flux, density and direction for the spacecraft velocity have not been included; b) the flux has been evaluated for an energy of 40 eV rather than 45 eV as in the prior data set; c) the data set has been expanded in coverage to orbit 3681.

Any questions or problems with the data or the data tapes should be communicated to:

W.T. Kasprzak

301-286-8253

07-NOV-1989

NSSDC DOCUMENTATION FOR  
PIONEER VENUS ORBITER NEUTRAL MASS SPECTROMETER

## LOW RESOLUTION ENERGETIC ION DATA

## I. The Orbiter Neutral Mass Spectrometer (ONMS)

The instrument was primarily designed to determine the composition of the neutral exosphere/thermosphere of Venus. However, it has also detected energetic or fast ions whose energy exceeds 40 eV in the spacecraft frame of reference. These ions were observed in early orbits at an altitude higher than that required for measuring the neutral density at periapsis. Once the periapsis altitude had risen above the point where sensible neutral density measurements could be made the instrument was configured specifically to detect energetic ions.

The ONMS instrument has been described in "Pioneer Venus Orbiter Neutral Gas Mass Spectrometer Experiment," IEEE Transactions on Geoscience and Remote Sensing, GE-18 (1), 1980. A summary of the early results for energetic ions has been described in "Observations of Energetic Ions near the Venus Ionopause," Planet. Sp. Sci., 30, 1107-1115, 1982. The method used to reduce the energetic ion data to a flux and density has been described in "Observations of Energetic Ions on the Nightside of Venus," J. Geophys. Res., 92, 291-298, 1987. The data has been used as part of a study of the iontail of Venus in "The Iontail of Venus: Its Configuration and Evidence for Ion Escape," J. Geophys. Res., 92, 15-26, 1987. The global nature of the data has been summarized for the first 2500 orbits in "Fast O<sup>+</sup> Ion Flow Observed Around Venus at Low Altitudes," NASA TM 100717. The angular response and minimum energy have been evaluated in "Pioneer Venus Neutral Mass Spectrometer," a GSFC summer institute project report by Yvette Guenther. The method used to reduce the data assumes cylindrical symmetry of the ion source but in actual fact the source is asymmetrical in its angular response. This can introduce scatter in the data that is a function of the angle of attack. No simple solution has been found for modeling this asymmetry since the actual ion drift vector is unknown. The minimum energy of an ion detectable by the ONMS in energetic ion mode is 35.9 eV, the maximum transmission is assumed to occur about 10 V above this value. On the nightside of Venus the spacecraft potential is negative and the most probable ion energy is near 40 eV. The papers are reproduced here for convenient reference.

## II. Reduction to flux and number density

Reference to the basic data reduction has been given in Section I. Because of the paucity of data at other mass numbers only mass 16 (atomic oxygen) has been reduced to a flux and number density. As part of the reduction process the angle in the ecliptic plane of the apparent ion flow in space-craft reference frame has been deduced. No correction has been applied to the angle, density or flux in order to remove the space-craft velocity. In order to fit the data a minimum of 30 points were required in 36 seconds. In addition the maximum to minimum count ratio was required to be a factor of 3 or greater in order to insure that there was a definitive spin modulation. For those masses not fit by this process (all masses except 16 [atomic oxygen]) or those data that did not satisfy the above criteria a separate plot of the maximum count rate per 12 seconds was included in the microfiche data set. A rough conversion of  $4 \times 10^7 \text{ cm}^{-2} \text{ s}^{-1} / 10^4 \text{ counts s}^{-1}$  can be used to convert to a flux and a speed of  $2.2 \times 10^6 \text{ cm s}^{-1}$  can be used to convert to number density. A constant spacecraft potential of  $-5 \text{ v}$  has been assumed in assigning the effective energy of the ions to 40 eV. The minimum count rate is 1 per integration period or about 6 to 12 counts/s, depending on the bit rate and format of the telemetry data. The ion species regularly monitored include: He, N, O,  $\text{N}_2/\text{CO}$  and  $\text{CO}_2$ .

In general for orbit numbers 1 to 645 data were taken from RPA mode since the gas background with the filament on was considerably less than in non-RPA mode. For orbit numbers above 923 the instrument was deliberately configured with the filament off and non-RPA mode data was used. For mass 16 the RPA voltage is about +3.8 volts.

## III. Summary data.

All orbits have been processed where data exists or can be visually determined to exist. For orbits 1 to 645 a visual examination of the neutral mode data is required in order to identify the regions of energetic ions. For orbits beyond 923 no visual examination was needed. The ONMS instrument was not on for all orbits nor were energetic ions seen on all those orbits in which it was in operation. On the dayside of Venus energetic ions were seen only near the ionopause and when periapsis rose above it energetic ions were no longer observed. The flux values are estimated in the spacecraft reference frame. The density is computed from the flux by dividing it by a speed corresponding to 40 eV.

The data values are constructed for UT times supplied by the Pioneer Venus Project.

IV. Summary data tape.

The summary data tape was constructed in accordance with the recommendations of the Pioneer Venus archiving committee. A copy of that format is included for reference. The data tape has the following characteristics:

MEDIUM:	MAGNETIC TAPE
FORMAT:	ASCII
DENSITY:	1600 BPI
TRACKS:	9
PHYSICAL BLOCKSIZE:	3900 BYTES
LOGICAL RECORD SIZE:	78 BYTES
RECORDS/PHYSICAL BLOCK:	50
PHYSICAL RECORD TYPE:	FIXED BLOCK
TAPE LABEL:	UNLABELED
DENSITY:	1600 BPI
FORMAT:	ASCII
COMPUTER USED:	VAX 780

The orbits on the tape have been arranged sequentially. The format of the tape is briefly:

RECORD 1:  
 DESCRIPTION: number of variables and 4 character variable names  
 FORMAT: (I3,<N> (1X,A4)) where N=number of variables

RECORD 2:  
 DESCRIPTION: FORTRAN format of succeeding data records  
 FORMAT: (<M>A1) where M=number of bytes per logical record

RECORD 3:  
 DESCRIPTION: fill data definition for each data field  
 FORMAT: format contained in record 2

RECORD 4...:  
 DESCRIPTION: summary data  
 FORMAT: format contained in record 2

The variables listed in RECORD 1 have the following are:

<u>VARIABLE</u>	<u>COMMENT</u>
DO+	Density of energetic atomic oxygen in $\text{cm}^{-3}$
FO+	Flux of energetic atomic oxygen in $\text{cm}^{-2} \text{ s}^{-1}$
FANG	Apparent angle, in degrees, of the ion flow in the ecliptic plane measured with respect to the sun
VALT	Altitude above the mean surface of Venus in km
VLAT	Venus latitude in degrees
VLST	Venus local solar time in hr
VSZA	Venus solar zenith angle in degrees

V. Description of microfiche plots.

Each orbit processed consists of 5 plots.

<u>PAGE</u>	<u>COMMENT</u>
1	Header page identifying the spacecraft and instrument, orbit number, UT date and time of periapsis, and the principal investigator telephone and address .
2	Maximum pulse counts/sec for a selected set of mass numbers plotted versus time from periapsis; the data are multiplied by a factor in order to put them on a common vertical axis (the multipliers are indicated by the numbers following the X on the left hand side of the plot).
3	The 12 second average density for atomic oxygen plotted versus periapsis time.
4	The 12 second average flux for atomic oxygen plotted versus periapsis time.
5	The angle of the apparent atomic oxygen flow vector in the ecliptic plane.

Positional parameters for the data are available on the summary tape.

An example of a plot set has been included for reference.

VI. Energetic ion event list

A list of start and stop times for sections of the orbit where energetic ions have been observed for orbits 1 to 706 along with several location parameters for the spacecraft corresponding to these times. This list is included because the instrument was not optimally configured for measurement of energetic ions in this orbit range. Time limits were determined by a visual examination of the data.

ONMS-5  
(LR)

[26-FEB-90]

Several orbits of energetic ion data show individual points that that are erroneous and probably wrong.

ORBIT	LOW RESOLUTION DATA PERIAPSIS TIME TAG	UNIVERSAL TIME OF TIME TAG (ms)
3453	-180	8722030
	-168	8734030
3660	-576	10603177
	-564	10615177
	-468	10711177
	-456	10723177
	-336	10843177
3681	-648	10915226
	-636	10927226

High resolution data in the same time frame, plus or minus 12 seconds, is most likely wrong.

PIONEER VENUS ORBITER NEUTRAL MASS SPECTROMETER (ONMS)

Energetic Ion Location File

ORBITS 1 TO 706

A summary of the location of energetic ions detected by the ONMS instrument is given in this file. The file contains the start and stop times for each energetic ion segment. The file header description:

Name	Comment
-----	-----
ORBIT	Orbit number
MS	Mass number of species (e.g. 16 would be nominally O+)
YYDDD	YY = last two digits of year
	DD = day of year
HH:MM:SS	HH = hour
	MM = minutes
	SS = seconds
PER TIM	Time from periapsis (sec)
ALT	Altitude in (km)
SZA	Solar zenith angle (deg)
LST	Local solar time (hr)

PIONEER VENUS NEUTRAL MASS SPECTROMETER ENERGETIC ION EVENT LIST

ORBIT MS	-----START-----						-----FINISH-----					
	YYDDD HH:MM:SS	PER TIM	ALT	SAZ	HOUR	YYDDD HH:MM:SS	PER TIM	ALT	SAZ	HOUR		
1 16	78339 15: 6:35	-278.4	625.3	63.5	15.5	78339 15: 9:19	-114.2	420.8	62.8	15.9		
1 16	78339 15:13:26	133.3	436.2	64.8	16.3	78339 15:14:46	213.2	524.9	66.2	16.4		
3 16	78341 14:25:51	-356.3	624.0	66.4	15.5	78341 14:27: 2	-285.4	476.5	65.8	15.7		
6 16	78344 14:47:58	-496.8	976.0	70.6	15.3	78344 14:50:46	-328.8	544.8	69.5	15.9		
9 16	78347 15:15:22	-246.4	368.7	74.1	16.5	78347 15:16:59	-149.8	237.0	74.6	16.7		
9 16	78347 15:22:30	181.1	272.9	78.8	17.2	78347 15:22:43	194.6	290.5	79.0	17.3		
9 16	78347 15:23:44	255.6	384.3	80.1	17.3	78347 15:24:22	293.1	453.3	80.8	17.4		
9 16	78347 15:26: 0	391.4	672.0	82.7	17.5	78347 15:26: 0	391.4	672.0	82.7	17.5		
22 16	78360 17: 6: 1	-442.8	799.8	85.6	17.3	78360 17: 7: 3	-380.2	637.7	86.9	17.5		
26 16	78364 17:37:15	-506.2	984.1	87.9	17.4	78364 17:38:51	-410.5	715.5	90.4	17.8		
26 16	78364 17:40:31	-310.4	482.6	93.3	18.1	78364 17:41:55	-226.4	331.0	95.7	18.3		
27 16	78365 17:46:53	-407.4	708.6	91.6	17.9	78365 17:46:53	-407.4	708.6	91.6	17.9		
27 16	78365 18: 0:14	393.0	671.9	111.3	19.5	78365 18: 0:14	393.0	671.9	111.3	19.5		
27 16	78365 18: 6:28	767.2	1888.8	112.1	20.1	78365 18: 7:15	814.3	2071.8	112.0	20.1		
30 16	79003 18: 7: 8	-616.7	1331.5	88.2	17.3	79003 18: 7:39	-585.2	1225.1	89.1	17.5		
30 16	79003 18:30:17	773.0	1903.7	115.5	20.4	79003 18:45: 3	1658.4	5745.5	107.4	22.3		
32 16	79005 18:16:48	-633.9	1399.3	89.1	17.4	79005 18:16:48	-633.9	1399.3	89.1	17.4		
33 16	79006 18:39:19	423.2	749.9	120.7	20.2	79006 18:39:19	423.2	749.9	120.7	20.2		
38 16	79011 19: 6:30	596.3	1269.8	127.0	21.0	79011 19: 7:17	642.8	1429.3	126.4	21.1		
41 16	79014 19: 6: 4	-210.6	314.4	115.9	20.0	79014 19: 7:16	-138.6	227.4	119.4	20.2		
42 16	79015 19: 8:44	-309.5	490.7	112.0	19.9	79015 19:11: 2	-171.3	266.1	119.1	20.2		
42 16	79015 19:21:32	458.9	854.6	133.9	21.3	79015 19:22:31	517.7	1027.1	133.2	21.3		
43 16	79016 19:21:56	222.7	339.1	135.1	21.0	79016 19:24:17	363.7	612.4	136.0	21.2		
43 16	79016 19:28:38	625.6	1380.2	132.5	21.6	79016 19:30:28	735.5	1775.5	130.0	21.8		
44 16	79017 19:33:41	677.6	1551.1	132.4	21.8	79017 19:33:41	677.4	1550.4	132.4	21.8		
46 16	79019 19:41:22	713.3	1686.4	133.4	22.1	79019 19:42:56	807.3	2044.7	130.6	22.2		
49 16	79022 19:48:54	531.7	1073.8	141.7	22.1	79022 19:51:31	688.4	1602.6	136.8	22.4		
50 16	79023 19:55:43	728.9	1754.1	136.3	22.5	79023 19:57:41	846.6	2208.1	132.1	22.7		
52 16	79025 19:59:52	631.7	1389.9	141.2	22.6	79025 20: 4:19	898.4	2406.7	131.0	23.1		
54 16	79027 20: 3:44	573.5	1200.1	145.3	22.8	79027 20: 7:23	792.5	1988.7	136.1	23.1		
55 16	79028 20: 6:33	598.8	1287.2	145.0	22.9	79028 20: 6:57	622.0	1365.9	144.0	22.9		
56 16	79029 20: 4:15	316.0	508.8	155.9	22.6	79029 20: 8:33	574.0	1208.6	146.9	23.0		
57 16	79030 20: 8:35	431.3	787.3	153.9	22.9	79030 20:12:31	666.8	1528.3	143.2	23.2		
68 16	79041 20:15:55	448.1	819.0	159.0	0.1	79041 20:17:21	534.2	1072.6	153.0	0.2		
68 16	79041 20:20:36	729.9	1748.2	140.8	0.5	79041 20:21:24	777.1	1927.4	138.2	0.6		
70 16	79043 20:13: 7	322.3	519.2	168.4	0.1	79043 20:14: 6	380.9	652.2	163.8	0.2		
70 16	79043 20:18:38	653.6	1476.4	144.8	0.6	79043 20:22:15	870.1	2298.3	132.8	1.0		
77 16	79050 19:44:23	-905.0	2438.0	100.6	20.0	79050 19:46:12	-795.3	2000.4	106.2	21.0		
77 16	79050 19:54:40	-288.0	446.7	140.1	23.7	79050 19:56:13	-194.4	294.0	147.8	23.9		
77 16	79050 20: 3:33	245.7	371.1	167.8	0.7	79050 20: 6:10	402.5	702.8	157.4	1.0		
77 16	79050 20:10: 5	637.2	1416.8	141.9	1.4	79050 20:11:54	746.8	1814.8	135.6	1.5		
79 16	79052 20: 4:18	483.0	908.8	149.7	1.3	79052 20: 5:36	561.3	1150.1	144.7	1.5		
80 16	79053 19:59:54	368.9	606.2	156.1	1.3	79053 20: 0:41	415.9	723.6	153.1	1.3		
80 16	79053 20: 4:36	650.9	1454.2	138.6	1.7	79053 20: 5:38	713.5	1680.9	135.1	1.8		
82 16	79055 19:51:41	182.0	267.8	162.4	1.2	79055 19:53:33	293.6	448.1	157.9	1.4		
85 16	79058 19:49:27	524.0	1029.7	141.0	2.0	79058 19:52: 3	680.4	1557.1	132.4	2.3		
87 16	79060 19:38:30	264.5	389.6	151.7	1.8	79060 19:38:52	287.1	431.5	150.8	1.9		
87 16	79060 19:38:30	264.3	389.3	151.8	1.8	79060 19:38:54	288.3	433.8	150.8	1.9		
95 16	79068 19: 9: 9	189.5	284.7	141.5	2.6	79068 19: 9:41	221.6	329.9	140.7	2.6		
95 16	79068 19:10:53	294.2	456.0	138.4	2.7	79068 19:10:57	298.2	463.9	138.3	2.7		

Π

95	16	79068	19:10:55	295.7	459.0	138.4	2.7	79068	19:11:10	310.8	489.3	137.8	2.8
98	16	79071	19: 3:53	523.5	1042.7	125.0	3.4	79071	19: 3:53	523.5	1042.7	125.0	3.4
104	16	79077	19:21:52	438.6	798.0	119.9	3.9	79077	19:23:42	548.4	1121.8	116.1	4.1
112	16	79085	20: 1: 6	624.1	1370.0	103.3	5.0	79085	20: 2: 9	686.7	1591.2	101.6	5.1
116	16	79089	19:54:50	-812.2	2064.4	106.6	1.2	79089	20: 3:19	-303.3	471.4	112.5	3.8
116	16	79089	20:13:29	307.1	479.0	105.7	5.0	79089	20:15:58	455.8	840.1	102.1	5.2
117	16	79090	20:17:32	287.8	440.1	104.6	5.0	79090	20:17:34	289.6	443.6	104.5	5.0
117	16	79090	20:17:33	289.3	443.0	104.5	5.0	79090	20:18:33	349.3	569.0	103.1	5.1
127	16	79100	20:58:57	257.9	380.1	89.6	6.0	79100	20:59:35	295.3	449.5	88.8	6.1
137	16	79110	21:22:47	-383.1	645.9	89.9	5.8	79110	21:23:50	-320.1	502.2	88.2	6.0
137	16	79110	21:25:47	-203.1	296.0	85.0	6.3	79110	21:25:47	-203.1	296.0	85.0	6.3
137	16	79110	21:34:34	323.2	508.8	72.9	7.2	79110	21:35:13	362.4	596.4	72.4	7.2
138	16	79111	21:23:50	-484.7	920.3	91.6	5.5	79111	21:24:37	-437.8	788.0	90.3	5.7
138	16	79111	21:18:21	-813.7	2068.5	98.6	3.5	79111	21:19: 8	-766.9	1886.8	97.7	3.9
138	16	79111	21:18:21	-813.5	2067.7	98.6	3.5	79111	21:19: 8	-766.7	1886.1	97.7	3.9
138	16	79111	21:36:54	299.2	460.1	71.7	7.3	79111	21:38:52	417.8	734.5	70.3	7.4
139	16	79112	21:28:36	-355.3	581.6	87.0	6.1	79112	21:28:48	-343.6	555.0	86.6	6.1
151	16	79124	21:36:45	-683.0	1297.7	84.8	6.3	79124	21:39:22	-446.5	816.8	78.1	7.0
151	16	79124	21:51:31	282.4	433.4	51.6	8.6	79124	21:51:42	293.5	454.9	51.4	8.6
151	16	79124	21:52: 6	318.1	504.6	51.3	8.7	79124	21:52: 6	318.1	504.6	51.3	8.7
152	16	79125	21:38:48	-444.9	814.6	77.1	7.2	79125	21:41:24	-288.9	448.5	69.6	7.6
161	16	79134	21:22:24	-411.9	735.0	67.0	8.2	79134	21:23:11	-365.0	619.7	64.2	8.4
162	16	79135	21:19:39	-413.1	741.4	66.1	8.3	79135	21:20:50	-342.9	572.9	61.9	8.5
162	16	79135	21:31: 9	276.7	438.6	34.5	9.8	79135	21:31:12	279.3	443.7	34.5	9.8
162	16	79135	21:31: 1	268.5	423.7	34.5	9.8	79135	21:31:12	280.0	444.7	34.5	9.8
164	16	79137	21:15: 1	-285.2	437.3	56.4	8.9	79137	21:15:59	-227.0	336.7	52.6	9.1
164	16	79137	21:23:17	211.0	312.6	31.8	9.9	79137	21:24:32	285.8	438.2	31.4	10.0
173	16	79146	20:31:16	-406.5	712.2	56.8	9.5	79146	20:31:16	-406.5	712.2	56.8	9.5
173	16	79146	20:42: 5	242.1	364.3	17.6	10.9	79146	20:42:41	278.7	428.4	18.1	11.0
175	16	79148	20:18:56	-382.9	661.3	53.6	9.8	79148	20:21:22	-237.1	365.3	42.5	10.2
175	16	79148	20:28:30	190.8	297.8	14.7	11.0	79148	20:28:56	217.4	335.0	14.5	11.1
185	16	79158	20:49:25	-513.9	1009.7	57.8	10.3	79158	20:54:51	-188.1	279.5	32.0	11.4
185	16	79158	21: 1:51	232.7	344.1	5.6	12.2	79158	21: 2:32	273.8	414.5	9.0	12.2
186	16	79159	20:57:21	-405.9	709.8	49.5	10.9	79159	20:57:45	-382.4	651.1	47.7	10.9
188	16	79161	21:10:42	-317.7	511.7	42.0	11.4	79161	21:12:54	-185.8	288.3	31.0	11.7
194	16	79167	21:42:13	-269.2	407.4	37.8	12.1	79167	21:43:18	-203.8	302.3	32.8	12.3
195	16	79168	21:45:26	-292.2	453.3	39.7	12.2	79168	21:46:28	-229.5	343.2	35.0	12.3
195	16	79168	21:54: 8	222.5	332.4	18.7	13.2	79168	21:54:39	261.2	395.9	20.4	13.3
198	16	79171	21:51:31	-525.3	1053.7	55.8	11.7	79171	21:52:57	-439.2	804.2	50.3	12.8
198	16	79171	22: 4:42	265.5	410.9	25.1	13.6	79171	22: 5:53	336.0	550.9	28.5	13.7
202	16	79175	22: 5:48	-246.3	366.0	39.4	13.1	79175	22: 6:36	-198.8	292.6	36.6	13.2
209	16	79182	22:11:45	-240.3	363.9	44.6	13.8	79182	22:12:47	-178.0	274.7	42.2	14.0
209	16	79182	22:18:50	184.7	283.0	39.9	14.7	79182	22:20:25	279.6	432.5	42.6	14.8
218	16	79191	22:11:35	-262.4	402.8	54.5	14.8	79191	22:12:36	-208.9	306.0	53.3	14.9
218	16	79191	22:19:29	212.3	322.1	54.9	15.7	79191	22:20:49	292.3	458.0	57.1	15.8
235	16	79208	21:59:48	-509.6	995.8	74.3	15.8	79208	21:59:48	-509.6	995.8	74.3	15.8
238	16	79211	22: 5: 8	-499.3	963.5	76.9	16.2	79211	22: 7:13	-373.6	623.8	77.8	16.6
297	16	79271	0:48:35	433.0	772.8	157.3	0.6	79271	0:48:35	432.9	772.6	157.3	0.6
316	16	79290	3: 3:59	496.9	960.9	133.7	2.7	79290	3: 5: 1	559.6	1155.1	130.6	2.8
320	16	79294	3:31:59	677.4	1559.5	120.7	3.4	79294	3:33: 2	740.2	1790.7	118.0	3.5
323	16	79297	3:45:57	402.1	702.8	128.4	3.3	79297	3:48:34	558.7	1155.3	122.0	3.5
334	16	79308	4:40:40	-328.7	527.4	119.5	3.1	79308	4:40:40	-328.7	527.4	119.5	3.1
334	16	79308	4:43:16	-172.7	264.0	121.3	3.5	79308	4:43:40	-148.7	237.2	121.4	3.5
334	16	79308	4:49: 8	179.3	272.1	118.3	4.1	79308	4:50:58	288.7	446.0	115.6	4.3

Π

337	16	79311	5:10:50	408.7	714.9	107.8	4.8	79311	5:11:53	471.7	886.4	106.1	4.9
344	16	79318	5:51:29	402.5	694.8	96.7	5.6	79318	5:52:1	433.9	777.1	96.0	5.6
348	16	79322	6:13:51	405.2	699.2	91.6	5.9	79322	6:14:54	468.1	869.7	90.4	6.0
354	16	79328	6:45:58	446.0	806.0	82.8	6.6	79328	6:46:21	469.4	871.8	82.5	6.6
379	16	79353	7:37:57	-518.9	1021.5	77.5	7.2	79353	7:39:59	-397.7	681.4	71.5	7.6
379	16	79353	7:51:36	300.1	460.4	45.7	9.1	79353	7:52:15	339.1	542.5	45.6	9.1
382	16	79356	7:36:43	-491.5	946.9	73.5	7.6	79356	7:37:7	-468.1	879.2	72.2	7.7
382	16	79356	7:50:26	331.1	534.4	41.2	9.4	79356	7:51:29	394.1	681.2	41.6	9.5
384	16	79358	7:34:55	-498.8	974.0	72.1	7.8	79358	7:37:8	-365.6	618.7	64.7	8.3
384	16	79358	7:46:21	187.5	292.0	38.9	9.4	79358	7:47:59	284.8	447.4	38.1	9.6
386	16	79360	7:34:12	-429.3	784.9	66.4	8.3	79360	7:37:0	-261.3	412.0	56.3	8.8
386	16	79360	7:44:14	172.3	281.0	36.0	9.6	79360	7:45:37	255.3	401.7	35.0	9.7
402	16	80011	7:1:43	-333.2	539.5	46.8	10.2	80011	7:3:56	-200.0	301.8	36.1	10.6
403	16	80012	7:7:56	-311.3	497.5	44.4	10.4	80012	7:10:10	-176.7	276.0	33.3	10.8
403	16	80012	7:16:32	204.5	312.3	9.0	11.5	80012	7:17:45	277.9	432.1	11.9	11.6
405	16	80014	7:18:9	-389.0	680.6	49.2	10.4	80014	7:21:38	-180.1	288.6	32.2	11.0
405	16	80014	7:27:28	170.3	276.6	5.8	11.6	80014	7:29:45	307.7	497.8	12.6	11.8
410	16	80019	7:41:35	-368.1	620.7	45.3	11.0	80019	7:41:35	-368.1	620.7	45.3	11.0
414	16	80023	7:50:28	-689.7	1596.8	66.2	10.0	80023	7:58:11	-226.6	329.4	32.9	11.8
414	16	80023	8:5:5	188.1	274.4	9.6	12.6	80023	8:6:29	272.1	406.3	14.7	12.8
423	16	80032	8:1:52	-429.5	769.4	48.5	12.2	80032	8:1:52	-429.5	769.4	48.5	12.2
434	16	80043	8:27:48	-247.5	381.4	44.8	13.9	80043	8:29:7	-169.0	269.7	42.1	14.1
434	16	80043	8:34:53	177.6	280.1	41.1	14.7	80043	8:35:40	224.3	344.4	42.3	14.8
439	16	80048	8:47:23	-398.7	700.2	54.7	14.1	80048	8:47:59	-362.7	613.0	53.5	14.2
439	16	80048	8:59:9	307.5	492.8	52.8	15.5	80048	8:59:24	323.0	524.9	53.4	15.5
444	16	80053	9:5:56	-523.0	1046.8	62.2	14.2	80053	9:6:19	-499.5	975.8	61.6	14.3
447	16	80056	9:36:12	597.6	1285.0	73.9	16.8	80056	9:36:12	597.6	1285.0	73.9	16.8
447	16	80056	9:17:48	-506.8	996.0	63.9	14.6	80056	9:18:59	-436.3	794.8	62.5	14.8
448	16	80057	9:23:37	-381.0	652.6	62.4	15.1	80057	9:23:37	-381.0	652.6	62.4	15.1
452	16	80061	9:34:1	-598.4	1284.7	69.1	14.7	80061	9:34:1	-598.4	1284.7	69.1	14.7
453	16	80062	9:39:7	-488.8	938.9	68.5	15.3	80062	9:40:19	-416.8	739.1	67.8	15.5
461	16	80070	10:3:8	-405.2	704.3	76.2	16.4	80070	10:3:8	-405.2	704.3	76.2	16.4
461	16	80070	10:17:53	480.2	909.3	90.5	18.1	80070	10:17:53	480.2	909.3	90.5	18.1
462	16	80071	10:6:40	-335.6	538.6	77.9	16.8	80071	10:6:40	-335.6	538.6	77.9	16.8
464	16	80073	10:9:13	-451.0	825.5	79.0	16.6	80073	10:12:23	-261.1	390.3	81.2	17.2
464	16	80073	10:21:57	313.1	490.0	92.0	18.2	80073	10:24:58	493.4	947.1	95.0	18.4
471	16	80080	10:20:47	-569.9	1185.5	83.9	16.9	80080	10:22:26	-470.9	882.0	85.8	17.3
471	16	80080	10:25:15	-301.6	467.0	89.5	17.8	80080	10:25:37	-279.4	424.0	90.1	17.9
472	16	80081	10:22:10	-594.2	1266.3	84.3	16.9	80081	10:24:31	-453.3	832.6	87.2	17.5
474	16	80083	10:25:41	-594.9	1269.5	85.9	17.1	80083	10:29:47	-348.2	568.3	92.0	18.0
474	16	80083	10:38:6	150.3	236.6	105.1	19.0	80083	10:40:6	270.5	409.7	107.2	19.2
479	16	80088	10:57:51	815.9	2082.1	115.1	20.6	80088	10:59:25	909.9	2459.7	114.2	20.7
490	16	80099	10:46:39	-700.4	1645.4	94.5	18.2	80099	10:48:54	-565.4	1179.3	100.3	19.0
490	16	80099	10:52:30	-349.4	579.7	110.6	19.7	80099	10:55:10	-189.5	292.4	118.5	20.1
490	16	80099	11:0:44	143.8	239.8	131.0	20.7	80099	11:5:35	434.8	791.5	132.5	21.2
490	16	80099	11:7:53	573.5	1205.7	130.5	21.4	80099	11:8:56	636.2	1416.8	129.3	21.5
496	16	80105	10:48:48	-590.7	1260.2	103.8	19.5	80105	10:50:48	-470.8	888.8	110.1	20.0
499	16	80108	11:5:32	513.6	1001.3	142.2	22.3	80108	11:5:32	513.6	1001.3	142.2	22.3
506	16	80115	10:58:24	741.4	1785.4	137.3	23.4	80115	11:1:1	897.8	2401.9	130.2	23.7
513	16	80122	10:29:41	216.3	309.4	168.6	23.3	80122	10:35:26	561.2	1150.6	148.6	23.9
520	16	80129	10:6:47	550.7	1116.4	147.5	0.6	80129	10:10:18	762.5	1865.1	134.4	1.0
566	16	80175	12:51:39	-225.2	331.1	111.3	4.2	80175	12:52:47	-157.1	241.2	111.0	4.3
579	16	80188	13:58:53	-496.3	951.1	98.5	4.8	80188	13:58:53	-496.3	951.1	98.5	4.8
585	16	80194	14:26:33	-491.7	939.1	92.7	5.5	80194	14:28:24	-379.9	637.0	90.0	5.8

587	16	80196	14:35:23	-431.3	770.1	89.2	5.9	80196	14:36:35	-359.3	589.6	87.2	6.1
606	16	80215	15:32:41	-405.6	739.5	68.2	7.9	80215	15:33:30	-356.2	620.8	65.6	8.1
607	16	80216	15:32:30	-580.0	1249.7	76.3	7.4	80216	15:38:58	-191.9	327.4	55.6	8.6
607	16	80216	15:45:50	219.9	366.5	40.7	9.3	80216	15:46:39	269.4	447.4	40.3	9.4
608	16	80217	15:34:38	-615.1	1368.6	77.2	7.4	80217	15:39:57	-296.4	501.1	60.1	8.5
608	16	80217	15:48:31	217.7	366.7	39.1	9.4	80217	15:49:42	288.3	485.6	38.9	9.5
609	16	80218	15:40: 6	-450.9	867.5	67.8	8.1	80218	15:44:44	-173.4	311.6	52.0	8.8
609	16	80218	15:50:24	166.3	303.5	38.2	9.5	80218	15:51:13	215.7	367.5	37.5	9.5
612	16	80221	15:49:33	-378.8	693.1	60.7	8.7	80221	15:53:36	-135.8	283.6	45.9	9.2
612	16	80221	15:57:34	102.5	256.3	35.0	9.7	80221	16: 0:29	277.4	479.7	32.7	9.9
615	16	80224	15:58:21	-348.6	634.7	55.8	9.1	80224	16: 2:21	-108.6	273.2	40.4	9.6
615	16	80224	16: 5:25	75.1	252.0	31.1	9.9	80224	16: 7:13	183.1	347.0	28.4	10.1
616	16	80225	15:58:30	-506.4	1047.6	64.9	8.7	80225	15:58:54	-482.6	978.6	63.4	8.7
617	16	80226	16:12:45	181.3	353.1	25.2	10.3	80226	16:14:47	302.4	546.0	25.7	10.5
620	16	80229	16:10:35	-453.8	912.2	58.3	9.3	80229	16:12:35	-333.9	621.8	50.1	9.6
620	16	80229	16:21:54	224.9	424.5	20.4	10.7	80229	16:23:56	346.7	649.2	23.1	10.9
621	16	80230	16:15:29	-329.7	616.8	48.9	9.8	80230	16:16:31	-267.0	496.6	44.4	9.9
624	16	80233	16:21:17	-491.6	1030.8	57.9	9.6	80233	16:23:54	-333.9	637.0	46.7	10.1
624	16	80233	16:31:14	105.7	309.5	16.0	11.0	80233	16:33:25	236.4	458.4	14.7	11.2
625	16	80234	16:28: 9	-249.5	483.2	39.5	10.4	80234	16:29:10	-189.2	396.2	34.8	10.5
626	16	80235	16:31:10	-239.6	471.3	37.9	10.5	80235	16:34: 1	-69.2	296.4	24.4	10.9
628	16	80237	16:41:33	40.4	293.9	13.9	11.3	80237	16:45:46	293.5	571.7	12.8	11.7
629	16	80238	16:35:31	-493.2	1051.4	54.8	10.1	80238	16:39:37	-247.6	495.5	36.3	10.8
629	16	80238	16:33: 4	-640.4	1511.5	64.4	9.5	80238	16:33: 4	-640.3	1511.2	64.4	9.5
629	16	80238	16:48:45	301.1	589.7	12.8	11.8	80238	16:49: 1	317.0	620.8	13.9	11.8
631	16	80240	16:43:44	-344.8	685.5	42.8	10.8	80240	16:48:56	-32.9	304.0	16.9	11.5
631	16	80240	16:50:21	52.4	309.6	9.7	11.6	80240	16:52:48	199.1	432.3	4.8	11.9
632	16	80241	16:48:26	-234.7	486.2	33.4	11.2	80241	16:51:41	-40.0	309.5	16.9	11.6
633	16	80242	16:51: 1	-252.0	517.0	34.4	11.2	80242	16:54: 0	-73.2	325.8	19.3	11.6
633	16	80242	16:56:16	62.5	320.9	7.4	11.8	80242	16:57:52	158.5	391.6	0.9	12.0
636	16	80245	16:59:26	-265.0	548.3	34.4	11.5	80245	17: 0:33	-198.4	448.6	29.0	11.7
638	16	80247	17: 6:39	-178.3	430.6	27.1	11.9	80247	17: 9:19	-18.4	326.4	14.5	12.2
644	16	80253	17:21:57	-292.9	617.9	36.5	12.3	80253	17:22:59	-231.4	515.7	32.2	12.5
657	16	80266	17:56: 6	-441.3	961.8	50.7	13.3	80266	18: 0:14	-192.7	478.7	40.5	14.0
670	16	80279	18:30:23	-486.8	1080.4	61.6	14.6	80279	18:31:10	-439.7	954.5	60.6	14.8
670	16	80279	18:39:36	66.0	367.9	57.8	15.8	80279	18:43:47	316.5	674.5	63.3	16.2
671	16	80280	18:34:36	-391.9	836.3	60.6	15.0	80280	18:38: 6	-181.6	460.8	58.2	15.5
678	16	80287	18:54:57	-258.5	563.5	67.8	16.1	80287	18:56:57	-138.5	409.9	68.2	16.3
684	16	80293	19: 4:30	-601.0	1414.7	74.6	15.8	80293	19: 6: 4	-507.0	1128.7	74.6	16.1
692	16	80301	19:28:52	-347.1	724.8	85.0	17.4	80301	19:29: 3	-336.3	702.1	85.2	17.4
699	16	80308	19:41:31	-646.6	1565.6	86.4	17.2	80308	19:43:17	-540.0	1226.6	88.8	17.6
706	16	80315	20: 4:27	-342.4	727.8	102.5	18.9	80315	20: 4:37	-331.6	705.5	102.8	19.0

01-OCT-1987

TO: Kent Hills  
Code 633.0  
FROM: W. T. Kasprzak  
Code 615.1  
SUBJECT: Energetic ion data from the Pioneer Venus Orbiter  
Neutral Mass Spectrometer (ONMS)  
Updated energetic ion data tape

The tape, microfiche and assorted documentation represent an added section of energetic processed data from the ONMS instrument. The magnetic tape contains data for orbit 1 to 2043 and replaces the previous energetic ion data tape submitted on 20-AUG-1987. Note that this does not replace the neutral density measurement data from the same instrument (ONMS). This new tape refers to measurements of energetic ions. Both measurement types occurred during the first 645 orbits and therefore overlap. The microfiche contains the plots for orbits 1134 to 2043 and therefore is an addition to the previous set of microfiche submitted and does not replace it.

A tape dump of the first few blocks has been included for reference.

Any questions or problems with the data or the data tape should be communicated to:

H. B. Niemann	301-286-8706
W. T. Kasprzak	301-286-8253

PV OMS ENERGETIC ION DATA FOR NSSDC

AN ASTERISK (\*) INDICATES NO UADS DATA FOR THE ORBIT

0001	0003	0006*	0009	0022*	0026*	0027*	0030*	0032*	0038*	0041
0042	0043*	0044*	0046*	0049*	0050*	0052*	0054*	0055*	0056	0057*
0068*	0070	0077	0079*	0080*	0082	0085*	0087*	0095*	0098*	0104*
0111*	0116*	0117*	0127*	0137*	0138*	0139*	0151*	0152*	0161*	0162*
0111	0173	0175	0185	0186*	0188	0194	0195	0198*	0202	0209
0218	0235*	0238*	0297*	0334	0354*	0379	0382*	0384	0402*	0403
0405	0410*	0414	0423*	0434	0439*	0444*	0447*	0448*	0452*	0453
0461*	0462*	0464	0471	0472*	0474	0479*	0490	0496	0499*	0506*
0513*	0520*	0566	0579*	0585	0587	0606	0607	0608	0609	0612
0615	0616*	0617	0620	0621	0624	0625*	0629*	0631	0632*	0633
0636	0638	0644	0935	0937	0939	0946	0949	0951	0953	0954
0956	0958	0967	0968	0970	0974	0975	0979	0981	0982	0986
0991	0998	1000	1003*	1005	1007	1016	1017	1019	1023	1024*
1030	1031	1035*	1037*	1038*	1040*	1042	1044*	1047	1049*	1054*
1056	1065	1066*	1068*	1072*	1073*	1077	1079*	1080*	1089*	1093
1096	1098*	1103*	1105	1115*	1121	1122*	1126*	1128*	1129*	1133*
1140	1145	1147*	1150*	1152*	1154	1163*	1164	1166	1170	1171
1175	1177	1114*	1182	1187	1189	1191	1194	1196	1199	1201
1203	1212	1213	1215	1219	1220	1224	1227	1231	1236	1238*
1240	1243*	1245	1248	1250	1252	1261*	1262*	1264*	1268*	1269*
1273*	1275*	1276	1280*	1285*	1287*	1289*	1292*	1294*	1297*	1299*
1301*	1310*	1313*	1317*	1318*	1322*	1324*	1325*	1329*	1334*	1336*
1338*	1341*	1343*	1346*	1348*	1350*	1359*	1360*	1362*	1366*	1367
1371*	1373	1374*	1378*	1383	1385*	1387	1390	1392	1395	1397
1399	1408	1409	1411*	1446	1448	1457*	1458	1460*	1464*	1465*
1469*	1471*	1472*	1476*	1481*	1483*	1485*	1488*	1490*	1492*	1495*
1497*	1506*	1507*	1509*	1513*	1514*	1518*	1520*	1521*	1525*	1530*
1531*	1532*	1533*	1534*	1537*	1539*	1542*	1544*	1546*	1555*	1556*
1558*	1562*	1563*	1567*	1569*	1570*	1574*	1579*	1581*	1583*	1586*
1511*	1593*	1595*	1604*	1605	1607	1611	1612*	1614*	1616	1618
1623	1628	1630	1632	1635	1637	1640	1642	1644	1653	1654
1656	1661	1665	1667	1668	1672	1677	1679*	1681	1684*	1686*
1689*	1691*	1693*	1702*	1703*	1705*	1709*	1710*	1716*	1717*	1721*
1726*	1728*	1730*	1733*	1735*	1738*	1740*	1742*	1751*	1752*	1754*
1758*	1759*	1763*	1765*	1766	1770*	1775*	1777*	1779*	1782*	1784*
1787*	1789*	1791*	1800*	1801*	1803*	1807*	1814*	1828*	1831*	1833*
1840*	1847	1850	1857*	1864	1868	1871	1875	1878	1882	1885
1892	1896	1899*	1906*	1913*	1920*	1924*	1927*	1931*	1934*	1938*
1941*	1948*	1952*	1955*	1959*	1962*	1966*	1969*	1976*	1983*	1987*
1994*	1997*	2036*	2039*	2043*						

ORBIT	DATE	TYPE	COMMENTS	EOT	EON	LED	UTP	OUP	PLT
***** NEUT, RPR, FILA OFF DATA WITH TIME SELECTED FROM ENERGETIC ION ***** MARKING FILE									
0001	30-DEC-86	EDR	INBOUND AND OUTBOUND DATA	YES	YES	YES	YES	YES	YES
0003	30-DEC-86	EDR	INBOUND DATA	YES	YES	YES	YES	YES	YES
0006	30-DEC-86	EDR	INBOUND DATA	YES	NO	NO	YES	YES	YES
0009	30-DEC-86	EDR	INBOUND AND OUTBOUND DATA	YES	YES	YES	YES	YES	YES
0022	31-DEC-86	EDR	ISOLATED POINTS ON INBOUND	YES	NO	NO	YES	YES	YES
0026	31-DEC-86	EDR	INBOUND DATA, SPARSE	YES	NO	NO	YES	YES	YES
0027	31-DEC-86	EDR	1 ISOLATED POINT	YES	NO	NO	YES	YES	YES
0030	31-DEC-86	EDR	SEVERAL ISOLATED POINTS	YES	NO	NO	YES	YES	YES
0032	07-JAN-87	EDR	1 POINT ONLY	YES	NO	NO	NO	YES	YES
0033	07-JAN-87	EDR	1 POINT ONLY	NO	NO	NO	NO	NO	NO
0038	07-JAN-87	EDR	2 ISOLATED POINTS NRPA DATA ONLY	YES	NO	NO	NO	YES	YES
0041	07-JAN-87	TYM	INBOUND DATA ONLY	YES	YES	YES	YES	YES	YES
0042	07-JAN-87	EDR		YES	YES	YES	YES	YES	YES
0043	07-JAN-87	EDR	NRPA DATA ONLY	YES	NO	NO	NO	YES	YES
0044	14-JAN-87	EDR	1 POINT OUT BOUND NRPA	YES	NO	NO	NO	YES	YES
0046	20-JAN-87	EDR	NRPA OUTBOUND DATA ONLY	YES	NO	NO	YES	YES	YES
0049	14-JAN-87	EDR	ISOLETED POINTS NRPA OUTBOUND	YES	NO	NO	NO	YES	YES
0050	14-JAN-87	EDR	ISOLETED POINTS NRPA OUTBOUND	YES	NO	NO	NO	YES	YES
0052	14-JAN-87	EDR	ISOLETED POINTS NRPA OUTBOUND	YES	NO	NO	NO	YES	YES
0054	14-JAN-87	EDR	ISOLETED POINTS NRPA OUTBOUND	YES	NO	NO	NO	YES	YES
0055	14-JAN-87	EDR	SEVERAL POINTS NRPA OUTBOUND	YES	NO	NO	NO	YES	YES
0056	14-JAN-87	EDR	SEVERAL POINTS NRPA OUTBOUND	YES	YES	YES	NO	YES	YES
0057	14-JAN-87	EDR	ISOLATED POINTS NRPA OUTBOUND	YES	NO	NO	NO	YES	YES
0068	14-JAN-87	EDR	ISOLATED POINTS NRPA OUTBOUND	YES	NO	NO	NO	YES	YES
0070	14-JAN-87	EDR	1 POINT RPA OUTBOUND	YES	YES	YES	NO	YES	YES
0077	14-JAN-87	EDR	INBOUND RPA/ISOLATED POINTS IN NRPA OUTBOUND	YES	YES	YES	NO	YES	YES
0079	14-JAN-87	EDR	ISOLATED POINTS NRPA MODE OUTBOUND	YES	NO	NO	NO	YES	YES
0080	20-JAN-87	EDR	ISOLATED POINTS OUTBOUND ONLY	YES	NO	NO	YES	YES	YES
0082	20-JAN-87	EDR	ISOLATED POINTS OUTBOUND ONLY	YES	YES	YES	YES	YES	YES
0085	20-JAN-87	EDR	ISOLATED POINTS OUTBOUND ONLY	YES	NO	NO	YES	YES	YES
0087	20-JAN-87	EDR	OUTBOUND DATA ONLY	YES	YES	NO	YES	YES	YES
0095	20-JAN-87	EDR	OUTBOUND DATA ONLY	YES	YES	NO	YES	YES	YES
0098	20-JAN-87	EDR	NRPA DATA OUTBOUND ONLY	YES	NO	NO	YES	YES	YES
0104	20-JAN-87	EDR	ISOLATED POINTS OUTBOUND ONLY	YES	NO	NO	YES	YES	YES
0112	20-JAN-87	EDR	ISOLATED POINTS OUTBOUND ONLY	YES	NO	NO	YES	YES	YES
0116	20-JAN-87	EDR	ION MODE INBOUND & OUTBOUND	YES	NO	NO	YES	YES	YES
0117	26-FEB-87	EDR	FEW ISOLATED POINTS	YES	NO	NO	YES	YES	YES
0127	26-FEB-87	EDR	FEW ISOLATED POINTS	YES	YES	NO	YES	YES	YES
0137	20-JAN-87	EDR	ONE POINT	YES	NO	NO	YES	YES	YES
0138	30-JAN-87	EDR	FEW ISOLATED POINTS RPA MODE	YES	YES	NO	YES	YES	YES
0139	20-JAN-87	EDR	NRPA MODE ONLY	YES	NO	NO	YES	YES	YES
0151	30-JUN-87	EDR	INBOUND AND SEVERAL POINTS OUTBOUND	YES	YES	YES	YES	YES	YES
0152	30-JUN-87	EDR	INBOUND ONLY	YES	YES	YES	YES	YES	YES
0161	30-JAN-87	EDR	FEW ISOLATED POINTS RPA MODE	YES	NO	NO	YES	YES	YES
0162	30-JAN-87	EDR	FEW ISOLATED POINTS RPA MODE	YES	NO	NO	YES	YES	YES
0164	30-JAN-87	EDR	INBOUND/OUTBOUND RPA MODE	YES	YES	YES	YES	YES	YES
0173	30-JAN-87	EDR	OUTBOUND RPA DATA	YES	YES	YES	YES	YES	YES
0175	30-JAN-87	EDR	INBOUND/OUTBOUND RPA DATA	YES	YES	YES	YES	YES	YES
0185	30-JAN-87	EDR	INBOUND/OUTBOUND RPA DATA	YES	YES	YES	YES	YES	YES

0186	10-FEB-87	EDR	2 ISOLATED POINTS	YES	NO	NO	YES	YES	YES
0188	10-FEB-87	EDR	INBOUND DATA	YES	YES	YES	YES	YES	YES
0194	10-FEB-87	EDR	INBOUND DATA	YES	YES	YES	YES	YES	YES
195	10-FEB-87	EDR	INBOUND/OUTBOUND DATA	YES	YES	YES	YES	YES	YES
198	10-FEB-87	EDR	1 ISOLATED POINTS INBOUND SEVERAL POINTS OUTBOUND	YES	NO	NO	YES	YES	YES
0202	10-FEB-87	EDR	INBOUND DATA	YES	YES	YES	YES	YES	YES
0209	10-FEB-87	EDR	INBOUND/OUTBOUND	YES	YES	YES	YES	YES	YES
0218	10-FEB-87	EDR	INBOUND/OUTBOUND	YES	YES	YES	YES	YES	YES
0235	10-FEB-87	EDR	1 POINT INBOUND	YES	NO	NO	YES	YES	YES
0238	10-FEB-87	EDR	SEVERAL ISOLATED POINTS INBOUND	YES	NO	NO	YES	YES	YES
0297	16-MAR-87	EDR	ONE ISOLATED POINT	YES	NO	NO	YES	YES	YES
0316	16-MAR-87	EDR	SEVERAL ISOLATED POINTS	NO	NO	NO	NO	NO	YES
0320	16-MAR-87	EDR	SEVERAL ISOLATED POINTS	NO	NO	NO	NO	NO	YES
0323	16-MAR-87	EDR	ISOLATED POINTS	NO	NO	NO	NO	NO	YES
0334	16-MAR-87	EDR	INBOUND/OUTBOUND DATA	YES	YES	YES	YES	YES	YES
0337	16-MAR-87	EDR	SEVERAL ISOLATED POINTS OUTBOUND	NO	NO	NO	NO	NO	YES
0344	26-MAR-87	EDR	ION MODE DATA SEVERAL ISOLATED POINTS	NO	NO	NO	NO	NO	YES
0348	26-MAR-87	EDR	ION MODE DATA SEVERAL ISOLATED POINTS	NO	NO	NO	NO	NO	YES
0354	26-MAR-87	EDR	OUTBOUND DATA SEVERAL ISOLATED POINTS	YES	NO	NO	YES	YES	YES
0379	26-MAR-87	EDR	INBOUND DATA	YES	YES	YES	YES	YES	YES
0382	26-MAR-87	EDR	INBOUND/OUTBOUND SEVERAL ISOLATED POINTS	YES	NO	NO	YES	YES	YES
0384	26-MAR-87	EDR	INBOUND/OUTBOUND DATA	YES	YES	YES	YES	YES	YES
386	26-MAR-87	EDR	NO ATTITUDE DATA	NO	NO	NO	NO	NO	YES
402	26-MAR-87	EDR	SEVERAL ISOLATED POINTS INBOUND	YES	NO	NO	YES	YES	YES
0403	26-MAR-87	EDR	INBOUND/OUTBOUND DATA	YES	YES	YES	YES	YES	YES
0405	26-MAR-87	EDR	INBOUND/OUTBOUND DATA	YES	YES	YES	YES	YES	YES
0410	26-MAR-87	EDR	SEVERAL ISOLATED POINTS INBOUND	YES	NO	NO	YES	YES	YES
0414	13-APR-87	EDR	INBOUND DATA	YES	YES	YES	YES	YES	YES
0423	13-APR-87	EDR	1 ISOLATED POINT INBOUND	YES	NO	NO	YES	YES	YES
0434	13-APR-87	EDR	INBOUND/OUTBOUND DATA	YES	YES	YES	YES	YES	YES
0439	13-APR-87	EDR	INBOUND DATA	YES	YES	YES	NO	YES	YES
0444	13-APR-87	EDR	FEW ISOLATED POINTS INBOUND	YES	NO	NO	YES	YES	YES
0447	13-APR-87	EDR	FEW ISOLATED POINTS INBOUND	YES	NO	NO	YES	YES	YES
0448	13-APR-87	EDR	1 ISOLATED POINT INBOUND	YES	NO	NO	YES	YES	YES
0452	13-APR-87	EDR	1 ISOLATED POINT INBOUND	YES	NO	NO	YES	YES	YES
0453	13-APR-87	EDR	INBOUND DATA	YES	YES	YES	YES	YES	YES
0461	13-APR-87	EDR	1 ISOLATED POINT INBOUND OUTBOUND	YES	NO	NO	YES	YES	YES
0462	13-APR-87	EDR	1 ISOLATED POINT INBOUND	YES	NO	NO	YES	YES	YES
0464	15-APR-87	EDR	INBOUND/OUTBOUND DATA	YES	YES	YES	YES	YES	YES
0471	15-APR-87	EDR	INBOUND ONLY	YES	YES	YES	YES	YES	YES
0472	15-APR-87	EDR	ISOLATED POINTS	YES	NO	NO	YES	YES	YES
0474	15-APR-87	EDR	INBOUND/OUTBOUND DATA	YES	YES	YES	YES	YES	YES
0479	15-APR-87	EDR	SEVERAL ISOLATED POINTS OUTBOUND	YES	NO	NO	YES	YES	YES
490	15-APR-87	EDR	INBOUND/OUTBOUND DATA	YES	YES	YES	YES	YES	YES
96	15-APR-87	EDR	INBOUND ONLY	YES	YES	YES	YES	YES	YES
0499	15-APR-87	EDR	ISOLATED POINTS OUTBOUND	YES	NO	NO	YES	YES	YES
0506	15-APR-87	EDR	OUTBOUND ONLY	YES	NO	NO	YES	YES	YES
0513	15-APR-87	EDR	OUTBOUND SCATTERED POINTS	YES	NO	NO	YES	YES	YES
0520	15-APR-87	EDR	ISOLATED POINTS	YES	NO	NO	YES	YES	YES

0566	17-APR-87	EDR	INBOUND DATA ONLY	YES	YES	YES	YES	YES	YES
0579	17-APR-87	EDR	1 ISOLATED POINT	YES	NO	NO	YES	YES	YES
0585	17-APR-87	EDR	INBOUND DATA ONLY	YES	YES	YES	YES	YES	YES
0587	17-APR-87	EDR	INBOUND DATA ONLY	YES	YES	YES	YES	YES	YES
0606	17-APR-87	EDR	INBOUND DATA ONLY	YES	YES	YES	YES	YES	YES
0607	17-APR-87	EDR	INBOUND AND OUTBOUND DATA	YES	YES	YES	YES	YES	YES
0608	17-APR-87	EDR	INBOUND AND OUTBOUND DATA	YES	YES	YES	YES	YES	YES
0609	17-APR-87	EDR	INBOUND AND OUTBOUND DATA	YES	YES	YES	YES	YES	YES
0612	17-APR-87	EDR	INBOUND AND OUTBOUND DATA	YES	YES	YES	YES	YES	YES
0615	17-APR-87	EDR	INBOUND AND OUTBOUND DATA	YES	YES	YES	YES	YES	YES
0616	17-APR-87	EDR	SEVERAL ISOLATED PNTS INBOUND	YES	YES	NO	YES	YES	YES
0617	17-APR-87	EDR	OUTBOUND DATA ONLY	YES	YES	YES	YES	YES	YES
0620	20-APR-87	EDR	INBOUND/OUTBOUND	YES	YES	YES	YES	YES	YES
0621	20-APR-87	EDR	INBOUND DATA ONLY	YES	YES	YES	YES	YES	YES
0624	20-APR-87	EDR	INBOUND/OUTBOUND	YES	YES	YES	YES	YES	YES
0625	20-APR-87	EDR	INBOUND DATA ONLY	YES	NO	NO	YES	YES	YES
0626	20-APR-87	EDR	INBOUND DATA ONLY	YES	YES	YES	YES	YES	YES
0628	20-APR-87	EDR	OUTBOUND DATA ONLY	YES	YES	YES	YES	YES	YES
0629	20-APR-87	EDR	INBOUND/OUTBOUND DATA	YES	NO	NO	YES	YES	YES
0631	20-APR-87	EDR	INBOUND/OUTBOUND FILA B	YES	YES	YES	YES	YES	YES
0632	20-APR-87	EDR	INBOUND DATA ONLY	YES	NO	NO	YES	YES	YES
0633	20-APR-87	EDR	INBOUND/OUTBOUND	YES	YES	YES	YES	YES	YES
0636	20-APR-87	EDR	INBOUND DATA ONLY	YES	NO	NO	YES	YES	YES
0638	20-APR-87	EDR	INBOUND DATA ONLY	YES	YES	YES	YES	YES	YES
0644	20-APR-87	EDR	FEW POINTS INBOUND	YES	YES	YES	YES	YES	YES

\*\*\*\*\* FOR ORBITS 935 AND UP NEUT, NRPA, FILA OFF DATA WILL BE USED \*\*\*\*\*

0935	15-JAN-87	EDR		YES	YES	YES	YES	YES	YES
0937	15-JAN-87	EDR		YES	YES	YES	YES	YES	YES
0939	15-JAN-87	EDR		YES	YES	YES	YES	YES	YES
0946	15-JAN-87	EDR		YES	YES	YES	YES	YES	YES
0949	15-JAN-87	EDR		YES	YES	YES	YES	YES	YES
0951	15-JAN-87	EDR		YES	YES	YES	YES	YES	YES
0953	15-JAN-87	EDR		YES	YES	YES	YES	YES	YES
0954	15-JAN-87	EDR		YES	YES	YES	YES	YES	YES
0956	15-JAN-87	EDR		YES	YES	YES	YES	YES	YES
0958	15-JAN-87	EDR		YES	YES	YES	YES	YES	YES
0967	15-JAN-87	EDR		YES	YES	YES	YES	YES	YES
0968	15-JAN-87	EDR		YES	YES	YES	YES	YES	YES
0970	15-JAN-87	EDR		YES	YES	YES	YES	YES	YES
0974	15-JAN-87	EDR		YES	YES	YES	YES	YES	YES
0975	15-JAN-87	EDR		YES	YES	YES	YES	YES	YES
0979	15-JAN-87	EDR		YES	YES	YES	YES	YES	YES
0981	15-JAN-87	EDR		YES	YES	YES	YES	YES	YES
0982	20-APR-87	EDR		YES	YES	YES	YES	YES	YES
0986	20-APR-87	EDR		YES	YES	YES	YES	YES	YES
0991	20-APR-87	EDR		YES	YES	YES	YES	YES	YES
0998	20-APR-87	EDR		YES	YES	YES	YES	YES	YES
1000	20-APR-87	EDR		YES	YES	YES	YES	YES	YES
1003	20-APR-87	EDR		YES	YES	NO	YES	YES	YES
1005	20-APR-87	EDR		YES	YES	YES	YES	YES	YES
1007	27-APR-87	EDR		YES	YES	YES	YES	YES	YES
1016	27-APR-87	EDR		YES	YES	YES	YES	YES	YES
1017	27-APR-87	EDR		YES	YES	YES	YES	YES	YES
1019	29-APR-87	EDR		YES	YES	YES	YES	YES	YES
1023	27-APR-87	EDR		YES	YES	YES	YES	YES	YES
1024	27-APR-87	EDR		YES	NO	NO	YES	YES	YES
1028	27-APR-87	EDR	NO DATA FROM -1000<TP<1000	NO	NO	NO	NO	YES	YES
1030	27-APR-87	EDR		YES	YES	YES	YES	YES	YES

1031	27-APR-87	EDR	YES						
1035	27-APR-87	EDR	YES	NO	NO	YES	YES	YES	YES
1037	27-APR-87	EDR	YES	NO	NO	YES	YES	YES	YES
1038	27-APR-87	EDR	YES	NO	NO	YES	YES	YES	YES
1040	27-APR-87	EDR	YES	NO	NO	YES	YES	YES	YES
1042	27-APR-87	EDR	YES						
1044	27-APR-87	EDR	YES	NO	NO	YES	YES	YES	YES
1047	27-APR-87	EDR	YES						
1049	27-APR-87	EDR	YES	NO	NO	YES	YES	YES	YES
1052	27-APR-87	EDR	YES	NO	NO	YES	YES	YES	YES
1054	27-APR-87	EDR	YES	NO	NO	YES	YES	YES	YES
1056	13-MAY-87	EDR	YES						
1065	13-MAY-87	EDR	YES						
1066	13-MAY-87	EDR	YES	NO	NO	YES	YES	YES	YES
1068	13-MAY-87	EDR	YES	NO	NO	YES	YES	YES	YES
1072	13-MAY-87	EDR	YES	NO	NO	YES	YES	YES	YES
1073	13-MAY-87	EDR	YES	NO	NO	YES	YES	YES	YES
1077	13-MAY-87	EDR	YES						
1079	13-MAY-87	EDR	YES	NO	NO	YES	YES	YES	YES
1080	13-MAY-87	EDR	YES	NO	NO	YES	YES	YES	YES
1084	13-MAY-87	EDR	YES						
1089	13-MAY-87	EDR	YES	NO	NO	YES	YES	YES	YES
1093	13-MAY-87	EDR	YES						
1096	13-MAY-87	EDR	YES						
1098	13-MAY-87	EDR	YES	NO	NO	YES	YES	YES	YES
1103	13-MAY-87	EDR	YES	NO	NO	YES	YES	YES	YES
1105	05-JUN-87	EDR	YES						
1114	05-JUN-87	EDR	YES	NO	NO	YES	YES	YES	YES
1115	05-JUN-87	EDR	YES	NO	NO	YES	YES	YES	YES
1121	05-JUN-87	EDR	YES						
1122	05-JUN-87	EDR	YES	NO	NO	YES	YES	YES	YES
1126	05-JUN-87	EDR	YES	NO	NO	YES	YES	YES	YES
1128	05-JUN-87	EDR	YES	NO	NO	YES	YES	YES	YES
1129	05-JUN-87	EDR	YES	NO	NO	YES	YES	YES	YES
1133	05-JUN-87	EDR	YES	NO	NO	YES	YES	YES	YES
1138	04-AUG-87	EDR	YES	NO	NO	YES	YES	YES	YES
1140	04-AUG-87	EDR	YES						
1145	04-AUG-87	EDR	YES						
1147	04-AUG-87	EDR	YES	NO	NO	YES	YES	YES	YES
1150	04-AUG-87	EDR	YES	NO	NO	YES	YES	YES	YES
1152	04-AUG-87	EDR	YES	NO	NO	YES	YES	YES	YES
1154	04-AUG-87	EDR	YES						
1163	04-AUG-87	EDR	YES	NO	NO	YES	YES	YES	YES
1164	04-AUG-87	EDR	YES						
1166	04-AUG-87	EDR	YES						
1170	04-AUG-87	EDR	YES						
1171	04-AUG-87	EDR	YES						
1175	05-AUG-87	EDR	YES						
1177	05-AUG-87	EDR	YES						
1178	05-AUG-87	EDR	YES						
1182	05-AUG-87	EDR	YES						
1187	05-AUG-87	EDR	YES						
1189	05-AUG-87	EDR	YES						
1191	05-AUG-87	EDR	YES						
1194	05-AUG-87	EDR	YES						
1196	05-AUG-87	EDR	YES						
1199	05-AUG-87	EDR	YES						
1201	05-AUG-87	EDR	YES						
1203	05-AUG-87	EDR	YES						
1212	10-AUG-87	EDR	YES						





1591	24-AUG-87	EDR		YES	NO	NO	YES	YES	YES
1593	24-AUG-87	EDR		YES	NO	NO	YES	YES	YES
1595	24-AUG-87	EDR		YES	NO	NO	YES	YES	YES
1604	24-AUG-87	EDR		YES	NO	NO	YES	YES	YES
1605	24-AUG-87	EDR		YES	YES	YES	YES	YES	YES
1607	24-AUG-87	EDR		YES	YES	YES	YES	YES	YES
1611	24-AUG-87	EDR		YES	YES	YES	YES	YES	YES
1612	26-AUG-87	EDR		YES	NO	NO	YES	YES	YES
1614	26-AUG-87	EDR		YES	NO	NO	YES	YES	YES
1616	26-AUG-87	EDR		YES	YES	YES	YES	YES	YES
1618	26-AUG-87	EDR		YES	YES	YES	YES	YES	YES
1619	26-AUG-87	EDR	0 DATA; DATAGAP -340<TP<1200 S	NO	NO	NO	NO	YES	YES
1623	26-AUG-87	EDR		YES	YES	YES	YES	YES	YES
1628	26-AUG-87	EDR		YES	YES	YES	YES	YES	YES
1630	02-SEP-87	EDR		YES	YES	YES	YES	YES	YES
1632	02-SEP-87	EDR		YES	YES	YES	YES	YES	YES
1635	02-SEP-87	EDR		YES	YES	YES	YES	YES	YES
1637	02-SEP-87	EDR		YES	YES	YES	YES	YES	YES
1640	02-SEP-87	EDR		YES	YES	YES	YES	YES	YES
1642	02-SEP-87	EDR		YES	YES	YES	YES	YES	YES
1644	02-SEP-87	EDR		YES	YES	YES	YES	YES	YES
1653	02-SEP-87	EDR		YES	YES	YES	YES	YES	YES
1654	02-SEP-87	EDR		YES	YES	YES	YES	YES	YES
1656	02-SEP-87	EDR		YES	YES	YES	YES	YES	YES
1661	02-SEP-87	EDR		YES	YES	YES	YES	YES	YES
1665	02-SEP-87	EDR		YES	YES	YES	YES	YES	YES
1667	02-SEP-87	EDR		YES	YES	YES	YES	YES	YES
1668	02-SEP-87	EDR		YES	YES	YES	YES	YES	YES
1672	02-SEP-87	EDR		YES	YES	YES	YES	YES	YES
1677	02-SEP-87	EDR		YES	YES	YES	YES	YES	YES
1679	02-SEP-87	EDR		YES	NO	NO	YES	YES	YES
1681	02-SEP-87	EDR		YES	YES	YES	YES	YES	YES
1684	02-SEP-87	EDR		YES	NO	NO	YES	YES	YES
1686	02-SEP-87	EDR		YES	NO	NO	YES	YES	YES
1689	04-SEP-87	EDR		YES	NO	NO	YES	YES	YES
1691	04-SEP-87	EDR		YES	NO	NO	YES	YES	YES
1693	04-SEP-87	EDR		YES	NO	NO	YES	YES	YES
1702	04-SEP-87	EDR		YES	NO	NO	YES	YES	YES
1703	04-SEP-87	EDR		YES	NO	NO	YES	YES	YES
1705	04-SEP-87	EDR		YES	NO	NO	YES	YES	YES
1709	04-SEP-87	EDR		YES	NO	NO	YES	YES	YES
1710	04-SEP-87	EDR		YES	NO	NO	YES	YES	YES
1716	04-SEP-87	EDR		YES	NO	NO	YES	YES	YES
1717	04-SEP-87	EDR		YES	NO	NO	YES	YES	YES
1719	04-SEP-87	EDR	NO DATA FOR THIS ORBIT	NO	NO	NO	NO	NO	NO
1721	04-SEP-87	EDR		YES	NO	NO	YES	YES	YES
1726	04-SEP-87	EDR		YES	NO	NO	YES	YES	YES
1728	04-SEP-87	EDR		YES	NO	NO	YES	YES	YES
1730	08-SEP-87	EDR		YES	NO	NO	YES	YES	YES
1733	08-SEP-87	EDR		YES	NO	NO	YES	YES	YES
1735	08-SEP-87	EDR		YES	NO	NO	YES	YES	YES
1738	08-SEP-87	EDR		YES	NO	NO	YES	YES	YES
1740	08-SEP-87	EDR		YES	NO	NO	YES	YES	YES
1742	08-SEP-87	EDR		YES	NO	NO	YES	YES	YES
1751	08-SEP-87	EDR		YES	NO	NO	YES	YES	YES
1752	08-SEP-87	EDR		YES	NO	NO	YES	YES	YES
1754	08-SEP-87	EDR		YES	NO	NO	YES	YES	YES
1758	08-SEP-87	EDR		YES	NO	NO	YES	YES	YES
1759	08-SEP-87	EDR		YES	NO	NO	YES	YES	YES
1763	08-SEP-87	EDR		YES	NO	NO	YES	YES	YES

1765	08-SEP-87	EDR	YES	NO	NO	YES	YES	YES
1766	08-SEP-87	EDR	YES	YES	YES	YES	YES	YES
1770	08-SEP-87	EDR	YES	NO	NO	YES	YES	YES
1775	08-SEP-87	EDR	YES	NO	NO	YES	YES	YES
1777	08-SEP-87	EDR	YES	NO	NO	YES	YES	YES
1779	08-SEP-87	EDR	YES	NO	NO	YES	YES	YES
1782	08-SEP-87	EDR	YES	NO	NO	YES	YES	YES
1784	08-SEP-87	EDR	YES	NO	NO	YES	YES	YES
1787	08-SEP-87	EDR	YES	NO	NO	YES	YES	YES
1789	08-SEP-87	EDR	YES	NO	NO	YES	YES	YES
1791	08-SEP-87	EDR	YES	NO	NO	YES	YES	YES
1800	08-SEP-87	EDR	YES	NO	NO	YES	YES	YES
1801	08-SEP-87	EDR	YES	NO	NO	YES	YES	YES
1803	08-SEP-87	EDR	YES	NO	NO	YES	YES	YES
1807	08-SEP-87	EDR	YES	NO	NO	YES	YES	YES
1814	08-SEP-87	EDR	YES	NO	NO	YES	YES	YES
1828	08-SEP-87	EDR	YES	NO	NO	YES	YES	YES
1831	08-SEP-87	EDR	YES	NO	NO	YES	YES	YES
1833	08-SEP-87	EDR	YES	NO	NO	YES	YES	YES
1840	08-SEP-87	EDR	YES	YES	YES	YES	YES	YES
1847	08-SEP-87	EDR	YES	NO	NO	YES	YES	YES
1850	08-SEP-87	EDR	YES	YES	YES	YES	YES	YES
1857	08-SEP-87	EDR	YES	YES	YES	YES	YES	YES
1857	08-SEP-87	EDR	YES	NO	NO	YES	YES	YES
1864	08-SEP-87	EDR	YES	YES	YES	YES	YES	YES
1868	08-SEP-87	EDR	YES	YES	YES	YES	YES	YES
1871	08-SEP-87	EDR	YES	YES	YES	YES	YES	YES
1875	08-SEP-87	EDR	YES	YES	YES	YES	YES	YES
1878	08-SEP-87	EDR	YES	YES	YES	YES	YES	YES
1882	08-SEP-87	EDR	YES	YES	YES	YES	YES	YES
1885	08-SEP-87	EDR	YES	YES	YES	YES	YES	YES
1892	08-SEP-87	EDR	YES	YES	YES	YES	YES	YES
1896	08-SEP-87	EDR	YES	YES	YES	YES	YES	YES
1899	11-SEP-87	EDR	YES	YES	YES	YES	YES	YES
1906	11-SEP-87	EDR	YES	NO	NO	YES	YES	YES
1910	11-SEP-87	EDR	YES	NO	NO	YES	YES	YES
1913	11-SEP-87	EDR	NO	NO	NO	NO	NO	NO
1920	11-SEP-87	EDR	YES	NO	NO	YES	YES	YES
1924	11-SEP-87	EDR	YES	NO	NO	YES	YES	YES
1927	11-SEP-87	EDR	YES	NO	NO	YES	YES	YES
1931	11-SEP-87	EDR	YES	NO	NO	YES	YES	YES
1934	11-SEP-87	EDR	YES	NO	NO	YES	YES	YES
1938	11-SEP-87	EDR	YES	NO	NO	YES	YES	YES
1941	11-SEP-87	EDR	YES	NO	NO	YES	YES	YES
1948	11-SEP-87	EDR	YES	NO	NO	YES	YES	YES
1952	11-SEP-87	EDR	YES	NO	NO	YES	YES	YES
1955	11-SEP-87	EDR	YES	NO	NO	YES	YES	YES
1959	11-SEP-87	EDR	YES	NO	NO	YES	YES	YES
1962	11-SEP-87	EDR	YES	NO	NO	YES	YES	YES
1966	11-SEP-87	EDR	YES	NO	NO	YES	YES	YES
1969	11-SEP-87	EDR	YES	NO	NO	YES	YES	YES
1976	11-SEP-87	EDR	YES	NO	NO	YES	YES	YES
1983	11-SEP-87	EDR	YES	NO	NO	YES	YES	YES
1987	11-SEP-87	EDR	YES	NO	NO	YES	YES	YES
1994	11-SEP-87	EDR	YES	NO	NO	YES	YES	YES
1997	11-SEP-87	EDR	YES	NO	NO	YES	YES	YES
2036	16-SEP-87	EDR	YES	NO	NO	YES	YES	YES
2039	16-SEP-87	EDR	YES	NO	NO	NO	YES	YES
2043	16-SEP-87	EDR	YES	NO	NO	NO	YES	YES
			YES	NO	NO	NO	YES	YES

NO DATA FOR THIS ORBIT

## Purpose of Revised Pioneer Venus NSSDC Data Format

1. standardize and improve the data formats for each experiment so that the tapes can be easily read by a requestor.
2. store the data by experiment,
3. provide for orderly updating of data,
4. provide for ultimate replacement of existing UADS generated archival tapes.

A new format was designed which is to be used by each experimenter for PVO NSSDC data experimenter, and can be easily read by computers expected to be accessible to a requester. One major difference between this and the existing LFD format is the use of text (ASCII) data formats, eliminating both binary and IBM floating point formats.

The proposed new submission format is self-defining in the sense that the first three records on each tape define the data parameters, value representations, and missing data (file) indicators. The first tape record defines the order in which the variables appear in the subsequent data records, in a manner similar to that used for SEDR trajectory data (SEDR file 5). The second tape record will contain a FORTRAN-compatible format list describing the field sizes and representations of each data value in the order defined in record 1. This format may be used to decode all subsequent records on the tape.

The third tape record will define a unique value associated with filler (missing) data for all variable fields. It is formatted according to the format used in record 2, and is immediately followed by the start of actual data records (records 4 and beyond).

The following is the proposed new format, with examples as applied to OETP instructions.

### PROPOSED PIONEER VENUS NSSDC LOW-FREQUENCY DATA FORMAT

This document describes a suggested format to be used by all investigators for the submission of their data to the National Space Sciences Data Center. The overall specification will require that all data be coded into ASCII, and written onto standard 1/2 inch 1600-bpi 9-track tapes. The logical record length will be fixed for a given tape, as well as the physical blocksize. Blocksizes should be large enough to avoid wasting tape, but should not exceed 8000 bytes in order to avoid making excessive demands on user programs for memory. The first three records of any of these tapes will be formatted as follows:

Record 1: The format to be used is (I3,n(1X,A4)) where "n" is the number of data items in each record.

* 4	ELTE	ELNE	MI	VS				(for OETP)
7	ETEM	SPOT	TONE	TTWO	XVEL	YVEL	ZVEL	(for ORPA)
↑	↑	↑	↑	↑	↑	↑	↑	
3	5	10	15	20	25	30	35	

Example 1: The first record in each tape file. Note that new value types with new 4-character designations can be added as necessary. The date, time, orbit and time-tag items are not included in the list, because they are common to all data records.

\* number of data items "n"

Record 2: This record contains the format in which all succeeding records are written. The first 4 format items specify the date, time, orbit, and time-tag, and will appear in the same format on all tapes.

(I8,I9,I5,I6,4F9.2)	(Appropriate for OETP)
↑	
1	

Example 2: The second record in each tape file

Record 3: This record will contain zeroes for the first four fields (date, time, orbit, and time-tag), and in addition will have a fill value in each data value location. This value will be used by any program reading the data to identify fill data in subsequent input records.

0	0	0	09999999.99999999.99999999.99999999.99
↑	↑	↑	↑
8	17	22	28 . 37 46 55 64

Example 3: The third record in each tape file. (Appropriate for OETP).

Record 4 to : These records contain the date, time, orbit, and time-tag for each time which has any non-fill data.

1981207	43527786	879	-1788	2345.67	78543.89999999.99	16.20	
↑	↑	↑	↑	↑	↑	↑	
8	17	22	28	37	46	55	64

Example 4: All records after the third in a tape file. (Appropriate for OETP).

As can be inferred from the above example, the date is coded as YEAR, DAY OF YEAR (1-366) with 19 included in the year. The time is in milliseconds of the day, orbit number is self-explanatory, and the time tag is the usual value ranging of the day from -1800 to 1800 in increments of 12.

The project-provided tape of SEDR information would be the source of the official dates and times to be used by all other investigators.

Nothing in the above format would preclude investigators from producing a tape containing the data from more than one experiment.

The external label on the tape should be type-written, and contain the following information:

- o Full name of experiment data contained on tape.<sup>1</sup>
- o Start date, time, and orbit number of data on the tape.
- o Stop date, time, and orbit number of data on the tape.
- o Production date of the tape.
- o The density (1600-bpi) and number of tracks (9) at which the tape was recorded.
- o An estimate of the amount of tape used.
- o The physical blocksize used in writing the tape.
- o A name and phone number of the individual responsible for the tape.

<sup>1</sup> Example: "Pioneer Venus Orbiter Electron Temperature Probe".

# PIIONEER VENUS

ORBITER NEUTRAL MASS SPECTROMETER

ORBIT

1105

DATE

81349

UT

PERIAPSIS

01 : 51 : 27

COMMENTS:

H. B. NIEMANN 301-286-8706

CODE 615

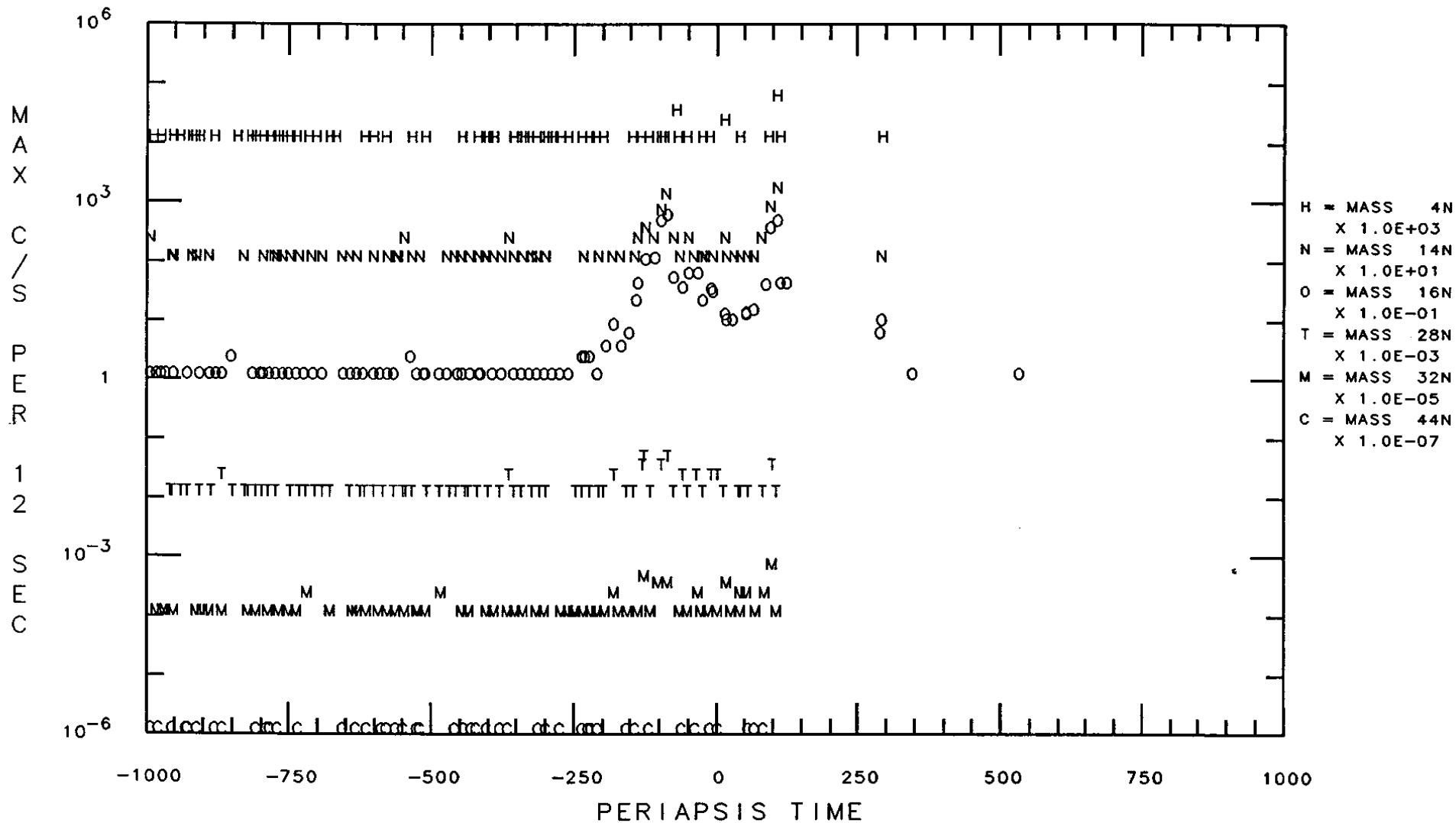
GODDARD SPACE FLIGHT CENTER  
GREENBELT, MD. 20771

*Plots 1*

# PV-ONMS DATA SUMMARY

SOURCE: E1

MAX DATA



Plots 2

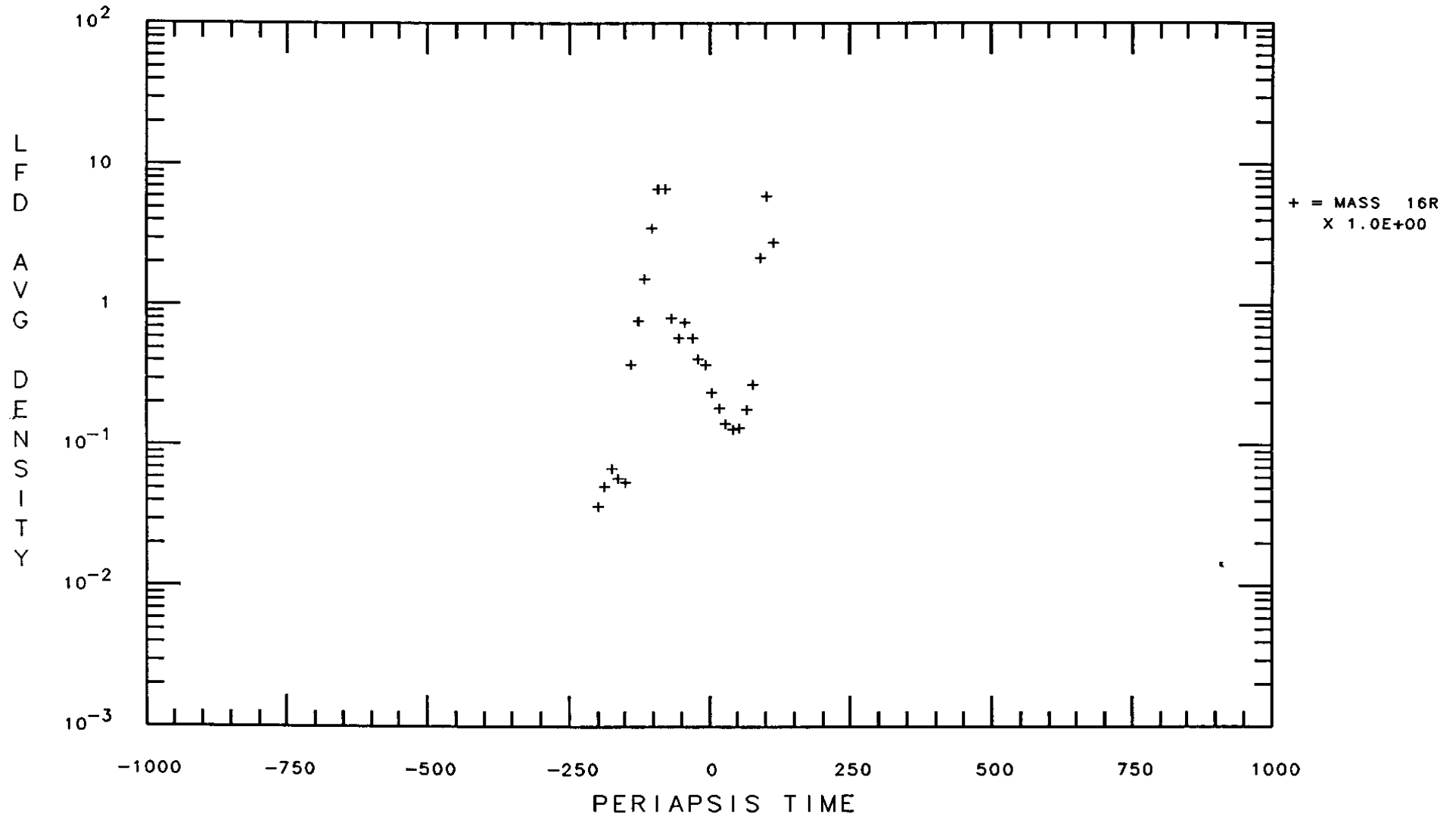
DATA SELECTION:    ORBITS    FROM 1105. TO 1105.

15:21:29  
05-JUN-87

# PV-ONMS DATA SUMMARY

SOURCE: E1

LED DATA



DATA SELECTION: ORBITS FROM 1105. TO 1105.

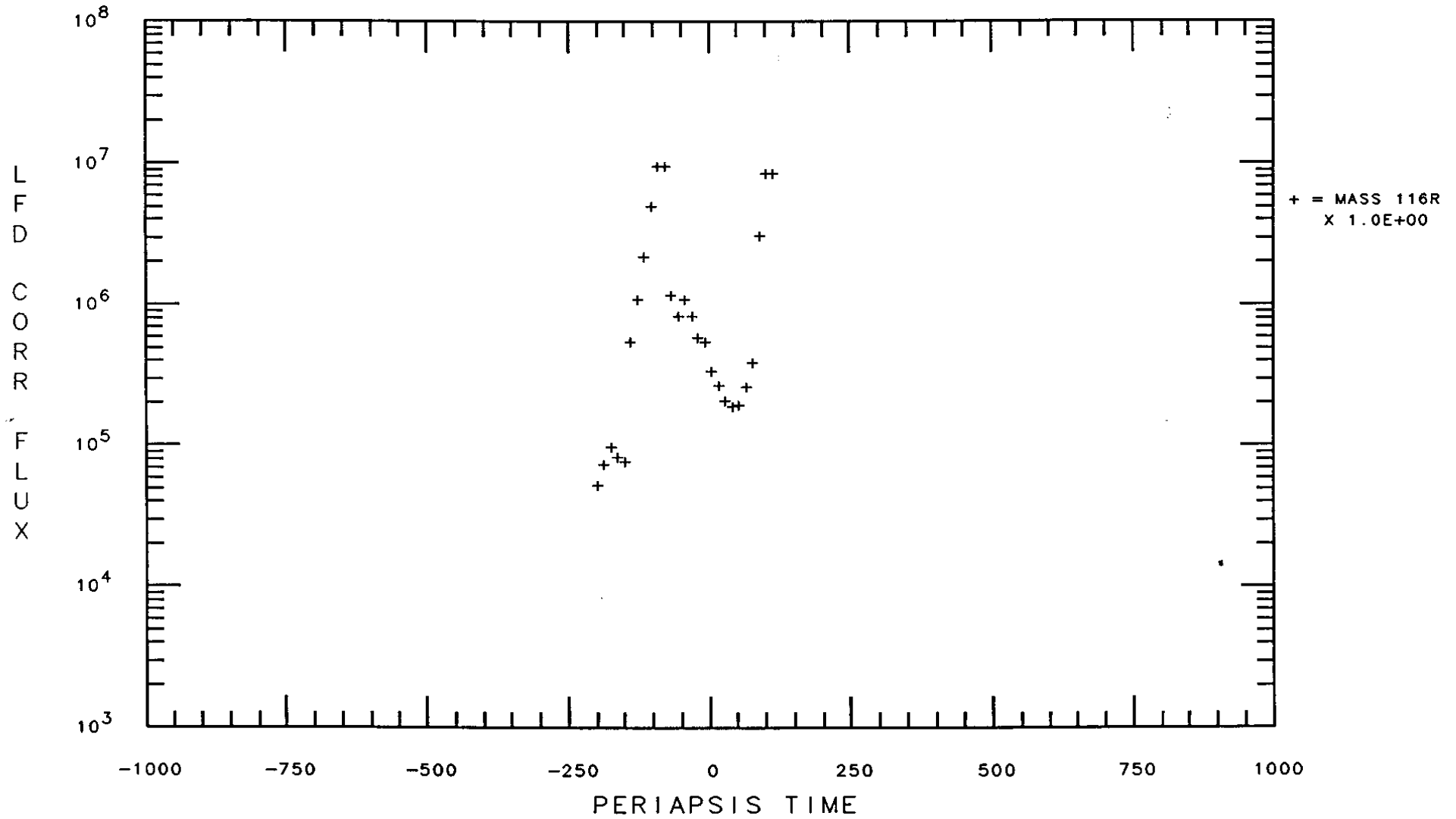
15:21:18  
05-JUN-87

*Plots 3*

# PV-ONMS DATA SUMMARY

SOURCE: E1

LED DATA



DATA SELECTION: ORBITS FROM 1105. TO 1105.

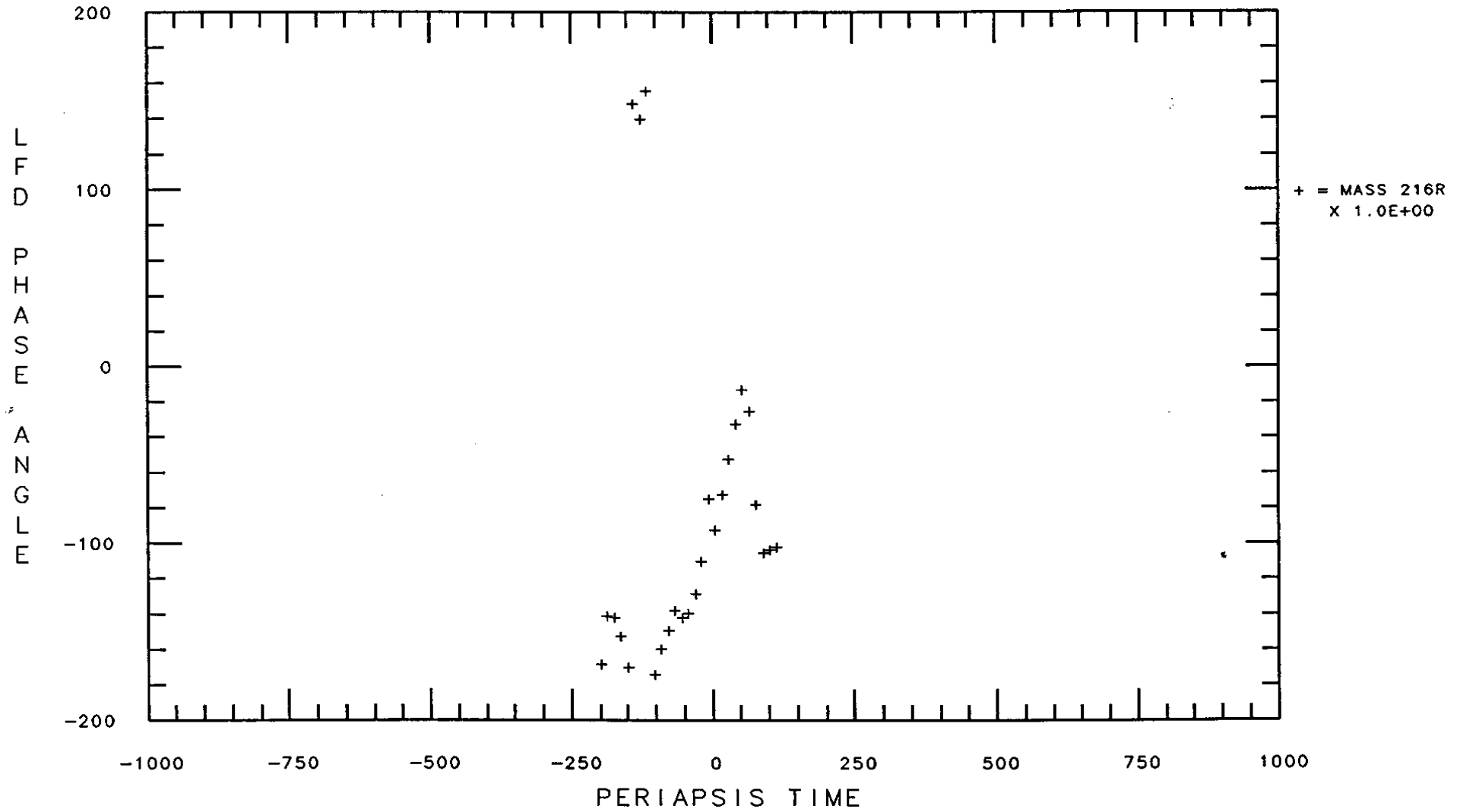
15:21:07  
05-JUN-87

*Plots 4*

# PV-ONMS DATA SUMMARY

SOURCE: E1

LED DATA



DATA SELECTION: ORBITS FROM 1105. TO 1105.

15:20:56  
05-JUN-87

*Plots 5*

ASCII LIST OF IN

FILE 1 RECORD 1 3900 BYTES

Y DO+ FO+ LANG VALT VLAT VLST WSTA  
 0 0 0 0 1.00E+35 1.00E+38 999. (18.19.15.16.1F69.2.1F69.2.0FF6.0.F6.1.F6.1.F5.1.F7.1)  
 999.0 999.0999.0 999.0 78339 54442817 1 -240 7  
 .01E-01 1.54E+05 123. 548.5 35.7 15.6 531.1 78339 54454817 1 -228 5.11E-01 1.12E+05 125. 531.5 34.8 15.7 63.1 783  
 39 54466817 1 -216 6.79E-01 1.48E+05 127. 515.3 33.8 15.7 63.0 78339 54478817 1 -204 4.17E-01 9.16E+05 124. 500.0  
 32.9 15.7 42.9 78339 54500817 1 -144 3.81E-02 6.36E+04 143. 436.8 28.1 15.8 62.6 78339 54638817 1 168 6.33E-0  
 2 1.19E+05 125. 467.6 3.6 10.0 65.4 78339 54850817 1 180 5.49E-02 1.21E+05 138. 480.9 2.6 16.4 65.6 78341 519  
 71000 3 100 2.46E-01 5.40E+05 100. 579.7 44.4 15.6 66.2 78341 51963000 3 -336 1.68E-01 4.12E+05 96. 553.1 43.5  
 15.0 66.1 78341 51995000 3 -324 2.91E+01 6.18E+05 110. 528.3 42.6 15.6 66.0 78341 52007000 3 -312 3.22E-01 7.06  
 E+05 115. 599.3 41.7 15.7 66.9 78347 54952817 9 -216 6.50E+00 1.43E+07 -99. 320.4 35.1 16.6 74.2 78347 54964817  
 3 -204 1.20E+01 2.33E+07 -99. 303.1 34.1 16.6 74.2 78347 54976817 9 -192 1.99E+01 4.37E+07 -99. 286.7 33.1 16.6  
 74.3 78347 54988817 9 -180 1.46E+01 5.12E+07 -99. 271.3 32.1 16.7 74.4 78347 55000817 9 -168 9.61E+00 2.11E+07  
 -99. 256.9 31.1 16.7 74.4 78347 55012817 9 -156 7.41E+00 1.63E+07 -99. 243.4 30.0 16.7 74.5 79014 68794816 41  
 -180 2.34E-01 1.13E+05 174. 203.0 32.4 20.0 117.4 79014 68806816 41 -168 8.98E-02 1.97E+05 176. 258.6 31.4 20.1 118.0  
 79014 68818816 41 -156 5.19E-02 1.13E+05 -175. 245.1 30.4 20.1 118.6 79015 68945816 42 -288 1.60E-01 3.51E+05 102.  
 447.6 41.0 18.9 113.1 79015 68957816 42 -276 1.78E-01 3.90E+05 84. 425.0 40.1 19.9 113.7 79015 68969816 42 -264 1  
 .50E-01 3.90E+05 96. 403.3 30.1 20.0 114.0 79015 68981816 42 -252 1.04E-01 2.30E+05 172. 382.5 38.2 20.0 115.0 790  
 15 68993816 42 -240 1.56E-01 3.43E+05 142. 362.5 37.2 20.0 115.6 79015 69005816 42 -228 2.42E-01 5.31E+05 159. 343.5  
 39.3 20.1 11.2 79015 69017816 42 -216 2.21E-01 4.68E+05 144. 325.3 35.3 20.1 115.8 79015 69029816 42 -204 1.40E-0  
 1 3.08E+05 141. 308.1 34.3 20.1 117.5 79015 69041816 42 -192 8.52E-02 1.87E+05 104. 291.8 33.3 20.2 118.1 79015 690  
 53816 42 -180 8.39E-02 1.18E+05 78. 278.4 32.3 20.2 118.7 79029 72370815 56 432 2.69E-01 5.91E+05 15. 784.0 -18.2  
 22.0 152.3 79029 72382815 56 444 1.07E-01 2.35E+05 30. 817.2 -19.0 22.8 152.3 79029 72394815 56 456 2.27E-01 5.00  
 E+05 40. 61.3 -19.9 22.8 151.8 79029 72406815 56 468 5.38E-01 1.18E+06 23. 884.0 -20.7 22.8 151.4 79029 72454815  
 50 516 8.00E-01 1.46E+05 171. 8025.1 -20.9 22.9 149.4 79043 72613000 70 360 1.34E-01 2.94E+05 58. 576.1 -12.2 0.2  
 167.3 79043 72625000 70 372 1.25E-01 3.74E+05 56. 603.6 -13.1 0.2 165.4 79043 73137000 70 684 2.04E-01 4.47E+05  
 -27. 1543.1 -1.7 0.7 143.7 79043 73149000 70 696 2.41E-01 5.30E+05 -21. 1586.2 -34.4 0.7 143.0 79043 73161000 70  
 700 2.01E-01 3.42E+05 -7. 1909.8 -35.1 0.7 142.2 79043 73173000 70 720 1.79E-01 3.92E+05 -4. 1673.7 -35.8 0.7 141.5  
 79043 73185000 70 732 1.48E-01 3.27E+05 -4. 1718.2 -36.4 0.7 140.8 79043 73197000 70 744 9.57E-02 2.10E+05 -10.  
 1762.7 -37.1 0.8 140.2 79043 73209000 70 756 1.16E-01 2.55E+05 -6. 1807.7 -37.7 0.8 139.5 79043 73221000 70 768 1  
 .61E-01 3.50E+05 -10. 1853.0 -38.0 0.0 138.6 79050 7104000 77 -264 2.15E-01 4.72E+05 -31. 401.7 38.6 23.7 142.1 790  
 55 71583000 264 2.22E-01 4.37E+05 -73. 392.8 -5.9 1.3 159.4

ASCII LIST OF IN

FILE 1 RECORD 133 3900 BYTES

89003 11169226 3681 -408 7.94E-02 1.61E+05 -93. 2226.1 18.4 1.2 154.7 89003 11167226 3681 -396 8.58E-02 1.89E+05 -85.  
 2207.9 17.8 1.2 155.0 89003 11179226 3681 -384 9.04E-02 1.99E+05 -86. 2190.3 17.1 1.2 155.3 89003 11191226 3681 -372 8  
 .89E-02 1.95E+05 -92. 2173.2 16.4 1.2 156.6 89003 11203226 3681 -360 1.03E-01 2.27E+05 -99. 2156.6 15.8 1.2 155.9 890  
 03 11215226 3681 -348 1.13E-01 2.49E+05 -104. 2140.5 15.1 1.3 156.2 89003 11227226 3681 -336 9.45E-02 2.08E+05 -106. 2124.9  
 14.4 1.3 157.4 89003 11239226 3681 -324 7.92E-02 1.70E+05 -105. 2109.9 13.7 1.3 156.7 89003 11251226 3681 -312 6.68E-0  
 2 1.47E+05 -107. 2095.4 13.1 1.3 156.9 89003 11263226 3681 -300 6.54E-02 1.44E+05 -96. 2081.4 12.4 1.3 157.1 89003 112  
 75226 3681 -288 5.76E-02 1.27E+05 -98. 2067.9 11.7 1.3 157.3 89003 11287226 3681 -276 5.81E-02 1.28E+05 -97. 2055.0 11.0  
 1.3 157.4 89003 11299226 3681 -264 6.28E-02 1.38E+05 -103. 2042.7 10.3 1.3 157.6 89003 11311226 3681 -252 6.05E-02 1.33  
 E+05 105. 2027.9 9.6 1.4 157.7 89003 11323226 3681 -240 5.68E-02 1.25E+05 -109. 2019.6 8.9 1.4 157.8 89003 11335226  
 3681 -228 5.00E-02 1.22E+05 -115. 2008.9 8.2 1.4 157.9 89003 11347226 3681 -216 5.62E-02 1.23E+05 -115. 1998.8 7.5 1.4  
 157.9 89003 11359226 3681 -204 5.97E-02 1.09E+05 -119. 1989.2 6.8 1.4 157.9 89003 11371226 3681 -192 6.45E-02 1.42E+05 -  
 121. 1980.2 5.1 1.4 158.0 89003 11383226 3681 -180 6.84E-02 1.94E+05 -112. 1971.8 5.4 1.4 157.9 89003 11395226 3681  
 -168 1.03E-01 1.95E+05 -114. 1961.8 4.7 1.4 157.9 89003 11407226 3681 -156 6.50E-02 1.87E+05 -111. 1956.6 4.0 1.4 157.8  
 89003 11419226 3681 -144 8.93E-02 1.96E+05 -105. 1949.5 3.3 1.5 157.8 89003 11599226 3681 48 1.09E+00 2.39E+05 -176.  
 1938.1 -7.4 1.4 154.1 89003 11611226 3681 60 5.06E-02 1.11E+05 -139. 1921.7 -8.1 1.7 153.7 89003 11623226 3681 72 1  
 .61E-01 3.50E+05 -17. 1915.0 1.7 1.7 153.7 89003 11705226 3681 84 1.15E+00 2.52E+05 -15. 1928.8 -9.5 1.7 152.9 890



REQ. AGENT

RAND NO.

ACQ. AGENT

RLR

DKB

PIONEER VENUS-1

HIGH RESOL-ENERGETIC ION (>40EV)

78-051A-11F PSPA-00183

This data set consists of 1 tape. The tape is 6250 bpi, 9-track, multifiled, ascii, and created on the IBM 360. The D and C numbers, time spans, and number of files are as follows:

D#	C#	FILES	TIME SPANS
--	--	-----	-----
D-85844	C-28934	08	12/05/78 - 01/03/89

07-MAR-90

TO: 633/P. Butterworth  
National Space Science Data Center

FROM: 615.1/W.T. Kasprzak

SUBJECT: Pioneer Venus Orbiter Neutral Mass Spectrometer  
(ONMS) high resolution energetic ion data

Enclosed is a tape and assorted documentation for the above new data set. The tape contains the high time resolution ("every point") energetic ion data from the ONMS. Also included on the tape are several auxiliary parameters derived from the data. Orbits 1 to 3681 are covered and represent all of the accumulated energetic ion data from the ONMS that is available and processed.

Any questions or problems with the data or the data tapes should be communicated to:

W.T. Kasprzak 301-286-8253

ONMS-1  
(HR ion)

07-NOV-1989

NSSDC DOCUMENTATION FOR  
PIONEER VENUS ORBITER NEUTRAL MASS SPECTROMETER

HIGH RESOLUTION ENERGETIC ION DATA

I. The Orbiter Neutral Mass Spectrometer (ONMS)

The instrument was primarily designed to determine the composition of the neutral exosphere/thermosphere of Venus. However, it has also detected energetic or fast ions whose energy exceeds 40 eV in the spacecraft frame of reference. These ions were observed in early orbits at an altitude higher than that required for measuring the neutral density at periapsis. Once the periapsis altitude had risen above the point where sensible neutral density measurements could be made the instrument was configured specifically to detect energetic ions.

The ONMS instrument has been described in "Pioneer Venus Orbiter Neutral Gas Mass Spectrometer Experiment," IEEE Transactions on Geoscience and Remote Sensing, GE-18 (1), 1980. A summary of the early results for energetic ions has been described in "Observations of Energetic Ions near the Venus Ionopause," Planet. Sp. Sci., 30, 1107-1115, 1982. The method used to reduce the energetic ion data to a flux and density has been described in "Observations of Energetic Ions on the Nightside of Venus," J. Geophys. Res., 92, 291-298, 1987. The data has been used as part of a study of the iontail of Venus in "The Ion tail of Venus: Its Configuration and Evidence for Ion Escape," J. Geophys. Res., 92, 15-26, 1987. The global nature of the data has been summarized for the first 2500 orbits in "Fast O<sup>+</sup> Ion Flow Observed Around Venus at Low Altitudes," NASA TM 100717. The angular response and minimum energy have been evaluated in "Pioneer Venus Neutral Mass Spectrometer," a GSFC summer institute project report by Yvette Guenther. The method used to reduce the data assumes cylindrical symmetry of the ion source but in actual fact the source is asymmetrical in its angular response. This can introduce scatter in the data that is a function of the angle of attack. No simple solution has been found for modeling this asymmetry since the actual ion drift vector is unknown. The minimum energy of an ion detectable by the ONMS in energetic ion mode is 35.9 eV, the maximum transmission is assumed to occur about 10 V above this value. On the nightside of Venus the spacecraft potential is negative and the most probable ion energy is near 40 eV. The papers are reproduced here for convenient reference.

## II. Reduction to flux and number density

Reference to the basic data reduction has been given in Section I. Because of the paucity of data at other mass numbers only mass 16 (atomic oxygen) has been reduced to a flux and number density. As part of the reduction process the angle in the ecliptic plane of the apparent ion flow in spacecraft reference frame has been deduced. No correction has been applied to the angle, number density or flux in order to remove the spacecraft velocity. One component of the ion drift can also be deduced perpendicular to the plane containing the axis on the ONMS and the spin axis of the spacecraft. In order to fit the data a minimum of 30 points were required in 36 seconds. In addition the maximum to minimum count ratio was required to be a factor of 3 or greater in order to insure that there was a definitive spin modulation. Only mass 16 (atomic oxygen) is fitted by this process. A constant spacecraft potential of -5 v has been assumed in assigning the effective energy of the ions to 40 eV. The minimum count rate is 1 per integration period or about 6 to 12 counts/s, depending on the bit rate and format of the telemetry data.

In general for orbit numbers 1 to 645 data were taken from RPA mode since the gas background with the filament on was considerably less than in non-RPA mode. For orbit numbers above 923 the instrument was deliberately configured with the filament off and non-RPA mode data was used. For mass 16 the RPA voltage is about +3.8 volts.

## III. The high resolution data.

All orbits have been processed where data exists or can be visually determined to exist. For orbits 1 to 645 a visual examination of the neutral mode data is required in order to identify the regions of energetic ions. For orbits beyond 923 no visual examination was needed. The ONMS instrument was not on for all orbits nor were energetic ions seen on all those orbits in which it was in operation. On the dayside of Venus energetic ions were seen only near the ionopause and when periapsis rose above it energetic ions were no longer observed. The flux values are estimated in the spacecraft reference frame. The density is computed from the flux by dividing it by a speed corresponding to 40 eV.

A time interval of 36 seconds is used in the least squares fit. The center 12 seconds of data is divided by the fitting function to derive the equivalent flux for that point. The center of the new fitting interval is adjusted so that it is centered on the expected signal maximum predicted from the previous interval fit. As a result of this method of fitting discontinuities may exist near minimum angle of attack where one 12 second interval adjoins the next

ONMS-3  
(HR ion)

interval. Several parameters result from the fit: 1) the best estimate of the flux for the interval (used to generate the low resolution UADS data set); 2) the phase shift of signal maximum with respect to that predicted by the position of the velocity vector and its error; 3) the fitting parameter B (Kasprzak et al., 1987); and 4) the effective angle of attack. Other items can be derived from this data: 1) the apparent direction of the ion flow projected into the ecliptic plane; and 2) one component of the ion drift perpendicular to the plane of axis of the ONMS and the spin axis. The phase angle is negative if the predicted signal maximum from the spacecraft velocity is ahead of the true signal maximum when viewed along the -Z spacecraft axis with clockwise rotation. The drift component is derived from the condition that the total relative velocity in the moving reference frame has no component perpendicular to the (ONMS axis, Z axis) plane. Therefore the drift component along this axis is equal to the spacecraft velocity component along this axis.

ONMS-4  
(HR ion)

IV. High resolution data tape.

The data tape has the following characteristics:

MEDIUM:	MAGNETIC TAPE
FORMAT:	ASCII
DENSITY:	6250 BPI
TRACKS:	9
PHYSICAL BLOCKSIZE:	9700 BYTES
LOGICAL RECORD SIZE:	97 BYTES
RECORDS/PHYSICAL BLOCK:	100
PHYSICAL RECORD TYPE:	FIXED BLOCK
TAPE LABEL:	UNLABELED
FORMAT:	ASCII
FILES:	ONE FILE PER 500 ORBITS
COMPUTER USED:	VAX 780

The orbits on the tape have been arranged sequentially. The format of the tape is briefly:

RECORD 1:  
DESCRIPTION: variable field names

RECORD 2:  
DESCRIPTION: FORTRAN format of succeeding data records

RECORD 3:  
DESCRIPTION: fill data definition for each data field

RECORD 4...:  
DESCRIPTION: data, one logical record per point

The field names listed in RECORD 1 are the following:

YYYYDDD	YYYY=4 digit year (e.g. 1978) DDD=3 digit day of year (e.g. 053)
UT(ms)	Universal time in ms
ORBIT	Orbit number
MS	Mass number - 16 for 0
F	Flag - D single data point flux, density A fitted parameters for interval
DENSITY	Effective number density assuming a 40 eV ion (particles/cm <sup>3</sup> )
FLUX	Flux (particles/cm <sup>2</sup> /s) AZ. ANG Azimuth angle of apparent ion flow direction projected into the ecliptic plane (deg)
PHASE	Phase shift of signal maximum with respect to that predicted by velocity vector (deg)
ERROR	Error in phase shift (deg)
ANGATK	Effective angle of attack (deg)
WP DIR	Direction of drift component perpendicular to (ONMS axis, Z axis) projected into the ecliptic plane (deg)
WP XY	Magnitude of drift component (m/s)

ONMS-5  
(HR ion)

B Fitting parameter

No spacecraft positional parameters have been included in the data set. These can be obtained from the SEDR data tape submitted separately by the Project.

Orbit parameters can be calculated with the orbit programs and data files include in the data set 78-051A-00I

[26-FEB-90]

Several orbits of energetic ion data show individual points that that are erroneous and probably wrong.

ORBIT	LOW RESOLUTION DATA PERIAPSIS TIME TAG	UNIVERSAL TIME OF TIME TAG (ms)
3453	-180	8722030
	-168	8734030
3660	-576	10603177
	-564	10615177
	-468	10711177
	-456	10723177
	-336	10843177
3681	-648	10915226
	-636	10927226

High resolution data in the same time frame, plus or minus 12 seconds, is most likely wrong.

2 March 1990

To: Wayne Kasprzak  
From: Joel Selekof *JAS*  
Re: HTP data tape for NSSDC

A tape has been created for NSSDC (and a duplicate for us) containing HTP high resolution energetic ion data for orbits 1-3681. The tape is 6250bpi, ascii records, each record has length of 97 bytes, blocked at 100 records per block (9700 bytes per block).

The tape consists of 8 files:

<u>file</u>	<u>orbit</u>
1	1 - 500
2	501 - 1000
3	1001 - 1500
4	1501 - 2000
5	2001 - 2500
6	2501 - 3000
7	3001 - 3500
8	3501 - 3681

Attached is a listing of the first 3 blocks of file 1. Also attached is a sample program for reading the data.

YYYYDD	UT(MS)	ORBIT	MS	F	DENSITY	FLUX	AZ.	ANG	PHASE	ERROR	ANGATK	WP	DIR	WP	XY	B
(17,19,15,13,1X,A1,1P2E9.2,0P5F7.1,1P2E9.2)																
0	0	0	0	0	1.00E+38	1.00E+38	999.0	999.0	999.0	999.0	999.0	999.0	999.0	1.00E+38	1.00E+38	
1978339	54427498	1	18	D	1.90E+00	4.17E+06	999.0	999.0	999.0	999.0	-30.5	999.0	999.0	1.00E+38	1.00E+38	
1978339	54430152	1	18	D	2.55E+00	5.60E+06	999.0	999.0	999.0	999.0	10.8	999.0	999.0	1.00E+38	1.00E+38	
1978339	54432808	1	18	D	4.76E-01	1.05E+06	999.0	999.0	999.0	999.0	44.6	999.0	999.0	1.00E+38	1.00E+38	
1978339	54435464	1	18	D	2.95E+00	6.49E+06	999.0	999.0	999.0	999.0	-58.9	999.0	999.0	1.00E+38	1.00E+38	
1978339	54432508	1	18	A	1.93E+00	4.23E+06	130.2	3.8	6.5	999.0	-3.8	3.38E+02	3.81E+00			
1978339	54438164	1	18	D	3.41E-01	7.49E+05	999.0	999.0	999.0	999.0	-45.0	999.0	999.0	1.00E+38	1.00E+38	
1978339	54440920	1	18	D	8.09E-01	1.78E+06	999.0	999.0	999.0	999.0	-11.2	999.0	999.0	1.00E+38	1.00E+38	
1978339	54443478	1	18	D	3.54E-01	7.78E+05	999.0	999.0	999.0	999.0	28.4	999.0	999.0	1.00E+38	1.00E+38	
1978339	54446132	1	18	D	2.09E+00	4.59E+06	999.0	999.0	999.0	999.0	55.3	999.0	999.0	1.00E+38	1.00E+38	
1978339	54441560	1	18	A	7.68E-01	1.69E+06	123.0	3.9	6.0	999.0	-4.0	3.40E+02	3.87E+00			
1978339	54448832	1	18	D	3.88E-01	8.08E+05	999.0	999.0	999.0	999.0	-52.5	999.0	999.0	1.00E+38	1.00E+38	
1978339	54451488	1	18	D	4.48E-01	9.83E+05	999.0	999.0	999.0	999.0	-23.4	999.0	999.0	1.00E+38	1.00E+38	
1978339	54454144	1	18	D	4.79E-01	1.05E+06	999.0	999.0	999.0	999.0	16.9	999.0	999.0	1.00E+38	1.00E+38	
1978339	54458800	1	18	D	2.41E-01	5.30E+05	999.0	999.0	999.0	999.0	48.8	999.0	999.0	1.00E+38	1.00E+38	
1978339	54453488	1	18	A	5.05E-01	1.11E+06	125.1	3.8	7.3	999.0	-4.6	3.31E+02	3.81E+00			
1978339	54459496	1	18	D	8.85E-01	2.16E+06	999.0	999.0	999.0	999.0	-56.9	999.0	999.0	1.00E+38	1.00E+38	
1978339	54462152	1	18	D	1.16E-01	2.56E+05	999.0	999.0	999.0	999.0	-35.2	999.0	999.0	1.00E+38	1.00E+38	
1978339	54464808	1	18	D	7.86E-01	1.73E+06	999.0	999.0	999.0	999.0	5.1	999.0	999.0	1.00E+38	1.00E+38	
1978339	54467464	1	18	D	4.04E-01	6.88E+05	999.0	999.0	999.0	999.0	38.9	999.0	999.0	1.00E+38	1.00E+38	
1978339	54470164	1	18	D	1.03E+00	2.27E+06	999.0	999.0	999.0	999.0	57.4	999.0	999.0	1.00E+38	1.00E+38	
1978339	54465048	1	18	A	6.57E-01	1.44E+06	126.7	3.8	7.8	999.0	-5.4	3.07E+02	3.57E+00			
1978339	54472820	1	18	D	2.46E-01	5.40E+05	999.0	999.0	999.0	999.0	-46.1	999.0	999.0	1.00E+38	1.00E+38	
1978339	54475476	1	18	D	6.58E-01	1.45E+06	999.0	999.0	999.0	999.0	-13.4	999.0	999.0	1.00E+38	1.00E+38	
1978339	54478132	1	18	D	2.56E-01	5.63E+05	999.0	999.0	999.0	999.0	25.9	999.0	999.0	1.00E+38	1.00E+38	
1978339	54480832	1	18	D	1.18E+00	2.61E+06	999.0	999.0	999.0	999.0	53.2	999.0	999.0	1.00E+38	1.00E+38	
1978339	54476644	1	18	A	5.19E-01	1.14E+06	125.3	3.1	11.1	999.0	-6.5	2.63E+02	3.10E+00			
1978339	54483488	1	18	D	1.32E-01	2.89E+05	999.0	999.0	999.0	999.0	-54.6	999.0	999.0	1.00E+38	1.00E+38	
1978339	54488144	1	18	D	5.14E-02	1.13E+05	999.0	999.0	999.0	999.0	-29.9	999.0	999.0	1.00E+38	1.00E+38	
1978339	54488800	1	18	D	1.20E-01	2.63E+05	999.0	999.0	999.0	999.0	8.8	999.0	999.0	1.00E+38	1.00E+38	
1978339	54491488	1	18	D	5.62E-02	1.23E+05	999.0	999.0	999.0	999.0	42.8	999.0	999.0	1.00E+38	1.00E+38	
1978339	54494152	1	18	D	1.55E-01	3.40E+05	999.0	999.0	999.0	999.0	-56.7	999.0	999.0	1.00E+38	1.00E+38	
1978339	54488348	1	18	A	1.10E-01	2.41E+05	117.9	2.2	16.2	999.0	-7.9	1.81E+02	2.15E+00			
1978339	54531484	1	18	D	3.76E-02	8.26E+04	999.0	999.0	999.0	999.0	-34.3	999.0	999.0	1.00E+38	1.00E+38	
1978339	54534164	1	18	D	3.35E-02	7.36E+04	999.0	999.0	999.0	999.0	2.9	999.0	999.0	1.00E+38	1.00E+38	
1978339	54536820	1	18	D	4.07E-02	8.94E+04	999.0	999.0	999.0	999.0	37.0	999.0	999.0	1.00E+38	1.00E+38	
1978339	54535996	1	18	A	3.55E-02	7.79E+04	141.6	0.7	10.6	999.0	-11.5	5.66E+01	7.08E-01			
1978339	54542132	1	18	D	3.30E-02	7.24E+04	999.0	999.0	999.0	999.0	-43.1	999.0	999.0	1.00E+38	1.00E+38	
1978339	54544832	1	18	D	3.57E-02	7.84E+04	999.0	999.0	999.0	999.0	-10.3	999.0	999.0	1.00E+38	1.00E+38	
1978339	54547488	1	18	D	5.14E-02	1.13E+05	999.0	999.0	999.0	999.0	26.5	999.0	999.0	1.00E+38	1.00E+38	
1978339	54550144	1	18	D	4.94E-02	1.09E+05	999.0	999.0	999.0	999.0	51.4	999.0	999.0	1.00E+38	1.00E+38	
1978339	54546028	1	18	A	4.49E-02	9.86E+04	144.9	1.2	7.0	999.0	-11.8	9.19E+01	1.18E+00			
1978339	54830138	1	18	D	4.30E-02	9.44E+04	999.0	999.0	999.0	999.0	42.2	999.0	999.0	1.00E+38	1.00E+38	
1978339	54832838	1	18	D	9.05E-02	1.99E+05	999.0	999.0	999.0	999.0	-43.9	999.0	999.0	1.00E+38	1.00E+38	
1978339	54834128	1	18	A	5.68E-02	1.25E+05	128.5	0.5	73.1	999.0	-34.8	2.93E+01	5.21E-01			
1978339	54838148	1	18	D	1.66E-02	3.65E+04	999.0	999.0	999.0	999.0	22.2	999.0	999.0	1.00E+38	1.00E+38	
1978339	54840804	1	18	D	4.47E-02	9.83E+04	999.0	999.0	999.0	999.0	42.8	999.0	999.0	1.00E+38	1.00E+38	
1978339	54843500	1	18	D	9.01E-02	1.98E+05	999.0	999.0	999.0	999.0	-43.0	999.0	999.0	1.00E+38	1.00E+38	
1978339	54843128	1	18	A	6.60E-02	1.45E+05	161.0	1.7	20.9	999.0	-34.8	9.56E+01	1.72E+00			
1978339	54846158	1	18	D	4.12E-02	9.05E+04	999.0	999.0	999.0	999.0	-31.5	999.0	999.0	1.00E+38	1.00E+38	
1978339	54848812	1	18	D	6.94E-02	1.52E+05	999.0	999.0	999.0	999.0	-7.7	999.0	999.0	1.00E+38	1.00E+38	
1978339	54851488	1	18	D	1.85E-02	4.07E+04	999.0	999.0	999.0	999.0	28.6	999.0	999.0	1.00E+38	1.00E+38	
1978339	54854168	1	18	D	3.88E-02	8.07E+04	999.0	999.0	999.0	999.0	45.0	999.0	999.0	1.00E+38	1.00E+38	

C READS 3 BLOCKS OF DATA FROM NSSDC TAPE.

C J SELEKOF 3/90

C

LOGICAL\*1 BLOCK(9700),REC(97)  
DATA NBLK /0/  
TYPE \*, 'ENTER TAPE DRIVE NUMBER'  
ACCEPT \*, LDRV  
CALL T\_RWND(LDRV)  
CALL T\_WAIT(LDRV,NS,NB)  
TYPE \*, 'HOW MANY FILES TO SKIP?'  
ACCEPT \*, NSKIP  
IF(NSKIP.EQ.0) GO TO 10  
CALL T\_SKPF(LDRV,NSKIP)

C

C READ IN A BLOCK OF DATA (100 RECS) OFF THE TAPE AND SEPARATE  
C INTO RECORDS.

C

10 NBLK=NBLK+1  
IF(NBLK.GT.3) GO TO 900  
WRITE(5,500) NBLK  
500 FORMAT(' READING BLOCK',I4)  
CALL T\_READ(LDRV,BLOCK,9700)  
CALL T\_WAIT(LDRV,NS,NB)  
IF(NS.EQ.1) GO TO 900  
N=0  
DO 100 I=1,100  
DO 110 J=1,97  
N=N+1  
REC(J)=BLOCK(N)  
110 CONTINUE  
WRITE(4,50) REC  
50 FORMAT(1X,97A1)  
100 CONTINUE

C

C GO TO NEXT BLOCK

C

GO TO 10

C

900 CALL T\_RWND(LDRV)  
CALL T\_WAIT(LDRV,NS,NB)  
STOP  
END





REQ. AGENT

RLR

RAND NO.

ACQ. AGENT

DKB

PIONEER VENUS-1

LOW & HIGH RESOL. NEUT. DENSITIES

78-051A-11G

PSPA-00392

This data set consists of 1 tape. The tape is 1600 bpi, 9-track, multifiled, ascii, and created on the IBM 360. The D and C numbers, time spans, and number of files are as follows:

<u>D#</u>	<u>C#</u>	<u>FILES</u>	<u>TIME SPANS</u>
D-85845	C-28935	02	12/07/78 - 09/05/80

Pioneer Venus Orbiter Neutral Mass Spectrometer  
High Resolution Neutral Density Data Set  
(13-DEC-1988)

1. The Orbiter Neutral Mass Spectrometer (ONMS)

The instrument was designed to determine the composition of the neutral thermosphere/exosphere of Venus. The term composition includes both the type of neutral gases present and their quantitative amount. The measurements begin at the orbit's periapsis altitude and extend to a limiting altitude at which the ambient signal becomes comparable to the the gas background and/or detector measurement threshold. The neutral composition includes helium, atomic nitrogen, atomic oxygen, molecular nitrogen, carbon monoxide and carbon dioxide.

The Pioneer Venus Project, its aims and early scientific results have been described in a special issue of Journal of Geophysical Research (1980). The instruments and spacecraft have been described in a special issue of the IEEE Transactions on Geoscience and Remote Sensing (1980). A more complete survey of results are contained in the book VENUS (Hunten et al., 1983). The reference section contains a list of relevant ONMS publications and some of these have been reproduced here for convenience. The instrument has been described in Niemann et al. (1980a) and the basic data reduction in Niemann et al. (1980b).

The spacecraft orbit is nearly polar (105.6 degrees inclination) with periapsis near the equator (17 degrees north celestial latitude) and has an average period of 24.03 hours. The local time of periapsis increases 1.6 degrees/day (or orbit) so that it takes 224.7 days to sample one complete diurnal cycle (dayside, evening terminator, nightside, and morning terminator). For the first 600 orbits the altitude of periapsis varied from 142 km to 250 km. After this period the periapsis altitude was no longer controlled and rose in response to the solar gravitational perturbations. The spacecraft spins with a nominal period of 12 seconds about an axis which points toward the south ecliptic pole. The ONMS instrument is mounted at an angle of 26.5 degrees with respect to the spin axis.

## 2. Data

The source of the data and their corrections are summarized below:

<u>SPECIES</u>	<u>M/E USED</u>	<u>COMMENTS</u>
He	4	
N	30	Surface recombined N and O
O	32	Surface recombined O to O <sub>2</sub> ; corrected for CO <sub>2</sub> fragmentation corrected for estimated surface recombination of O to CO <sub>2</sub> *
N <sub>2</sub> , CO	14, 28	m/e 14 corrected for NO, CO and CO <sub>2</sub> fragmentation; m/e 28 corrected for CO <sub>2</sub> fragmentation
CO <sub>2</sub>	44	Corrected for surface recombination of O to CO <sub>2</sub> *

\* the correction is based on matching scale height temperatures of O and CO<sub>2</sub>.

The data are from the nonretarding potential mode of the instrument. Data from the retarding mode are consistent with those obtained from the nonretarding mode and have not been included. The data set does not include the factor of 1.6 increase in density needed to maintain compatibility with other data sets as discussed by Hedin et al. (1983). Two data sets are provided: high resolution (HIRES), every point, composition; and low resolution (LORES), 12 second sampled, composition. The LORES data set represents the best estimated composition data and is derived from the HIRES data set. The orbit range covered is 1 to 640 for both data sets.

Several criteria were invoked when inserting data for a given orbit: orbit and attitude parameters must exist (project supplied); the spacecraft format and bit rate must be appropriate for acquisition of data by the ONMS; and the command sequence for the instrument must be appropriate for useful determination of atmospheric composition. Cases where useful composition cannot be determined include special test modes (e.g. retarding potential sweeps, filament off) and 1/8 unit amu sweep modes. In addition composition for the LORES data set cannot be easily determined for unit amu sweep mode. The ONMS was not operational for every orbit nor is every orbit complete due to data gaps introduced by use of telemetry formats for which the ONMS has no instrument output.

Useful composition data are gathered from the lowest periapsis altitude to a maximum altitude generally around 250

km (about 300 km for He). The actual maximum altitude depends on the accumulated surface gas buildup acquired from previous orbits which creates a gas background. The gas background was estimated from high altitude averages of the data and for all species, except helium, an inbound signal/background ratio of 2 and an outbound signal/background ratio of 4 were used as cutoff values. In some cases energetic ions (e.g. Kasprzak et al., 1982) were observed at low altitudes (e.g. below 300 km for orbit 219) and these were removed when visually detected. Some problems have been observed in the high altitude data very near cutoff, particularly for outbound N<sub>2</sub>. Several data points were never removed and appear higher than the expected extrapolation of the data to that time.

Residual spin modulation which had not been completely removed is evident in the processed data. The source of the spin residuals are the gas/surface adsorption/desorption effects which were not removed from the data and a noncosine behavior for the response of the ion source density with angle of attack. Another feature observed occasionally at large angles of attack (>40 degrees) is a reduction of the data when compared to data at lower angles of attack. This has been determined to be due to antenna shadowing; that is, the ONMS geometric view cone "sees" the spacecraft antenna at extreme angles of attack. Occasionally near minimum angle of attack (<10 degrees) enhanced data points are observed for m/e=4 (He channel) which are apparently high energy ions/neutrals travelling along the tube axis and being detected. The more extreme points in either of these two cases have been mass flagged.

The data time spacing depends on the spacecraft bit rate and format, and the particular instrument commands executed. Usually programmed mass format was used but occasionally unit amu and 1/8 amu sweeps were implemented. Several orbits switched from low electron energy to high electron energy and as a result there may be a discontinuity at the transition point. The 1/8 amu sweep data have not been included.

Atomic nitrogen was measured routinely only after orbit 190.

Orbits 1-19 generally do not have reliable relative composition due to the fact that gas-surface processes in the ion source had not stabilized. This affects all surface reactive species except He.

Isolated (one or two points per several spin cycles) high resolution data points are occasionally observed and they should be regarded as erroneous points which are more likely wrong than right.

The error associated with the points is more an

indication of data quality than of absolute uncertainty. It contains the statistical error of the data determined for the principle m/e used for the species from the detector signal plus the errors coming from any other species used to correct the data. It also contains a contribution which is proportional to the background/signal ratio. The total relative error is at least an additional 5-10% above this value.

The LORES data set is a companion data set created from the HIRES data and is generally more restricted since it requires all data to be available for the needed corrections in order to output a particular data point.

No spacecraft positional parameters have been included in the data sets. These can be obtained from the SEDR data submitted separately by the Project.

As of this date no known malfunction of the ONMS has been encountered.

① Spacecraft orbit parameters can be also obtained with the orbit programs and data files included in data set 78-051A-00I

### 3. HIRES Data tape

The data tape has the following characteristics:

TYPE:	9-TRACK
DENSITY:	1600 bpi
PHYSICAL BLOCK SIZE:	4800 bytes
LOGICAL RECORD SIZE:	60 bytes
LOGICAL RECORDS/PHYSICAL BLOCK:	80
FORMAT:	ASCII
LABEL:	NONE
FILES:	1

The first 3 records describe how to read and interpret the remaining portion of the tape. The following descriptions assume a FORTRAN code for reading the tape. The tape contains orbits in increasing orbit number order with data for each orbit in increasing time order.

#### 3.1 Record 1

This record contains the variable field names. It is read as:

```
CHARACTER*60 DESC
READ(UNIT, '(A)') DESC
```

The fields are:

YYYYDDD	YYYY=4 digit year (e.g. 1979) DDD=3 digit day of year (e.g. 053)
UT(ms)	Universal time in ms
ORBIT	Orbit number
MS	Mass number - 4 for He            28 for N2 14 for N            29 for CO 16 for O            44 for CO2
F	Flag - F for fully corrected P for preliminary (not fully corrected) M for mass flagged (problem point; probably wrong) N for final density negative (only preliminary density given)
ODENS	Preliminary density (part/cc)
FDENS	Final corrected density (part/cc)
ANGATK	Angle of attack (degrees)
PCERR	% error in density -1 if error >12%

Notes:

- 1) For CO2 both ODENS and FDENS are given since the final correction to this species depends on a model:  

$$\text{New CO2 density} = \text{Old CO2 density} - 0.019 \times \text{Old O density}$$

$$\text{New O density} = \text{Old O density} + 0.019 \times \text{Old O density}$$
 Only the New O density is given.
- 2) Mass flagged points are usually points that fall excessively beyond range of the main body of the data. They may be wild points, points with wrong mass designations or simply wrong for other reasons.
- 3) The best estimate of the density is to be found in the F data.
- 4) Data with errors greater than about 30% should be considered unreliable.
- 5) The angle of attack is included to help sort out low points due to antenna shadowing (all species) which occurs beyond 40 degrees and high ram points seen in He within 10 degrees angle of attack. Some of these points have already been mass flagged. In general, it would be best to not include data in these regions.

### 3.2 Record 2

This record contains FORTRAN format for the remaining records. It is read as follows:

```
CHARACTER*60 FMT
READ(UNIT,'(A)') FMT
```

### 3.3 Record 3

This record contains the fill values for the fields described in records 1 and 2. It is read as follows:

```
INTEGER*4 F1,F2,F3,F4
CHARACTER*1 F5
REAL F6,F7,F8,F9
READ(UNIT,FMT) F1,F2,F3,F4,F5,F6,F7,F8,F9
```

### 3.4 Record 4...

The main data records with one record per point. They are read as follows:

```
INTEGER*4 YYYYDDD,UT,ORBIT,MASS
CHARACTER*1 F
REAL ODENS,FDENS,ANGATK,PCERR
READ(UNIT,FMT,END=?) YYYYDDD,UT,ORBIT,MASS,F,
ODENS,FDENS,ANGATK,PCERR
```

4. LORES data

This data is a low time resolution, representative sample, of the high resolution data. It is constructed at designated times which have been supplied by the Project. Data with errors greater than 30% are not included nor are data with angles of attack greater than 40 degrees. An absolute altitude cutoff of 250 km was used for all species except for He for which 350 km was used.

Each representative data point is constructed using an exponentially weighted average of the data over a 24 second interval centered at the sample point time. Corrections to the number densities of CO2 and O for surface reactions were made at this time based on empirical model results. A minimum of 3 data points per species and all data available for corrections are required to be present in order for a sample point to be output. The total number density and total mass density are computed if all major species (CO2, CO, N2, and O) are present. The data spacing is nominally 12 seconds except for the -12, 0, 12 time tags. Although time tags from -1800 to 1800 seconds are generated only those data records are output for which at least one species has a valid value for that time tag.

The variable names used for the species:

<u>ITEM</u>	<u>NAME</u>	<u>DESCRIPTION</u>	<u>UNITS</u>
1	DHE	Number density of He	part/cc
2	DN	Number density of N	part/cc
3	DO	Number density of O	part/cc
4	DN2	Number density of N2	part/cc
5	DCO	Number density of CO	part/cc
6	DCO2	Number density of CO2	part/cc
7	DRHO	Total mass density	g/cc
8	DTOT	Total number density	part/cc

Additional fields included:

<u>NAME</u>	<u>DESCRIPTION</u>
YYYYDDD	YYYY=4 digit year DDD=3 digit day of year
UT	Universal time (ms)
ORBIT	Orbit number
TIMTAG	Nominal time tag assigned by project

The data tape has the following characteristics:

TYPE:	9-TRACK
DENSITY:	1600 bpi
PHYSICAL BLOCK SIZE:	1000 bytes
LOGICAL RECORD SIZE:	100 bytes
LOGICAL RECORDS/PHYSICAL BLOCK:	10
FORMAT:	ASCII

LABEL: NONE  
FILES: 1

The structure of the tape corresponds to the UADS structure defined by the Project and described in an accompanying document. The first 3 records describe how to read and interpret the remaining portion of the tape. The following descriptions assume FORTRAN code for reading the tape.

The tape contains the orbits in increasing orbit number order with data in increasing time order within each orbit.

#### 4.1 Record 1

This record contains the variable field names for each record excluding the first 4 fields which are the YYYYDDD, UT(ms), orbit number and nominal time tag. It is read as:

```
PARAMETER (NVAR=8)
CHARACTER*4 NAMES(NVAR)
READ(UNIT, '(I3,<NVAR>(1X,A4))') NV,(NAMES(I),I=1,NV)
```

The 8 field names correspond to the 8 items previously mentioned.

#### 4.2 Record 2

This record contains the FORTRAN format for the remaining records and includes the 4 leading fields and the 8 remaining fields. It is read as:

```
PARAMETER (NBYT=100)
BYTE FORMAT(NBYT)
READ(UNIT, '(<NBYT>A1)') FORMAT
```

#### 4.3 Record 3

This record contains the fill values for the fields described. It is read as:

```
PARAMETER (NV=8,NVAR=4+NV)
INTEGER*4 F1,F2
INTEGER*2 F3,F4
REAL*4 F5,F6,F7,F8,F9,F10,F11,F12
READ(UNIT,FORMAT,END=?) F1,F2,F3,F4,F5,F6,F7,F8,F9,
F10,F11,F12
```

#### 4.4 Record 4...

The main data records with one record per sample time point, maximum of 8 species per line:

```
PARAMETER (NV=8,NVAR=4+NV)
```

119-9

↑

```
INTEGER*4 YYYYDDD,UT
INTEGER*2 ORBIT,TIMTAG
REAL*4 DATA(NV)
READ(UNIT,FORMAT) YYYYDDD,UT,ORBIT,TIMTAG,
      (DATA(I),I=1,NV)
```

↑

↑

5. Auxiliary documents

The following documents have been included for further reference:

- a) Reproductions of relevant publications
- b) Summary list of orbits not included and list of possible anomalies for orbits included
- c) Plots illustrating possible problems in the data
- d) Proposed NSSDC low frequency data format from the Project
- e) Dump of first few records of each data tape

Any problems/questions should be directed to:

H.B. Niemann  
Code 615  
NASA/Goddard Space Flight Center  
Greenbelt MD 20771  
(301)-286-8705

W.T. Kasprzak  
Code 615.1  
NASA/Goddard Space Flight Center  
Greenbelt MD 20771  
(301)-286-8253

5. References

IEEE Transactions on Geoscience and Remote Sensing, GE-18, 1-130, 1980.

Journal of Geophysical Research, 85, 7575-8337, 1980.

Hedin, A.E., H.B. Niemann, and W.T. Kasprzak, Global empirical model of the Venus thermosphere, J. Geophys. Res., 88, 73-83, 1983.

Hunten, D.M., L. Colin, T.M. Donahue, and V.I. Moroz (ed.) VENUS, The University of Arizona Press, Tucson, Arizona, 1983.

Kasprzak, W.T., A.E. Hedin, H.B. Niemann, and N.W. Spencer, Atomic Nitrogen in the upper atmosphere of Venus, Geophys. Res. Lett., 7, 106-108, 1980.

Kasprzak, W.T., H.A. Taylor, L.H. Brace, and H.B. Niemann, Observations of energetic ions near the ionopause, Planet. Sp. Sci., 30, 1107-1115, 1982.

Kasprzak, W.T., A.E. Hedin, H.G. Mayr, and H.B. Niemann, Wavelike perturbations observed in the neutral thermosphere of Venus, J. Geophys. Res., 93, 11237-11245, 1988.

Keating, G.M., J.L. Bertaux, S.W. Bougher, T.E. Cravens, R.E. Dickenson, A.E. Hedin, V.A. Krasnopolsky, A.F. Nagy, J.Y. Nicholson, III, L.J. Paxton, and U. von Zahn, Models of Venus neutral upper atmosphere: Structure and composition, Adv. Sp. Res., 5, 117-171, 1985.

Niemann, H.B., R.E. Hartle, W.T. Kasprzak, N.W. Spencer, D.M. Hunten, and G.R. Carignan, Venus upper atmosphere neutral composition: Preliminary results from the Pioneer Venus Orbiter, Science, 203, 770-772, 1979a.

Niemann, H.B., R.E. Hartle, A.E. Hedin, W.T. Kasprzak, N.W. Spencer, D.M. Hunten, and G.R. Carignan, Venus upper atmosphere, neutral gas composition: First observations of the diurnal variations, Science, 205, 54-56, 1979b.

Niemann, H.B., J.R. Booth, J.E. Cooley, R.E. Hartle, W.T. Kasprzak, N.W. Spencer, S.H. Way, D.M. Hunten, and G.R. Carignan, Pioneer Venus Orbiter neutral gas mass spectrometer experiment, IEEE Trans. Geosci. Remote Sens., GE-18, 60-65, 1980a.

Niemann, H.B., W.T. Kasprzak, A.E. Hedin, D.M. Hunten, and N.W. Spencer, Mass Spectrometric measurements of the gas composition of the thermosphere and exosphere of Venus, J. Geophys. Res., 85, 7817-7827, 1980b.

von Zahn, U., S. Kumar, H. Niemann, and R. Prinn, Composition  
the Venus atmosphere, in VENUS, edited by D.M. Hunten,  
L. Colin, T.M. Donahue, and V.I. Moroz, pp. 299-430,  
University of Arizona Press, Tucson, Ariz., 1983.

COMMENTS ON ORBITS NOT ON THE NSSDC ONMS NEUTRAL ATMOSPHERE TAPE AND OTHER SPECIAL NOTES

The following is a list of orbits not contained in the data tape. Generally speaking the term 'NO DATA AVAILABLE FOR THIS ORBIT' means no telemetry tape was received or that, for this orbit, the telemetry format did not contain ONMS words. The term 'NO DATA AVAILABLE FOR ONMS NEAR PERIAPSIS' generally indicates that the telemetry format near periapsis did not contain ONMS words or that there was a loss of telemetry data; data were received at higher altitudes but well beyond the range of the sensible neutral atmosphere. 1/8 amu sweep mode has a very low data rate and it is very difficult to fully correct the composition so that where that mode is used there is no data. Engineering tests do not yield any useful atmospheric densities.

ORBIT COMMENT

- \*\* 1 PERIAPSIS ALTITUDE TOO HIGH FOR ATMOSPHERE DETECTION
- 2 RPA SWEEP MODE TEST-NO DATA AVAILABLE
- 2-19 GAS SURFACE REACTIONS FOR O AND CO2 NOT STABILIZED
- 8 RPA SWEEP MODE TEST-NO DATA AVAILABLE
- 10 UNIT SWEEP
- 15 NO DATA AVAILABLE FOR ONMS NEAR PERIAPSIS
- 23 UNIT SWEEP
- 24 RPA SWEEP MODE TEST-NO DATA AVAILABLE
- 31 1/8 SWEEP-NO DATA AVAILABLE
- 32 NO DATA AVAILABLE FOR ONMS NEAR PERIAPSIS
- 34 NO DATA AVAILABLE FOR ONMS NEAR PERIAPSIS
- 40 1/8 UNIT SWEEP-NO DATA AVAILABLE
- 47 NO DATA AVAILABLE FOR ONMS NEAR PERIAPSIS
- 48 RPA MODE SWEEP MODE TEST
- 55 NO DATA AVAILABLE FOR ONMS NEAR PERIAPSIS
- 56 NO DATA AVAILABLE FOR ONMS NEAR PERIAPSIS
- 58 UNIT SWEEP
- 63 LOW ELECTRON ENERGY PERIAPSIS TIME < 60 SEC
- 64 NO DATA AVAILABLE FOR ONMS NEAR PERIAPSIS
- 65 NO DATA AVAILABLE FOR ONMS NEAR PERIAPSIS
- 69 NO DATA AVAILABLE FOR ONMS NEAR PERIAPSIS
- 71 NO DATA AVAILABLE FOR ONMS NEAR PERIAPSIS
- 72 NO DATA AVAILABLE FOR ONMS NEAR PERIAPSIS
- 78 LOW ELECTON ENERGY
- 80 NO DATA AVAILABLE FOR ONMS NEAR PERIAPSIS
- 81 UNIT SWEEP
- 83 UNIT SWEEP
- 86 LOW ELECTRON ENERGY PERIAPSIS TIME < 60 SEC
- 88 NO DATA AVAILABLE FOR ONMS NEAR PERIAPSIS
- 89 NO DATA FOR THIS ORBIT
- 91 UNIT SWEEP
- 93 UNIT SWEEP
- 94 LOW ELECTRON ENERGY PERIAPSIS TIME < 60 SEC
- 96 NO DATA AVAILABLE FOR ONMS NEAR PERIAPSIS
- 99 UNIT SWEEP
- 100 UNIT SWEEP
- 102 LOW ELECTRON ENERGY PERIAPSIS TIME < 60 SEC
- 104 UNIT SWEEP

- 107 UNIT SWEEP
- 110 UNIT SWEEP
- 112 UNIT SWEEP
- 113 UNIT SWEEP
- 118 LOW ELECTRON ENERGY PERIAPSIS TIME < 60 SEC
- 120 UNIT SWEEP
- 123 UNIT SWEEP
- 125 RPA MODE SWEEP MODE TEST
- 126 LOW ELECTRON ENERGY PERIAPSIS TIME < 60 SEC
- 128 UNIT SWEEP
- 131 UNIT SWEEP
- 136 UNIT SWEEP
- 139 UNIT SWEEP
- 142 MASS 44 ONLY
- 144 UNIT SWEEP
- 147 UNIT SWEEP
- 150 LOW ELECTRON ENERGY PERIAPSIS TIME < 60 SEC
- 152 UNIT SWEEP
- 155 UNIT SWEEP
- 156 ENGINEERING TEST
- 158 LOW ELECTRON ENERGY PERIAPSIS TIME < 60 SEC
- 160 LOW ELECTRON ENERGY PERIAPSIS TIME < 60 SEC
- 163 MASS 44 ONLY
- 166 LOW ELECTRON ENERGY PERIAPSIS TIME < 60 SEC
- 168 UNIT SWEEP
- 171 UNIT SWEEP
- 174 NO DATA AVAILABLE FOR ONMS NEAR PERIAPSIS
- 176 ENGINEERING TEST-NO DATA AVAILABLE
- 182 NO DATA AVAILABLE FOR ONMS NEAR PERIAPSIS
- 190 UNIT SWEEP
- 192 MASS 44 ONLY
- 193 ENGINEERING TEST-NO DATA AVAILABLE
- 196 NO DATA AVAILABLE NEAR PERIAPSIS
- 198 UNIT SWEEP
- 200 MASS 44 ONLY
- 201 UNIT SWEEP
- 206 UNIT SWEEP
- 217 NO DATA AVAILABLE FOR ONMS NEAR PERIAPSIS
- 225 NO DATA AVAILABLE FOR ONMS NEAR PERIAPSIS
- 233 NO DATA AVAILABLE FOR ONMS NEAR PERIAPSIS
- 241 NO DATA AVAILABLE FOR ONMS NEAR PERIAPSIS
- 243 1/8 UNIT SWEEP-NO DATA AVAILABLE
- 248 UNIT SWEEP
- 249 NO DATA AVAILABLE FOR THIS ORBIT
- 250 NO DATA AVAILABLE FOR THIS ORBIT
- 251 NO DATA AVAILABLE FOR ONMS NEAR PERIAPSIS
- \*\*252-281 ORBITER TURNED OFF DURING PIONEER-SATURN ENCOUNTER
- 282 NO DATA FOR THIS ORBIT
- 284 NO DATA FOR THIS ORBIT
- 286 NO DATA AVAILABLE FOR ONMS NEAR PERIAPSIS
- 290 ATTITUDE DATA NECESSARY FOR PROCESSING NOT AVAILABLE
- 293 NO DATA AVAILABLE FOR ONMS NEAR PERIAPSIS
- 294 NO DATA AVAILABLE FOR ONMS NEAR PERIAPSIS
- 296 UNIT SWEEP

297 UNIT SWEEP  
303 NO DATA AVAILABLE FOR ONMS NEAR PERIAPSIS  
310 UNIT SWEEP  
317 NO DATA AVAILABLE FOR ONMS NEAR PERIAPSIS  
321 NO DATA FOR THIS ORBIT  
326 NO DATA AVAILABLE FOR ONMS NEAR PERIAPSIS  
327 NO DATA AVAILABLE FOR ONMS NEAR PERIAPSIS  
330 NO DATA AVAILABLE FOR ONMS NEAR PERIAPSIS  
331 UNIT SWEEP  
336 NO DATA AVAILABLE FOR ONMS NEAR PERIAPSIS  
338 UNIT SWEEP  
339 COMMANDS NOT PROPERLY LOADED-NO DATA AVAILABLE  
342 NO DATA AVAILABLE FOR ONMS NEAR PERIAPSIS  
345 NO DATA AVAILABLE FOR ONMS NEAR PERIAPSIS  
346 LOW DATA RATE (PERC @256 BPS)  
353 UNIT SWEEP  
358 NO DATA AVAILABLE FOR ONMS NEAR PERIAPSIS  
359 NO DATA FOR THIS ORBIT  
360 UNIT SWEEP  
362 NO DATA AVAILABLE FOR ONMS NEAR PERIAPSIS  
364 NO DATA AVAILABLE FOR ONMS NEAR PERIAPSIS  
367 UNIT SWEEP  
374 UNIT SWEEP  
378 NO DATA AVAILABLE FOR ONMS NEAR PERIPASIS  
381 UNIT SWEEP  
388 UNIT SWEEP  
395 UNIT SWEEP  
397 QUESTIONABLE TEPOCH FOR DATA SAMPLE-NO LORES DATA  
398 NO DATA FOR THIS ORBIT  
402 UNIT SWEEP  
406 NO DATA FOR THIS ORBIT  
409 UNIT SWEEP  
416 UNIT SWEEP  
418 COMMANDS NOT PROPERLY LOADED-NO DATA AVAILABLE  
423 UNIT SWEEP  
430 UNIT SWEEP  
432 RPA SWEEP MODE TEST  
434 LOW ELECTRON ENERGY  
436 NO DATA FOR THIS ORBIT  
437 UNIT SWEEP  
438 ENGINEERING TEST-NO DATA AVAILABLE  
443 COMMANDS NOT PROPERLY LOADED-NO DATA AVAILABLE  
444 UNIT SWEEP  
451 UNIT SWEEP  
455 COMMANDS NOT PROPERLY LOADED-NO DATA AVAILABLE  
458 UNIT SWEEP  
465 UNIT SWEEP  
467 RPA MODE SWEEP TEST  
469 NO DATA AVAILABLE FOR ONMS NEAR PERIAPSIS  
470 1/8 UNIT SWEEP-NO DATA AVAILABLE  
471 LOW ELECTRON ENERGY  
472 UNIT SWEEP  
479 UNIT SWEEP  
484 ENGINEERING TEST-NO DATA AVAILABLE

486 UNIT SWEEP  
 492 UNIT SWEEP  
 499 UNIT SWEEP  
 501 RPA MODE SWEEP TEST  
 503 1/8 UNIT SWEEP-NO DATA AVAILABLE  
 505 LOW ELECTRON ENERGY  
 506 UNIT SWEEP  
 510 NO DATA AVAILABLE FOR ONMS NEAR PERIAPSIS  
 513 UNIT SWEEP  
 518 NO DATA FOR THIS ORBIT  
 520 UNIT SWEEP  
 527 UNIT SWEEP  
 534 UNIT SWEEP  
 536 NO DATA AVAILABLE FOR ONMS NEAR PERIAPSIS  
 538 1/8 UNIT SWEEP-NO DATA AVAILABLE  
 540 LOW ELECTRON ENERGY  
 541 UNIT SWEEP  
 542 NO DATA AVAILABLE FOR ONMS NEAR PERIAPSIS  
 548 UNIT SWEEP  
 553 ENGINEERING TEST-NO DATA AVAILABLE  
 555 UNIT SWEEP  
 562 UNIT SWEEP  
 565 1/8 UNIT SWEEP-NO DATA AVAILABLE  
 569 UNIT SWEEP

\*\*\*\*\*  
 NOTE: ORBITS 570-583 HAVE SPIN RATE 15 RPM, ORBITS 584-586 HAVE SPIN RATE 10 RPM; NORMAL SPIN RATE IS 5 RPM  
 \*\*\*\*\*

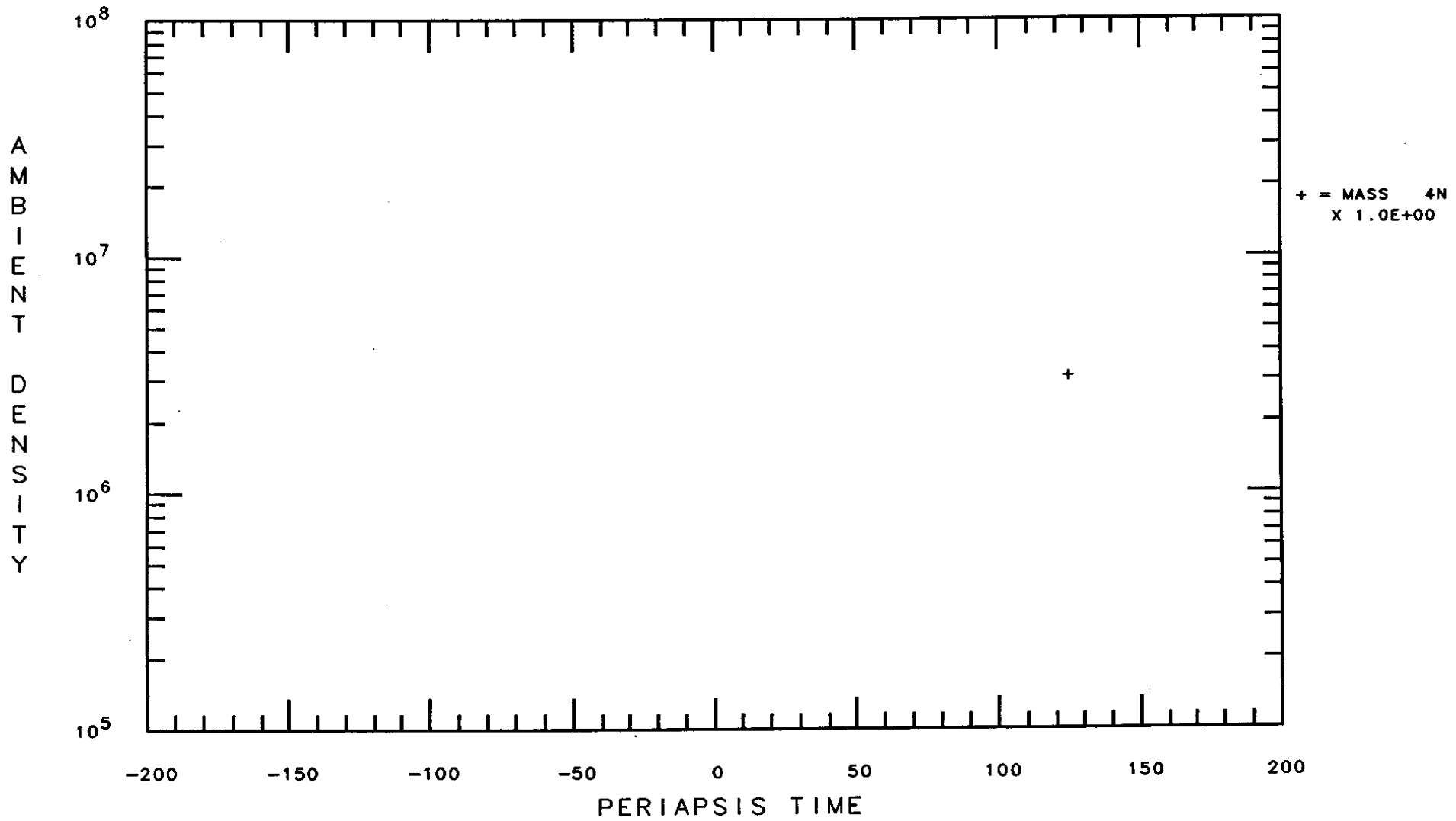
570 NO DATA AVAILABLE FOR ONMS NEAR PERIAPSIS  
 575 LOW ELECTRON ENERGY  
 576 UNIT SWEEP  
 583 UNIT SWEEP  
 588 ENGINEERING TEST-NO DATA AVAILABLE  
 590 UNIT SWEEP  
 597 UNIT SWEEP  
 600 1/8 UNIT SWEEP-NO DATA AVAILABLE

\*\*\*\*\*  
 NOTE: PERIAPSIS NO LONGER BEING CONTROLLED; AS IT RISES THE ATMOSPHERE SIGNAL APPROACHES THE LOWER LIMIT MEASUREMENT THRESHOLD OF ONMS; ORBIT 620 IT IS 254 KM;  
 \*\*\*\*\*

610 LOW ELECTRON ENERGY  
 611 UNIT SWEEP  
 618 UNIT SWEEP  
 621-626 DATA BELOW MEASUREMENT THRESHOLD  
 628-639 DATA BELOW MEASUREMENT THRESHOLD

# PV-ONMS DATA SUMMARY

NEW DATA



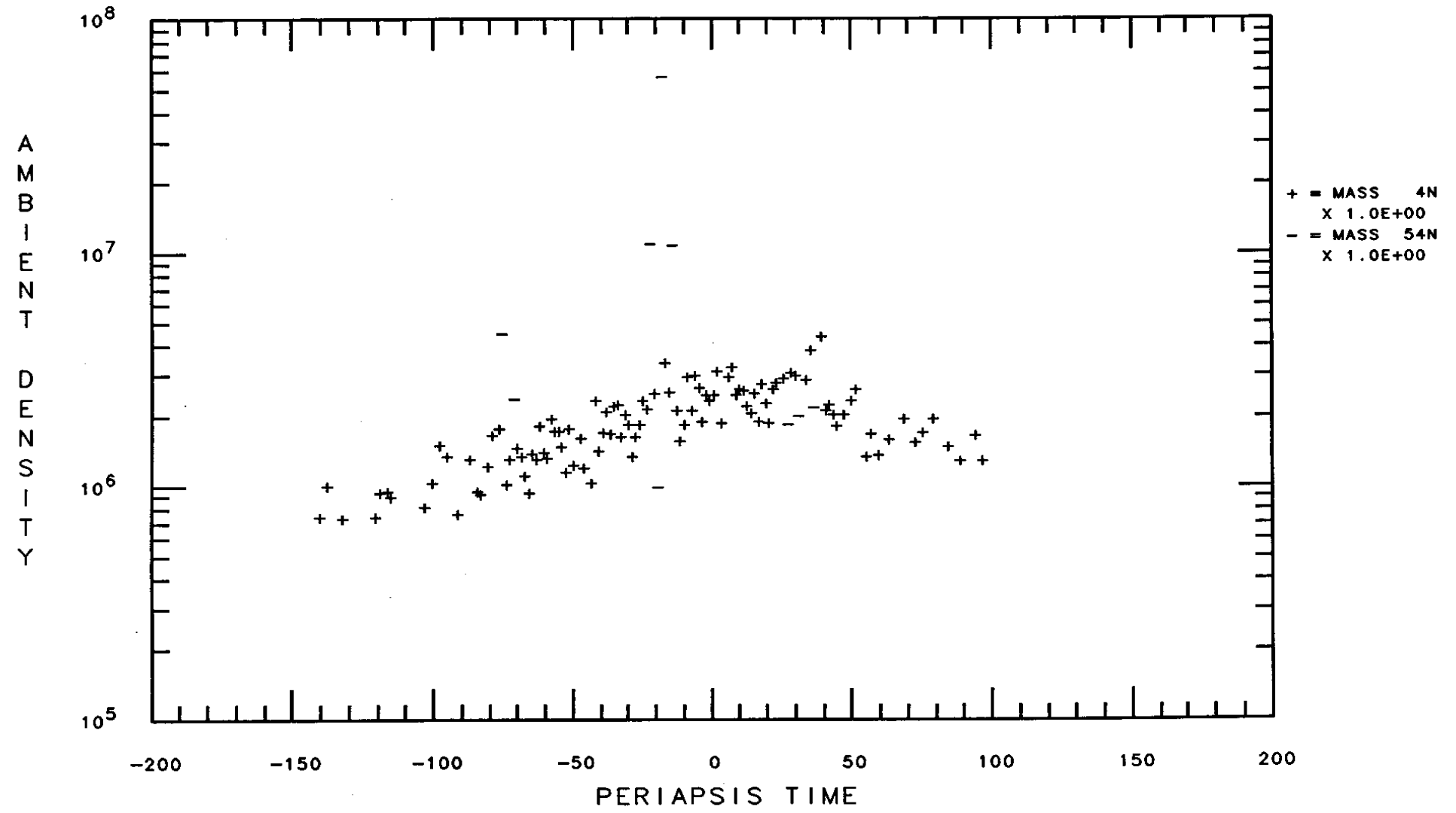
DATA SELECTION: ORBITS FROM 617. TO 617.

10:29:43  
08-DEC-88

# PV-ONMS DATA SUMMARY

- HIGH RAM POINTS FOR He  
ALL ANGLES OF ATTACK  
RAM POINTS MASS FLAGGED

NEW DATA



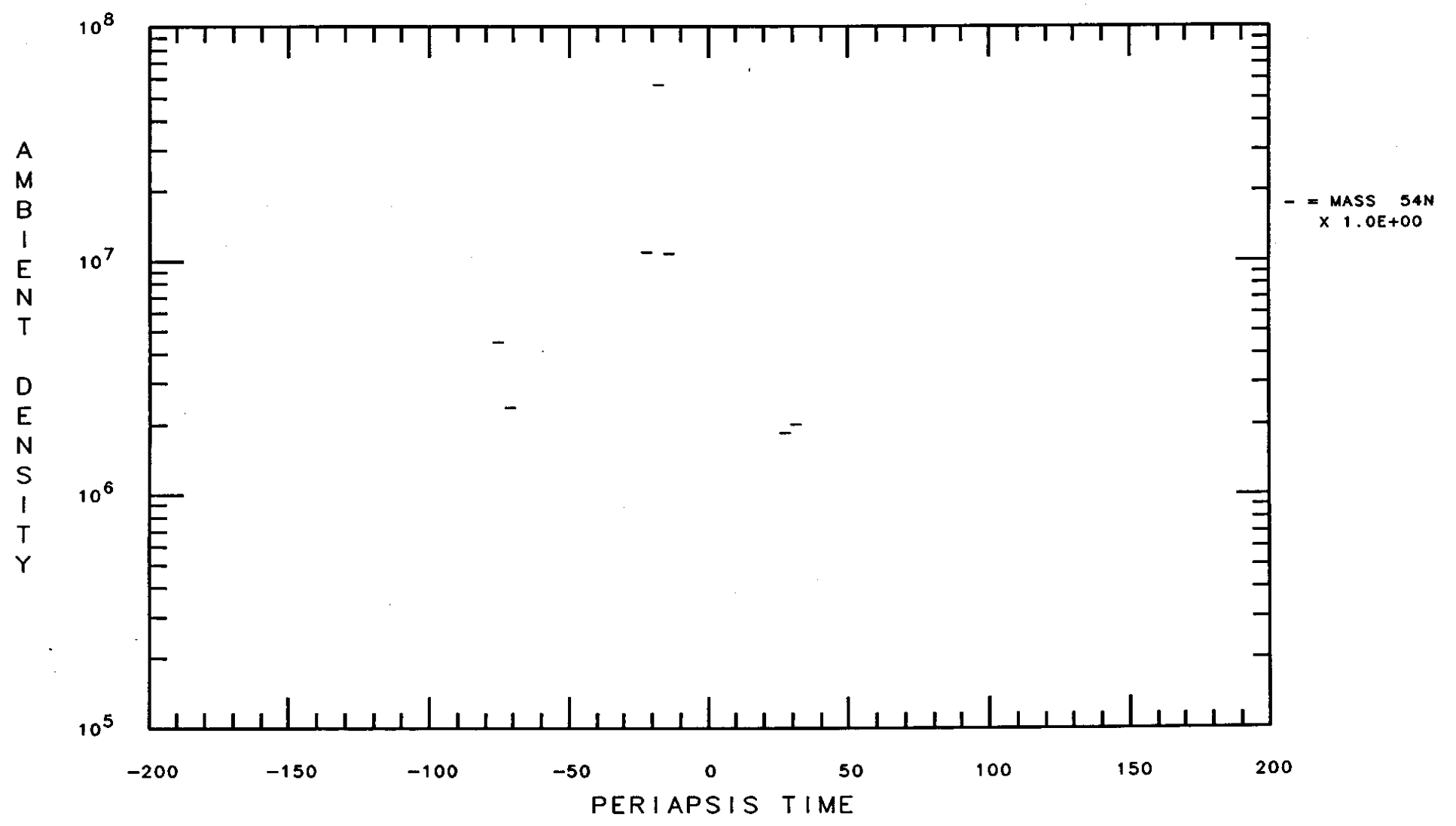
DATA SELECTION: ORBITS FROM 582. TO 582.

10:10:37  
08-DEC-88

# PV-ONMS DATA SUMMARY

- HIGH RAM POINTS FOR He  
ANGLE OF ATTACK < 10°

NEW DATA



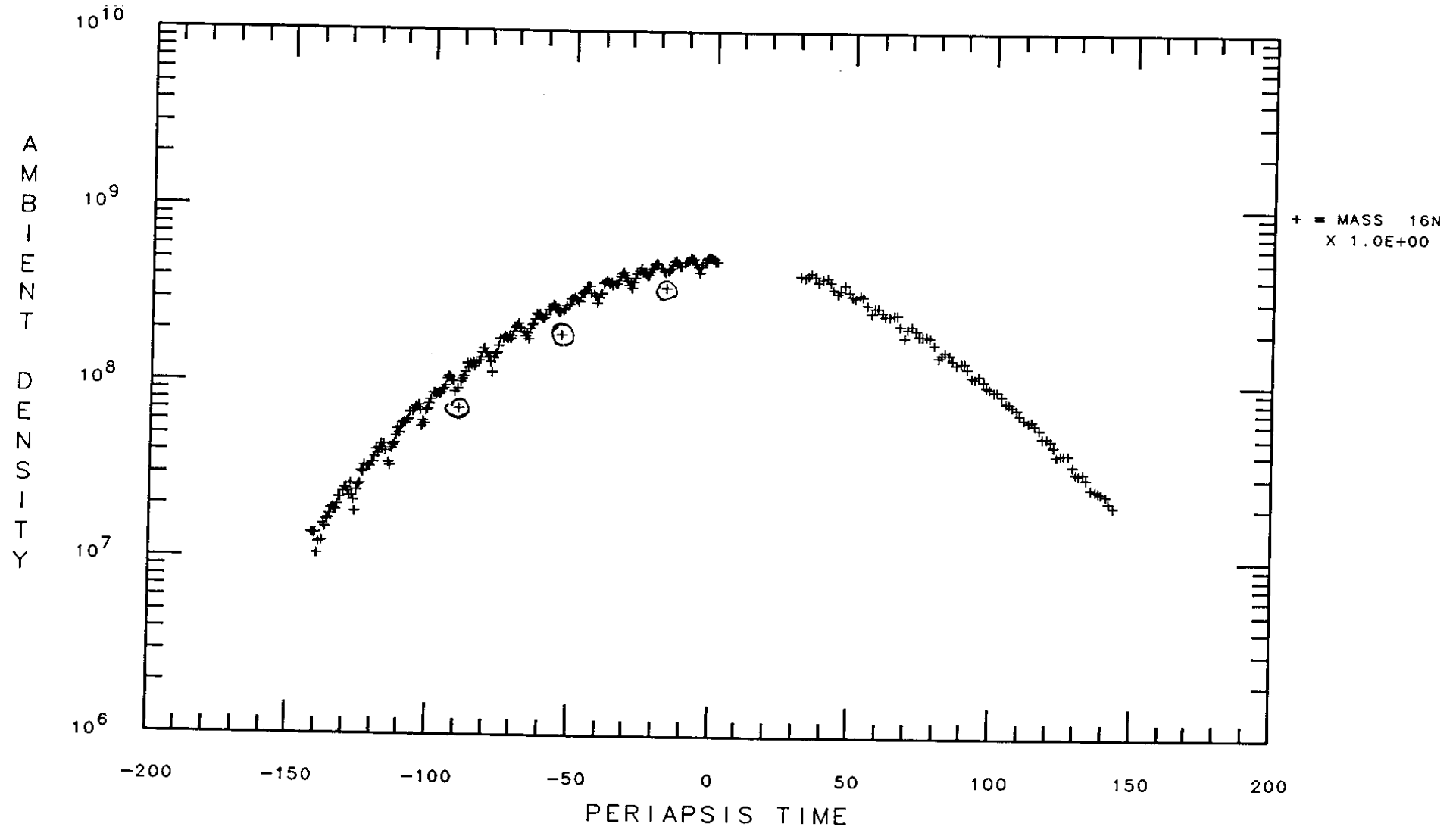
DATA SELECTION:    ORBITS            FROM 582. TO 582.  
                          ORBITS            FROM -10. TO 10.

10:11:11  
 08-DEC-88

# PV-ONMS DATA SUMMARY

- 1) SPIN MODULATION OF DATA
- 2) DATA GAP
- 3) ANTENNA SHADOWED POINTS (circled)

EXL DATA



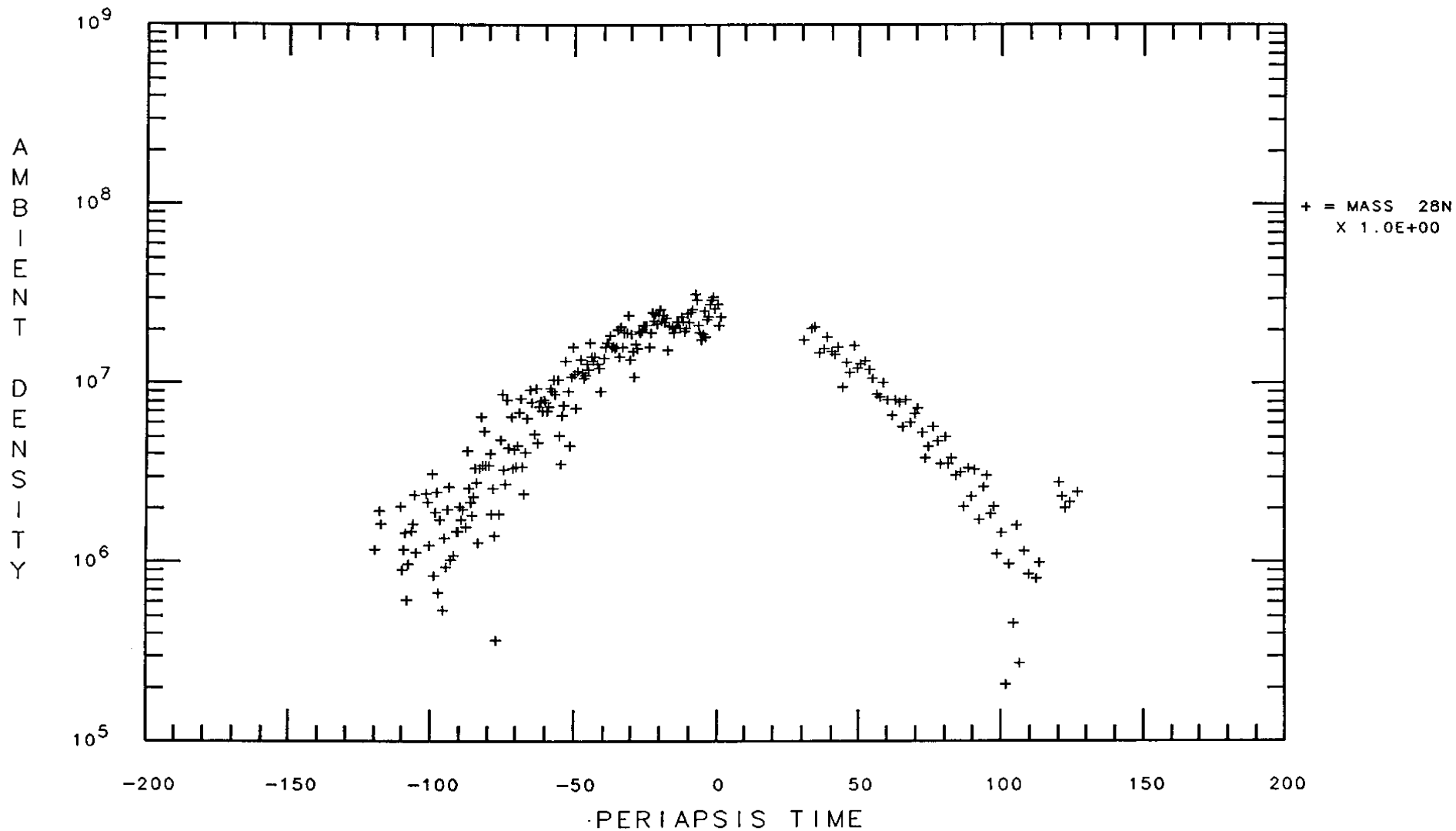
DATA SELECTION: ORBITS FROM 394. TO 394.



# PV-ONMS DATA SUMMARY

OUTBOUND PROBLEM POINTS  
NEAR HIGH ALTITUDE CUTOFF

EXL DATA



DATA SELECTION: ORBITS FROM 394. TO 394.

09:35:02  
08-DEC-88

## Purpose of Revised Pioneer Venus NSSDC Data Format

1. standardize and improve the data formats for each experiment so that the tapes can be easily read by a requestor.
2. store the data by experiment,
3. provide for orderly updating of data,
4. provide for ultimate replacement of existing UADS generated archival tapes.

A new format was designed which is to be used by each experimenter for PVO NSSDC data experimenter, and can be easily read by computers expected to be accessible to a requester. One major difference between this and the existing LFD format is the use of text (ASCII) data formats, eliminating both binary and IBM floating point formats.

The proposed new submission format is self-defining in the sense that the first three records on each tape define the data parameters, value representations, and missing data (file) indicators. The first tape record defines the order in which the variables appear in the subsequent data records, in a manner similar to that used for SEDR trajectory data (SEDR file 5). The second tape record will contain a FORTRAN-compatible format list describing the field sizes and representations of each data value in the order defined in record 1. This format may be used to decode all subsequent records on the tape.

The third tape record will define a unique value associated with filler (missing) data for all variable fields. It is formatted according to the format used in record 2, and is immediately followed by the start of actual data records (records 4 and beyond).

The following is the proposed new format, with examples as applied to OETP instructions.

### PROPOSED PIONEER VENUS NSSDC LOW-FREQUENCY DATA FORMAT

This document describes a suggested format to be used by all investigators for the submission of their data to the National Space Sciences Data Center. The overall specification will require that all data be coded into ASCII, and written onto standard 1/2 inch 1600-bpi 9-track tapes. The logical record length will be fixed for a given tape, as well as the physical blocksize. Blocksizes should be large enough to avoid wasting tape, but should not exceed 8000 bytes in order to avoid making excessive demands on user programs for memory. The first three records of any of these tapes will be formatted as follows:

Record 1: The format to be used is (I3,n(1X,A4)) where "n" is the number of data items in each record.

*	4	ELTE	ELNE	MI	VS							(for OETP)
	7	ETEM	SPOT	TONE	TTWO	XVEL	YVEL	ZVEL				(for ORPA)
	↑	↑	↑	↑	↑	↑	↑	↑				
	3	5	10	15	20	25	30	35				

Example 1: The first record in each tape file. Note that new value types with new 4-character designations can be added as necessary. The date, time, orbit and time-tag items are not included in the list, because they are common to all data records.

\* number of data items "n"

Record 2: This record contains the format in which all succeeding records are written. The first 4 format items specify the date, time, orbit, and time-tag, and will appear in the same format on all tapes.

(I8,I9,I5,I6,4F9.2)	(Appropriate for OETP)
↑	
1	

Example 2: The second record in each tape file

Record 3: This record will contain zeroes for the first four fields (date, time, orbit, and time-tag), and in addition will have a fill value in each data value location. This value will be used by any program reading the data to identify fill data in subsequent input records.

0	0	0	09999999.99999999.99999999.99999999.99
↑	↑	↑	↑
8	17	22	28 . 37 46 55 64

Example 3: The third record in each tape file. (Appropriate for OETP).

Record 4 to : These records contain the date, time, orbit, and time-tag for each time which has any non-fill data.

1981207	43527786	879	-1788	2345.67	78543.89999999.99	16.20	
↑	↑	↑	↑	↑	↑	↑	
8	17	22	28	37	46	55	64

Example 4: All records after the third in a tape file. (Appropriate for OETP).

As can be inferred from the above example, the date is coded as YEAR, DAY OF YEAR (1-366) with 19 included in the year. The time is in milliseconds of the day, orbit number is self-explanatory, and the time tag is the usual value ranging of the day from -1800 to 1800 in increments of 12.

The project-provided tape of SEDR information would be the source of the official dates and times to be used by all other investigators.

Nothing in the above format would preclude investigators from producing a tape containing the data from more than one experiment.

The external label on the tape should be type-written, and contain the following information:

- o Full name of experiment data contained on tape.<sup>1</sup>
- o Start date, time, and orbit number of data on the tape.
- o Stop date, time, and orbit number of data on the tape.
- o Production date of the tape.
- o The density (1600-bpi) and number of tracks (9) at which the tape was recorded.
- o An estimate of the amount of tape used.
- o The physical blocksize used in writing the tape.
- o A name and phone number of the individual responsible for the tape.

<sup>1</sup> Example: "Pioneer Venus Orbiter Electron Temperature Probe".

\$NOP  
\$NOP

\$NOP  
\$NOP ===== LIST OF OUT1

\$EXE TPLIST BS

D-85845  
12/7/78 - 9/5/80

INPUT PARAMETERS ARE: AS FL=5=5 2 1 1

TAPE NO. 1 FILE NO. 1  
RECORD 1 LENGTH 1000

2 DFE CN DC DN2 DCC DCO2 DRHC DTOT  
4digit Year DOY (I8,I9,I5,I6,1P8E9,2)  
0 0 0 0.00E-01 0.00E-01 0.00E-01 0.00E-01 0.00E-01 0.00E-01 0.00E-01 0.00E-01 0.00E-01  
-1 1978341 52247000 3 -72 0.00E-01 1.00E-01 2.75E+05 0.00E-01 3.87E+06 2.06E+06 0.00E-01 0.00  
E-01 1978341 52259000 3 -61 0.00E-01 0.00E-01 4.16E+05 0.00E-01 5.15E+06 3.20E+06 0.00E-01 0.0  
E-01 1978341 52271000 3 -48 0.00E-01 0.00E-01 5.47E+05 2.52E+06 7.17E+06 4.77E+06 8.13E-16 1.  
5E+07 1978341 52283000 3 -36 1.68E+06 0.00E-01 6.07E+05 3.47E+06 8.69E+06 6.56E+06 1.07E-15 2  
.1E+07 1978341 52295000 3 -24 0.00E-01 0.00E-01 7.05E+05 3.96E+06 9.62E+06 8.48E+06 1.27E-15  
2.28E+07 1978341 52307000 3 -12 0.00E-01 0.00E-01 9.01E+05 4.09E+06 1.02E+07 1.06E+07 1.46E-15  
2.58E+07 1978341 52307116 3 0 0.00E-01 0.00E-01 9.02E+05 4.09E+06 1.02E+07 1.06E+07 1.46E-1  
5 2.58E+07

TAPE NO. 1 FILE NO. 1  
RECORD 2 LENGTH 1000

1978341 52379000 3 72 0.00E-01 0.00E-01 3.47E+05 0.00E-01 3.31E+06 4.81E+06 0.00E-01 0.00E-0  
1 1978341 52391000 3 84 0.00E-01 0.00E-01 2.30E+05 0.00E-01 0.00E-01 3.80E+06 0.00E-01 0.00E-  
01 1978342 52714816 4 -18 0.00E-01 0.00E-01 2.65E+05 0.00E-01 3.45E+06 4.76E+06 0.00E-01 0.00E-  
-01 1978342 52726816 4 -26 0.00E-01 0.00E-01 5.34E+05 0.00E-01 6.54E+06 8.14E+06 0.00E-01 0.00  
E-01 1978342 52738816 4 -84 1.42E+06 0.00E-01 8.83E+05 2.72E+06 1.08E+07 1.28E+07 1.60E-15 2.8  
7E+7 1978342 52750816 4 -72 1.46E+06 0.00E-01 1.25E+06 4.23E+06 1.65E+07 1.93E+07 2.42E-15 4.  
27E+07 1978342 52762816 4 -60 1.43E+06 0.00E-01 1.91E+06 7.09E+06 2.65E+07 2.92E+07 3.75E-15 6  
.61E+07 1978342 52774816 4 -48 1.52E+06 0.00E-01 2.66E+06 1.11E+07 3.68E+07 4.17E+07 5.35E-15  
9.37E+07 1978342 52786816 4 -36 1.56E+06 0.00E-01 3.54E+06 1.50E+07 4.80E+07 5.58E+07 7.11E-15  
1.24E+08 1978342 52798816 4 -24 1.59E+06 0.00E-01 4.65E+06 1.79E+07 5.88E+07 6.89E+07 8.73E-1  
5 1.52E+08

TAPE NO. 1 FILE NO. 1  
RECORD 3 LENGTH 1000

1978343 53183000 5 -120 0.00E-01 0.00E-01 4.86E+05 0.00E-01 0.00E-01 4.29E+06 0.00E-01 0.00E-0  
1 1978343 53195000 5 -138 1.50E+06 0.00E-01 9.43E+05 0.00E-01 3.12E+06 7.62E+06 0.00E-01 0.00E-  
01 1978343 53207000 5 -96 1.39E+06 0.00E-01 1.96E+06 2.66E+06 6.12E+06 1.25E+07 1.39E-15 2.47E  
+07 1978343 53219000 5 -84 1.21E+06 0.00E-01 3.74E+06 4.05E+06 1.03E+07 1.88E+07 2.15E-15 3.81  
E+07 1978343 53231000 5 -72 1.37E+06 0.00E-01 6.56E+06 6.44E+06 1.64E+07 2.73E+07 3.24E-15 5.8  
1E+07 1978343 53243000 5 -60 1.40E+06 0.00E-01 1.07E+07 9.18E+06 2.39E+07 3.81E+07 4.62E-15 8.  
33E+07 1978343 53255000 5 -48 1.59E+06 0.00E-01 1.54E+07 1.25E+07 3.24E+07 4.85E+07 6.05E-15 1  
.10E+08 1978343 53267000 5 -36 1.56E+06 0.00E-01 2.12E+07 1.60E+07 4.28E+07 6.14E+07 7.79E-15  
1.43E+08 1978343 53279000 5 -24 1.56E+06 0.00E-01 3.54E+07 2.11E+07 5.72E+07 7.58E+07 9.92E-15  
1.83E+08 1978343 53291000 5 -12 1.67E+06 0.00E-01 0.00E-01 2.38E+07 6.38E+07 0.00E-01 0.00E-0  
1 0.00E-01

TAPE NO. 1 FILE NO. 1  
RECORD 4 LENGTH 1000

1978344 53807000 6 36 0.00E-01 0.00E-01 5.56E+07 7.34E+07 0.00E-01 4.72E+07 0.00E-01 0.00E-0  
1 1978344 53819000 6 48 0.00E-01 0.00E-01 4.37E+07 7.09E+07 0.00E-01 3.73E+07 0.00E-01 0.00E-  
01 1978344 53831000 6 60 0.00E-01 0.00E-01 3.62E+07 3.03E+07 0.00E-01 2.95E+07 0.00E-01 0.00E-  
-01 1978344 53843000 6 72 1.46E+06 0.00E-01 2.91E+07 0.00E-01 1.29E+07 2.91E+07 0.00E-01 0.00  
E-01 1978344 53855000 6 84 1.50E+06 0.00E-01 2.17E+07 4.12E+06 8.28E+06 1.83E+07 2.50E-15 5.3  
9E+7 1978344 53867000 6 96 1.39E+06 0.00E-01 1.53E+07 2.47E+06 5.19E+06 1.33E+07 1.75E-15 7.  
77E+7 1978344 53879000 6 108 1.11E+06 0.00E-01 9.61E+06 0.00E-01 0.00E-01 9.15E+06 0.00E-01 0  
.00E-01 1978344 53891000 6 120 1.22E+06 0.00E-01 5.43E+06 0.00E-01 0.00E-01 6.35E+06 0.00E-01  
0.00E-01 1978344 53903000 6 132 0.00E-01 0.00E-01 3.22E+06 0.00E-01 0.00E-01 4.37E+06 0.00E-01  
0.00E-01 1978345 54116816 7 -144 0.00E-01 0.00E-01 4.67E+05 0.00E-01 0.00E-01 1.10E+06 0.00E-0  
1 0.00E-01

TAPE NO. 1 FILE NO. 1  
RECORD 5 LENGTH 1000

Pioneer Venus

PIONEER VENUS 1

12 SECOND B & E FIELD DATA 1 HOUR AROUND PERIAPSIS

78-051A-12F PSFP-00055  
 78-051A-13E

This dataset consists of eleven 9-track tapes. 4 tapes are 1600 BPI, while the other seven are 6250 BPI. The tapes are ASCII and were created on the IBM computer. Each file contains 8 physical records (or blocks) which are 6080 bytes long. Each physical record contains 38 logical records which are 160 bytes long. The logical records are arranged as follows:

- Record 1: Data headers
- Record 2: Fortran Format
- Record 3: Data Fill examples
- Record 4: Time, Orbit, T-Peri, Data

Each file contains data for one orbit, one hour about periapsis (i.e. 2 hours of data within the nominal Venusian ionosphere). The data are 24 second averages taken 12 seconds apart.

The "D" and "C" numbers along with their time spans are as follows:

D#	C#	TIME SPAN	FILES	ORBIT #
D-66729	C-24987	12/05/78 - 04/18/80	500	1- 500
D-66730	C-24988	04/19/80 - 09/01/81	500	501-1000
D-74127	C-26131	09/02/81 - 01/14/83	500	1001-1500
D-74128	C-26132	01/15/83 - 05/28/83	500	1501-2000
D-83252	C-29214	05/28/84 - 01/17/86	600	2001-2600
D-98900	C-29873	01/30/86 - 02/22/87	388	2613-3000
D-98901	C-29874	02/22/87 - 08/25/88	550	3001-3550
D-101566	C-031192	08/26/88 - 10/16/88	52	3551-3602
D-101567	C-031193	10/17/88 - 06/06/90	598	3603-4200
D-101568	C-031194	06/07/90 - 07/11/91	399	4201-4600
D-101569	C-031195	07/12/91 - 10/08/92	455	4601-5055

PIONEER VENUS ORBITER  
MAGNETOMETER AND ELECTRIC FIELD DETECTOR  
LOW-FREQUENCY DATA SUBMISSION TO  
NATIONAL SPACE SCIENCE DATA CENTER

7P-051A-12F  
7P-051A-13E

Parameters on NSSDC Low-frequency Data Tape

This tape contain 24 second overlapped averages, every 12 seconds of both the PVO magnetometer (OMAG) and electric field data (OEFD), for an hour centered around the periapsis of each orbit for orbits 4201-4600. The time epochs were provided by the Pioneer Project at Ames Research Center.

During orbit 3602, the spin-plane magnetometer sensors failed, and so after this orbit the magnetic field data columns contain only the Bz component. We receive 3 values for the P-sensor (Bz) rather than 1 value for Bx, By and Bz. Due to this, the columns for Bx, By, Bt and DBTL are all flagged. We've left the columns in the files so they are the same format as orbits 1-3602. The magnetometer data for these orbits are in spacecraft coordinates. Also included are the standard deviations of Bz.

The OEFD data consists of the 24 second maximum and average from each of the four OEFD channels, in units of volts per meter per square root hertz. The four frequency bands are centered around 100 Hz, 730 Hz, 5.4kHz and 30kHz.

Tape Format

These tapes were created using the ASCII format described in "Pioneer Venus Mission Instructions for Data Submissions to the National Space Science Data Center". This document should be referenced for general tape information.

The tapes are standard 1/2 inch, 9 track, 6250 bpi, unlabeled, ASCII, with fixed length blocked records. The record length is 160 bytes, in blocks of 38, for a blocksize of 6080 bytes. There is a record for each 12 second interval for an hour about periapsis, resulting in 301 data records per orbit. With 3 header records there are then 304 records per orbit, which fill 8 complete blocks. There is a tape mark after the last record of each orbit, which splits the tape into 399 files with a double tape mark after the last file.

NOTE: There is no file for orbit 4435.

\*\*\*\*\*

PVO OMAG & OEFD LOW-FREQUENCY DATA TAPE

As specified in the "Pioneer Venus Mission Instructions for Data Submissions to the NSSDC" the first three records are information on the format of the data.

Record #1: Format: (I3,14(1x,A4)) Gives the number of data columns in each data record (14), and 4 character descriptors for each.

Record #2: Format: (A160) Gives the Fortran format to be used in reading each data record.

Record #3: Fortran format is given in record #2. Contains the fill values which occur when no data is available.

Record #4-end: Time, orbit, seconds from periapsis, data.

\*\*\*\*\*

ITEM	CONTENTS	FORMAT	EXAMPLE	FILL
1	YEAR * 1000 + DAY OF YEAR	I8	(b=blank) b1984001	0
2	MILLISECONDS OF DAY	I9	b86400000	0
3	ORBIT NUMBER	I5	b1901	0
4	SECONDS FROM PERIAPSIS	I6	-43200	0
5	BX AVERAGE (all flags)	F7.2	b-10.10	b999.00
6	BY AVERAGE (all flags)	"	"	"
7	BZ AVERAGE (P-sensor avg. S/C in	"	"	"
8	BT AVERAGE (all flags) GAMMAS	"	"	"
9	SD OF COMPONENTS (P-sensor avg)	"	"	"
10	SD OF TOTAL (all flags)	"	"	"
11	100 HZ ELEC MAX (V/(M*HZ**.5))	E10.3	b0.333E-07	1.0E+32
12	100 HZ ELEC AVERAGE	"	"	"
13	730 HZ ELEC MAX	"	"	"
14	730 HZ ELEC AVE	"	"	"
15	5.4 KHZ ELEC MAX	"	"	"

12f  
13E

2

16	5.4 KHZ ELEC AVE	"	"	"
17	30 KHZ ELEC MAX	"	"	"
18	30 KHZ ELEC AVE	"	"	"
19	BLANK FILL		10X	

TOTAL CHARACTERS = 160

\*\*\*\*\*

DATA = u3551.ffd  
 CDATE = 90 054 FEB 23 10:03:27 UPDATE = 90 054 FEB 23 10:03:35  
 RECL = 269  
 LINES = 20  
 NROWS = 301  
 OPSYS = SUN/UNIX

#	NAME	UNITS	SOURCE	FORMAT
001	UT	YR MON DY	HR MN SC MS	613.2,14.3
002	BX VSO	NT	PVO OMAG	G13.5
003	BY VSO	NT	PVO OMAG	G13.5
004	BZ VSO	NT	PVO OMAG	G13.5
005	BT	NT	PVO OMAG	G13.5
006	VSOX	RV	PVO SEDR/UCLA	G13.5
007	VSOY	RV	PVO SEDR/UCLA	G13.5
008	VSOZ	RV	PVO SEDR/UCLA	G13.5
009	PLAT	DEG	PVO SEDR/UCLA	G13.5
010	PLON	DEG	PVO SEDR/UCLA	G13.5
011	DBTR	NT	PVO SD OF B COMPONENTS	G13.5
012	DBTL	NT	PVO SD OF B TOTAL	G13.5
013	E100 MAX	V/M/RTHZ	PVO OEFD 100HZ CHANNEL	G13.5
014	E100 AVG	V/M/RTHZ	PVO OEFD 100 HZ CHANNEL	G13.5
015	E730 MAX	V/M/RTHZ	PVO OEFD 730 HZ CHANNEL	G13.5
016	E730 AVG	V/M/RTHZ	PVO OEFD 730 HZ CHANNEL	G13.5
017	E5.4KMAX	V/M/RTHZ	PVO OEFD 5.4K HZ CHANNEL	G13.5
018	E5.4KAVG	V/M/RTHZ	PVO OEFD 5.4K HZ CHANNEL	G13.5
019	E30K MAX	V/M/RTHZ	PVO OEFD 30K HZ CHANNEL	G13.5
020	E30K AVG	V/M/RTHZ	PVO OEFD 30K HZ CHANNEL	G13.5

ABSTRACT  
 FIRST TIME - 88 239 AUG 26 02:17:25.415  
 LAST TIME - 88 239 AUG 26 03:17:25.415  
 OWNER - GORDON  
 MISSING DATA FLAG - 1.000000E+32  
 ORBIT NUMBER(S) - 3551

ORBIT START TIME NREC  
 PVO UADS DATA - 12 SEC AVERAGES 1 HOUR ABOUT PERIAPSIS  
 Periapsis time: 88 239 AUG 26 02:47:25.415  
 NSSFF: 90 052 FEB 21 18:55:42.330

PVO OETP data received Jan 02, 1990 via SPAN mail.  
 MERGE: 90 053 FEB 22 08:28:56  
 Data columns extracted from DISK\$SCRATCH:[GORDON.OETP]OETPO.FFH;1  
 FMERGE: 90 054 FEB 23 10:03:28  
 Files A & B merged (nearest points from B)  
 File A: QSA2:[PVO.UADS]Y3551.FFH;1  
 File B: DISK\$SCRATCH:[GORDON.OETP]OETP.FFH;1  
 A columns: 1 - 20  
 B columns: 21 - 23

END  
 FORTRAN FORMAT:  
 (613.2,14.3,19G13.5)  
 MISSING DATA FLAGS:

00 00 00 00 00 00 000 0.10000E+33 0.10000E+33 0.10000E+33 0.10000E+33 0.10000E+33 0.10000  
 E+33 0.10000E+33 0.10000E+33 0.10000E+33 0.10000E+33 0.10000E+33 0.10000E+33 0.10000E+33  
 0.10000E+33 0.10000E+33 0.10000E+33 0.10000E+33 0.10000E+33 0.10000E+33

DATA:

88 08 26 02 17 25 415	11.929	-6.4944	-5.6719	14.863	0.52416	0.50853
1.9389	68.706	67.441	2.2697	0.89698	0.15350E-03	0.53216E-04
0.12478E-04	0.80742E-05	0.14739E-05	0.12898E-05	0.32623E-04	0.71307E-05	
88 08 26 02 17 37 415	12.287	-6.6868	-5.1625	15.090	0.53274	0.50735
1.9291	68.494	66.851	2.5602	1.0308	0.47323E-03	0.72020E-04
0.13479E-04	0.83521E-05	0.18433E-05	0.13380E-05	0.32623E-04	0.53662E-05	
88 08 26 02 17 49 415	12.144	-7.4500	-4.6707	15.274	0.54131	0.50615
1.9192	68.280	66.267	3.2585	1.3915	0.60776E-03	0.10911E-03
0.16347E-04	0.90034E-05	0.67950E-05	0.16462E-05	0.22435E-04	0.31645E-05	
88 08 26 02 18 01 415	12.165	-7.3945	-4.7181	15.371	0.54987	0.50494
1.9092	68.061	65.691	3.8349	1.7655	0.60776E-03	0.11919E-03
0.19825E-04	0.93375E-05	0.17909E-04	0.21872E-05	0.22435E-04	0.33034E-05	
88 08 26 02 18 13 415	12.356	-7.0215	-4.5552	15.291	0.55842	0.50372
1.8993	67.840	65.121	3.8544	1.8782	0.45390E-03	0.10301E-03
0.19825E-04	0.88679E-05	0.17909E-04	0.21072E-05	0.22435E-04	0.38103E-05	
88 08 26 02 18 25 415	11.840	-7.6666	-3.3047	14.889	0.56695	0.50248
1.8892	67.614	64.558	3.8173	1.5850	0.41758E-03	0.10939E-03
0.14560E-04	0.84276E-05	0.54332E-05	0.17172E-05	0.20052E-04	0.43844E-05	
88 08 26 02 18 37 415	11.524	-7.9920	-2.3347	14.549	0.57546	0.50123
1.8792	67.385	64.002	3.4306	1.4183	0.41758E-03	0.12777E-03
0.19825E-04	0.86016E-05	0.15429E-04	0.21001E-05	0.19315E-04	0.38766E-05	

88 08 26 02 18 49 415	12.504	-7.0965	-3.9372	15.338	0.58396	0.49997
1.8690	67.153	63.453	4.0800	1.8275	0.41758E-03	0.14340E-03
0.34024E-04	0.94414E-05	0.15429E-04	0.24545E-05	0.20052E-04	0.30038E-05	
88 08 26 02 19 01 415	12.750	-6.6224	-4.3016	15.356	0.59245	0.49870
1.8589	66.917	62.911	3.8877	2.0007	0.40053E-03	0.13108E-03
0.34024E-04	0.92763E-05	0.73209E-05	0.20780E-05	0.23291E-04	0.35882E-05	
08 26 02 19 13 415	11.698	-7.3801	-2.2878	14.309	0.60092	0.49741
1.8486	66.677	62.375	3.3282	1.6371	0.40053E-03	0.95494E-04
0.14560E-04	0.82771E-05	0.45094E-05	0.15582E-05	0.23291E-04	0.31306E-05	
88 08 26 02 19 25 415	11.537	-7.6560	-1.0969	14.117	0.60938	0.49611
1.8384	66.434	61.845	2.7907	1.1361	0.33899E-03	0.76555E-04
0.14560E-04	0.78273E-05	0.18433E-05	0.13370E-05	0.22435E-04	0.35479E-05	
88 08 26 02 19 37 415	12.244	-6.0923	0.46395	14.078	0.61782	0.49480
1.8281	66.187	61.322	3.5012	1.0368	0.33899E-03	0.64168E-04
0.14560E-04	0.75403E-05	0.17759E-05	0.13016E-05	0.22435E-04	0.36478E-05	
88 08 26 02 19 49 415	10.462	-5.3548	4.3894	13.669	0.62624	0.49348
1.8177	65.937	60.806	5.9408	2.2836	0.41758E-03	0.91204E-04
0.13479E-04	0.77981E-05	0.16483E-05	0.13105E-05	0.94834E-05	0.22858E-05	
88 08 26 02 20 01 415	4.6609	-3.8255	10.953	14.274	0.63464	0.49214
1.8073	65.684	60.296	7.5355	2.8915	0.41758E-03	0.10492E-03
0.15133E-04	0.84071E-05	0.16483E-05	0.13449E-05	0.91349E-05	0.14342E-05	

SAMPLE UADS FILE FOR ORBITS 3603-5055

DATA = u3809.ffd
CDATE = 91 205 JUL 24 14:22:20
BECL = 269
LS = 20
NEWS = 301
OPSYS = SUN/UNIX

Table with columns: # NAME, UNITS, SOURCE, FORMAT. Rows include UT, BX SC, BY SC, BZ SC, BT, VSOX, VSOY, VSOZ, PLAT, PLON, DBTR, DBTL, E100 MAX, E100 AVG, E730 MAX, E730 AVG, E5.4KMAX, E5.4KAVG, E30K MAX, E30K AVG.

ABSTRACT
FIRST TIME = 89 131 MAY 11 02:57:07.595
LAST TIME = 89 131 MAY 11 03:57:07.595
OWNER = debbie
MISSING DATA FLAG = 1.00000E+32
AVERAGE INTERVAL = 00:00:24.000
ORBIT NUMBER(S) = 3809
PVO EDR DATA PROCESSING, VERSION 1.5, UCLA, DATE: 91 205 JUL 24
PVOFLAGCAL: 91 205 JUL 24

Magnetic field data flagged during calibrate interval.
AVG: 91 205 JUL 24 14:21:48
input file: hima3809.ffh...
Output file: /scratch/debbie/uads\_mag3809.ffh
Processing options: AVG RMSDEV COUNT
Window width(sec)= 24.000 Output res= 12.000
Min pts= 1.00

ffcalc: 91 205 JUL 24 14:21:54
Input file: /scratch/debbie/uads\_mag3809.ffh
Output file: /scratch/debbie/uads\_mag3809.ffh
out: c1;
"BX SC" "NT" = FLAG;
"BY SC" "NT" = FLAG;
c2:
"BT" "NT" = FLAG;
"SDBZ" "NT" = sqrt((c3\*c3) \* c4 / (c4-1.));
"SDBT" "NT" = FLAG;

PVO EDR DATA PROCESSING, VERSION 1.5, UCLA, DATE: 91 205 JUL 24
ffcalc: 91 205 JUL 24 14:22:00
Input file: hiel3809
Output file: /scratch/debbie/hiel\_rt3809.ffh
var: skip {c1<" 89 131 MAY 11 02:56:55.595"};
var: stop {c1>" 89 131 MAY 11 03:57:19.595"};
out: c1;
"E100HZ" "V/M/HZ.5" = sqrt(c2);
"E730HZ" "V/M/HZ.5" = sqrt(c3);
"E5.4KHZ" "V/M/HZ.5" = sqrt(c4);
"E30KHZ" "V/M/HZ.5" = sqrt(c5);

FFAVG: 91 205 JUL 24 14:22:01
Input file: /scratch/debbie/hiel\_rt3809.ffh...
Output file: /scratch/debbie/uads\_ele3809.ffh
Processing options: MAX AVG
Window width(sec)= 24.000 Output res= 12.000
Min pts= 1.00 1.00 1.00 1.00
FFMERGE: 91 205 JUL 24 14:22:07
Files A & B merged (A union B)
File A: /scratch/debbie/uads\_mag3809.ffh
File B: /scratch/debbie/uads\_ele3809.ffh
A columns: 1 - 7

B columns: 8 - 15  
PVO EDR DATA PROCESSING, VERSION 1.5, UCLA, DATE: 91 205 JUL 24  
EPHFLAGDUP: 91 205 JUL 24

No duplicate ephemeris records found.  
FFMERGE: 91 205 JUL 24 14:22:13  
Files A & B merged (quadratic interpolation of B)  
File A: /scratch/debbie/uads\_magele3809.ffh  
File B: ephe3809.ffh ...

A columns: 1 - 15  
B columns: 16 - 20  
ffcalc: 91 205 JUL 24 14:22:20  
Input file: /scratch/debbie/uads\_mageleeph3809.ffh  
Output file: /prod/pvo/uads/u3809.ffh

out: c1; c2; c3; c4; c5;  
"VSOX" "RV" = c16;  
"VSOY" "RV" = c17;  
"VSOZ" "RV" = c18;  
"PLAT" "DEG" = c19;  
"PLON" "DEG" = c20;  
"DBTR" "NT" = c6;  
"DBTL" "NT" = c7;  
"E100 MAX" "V/M/rthZ" = c8;  
"E100 AVG" "V/M/rthZ" = c9;  
"E730 MAX" "V/M/rthZ" = c10;  
"E730 AVG" "V/M/rthZ" = c11;  
"E5.4KMAX" "V/M/rthZ" = c12;  
"E5.4KAVG" "V/M/rthZ" = c13;  
"E30K MAX" "V/M/rthZ" = c14;  
"E30K AVG" "V/M/rthZ" = c15;

END  
FORTRAN FORMAT:  
(6I3.2,I4.3,19G13.5)  
MISSING DATA FLAGS:

00 00 00 00 00 00 000 0.10000E+33 0.10000E+33 0.10000E+33 0.10000E+33 0.10000E+33 0.10000  
E+33 0.10000E+33 0.10000E+33 0.10000E+33 0.10000E+33 0.10000E+33 0.10000E+33 0.10000E+33  
0.10000E+33 0.10000E+33 0.10000E+33 0.10000E+33 0.10000E+33 0.10000E+33

DATA:  
89 05 11 02 57 07 595 0.10000E+33 0.10000E+33 0.10000E+33 0.10000E+33 0.70199 -0.11957  
1.9289 69.094 89.502 0.10000E+33 0.10000E+33 0.10000E+33 0.10000E+33  
0.10000E+33 0.10000E+33 0.10000E+33 0.10000E+33 0.10000E+33 0.10000E+33  
05 11 02 57 19 595 0.10000E+33 0.10000E+33 0.10000E+33 0.10000E+33 0.70611 -0.12706  
1.9189 68.881 88.905 0.10000E+33 0.10000E+33 0.10000E+33 0.10000E+33  
0.10000E+33 0.10000E+33 0.10000E+33 0.10000E+33 0.10000E+33 0.10000E+33  
89 05 11 02 57 31 595 0.10000E+33 0.10000E+33 0.10000E+33 0.10000E+33 0.71021 -0.13455  
1.9088 68.665 88.316 0.10000E+33 0.10000E+33 0.10000E+33 0.10000E+33  
0.10000E+33 0.10000E+33 0.10000E+33 0.10000E+33 0.10000E+33 0.10000E+33  
89 05 11 02 57 43 595 0.10000E+33 0.10000E+33 0.10000E+33 0.10000E+33 0.71430 -0.14204  
1.8987 68.445 87.734 0.10000E+33 0.10000E+33 0.10000E+33 0.10000E+33  
0.10000E+33 0.10000E+33 0.10000E+33 0.10000E+33 0.10000E+33 0.10000E+33  
89 05 11 02 57 55 595 0.10000E+33 0.10000E+33 0.10000E+33 0.10000E+33 0.71836 -0.14952  
1.8885 68.221 87.159 0.10000E+33 0.10000E+33 0.10000E+33 0.10000E+33  
0.10000E+33 0.10000E+33 0.10000E+33 0.10000E+33 0.10000E+33 0.10000E+33  
89 05 11 02 58 07 595 0.10000E+33 0.10000E+33 0.10000E+33 0.10000E+33 0.72241 -0.15700  
1.8783 67.994 86.591 0.10000E+33 0.10000E+33 0.10000E+33 0.10000E+33  
0.10000E+33 0.10000E+33 0.10000E+33 0.10000E+33 0.10000E+33 0.10000E+33  
89 05 11 02 58 19 595 0.10000E+33 0.10000E+33 0.10000E+33 0.10000E+33 0.72644 -0.16447  
1.8680 67.763 86.030 0.10000E+33 0.10000E+33 0.10000E+33 0.10000E+33  
0.10000E+33 0.10000E+33 0.10000E+33 0.10000E+33 0.10000E+33 0.10000E+33  
89 05 11 02 58 31 595 0.10000E+33 0.10000E+33 0.10000E+33 0.10000E+33 0.73045 -0.17194  
1.8577 67.528 85.476 0.10000E+33 0.10000E+33 0.10000E+33 0.10000E+33  
0.10000E+33 0.10000E+33 0.10000E+33 0.10000E+33 0.10000E+33 0.10000E+33  
89 05 11 02 58 43 595 0.10000E+33 0.10000E+33 0.10000E+33 0.10000E+33 0.73445 -0.17941  
1.8474 67.290 84.929 0.10000E+33 0.10000E+33 0.10000E+33 0.10000E+33  
0.10000E+33 0.10000E+33 0.10000E+33 0.10000E+33 0.10000E+33 0.10000E+33  
89 05 11 02 58 55 595 0.10000E+33 0.10000E+33 0.10000E+33 0.10000E+33 0.73842 -0.18687  
1.8370 67.048 84.389 0.10000E+33 0.10000E+33 0.10000E+33 0.10000E+33  
0.10000E+33 0.10000E+33 0.10000E+33 0.10000E+33 0.10000E+33 0.10000E+33  
89 05 11 02 59 07 595 0.10000E+33 0.10000E+33 0.10000E+33 0.10000E+33 0.74237 -0.19432  
1.8265 66.803 83.855 0.10000E+33 0.10000E+33 0.10000E+33 0.10000E+33  
0.10000E+33 0.10000E+33 0.10000E+33 0.10000E+33 0.10000E+33 0.10000E+33  
89 05 11 02 59 19 595 0.10000E+33 0.10000E+33 0.10000E+33 0.10000E+33 0.74630 -0.20177  
1.8160 66.553 83.328 0.10000E+33 0.10000E+33 0.10000E+33 0.10000E+33  
0.10000E+33 0.10000E+33 0.10000E+33 0.10000E+33 0.10000E+33 0.10000E+33  
89 05 11 02 59 31 595 0.10000E+33 0.10000E+33 0.10000E+33 0.10000E+33 0.75021 -0.20922  
1.8055 66.301 82.808 0.10000E+33 0.10000E+33 0.10000E+33 0.10000E+33  
0.10000E+33 0.10000E+33 0.10000E+33 0.10000E+33 0.10000E+33 0.10000E+33  
89 05 11 02 59 43 595 0.10000E+33 0.10000E+33 0.10000E+33 0.10000E+33 0.75411 -0.21666  
1.7949 66.044 82.294 0.10000E+33 0.10000E+33 0.10000E+33 0.10000E+33  
0.10000E+33 0.10000E+33 0.10000E+33 0.10000E+33 0.10000E+33 0.10000E+33  
89 05 11 02 59 55 595 0.10000E+33 0.10000E+33 0.10000E+33 0.10000E+33 0.75798 -0.22409





1988290 12120671 3602 1356 -21.47 0.57 -6.93 23.39 6.64 2.18 0.147E-03 0.421E-04 0.382E-04 0.107E-04 0.179E-04 0.474E-05 0  
 .718E-06 0.556E-06 1988290 12132671 3602 1368 -22.28 -0.44 -6.75 23.79 5.23 1.58 0.135E-03 0.435E-04 0.382E-04 0.1  
 28E-04 0.250E-04 0.554E-05 0.665E-06 0.561E-06 1988290 12144671 3602 1380 -21.86 0.63 -7.49 23.64 5.37 1.87 0.130  
 E-03 0.446E-04 0.327E-04 0.118E-04 0.250E-04 0.480E-05 0.744E-06 0.558E-06 1988290 12156671 3602 1392 -21.18 2.65 -6.9  
 4 23.00 5.83 2.74 0.755E-04 0.379E-04 0.157E-04 0.854E-05 0.338E-04 0.390E-05 0.744E-06 0.554E-06 1988290 12168671 36  
 02 1404 -18.30 1.78 -6.60 20.00 6.47 4.78 0.141E-03 0.362E-04 0.135E-04 0.800E-05 0.338E-04 0.302E-05 0.690E-06 0.544E-06  
 1988290 12180671 3602 1416 -16.70 3.45 -6.71 19.09 7.02 4.40 0.147E-03 0.475E-04 0.170E-04 0.803E-05 0.504E-05 0.1  
 75E-05 0.665E-06 0.548E-06 1988290 12192671 3602 1428 -20.70 4.01 -8.70 23.82 8.85 5.37 0.147E-03 0.464E-04 0.170  
 E-04 0.861E-05 0.590E-04 0.583E-05 0.297E-05 0.659E-06 1988290 12204671 3602 1440 -25.51 3.92 -9.62 28.50 8.20 3.  
 30 0.189E-03 0.497E-04 0.562E-04 0.106E-04 0.590E-04 0.895E-05 0.297E-05 0.670E-06 1988290 12216671 3602 1452 -25.97 5.  
 87 -9.74 29.11 6.95 1.68 0.189E-03 0.587E-04 0.765E-04 0.177E-04 0.111E-03 0.152E-04 0.121E-05 0.592E-06 1988290 122  
 28671 3602 1464 -26.28 2.45 -9.13 28.62 6.63 1.90 0.167E-03 0.482E-04 0.765E-04 0.174E-04 0.111E-03 0.131E-04 0.121E-05 0.5  
 78E-06 1988290 12240671 3602 1476 -24.38 0.05 -7.93 26.38 7.18 3.37 0.856E-04 0.398E-04 0.541E-04 0.125E-04 0.107  
 E-03 0.138E-04 0.130E-05 0.584E-06 1988290 12252671 3602 1488 -23.76 2.57 -9.16 26.50 7.86 3.53 0.856E-04 0.411E-  
 04 0.541E-04 0.111E-04 0.195E-03 0.221E-04 0.163E-05 0.635E-06 1988290 12264671 3602 1500 -26.54 2.64 -10.10 29.14 6  
 .38 1.76 0.105E-03 0.446E-04 0.191E-04 0.936E-05 0.195E-03 0.163E-04 0.163E-05 0.611E-06 1988290 12276671 3602 1512 -27  
 .33 0.95 -10.91 30.01 6.67 3.01 0.125E-03 0.474E-04 0.327E-04 0.101E-04 0.103E-03 0.139E-04 0.897E-06 0.579E-06 198  
 8290 12288671 3602 1524 -28.55 1.08 -11.68 31.56 7.59 3.57 0.206E-03 0.461E-04 0.327E-04 0.108E-04 0.139E-03 0.171E-04 0.897  
 E-06 0.591E-06 1988290 12300671 3602 1536 -30.28 2.58 -11.00 32.89 6.54 2.00 0.206E-03 0.483E-04 0.584E-04 0.141E-  
 04 0.144E-03 0.227E-04 0.332E-05 0.692E-06 1988290 12312671 3602 1548 -28.99 3.13 -11.28 31.64 5.38 2.19 0.115E-03  
 0.478E-04 0.584E-04 0.137E-04 0.144E-03 0.165E-04 0.332E-05 0.683E-06 1988290 12324671 3602 1560 -29.91 2.40 -12.59 3  
 2.79 5.06 2.95 0.287E-03 0.556E-04 0.303E-04 0.104E-04 0.590E-04 0.632E-05 0.744E-06 0.559E-06 1988290 12336671 3602  
 1572 -33.67 2.80 -12.55 36.22 4.21 2.04 0.287E-03 0.519E-04 0.303E-04 0.992E-05 0.590E-04 0.543E-05 0.665E-06 0.552E-06  
 1988290 12348671 3602 1584 -33.50 2.21 -11.66 35.97 6.16 2.38 0.253E-03 0.485E-04 0.584E-04 0.121E-04 0.166E-04 0.467E-  
 05 0.126E-05 0.591E-06 1988290 12360671 3602 1596 -31.22 1.80 -12.62 34.38 7.56 3.25 0.299E-03 0.625E-04 0.584E-04  
 0.126E-04 0.216E-04 0.533E-05 0.126E-05 0.592E-06 1988290 12372671 3602 1608 -31.76 4.52 -13.25 35.30 7.37 3.37 0  
 .299E-03 0.532E-04 0.315E-04 0.102E-04 0.216E-04 0.438E-05 0.204E-05 0.623E-06 1988290 12384671 3602 1620 -31.31 5.47 -  
 11.54 34.22 6.34 3.42 0.264E-03 0.466E-04 0.315E-04 0.113E-04 0.338E-04 0.779E-05 0.204E-05 0.631E-06 1988290 1239667  
 1 3602 1632 -32.17 4.31 -11.36 34.63 5.54 3.64 0.264E-03 0.448E-04 0.303E-04 0.100E-04 0.338E-04 0.692E-05 0.772E-06 0.557E-  
 06 1988290 12408671 3602 1644 -32.52 3.24 -11.69 34.92 5.28 3.56 0.135E-03 0.389E-04 0.163E-04 0.871E-05 0.950E-05  
 0.234E-05 0.104E-05 0.564E-06 1988290 12420671 3602 1656 -31.26 2.88 -10.80 33.43 4.89 2.76 0.135E-03 0.385E-04 0  
 .223E-04 0.935E-05 0.119E-04 0.294E-05 0.104E-05 0.569E-06 1988290 12432671 3602 1668 -31.45 4.23 -9.94 33.64 5.57  
 2.04 0.174E-03 0.383E-04 0.413E-04 0.105E-04 0.280E-04 0.470E-05 0.690E-06 0.557E-06 1988290 12444671 3602 1680 -29.90  
 4.27 -9.71 32.25 6.24 2.03 0.206E-03 0.448E-04 0.413E-04 0.108E-04 0.280E-04 0.434E-05 0.744E-06 0.566E-06 1988290  
 12456671 3602 1692 -30.73 3.07 -10.82 33.07 5.41 2.38 0.233E-03 0.594E-04 0.240E-04 0.944E-05 0.455E-04 0.423E-05 0.897E-06  
 0.579E-06 1988290 12468671 3602 1704 -33.26 2.60 -12.48 35.85 4.81 2.41 0.233E-03 0.535E-04 0.368E-04 0.119E-04 0  
 .455E-04 0.689E-05 0.897E-06 0.581E-06 1988290 12480671 3602 1716 -34.10 2.56 -11.69 36.42 5.12 2.11 0.115E-03 0.3  
 82E-04 0.368E-04 0.123E-04 0.241E-04 0.578E-05 0.744E-06 0.561E-06 1988290 12492671 3602 1728 -33.15 0.89 -10.02 34.87  
 4.44 1.73 0.115E-03 0.397E-04 0.163E-04 0.935E-05 0.250E-04 0.484E-05 0.744E-06 0.569E-06 1988290 12504671 3602 1740  
 -33.86 0.74 -11.03 35.87 5.01 2.47 0.197E-03 0.449E-04 0.340E-04 0.969E-05 0.250E-04 0.468E-05 0.772E-06 0.573E-06  
 1988290 12516671 3602 1752 -34.81 1.17 -10.84 36.71 4.80 2.44 0.197E-03 0.472E-04 0.340E-04 0.942E-05 0.179E-04 0.444E-05 0  
 .801E-06 0.569E-06 1988290 12528671 3602 1764 -32.80 2.82 -9.52 34.56 5.67 3.35 0.120E-03 0.449E-04 0.130E-04 0.8  
 17E-05 0.179E-04 0.363E-05 0.801E-06 0.566E-06 1988290 12540671 3602 1776 -30.97 3.57 -9.82 32.91 5.12 3.23 0.135  
 E-03 0.459E-04 0.103E-04 0.780E-05 0.260E-04 0.382E-05 0.665E-06 0.559E-06 1988290 12552671 3602 1788 -31.34 3.40 -10.4  
 3 33.33 3.61 2.08 0.135E-03 0.468E-04 0.170E-04 0.902E-05 0.260E-04 0.524E-05 0.665E-06 0.554E-06 1988290 12564671 36  
 02 1800 -32.93 4.60 -11.48 35.46 5.14 2.32 0.135E-03 0.460E-04 0.170E-04 0.917E-05 0.107E-03 0.987E-05 0.640E-06 0.550E-06



Pioneer Venus

PIONEER VENUS 1

2-MIN OVERLAPPED AVG, EVERY MIN.

78-051A-12G, 13D PSFP-00053

THIS DATA SET HAS BEEN RESTORED. THERE WERE ORIGINALLY 43 9-TRACK, 1600 BPI TAPES, WRITTEN IN ASCII. THERE ARE 22 RESTORED TAPES WRITTEN IN ASCII. THE DR TAPES ARE 3480 CARTRIDGES AND THE DS TAPES ARE 9-TRACK, 6250 BPI. THE TAPES ARE NOT IN TIME SEQUENTIAL ORDER. THE ORIGINAL TAPES WERE CREATED ON AN IBM 360 COMPUTER AND WERE RESTORED ON AN IBM 9021 COMPUTER. THE DR AND DS NUMBERS ALONG WITH THE CORRESPONDING D NUMBERS AND TIME SPANS ARE AS FOLLOWS:

DR#	DS#	DD#	FILES	TIME SPAN
DR006220	DS006220	D072906	1-26	12/06/78 - 12/31/78
		D072907	27-116	01/01/79 - 03/31/79
		D072908	117-217	04/01/79 - 06/30/79
DR006221	DS006221	D072909	92	07/01/79 - 09/30/79
DR006222	DS006222	D072910	1-92	10/01/79 - 12/31/79
		D072911	93-183	01/01/80 - 03/31/80
		D072912	184-274	04/03/80 - 06/30/80
DR006223	DS006223	D072913	1-92	07/02/80 - 09/30/80
		D072914	93-184	10/01/81 - 12/31/81
		D072915	185-274	12/31/81 - 03/31/82
DR006224	DS006224	D072916	1-91	04/01/82 - 06/30/82
		D072917	92-183	07/01/82 - 09/30/82
		D072918	184-275	09/29/82 - 12/31/82
DR006225	DS006225	D072919	1-90	01/01/83 - 03/31/83
		D072920	91-181	04/03/83 - 06/30/83
		D072921	182-273	07/04/83 - 09/30/83
DR006226	DS006226	D072922	1-92	10/02/83 - 12/31/83
		D072923	93-183	01/01/84 - 03/31/84
		D072924	184-274	04/02/84 - 06/30/84
DR006227	DS006227	D072925	1-92	07/01/84 - 09/30/84
		D074165	93-183	09/29/80 - 12/31/80
		D074166	184-274	01/01/81 - 03/31/81
DR006228	DS006228	D074167	1-91	04/01/81 - 06/30/81
		D074168	92-183	06/30/81 - 09/30/81

## PIONEER VENUS 1

78-051A-12G

DR#	DS#	DD#	FILES	TIME SPAN
DR006229	DS006229	D079502	1-90	01/01/85 - 03/31/85
		D079503	91-182	10/02/84 - 12/31/84
		D079504	183-273	04/01/85 - 06/30/85
DR006230	DS006230	D079505	1-92	07/01/85 - 09/30/85
		D079506	93-184	10/01/85 - 12/31/85
		D079507	185-274	01/01/86 - 03/31/86
DR006231	DS006231	D079508	1-91	04/01/86 - 05/30/86
		D101570	92-275	07/01/86 - 12/31/86
DR006232	DS006232	D101571	181	01/01/87 - 06/30/87
DR006233	DS006233	D101572	184	07/01/87 - 12/31/87
DR006234	DS006234	D101573	1-182	01/01/88 - 06/30/88
		D101574	183-366	07/01/88 - 12/31/88
DR006235	DS006235	D101575	181	01/01/89 - 06/30/89
DR006236	DS006236	D101576	184	07/01/89 - 12/31/89
DR006237	DS006237	D101577	181	01/01/90 - 06/30/90
DR006238	DS006238	D101578	184	07/01/90 - 12/31/90
DR006239	DS006239	D101579	181	01/01/91 - 06/30/91
DR006240	DS006240	D101580	184	07/01/91 - 12/31/91
DR006241	DS006241	D101581	282	01/01/92 - 10/08/92

PIONEER VENUS 1

2 MINUTE OVERLAPPED AVERAGES, EVERY MINUTE

78-051A-12G/13D

THESE TAPES ARE ADDITIONS TO THE OTHER 24 9-TRACK TAPES, TOTAL  
-ING 36 TAPES FOR THIS DATASET. THESE 12 TAPES ONLY, ARE STORED  
AT 6250 BPI. THE D AND C NUMBERS ALONG WITH THEIR TIME SPANS ARE  
AS FOLLOWS:

D#	C#	TIMESPANS	FILES
D-101570	C-031196	07/01/86-12/31/86	184
D-101571	C-031197	01/01/87-06/30/87	181
D-101572	C-031198	07/01/87-12/31/87	184
D-101573	C-031199	01/01/88-06/30/88	182
D-101574	C-031200	07/01/88-12/31/88	184
D-101575	C-031201	01/01/89-06/30/89	181
D-101576	C-031202	07/01/89-12/31/89	184
D-101577	C-031203	01/01/90-06/30/90	181
D-101578	C-031204	07/01/90-12/31/90	184
D-101579	C-031205	01/01/91-06/30/91	181
D-101580	C-031206	07/01/91-12/31/91	184
D-101581	C-031207	01/01/92-10/08/92	282

REQ. AGENT

DHG  
SAR

RAND NO.

V0326  
V0337

ACQ. AGENT

HKH  
HKH

PIONEER VENUS 1

2 MINUTE OVERLAPPED AVERAGES, EVERY MINUTE

78-051A-12G,13D

This data set consists of 24 9-track tapes. The data is stored at 1600 BPI in ASCII, with a blocking factor of 30 logical records per block. The first block contains data headers, the fortran format, and data fill. Each file contains 24 hours of data. The tapes were created on an ibm 360 computer. The 'D' and 'C' numbers and time spans are as follows:

<u>D #</u>	<u>C #</u>	<u>Time Span</u>	<u># Files</u>
D-72906	C-25666	12/06/78 - 12/31/78	26
D-72907	C-25667	01/01/79 - 03/31/79	90
D-72908	C-25668	04/01/79 - 06/30/79	91
D-72909	C-25669	07/01/79 - 09/30/79	92
D-72910	C-25670	10/01/79 - 12/31/79	92
D-72911	C-25671	01/01/80 - 03/31/80	91
D-72912	C-25672	04/01/80 - 06/30/80	91
D-72913	C-25673	07/01/80 - 09/30/80	92
D-74165	C-26151	10/01/80 - 12/31/80	92
D-74166	C-26152	01/01/81 - 03/31/81	90
D-74167	C-26153	04/01/81 - 06/30/81	91
D-74168	C-26154	07/01/81 - 09/30/81	92
D-72914	C-25674	10/01/81 - 12/31/81	92
D-72915	C-25675	01/01/82 - 03/31/82	90

D#	C#	TIMESPAN	#FILES
D-72916	C-25676	04/01/82-06/30/82	91
D-72917	C-25677	07/01/82-09/30/82	92
D-72918	C-25678	10/02/82-12/31/82	92
D-72919	C-25679	01/01/83-03/31/83	90
D-72920	C-25680	04/01/83-06/30/83	91
D-72921	C-25681	07/01/83-09/30/83	92
D-72922	C-25682	10/01/83-12/31/83	92
D-72923	C-25683	01/01/84-03/31/83	91
D-72924	C-25684	04/01/84-06/30/84	91
D-72925	C-25685	07/01/84-09/30/84	92
D-79502	C-27759	01/01/85-03/31/85	90
D-79503	C-27760	10/01/84-12/31/84	92
D-79504	C-27761	04/01/85-06/30/85	91
D-79505	C-27762	07/01/85-09/30/85	92
D-79506	C-27763	10/01/85-12/31/85	92
D-79507	C-27764	01/02/86-03/31/86	90
D-79508	C-27765	04/01/86-05/30/86	91

Rec'd with additional  
12 tapes

September 8, 1993

↑  
Enclosed in this package are 12 more Pioneer Venus Orbiter OMAG and OEFD Summary Tapes. These tapes are in the same format as the previous ones that we have sent to you. The tapes cover the time periods from:

1986	Jul 1 0000	- 87	Jan 01 0000	orbits 2765	- 2947
1987	Jan 1 0000	- 87	Jun 30 2359	orbits 2948	- 3128
1987	Jul 1 0000	- 88	Jan 01 0000	orbits 3129	- 3312
1988	Jan 1 0000	- 88	Jun 30 2359	orbits 3313	- 3494
1988	Jul 1 0000	- 89	Jan 01 0000	orbits 3495	- 3678
1989	Jan 1 0000	- 89	Jun 30 2359	orbits 3679	- 3859
1989	Jul 1 0000	- 90	Jan 01 0000	orbits 3860	- 4043
1990	Jan 1 0000	- 90	Jun 30 2359	orbits 4044	- 4224
1990	Jul 1 0000	- 91	Jan 01 0000	orbits 4225	- 4408
1991	Jan 1 0000	- 91	Jun 30 2359	orbits 4409	- 4589
1991	Jul 1 0000	- 92	Jan 01 0000	orbits 4590	- 4473
1992	Jan 1 0000	- 92	Oct 08 2359	orbits 4474	- 5055

If you have any questions please contact:

M. Kniffin  
Institute of Geophysics  
and Planetary Physics  
UCLA  
Los Angeles, CA 90024  
(310) 206-9955

SPAN ADDRESS: BRUNET::MURIEL  
INTERNET: [muriel@igpp.ucla.edu](mailto:muriel@igpp.ucla.edu)

↑

↑

Documentation for the Pioneer Venus Orbiter OMAG and OEFD Summary Tapes

These tapes contain two minute overlapped averages, with one minute centers, of the PVO magnetometer and electric field sensor experiments, OMAG and OEFD. Also included are spacecraft position and attitude data. The tapes contain data from the entire orbit of PVO and so contain both IMF and periapsis data. During orbit 3602 the spin-plane magnetometer sensors failed, and so after this orbit the magnetic field data columns contain only the Bz component. We receive 3 values for the P-sensor (Bz) rather than 1 value for Bx, By and Bz. Due to this, the columns for Bx, By and Bz are all flags. Bz is a 2 minute overlapped average of the 3 p-sensor values in Spacecraft coordinates.

The tapes were created using the ASCII format described in the "Pioneer Venus Mission Instructions for Data Submissions to the National Space Science Data Center". This should be referred to for general format information. These tapes are standard 1/2 inch, 9 track, unlabeled, ASCII, with fixed length blocked records. The blocksize is 7800 bytes, and the logical record length is 260 bytes. Thus there are 30 records per block.

As specified in the "Pioneer Venus Mission Instructions for Data Submissions to the NSSDC" the first three records are information on the format of the data.

- Record #1: Format: (I3,32(1x,A4)) Gives the number of data columns in each data record (32), and 4 character descriptors for each.
- Record #2: Format: (A260) Gives the Fortran format to be used in reading each data record.
- Record #3: Fortran format is given in record #2. Contains the fill values which occur when no data is available.
- Record #4-end: Time, orbit, seconds from periapsis, data.

On these tapes records 4-30 are also flagged with the fill values, and records 31 -1471 contain 24 hours of one minute data. Each 24 hours of data is then followed by a tape mark, separating the tape into files. There are two consecutive tape marks after the last file on the tape.

For more information contact:

M. Kniffin  
 Institute of Geophysics  
 and Planetary Physics  
 UCLA  
 Los Angeles, CA 90024  
 (310) 206-9955

internet: muriel@igpp.ucla.edu

\*\*\*\*\*

PVO OMAG & OEFD 1 MINUTE SUMMARY TAPE

\*\*\*\*\*

DESCRIPTION OF DATA FIELDS

HEADER TITLE	CONTENTS	FORMAT	EXAMPLE (b = blank)	FILL
	YEAR * 1000 + DAY OF YEAR	I8	b1984001	0
	MILLISECONDS OF DAY	I9	b86400000	0
	ORBIT NUMBER	I5	b1901	0
	SECONDS FROM PERIAPSIS	I6	-43200	0
BX	BX AVERAGE (GAMMAS IN VSO COORDS)	F6.1	b-40.5	999.
BY	BY AVERAGE (VSO-VENUS SOLAR ORBITAL)	"	"	"
BZ	BZ AVERAGE	"	"	"
BT	B TOTAL AVERAGE	"	"	"
VBXX	BX*BX COVARIANCE	F7.2	b100.10	"
VBXY	BX*BY COVARIANCE	"	"	"
VBXZ	BX*BZ COVARIANCE	"	"	"
VBYY	BY*BY COVARIANCE	"	"	"
VBYZ	BY*BZ COVARIANCE	"	"	"
BZZ	BZ*BZ COVARIANCE	"	"	"
.BTT	BT*BT COVARIANCE	"	"	"
NB	NUM OF HIRES MAG PTS AVERAGED	F6.0	b2880.	0.
100M	100 HZ ELEC MAXIMUM (V/(M*HZ**.5))	E9.3	b.333E-07	1.0E+32
100A	100 HZ ELEC AVERAGE	"	"	"
730M	730 HZ ELEC MAX	"	"	"

730A	730 HZ ELEC AVE	"	"	"
5.4K	5.4 KHZ ELEC MAX	"	"	"
5.4K	5.4 KHZ ELEC AVE	"	"	"
30KM	30 KHZ ELEC MAX	"	"	"
KA	30 KHZ ELEC AVE	"	"	"
JX	SC POSITION X (VEN. RADII IN	F8.3	b-13.055	999.
VSOY	Y (VSO COORDS)	"	"	"
VSOZ	Z	"	"	"
SPX	SPIN AXIS X (IN VSO COORDS)	F7.3	b-1.000	99.
SPY	Y	"	"	"
SPZ	Z	"	"	"
PLAT	PLANETARY LAT.OF SPACECRAFT (DEG)	F6.1	bb90.0	999.
PLON	PLANETARY LONG.	"	b360.0	"
SCLT	CELESTIAL LAT.OF SPACECRAFT (DEG)	"	bb90.0	"
SCLN	CELESTIAL LONG. OF S/C	"	b360.0	"
ELN	CELESTIAL LONG. OF EARTH	"	"	"
RSUN	DISTANCE TO SUN (AU)	F6.3	b1.000	9.
	TOTAL CHARACTERS -	260		

Note that the format and fill values do not need to be "hard coded" into a program, but can be read from the tape.

20 tapes

PVO Summary Tape

Generated by the UCLA Fluxgate Magnetometer Group

by

C. T. Russell

Institute of Geophysics and Planetary Physics

University of California

Los Angeles, California 90024

October 1985

12 ~~A~~  
13 —

## Introduction

The Pioneer Venus Orbiter was launched from earth on May 20, 1978 and arrived in Venus orbit on December 4, 1978. Overviews of the mission have been written by Colin (1980). Included in the instrument complement were an electric field detector measuring plasma waves in four frequency bands centered around 100 Hz, 730 Hz, 5.4 Hz and 30 kHz, and a fluxgate magnetometer measuring the magnetic field from D. C. to the Nyquist frequency of the instrument; often close to 1 Hz. These instruments have been described by Scarf et al. (1980a) and Russell et al. (1980). Measurements have been obtained almost continually from launch with the exception of a period of about one month every 19 months when Venus goes behind the sun as seen from the earth. Examples of the data obtained by these instruments can be found in papers by Scarf et al. (1980b) and Russell et al. (1981).

## Parameters on Summary Tape

The summary tapes contain two minute overlapped averages, every one minute of both the magnetometer (OMAG) and the electric field data (OEFD). In addition the tape contains the covariance matrix of magnetic field fluctuations and the maximum reading of the electric field detector in each of the channels. The magnetic field direction of the spacecraft position and the spin axis of the spacecraft are given in Venus Solar Orbital (VSO) coordinates. This coordinate system is analogous to the terrestrial GSE or Geocentric Solar Ecliptic coordinate system. The VSO X-direction points toward the sun; its Z-direction is normal to the orbital plane of Venus and its Y-direction is in the orbital plane pointing opposite to the direction of orbital motion. For purposes in which a knowledge of the field in spacecraft coordinates is needed, one can easily rotate the data using the spin axis orientation (cf. Russell, 1971). For purposes in which the sub-PVO planetary

position is important, the planetary longitude and latitude is given; for purposes in which the celestial position is important, the celestial longitude, and latitude of the spacecraft and the longitude of the earth are given, epoch 1950.0, as well as the heliocentric distance. The tapes contain data from the entire orbit of Pioneer Venus. The only data that has been removed is the daily calibration signal.

#### Tape Format

These tapes were created using the ASCII format described in "Pioneer Venus Mission Instructions for Data Submissions to the National Space Science Data Center". This document should be referenced for general tape information. The tapes are standard 1/2 inch, 9 track, 1600 BPI, unlabeled, ASCII with fixed length blocked records. The blocksize is 7800 bytes, and the logical record length is 260 bytes. Thus there are 30 records per block.

Each 24 hours of data is followed by a tape mark, separating the tape into files. The first three records of each file contain data headers, the Fortran format, and data fill as described in the NSSDC instructions. Records 4-30 of the first block are flagged with the fill values. Then each block after that is regular data (30 records = 1/2 hours of data in each block.) Thus there are 48 data blocks plus 1 header block per file. There are two consecutive tape marks after the last file on the tape. The description of the tape fields is given in Table 1.

#### Zero Levels of the Magnetometer

The amplitude of transverse waves is much greater than that of compressional waves in the interplanetary medium. Thus, the amplitude of the magnetic field usually remains roughly constant when the field direction changes. We used this

behavior to calculate the zero level of the magnetic field by solving for the zero levels that kept the field magnitude most constant. Only rotations of the field direction greater than  $30^{\circ}$  within a 2-hour period were used. Each month an average zero level was calculated as well as the standard deviation of this offset. Values greater than one standard deviation were discarded once the averages recalculated. The resulting spin axis zero levels are plotted in Figure 1. The slope of the least square fit to the line is 0.005 nT/yr with an initial value of 0.13 in December, 1978. These values have not been subtracted from the data.

#### Acknowledgments

The programming necessary for the production of these tapes was ably and rapidly performed by G. Maclean, and the checking of the magnetometer zero levels was performed by J. Dashkin. This work was supported by NASA contract NAS2-9491.

#### References

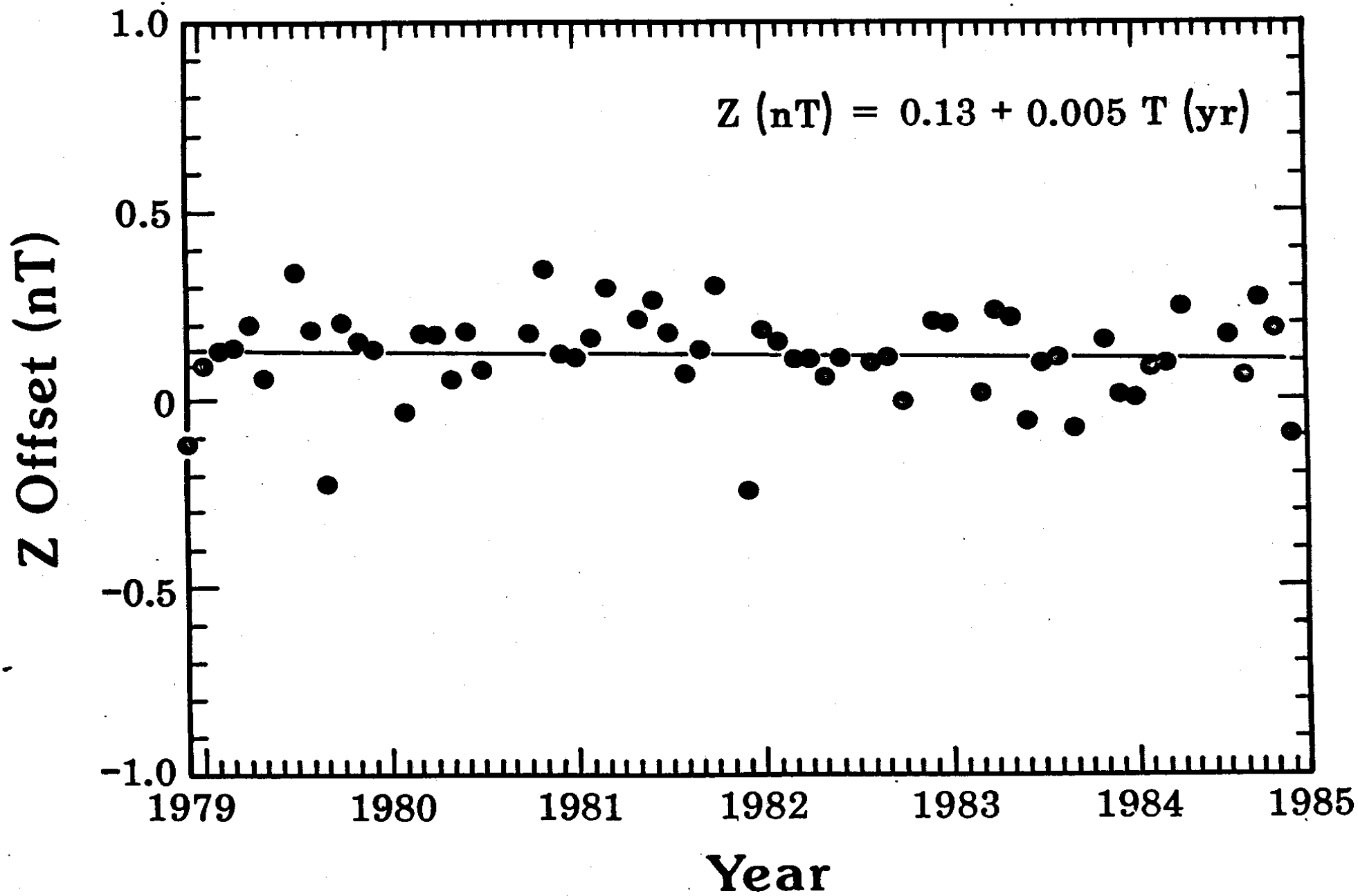
- Colin, L., The Pioneer Venus program, J. Geophys. Res., 85, 7575-7598, 1980.
- Russell, C. T., Geophysical coordinate transformations, Cosmic Electrodynamics (2), 184, 1971.
- Russell, C. T., R. C. Snare, J. D. Means, and R. C. Elphic, Pioneer Venus orbiter fluxgate magnetometer, IEEE Trans. Geosci. Remote Sensing GE-18, 32-35, 1980.
- Russell, C. T., J. G. Luhmann, R. C. Elphic, and F. L. Scarf, The distant bow shock and magnetotail of Venus: Magnetic field and plasma wave observations, Geophys. Res. Lett., 8, 843-846, 1981.
- Scarf, F. L., W. W. L. Taylor and F. Virobik, The Pioneer Venus orbiter plasma wave investigation, IEEE Trans. Geosci. Remote Sensing GE-18, 36, 1980a.
- Scarf, F. L., W. W. L. Taylor, C. T. Russell, and R. C. Elphic, Pioneer Venus plasma wave observations: The solar wind-Venus interaction, J. Geophys. Res., 85, 7599-7612, 1980b.

## DESCRIPTION OF DATA FIELDS

HEADER TITLE	CONTENTS	FORMAT	EXAMPLE (b = blank)	FILL
	YEAR * 1000 + DAY OF YEAR	I8	b1984001	0
	MILLISECONDS OF DAY	I9	b86400000	0
	ORBIT NUMBER	I5	b1901	0
	SECONDS FROM PERIAPSIS	I6	-43200	0
BX	BX AVERAGE (GAMMAS IN VSO COORDS)	F6.1	b-40.5	999.
BY	BY AVERAGE (VSO=VENUS SOLAR ORBITAL)	"	"	"
BZ	BZ AVERAGE	"	"	"
BT	B TOTAL AVERAGE	"	"	"
VBXX	BX*BX COVARIANCE	F7.2	b100.10	"
VBXY	BX*BY COVARIANCE	"	"	"
VBXZ	BX*BZ COVARIANCE	"	"	"
VBYY	BY*BY COVARIANCE	"	"	"
VBYZ	BY*BZ COVARIANCE	"	"	"
VBZZ	BZ*BZ COVARIANCE	"	"	"
VBTT	BT*BT COVARIANCE	"	"	"
NB	NUM OF HIRES MAG PTS AVERAGED	F6.0	b2880.	0.
100M	100 HZ ELEC MAXIMUM (V/(M*HZ**.5))	E9.3	b.333E-07	1.0E+32
100A	100 HZ ELEC AVERAGE	"	"	"
730M	730 HZ ELEC MAX	"	"	"
730A	730 HZ ELEC AVE	"	"	"
5.4K	5.4 KHZ ELEC MAX	"	"	"
5.4K	5.4 KHZ ELEC AVE	"	"	"
30KM	30 KHZ ELEC MAX	"	"	"
30KA	30 KHZ ELEC AVE	"	"	"
VSOX	SC POSITION X (VEN. RADII IN	F8.3	b-13.055	999.
VSOY	Y VSO COORDS)	"	"	"
VSOZ	Z	"	"	"
SPX	SPIN AXIS X (IN VSO COORDS)	F7.3	b-1.000	99.
SPY	Y	"	"	"
SPZ	Z	"	"	"
PLAT	PLANETARY LAT.OF SPACECRAFT (DEG)	F6.1	bb90.0	999.
PLON	PLANETARY LONG.	"	b360.0	"
SCLT	CELESTIAL LAT.OF SPACECRAFT (DEG)	"	bb90.0	"
SCLN	CELESTIAL LONG. OF S/C	"	b360.0	"
ELN	CELESTIAL LONG. OF EARTH	"	"	"
RSUN	DISTANCE TO SUN (AU)	F6.3	b1.000	9.
		TOTAL CHARACTERS = 260		

Note that the format and fill values do not need to be "hard coded" into a program, but can be read from the tape.

5





```

99.00 999.00 999.00 999.00 999.00 0. .100E+33 .100E+33 .100E+33 .100E+33 .100E+33 .100E+33 .100E+33 .100E+33 999.000 999.000 999.
000 99.000 99.000 99.000 999.0 999.0 999.0 999.0 999.0 9.000 0 0 0 0 999.0 999.0 999.0 999.0 999.00 999.00 999.0
0 999.00 999.00 999.00 999.00 0. .100E+33 .100E+33 .100E+33 .100E+33 .100E+33 .100E+33 .100E+33 .100E+33 999.000 999.000 999.000
99.000 99.000 99.000 999.0 999.0 999.0 999.0 999.0 9.000 0 0 0 0 999.0 999.0 999.0 999.0 999.00 999.00 999.00 99.0
9.00 999.00 999.00 999.00 0. .100E+33 .100E+33 .100E+33 .100E+33 .100E+33 .100E+33 .100E+33 .100E+33 999.000 999.000 999.000 99.0
00 99.000 99.000 999.0 999.0 999.0 999.0 999.0 9.000 0 0 0 0 999.0 999.0 999.0 999.0 999.00 999.00 999.00 999.00
999.00 999.00 999.00 0. .100E+33 .100E+33 .100E+33 .100E+33 .100E+33 .100E+33 .100E+33 .100E+33 999.000 999.000 999.000 99.000 9
9.000 99.000 999.0 999.0 999.0 999.0 999.0 9.000 0 0 0 0 999.0 999.0 999.0 999.0 999.00 999.00 999.00 999.00 999
.00 999.00 999.00 0. .100E+33 .100E+33 .100E+33 .100E+33 .100E+33 .100E+33 .100E+33 .100E+33 999.000 999.000 999.000 99.000 99.00
0 99.000 999.0 999.0 999.0 999.0 999.0 9.000 0 0 0 0 999.0 999.0 999.0 999.0 999.00 999.00 999.00 999.00 999.00
999.00 999.00 0. .100E+33 .100E+33 .100E+33 .100E+33 .100E+33 .100E+33 .100E+33 .100E+33 999.000 999.000 999.000 99.000 99.000 99
.000 999.0 999.0 999.0 999.0 999.0 9.000 0 0 0 0 999.0 999.0 999.0 999.0 999.00 999.00 999.00 999.00 999.00 999.
00 999.00 0. .100E+33 .100E+33 .100E+33 .100E+33 .100E+33 .100E+33 .100E+33 .100E+33 999.000 999.000 999.000 99.000 99.000 99.000
999.0 999.0 999.0 999.0 999.0 9.000 0 0 0 0 999.0 999.0 999.0 999.0 999.00 999.00 999.00 999.00 999.00 999.00 999.00 9
99.00 0. .100E+33 .100E+33 .100E+33 .100E+33 .100E+33 .100E+33 .100E+33 .100E+33 999.000 999.000 999.000 99.000 99.000 99.000 999
.0 999.0 999.0 999.0 999.0 9.000 0 0 0 0 999.0 999.0 999.0 999.0 999.00 999.00 999.00 999.00 999.00 999.00 999.00 999.0
0 0. .100E+33 .100E+33 .100E+33 .100E+33 .100E+33 .100E+33 .100E+33 .100E+33 999.000 999.000 999.000 99.000 99.000 99.000 999.0 9
99.0 999.0 999.0 999.0 9.000 0 0 0 0 999.0 999.0 999.0 999.0 999.00 999.00 999.00 999.00 999.00 999.00 999.00 999.00
0. .100E+33 .100E+33 .100E+33 .100E+33 .100E+33 .100E+33 .100E+33 .100E+33 999.000 999.000 999.000 99.000 99.000 99.000 999.0 999.0
999.0 999.0 999.0 9.000 0 0 0 0 999.0 999.0 999.0 999.0 999.00 999.00 999.00 999.00 999.00 999.00 999.00 999.00 0.
.100E+33 .100E+33 .100E+33 .100E+33 .100E+33 .100E+33 .100E+33 .100E+33 999.000 999.000 999.000 99.000 99.000 99.000 999.0 999.0 999
.0 999.0 999.0 9.000 0 0 0 0 999.0 999.0 999.0 999.0 999.00 999.00 999.00 999.00 999.00 999.00 999.00 999.00 0. .100
E+33 .100E+33 .100E+33 .100E+33 .100E+33 .100E+33 .100E+33 .100E+33 999.000 999.000 999.000 99.000 99.000 99.000 999.0 999.0 999.0 9
99.0 999.0 9.000 0 0 0 0 999.0 999.0 999.0 999.0 999.00 999.00 999.00 999.00 999.00 999.00 999.00 999.00 0. .100E+33
.100E+33 .100E+33 .100E+33 .100E+33 .100E+33 .100E+33 .100E+33 999.000 999.000 999.000 99.000 99.000 99.000 999.0 999.0 999.0 999.0
999.0 9.000

```

ASCII LIST OF D64168

██████████ 7800 BYTES

```

██████████ 0 938 -7102 .4 2.0 4.8 5.3 .16 -.18 .07 .57 -.26 .17 .04 259. .418E-03 .492E-04 .120E-
04 .820E-05 .184E-05 .139E-05 .832E-06 .570E-06 3.268 3.001 2.658 .052 .006 -.999 29.4 281.4 3.3 154.0 279.1 .718 198
1182 60000 938 -7042 .1 2.6 4.4 5.2 .18 -.13 .05 .47 -.20 .13 .05 234. .418E-03 .538E-04 .120E-04 .
829E-05 .184E-05 .140E-05 .690E-06 .563E-06 3.246 2.974 2.660 .052 .006 -.999 29.6 281.3 3.3 154.0 279.1 .718 1981182
120000 938 -6982 .1 2.7 4.2 5.0 .20 -.12 -.00 .15 .00 .02 .06 235. .493E-03 .451E-04 .125E-04 .833E
-05 .178E-05 .140E-05 .690E-06 .560E-06 3.224 2.946 2.662 .052 .006 -.999 29.8 281.3 3.3 154.0 279.1 .718 1981182 1
80000 938 -6922 .3 2.7 4.2 5.0 .11 -.02 -.02 .08 -.00 .03 .04 258. .608E-03 .524E-04 .125E-04 .826E-05

```

.178E-05	.140E-05	.772E-06	.567E-06	3.202	2.919	2.663	.052	.006	-.999	30.1	281.2	3.3	154.0	279.1	.718	1981182	24000																			
0	938	-6862	.1	2.7	4.2	5.1	.63	-.15	.08	.10	-.05	.09	.08	232.	.608E-03	.534E-04	.116E-04	.816E-05	.178																	
E-05	.139E-05	.931E-06	.581E-06	3.180	2.891	2.665	.052	.006	-.999	30.3	281.1	3.3	154.0	279.1	.718	1981182	300000	9																		
38	-6802	-1.2	3.3	4.3	5.9	2.36	-.93	.77	.48	-.23	.63	.37	234.	.214E-03	.406E-04	.116E-04	.811E-05	.178E-05																		
.139E-05	.931E-06	.587E-06	3.157	2.863	2.666	.052	.006	-.999	30.5	281.0	3.3	154.0	279.1	.718	1981182	360000	938	-																		
6742	-2.2	3.6	3.8	5.8	1.20	-.36	.71	.30	.07	1.21	.80	260.	.368E-03	.414E-04	.135E-04	.821E-05	.178E-05	.13																		
9E-05	.931E-06	.580E-06	3.135	2.835	2.668	.052	.006	-.999	30.7	280.9	3.3	154.0	279.1	.718	1981182	420000	938	-6682																		
-2.2	3.1	3.0	4.9	.77	-.26	.20	.48	.22	.80	.92	234.	.368E-03	.496E-04	.135E-04	.830E-05	.178E-05	.140E-0																			
5	.801E-06	.571E-06	3.112	2.807	2.669	.052	.006	-.999	30.9	280.8	3.3	154.0	279.1	.718	1981182	480000	938	-6622	-2																	
.0	2.5	3.1	4.5	.31	.12	.12	.50	-.05	.49	.27	233.	.368E-03	.526E-04	.120E-04	.836E-05	.178E-05	.141E-05	.6																		
90E-06	.563E-06	3.089	2.778	2.670	.052	.006	-.999	31.2	280.8	3.3	154.0	279.1	.718	1981182	540000	938	-6562	-1.8																		
2.6	3.4	4.7	.20	.24	.03	.51	.04	.14	.15	232.	.781E-03	.474E-04	.130E-04	.851E-05	.184E-05	.141E-05	.716E-																			
06	.561E-06	3.066	2.750	2.671	.052	.006	-.999	31.4	280.7	3.3	154.0	279.1	.718	1981182	600000	938	-6502	-1.5	2.5																	
3.1	4.4	.28	.02	.12	.39	.11	.27	.29	233.	.781E-03	.558E-04	.130E-04	.843E-05	.184E-05	.141E-05	.801E-06	.																			
570E-06	3.043	2.721	2.672	.052	.006	-.999	31.7	280.6	3.3	154.0	279.1	.718	1981182	660000	938	-6442	-.9	2.4	3																	
.3	4.3	.68	.28	.34	.49	.13	.30	.28	260.	.781E-03	.533E-04	.125E-04	.819E-05	.184E-05	.140E-05	.966E-06	.585E																			
-06	3.020	2.693	2.672	.052	.006	-.999	31.9	280.5	3.3	154.0	279.1	.718	1981182	720000	938	-6382	-.1	2.8	3.6																	
4.6	.27	.13	.01	.36	.11	.12	.27	234.	.206E-03	.415E-04	.116E-04	.813E-05	.184E-05	.139E-05	.966E-06	.588E-06																				
2.997	2.664	2.673	.052	.006	-.999	32.1	280.4	3.3	154.0	279.1	.718	1981182	780000	938	-6322	.3	2.4	3.3	4.4																	
1.47	-.62	-.31	.75	.35	.27	.41	234.	.435E-03	.468E-04	.125E-04	.825E-05	.184E-05	.140E-05	.931E-06	.577E-06	2.																				
973	2.635	2.673	.052	.006	-.999	32.4	280.3	3.3	154.0	279.1	.718	1981182	840000	938	-6262	1.3	1.6	2.9	4.0	2																
.21	-.77	-.41	.75	.24	.19	.31	260.	.435E-03	.542E-04	.125E-04	.834E-05	.184E-05	.140E-05	.772E-06	.568E-06	2.949																				
2.606	2.673	.052	.006	-.999	32.6	280.2	3.3	154.0	279.1	.718	1981182	900000	938	-6202	1.8	1.4	2.6	3.6	.61																	
.05	.03	.28	-.02	.19	.27	232.	.435E-03	.531E-04	.120E-04	.840E-05	.178E-05	.141E-05	.665E-06	.563E-06	2.925	2.																				
577	2.674	.052	.006	-.999	32.9	280.1	3.3	154.0	279.1	.718	1981182	960000	938	-6142	1.0	1.8	2.3	3.2	.33	.																
09	.03	.27	.10	.27	.41	232.	.961E-03	.571E-04	.125E-04	.841E-05	.178E-05	.141E-05	.744E-06	.564E-06	2.901	2.547																				
2.674	.052	.006	-.999	33.1	280.0	3.3	154.0	279.1	.718	1981182	1020000	938	-6082	.9	2.1	2.1	3.2	.37	.36																	
.20	.56	.36	.44	1.04	234.	.961E-03	.625E-04	.130E-04	.833E-05	.178E-05	.141E-05	.832E-06	.574E-06	2.877	2.518	2.																				
674	.052	.006	-.999	33.4	279.9	3.3	154.0	279.1	.718	1981182	1080000	938	-6022	.5	2.7	3.1	4.5	1.74	.61	-1.0																
4	1.03	.45	1.79	2.06	234.	.473E-03	.522E-04	.130E-04	.816E-05	.184E-05	.139E-05	.966E-06	.589E-06	2.853	2.488	2.673																				
.052	.006	-.999	33.7	279.8	3.3	154.0	279.1	.718	1981182	1140000	938	-5962	-.3	3.2	4.5	5.7	1.40	.54	-.91																	
.47	-.23	.87	.27	260.	.174E-03	.426E-04	.116E-04	.812E-05	.184E-05	.139E-05	.966E-06	.586E-06	2.829	2.459	2.673	.0																				
52	.006	-.999	33.9	279.7	3.3	154.0	279.1	.718	1981182	1200000	938	-5902	-.6	3.4	4.9	6.0	.19	.10	-.03	.18																
-.09	.07	.02	234.	.454E-03	.473E-04	.125E-04	.825E-05	.184E-05	.139E-05	.931E-06	.575E-06	2.804	2.429	2.672	.052	.006	-.999	34.2	279.6	3.3	154.0	279.1	.718	1981182	1260000	938	-5842	-.3	3.7	4.7	6.0	.41	.06	-.03	.11	-
.05	.06	.02	234.	.454E-03	.540E-04	.125E-04	.830E-05	.178E-05	.139E-05	.744E-06	.565E-06	2.779	2.399	2.672	.052	.006	-.999	34.5	279.5	3.3	154.0	279.1	.718	1981182	1320000	938	-5782	-.5	3.8	4.6	6.0	.75	.06	.04	.09	-.03
6	-.999	34.5	279.5	3.3	154.0	279.1	.718	1981182	1380000	938	-5722	-1.4	3.9	4.4	6.1	.18	.04	.02	.26	-.16	.															
.04	.03	213.	.339E-03	.494E-04	.130E-04	.844E-05	.178E-05	.141E-05	.665E-06	.563E-06	2.754	2.369	2.671	.052	.006	-.999	34.7	279.4	3.3	154.0	279.1	.718	1981182	1440000	938	-5662	-2.8	3.6	3.7	6.1	1.79	.99	.50	.81	.16	.36
.05	151.	.401E-03	.499E-04	.120E-04	.792E-05	.178E-05	.137E-05	.931E-06	.578E-06	2.704	2.308	2.669	.052	.006	-.999	35																				
.3	279.1	3.3	154.0	279.1	.718	1981182	1500000	938	-5602	-1.5	3.9	4.1	6.3	4.57	1.61	1.26	.79	.40	.46	.1																
0	234.	.401E-03	.460E-04	.120E-04	.811E-05	.184E-05	.139E-05	.966E-06	.589E-06	2.679	2.278	2.668	.052	.006	-.999	35.6	2																			

79.0 3.3 154.0 279.1 .718 1981182 1560000 938 -5542 .8 4.6 4.7 6.7 1.34 .45 .32 .24 .09 .13 .09 2  
26. .174E-03 .392E-04 .120E-04 .817E-05 .184E-05 .138E-05 .966E-06 .583E-06 2.653 2.247 2.666 .052 .006 -.999 35.9 278.9  
3.3 154.0 279.1 .718 1981182 1620000 938 -5482 1.3 4.8 4.8 6.9 .17 .07 .01 .09 -.00 .04 .09 127.  
.174E-03 .407E-04 .120E-04 .815E-05 .178E-05 .138E-05 .897E-06 .579E-06 2.628 2.216 2.665 .052 .006 -.999 36.2 278.8 3  
.3 154.0 279.1 .718 1981182 1680000 938 -5422 1.5 5.3 4.9 7.4 .01 -.01 -.00 .02 .01 .01 .02 5. .174  
E-03 .521E-04 .107E-04 .776E-05 .165E-05 .133E-05 .716E-06 .586E-06 2.602 2.186 2.663 .052 .006 -.999 36.5 278.6 3.3 1  
54.0 279.1 .718 1981182 1740000 938 -5362 -1.2 4.1 5.1 6.7 .10 .08 -.03 .21 -.02 .06 .09 107. .174E-03  
.380E-04 .116E-04 .827E-05 .178E-05 .141E-05 .665E-06 .558E-06 2.576 2.155 2.661 .052 .006 -.999 36.8 278.5 3.3 154.0  
279.1 .718

\$NOP  
\$NOP  
\$NOP \*\*\*\* D1OUT1 \*\*\*  
\$EXEC TPLIST BS

D 72906

12/6/78-12/31/78

INPUT PARAMETERS ARE: AS AL 1

TAPE NO. 1 FILE NO. 1  
RECORD 1 LENGTH 7800  
32 BX BY BZ BT VBXX VBXY VBZ VBYV VBZZ VBIT NR 100M 100A 730M 730A 5.4K 5.4K 30KM  
30KA VSOX VSOY VSOZ SPX SPY SPZ PLAT PLON SCLT SCLN ELN RSUN SOURCE: PVO OMA6, OEFD PROCE  
SSED: IGPP/UCLA DATE: 85 320 NOV 16 (I8, I9, I5, I6, 4F6.1, 7F7.2, F6.0, 8E9.3, 3  
F8.3, 3F7.3, 5F6.1, F6.3)

Fortran Format

0 0 0 0 999.0 999.0 999.0 999.0 999.0 999.0 999.0 999.0  
999.00 999.00 999.00 999.00 0. .100E+33 .100E+33 .100E+33 .100E+33 .100E+33 .100E+33 .100E+33 .1  
00E+33 999.000 999.000 999.000 999.000 999.000 999.000 999.000 999.000 999.000 999.000 999.000 999.000  
0 0 999.0 999.0 999.0 999.0 999.0 999.0 999.0 999.0 999.0 999.0 999.0 999.0 999.0 999.0 999.0  
0E+33 .100E+33 .100  
99.000 99.000 999.0 999.0 999.0 999.0 999.0 999.0 9.000 0 0 0 999.0 999.0 999.0 999.0 99  
9.0 999.00 999.00 999.00 999.00 999.00 999.00 999.00 999.00 0. .100E+33 .100E+33 .100E+33 .100E+33 .100  
E+33 .100E+33 .100  
0 999.0 9.000 0 0 0 0 999.0 999.0 999.0 999.0 999.0 999.0 999.0 999.0 999.0 999.0 999.0  
0 999.00 999.00 0. .100E+33 .100E+33 .100E+33 .100E+33 .100E+33 .100E+33 .100E+33 .100E+33 .100E+33 999.0  
00 999.000 999.000 99.000 99.000 99.000 99.000 999.0 999.0 999.0 999.0 999.0 999.0 9.000 0 0  
0 999.0 999.0 999.0 999.0 999.0 999.0 999.0 999.0 999.0 999.0 999.0 999.0 999.0 999.0 999.0 999.0  
33 .100E+33 .100E+33 .100E+33 .100E+33 .100E+33 .100E+33 .100E+33 .100E+33 999.000 999.000 999.000 99.000 99.000 99.0  
00 999.0 999.0 999.0 999.0 999.0 999.0 9.000 0 0 0 999.0 999.0 999.0 999.0 999.0 999.0 999.0 999.0 9  
99.000 999.00 999.00 999.00 999.00 999.00 999.00 0. .100E+33 .100E+33 .100E+33 .100E+33 .100E+33 .100E+3  
3 .100E+33 .100E+33 999.000 999.000 999.000 999.000 99.000 99.000 99.000 999.0 999.0 999.0 999.0 999.0 9.00  
0 0 0 0 999.0 999.0 999.0 999.0 999.0 999.0 999.0 999.0 999.0 999.0 999.0 999.0 999.0 999.0 999.0  
.00 0. .100E+33 999.000 999.000 9  
99.000 99.000 99.000 99.000 999.0 999.0 999.0 999.0 999.0 999.0 999.0 999.0 9.000 0 0 0 999.0 999.0 9  
99.0 999.0 999.0 999.0 999.0 999.0 999.0 999.0 999.0 999.0 0. .100E+33 .100E+33 .100E+33  
.100E+33 .100E+33 .100E+33 .100E+33 .100E+33 .100E+33 999.000 999.000 999.000 99.000 99.000 99.000 999.0 999  
.0 999.0 999.0 999.0 9.000 0 0 0 999.0 999.0 999.0 999.0 999.0 999.0 999.0 999.0 999.0 999.0  
999.00 999.00 999.00 999.00 0. .100E+33 .100E+33 .100E+33 .100E+33 .100E+33 .100E+33 .100E+33 .100E+33 .  
100E+33 999.000 999.000 999.000 999.000 99.000 99.000 99.000 999.0 999.0 999.0 999.0 999.0 9.000 0  
0 0 999.0 999.0 999.0 999.0 999.0 999.0 999.0 999.0 999.0 999.0 999.0 999.0 999.0 999.0 999.0  
00E+33 .100E+33 .100  
0 99.000 99.000 999.0 999.0 999.0 999.0 999.0 9.000 0 0 0 999.0 999.0 999.0 999.0 999.0 999.0 999.0 9  
99.0 999.00 999.00 999.00 999.00 999.00 999.00 999.00 0. .100E+33 .100E+33 .100E+33 .100E+33 .10  
0E+33 .100E+33 .100E+33 .100E+33 .100E+33 999.000 999.000 999.000 99.000 99.000 99.000 999.0 999.0 999.0 999  
.0 999.0 9.000 0 0 0 0 999.0 999.0 999.0 999.0 999.0 999.0 999.0 999.0 999.0 999.0 999.0  
00 999.00 999.00 0. .100E+33 .100E+33 .100E+33 .100E+33 .100E+33 .100E+33 .100E+33 .100E+33 .100E+33 999.  
000 999.000 999.000 99.000 99.000 99.000 999.0 999.0 999.0 999.0 999.0 999.0 9.000 0 0  
0 999.0 999.0 999.0 999.0 999.0 999.0 999.0 999.0 999.0 999.0 999.0 999.0 999.0 999.0 999.0 999.0  
+33 .100E+33 .100E+33 .100E+33 .100E+33 .100E+33 .100E+33 .100E+33 .100E+33 999.000 999.000 999.000 99.000 99.000 99.  
000 999.0 999.0 999.0 999.0 999.0 999.0 9.000 0 0 0 999.0 999.0 999.0 999.0 999.0 999.0 999.0 999.0 999.0  
999.00 999.00 999.00 999.00 999.00 999.00 999.00 0. .100E+33 .100E+33 .100E+33 .100E+33 .100E+33 .100E+  
33 .100E+33 .100E+33 999.000 999.000 999.000 999.000 99.000 99.000 99.000 999.0 999.0 999.0 999.0 999.0 9.0  
00 0 0 0 999.0 999.0 999.0 999.0 999.0 999.0 999.0 999.0 999.0 999.0 999.0 999.0 999.0 999.0 999.0  
9.00 0. .100E+33 999.000 999.000  
999.000 99.000 99.000 99.000 999.0 999.0 999.0 999.0 999.0 999.0 999.0 999.0 9.000 0 0 0 999.0 999.0  
999.0 999.0 999.0 999.0 999.0 999.0 999.0 999.0 999.0 999.0 0. .100E+33 .100E+33 .100E+33 .100E+33  
.100E+33 .100E+33 .100E+33 .100E+33 .100E+33 .100E+33 999.000 999.000 999.000 99.000 99.000 99.000 999.0 99  
9.0 999.0 9.000 0 0 0 0 999.0 999.0 999.0 999.0 999.0 999.0 999.0 999.0 999.0 999.0 999.0 999.0  
0.00 999.00 999.00 0. .100E+33 .100E+33 .100E+33 .100E+33 .100E+33 .100E+33 .100E+33 .100E+33 .100E+33 999

filler record

.000	999.000	999.000	99.000	99.000	99.000	99.000	999.0	999.0	999.0	999.0	999.0	9.000	0	0	
0	999.0	999.0	999.0	999.0	999.00	999.00	999.00	999.00	999.00	999.00	999.00	999.00	0.	.100E+33	.100
E+33	.100E+33														
.000	999.0	999.0	999.0	999.0	999.0	9.000	0	0	0	999.0	999.0	999.0	999.0	999.0	999.0
999.00	999.00	999.00	999.00	999.00	999.00	999.00	0.	.100E+33							
+33	.100E+33														
.000	0	0	0	0	999.0	999.0	999.0	999.0	999.0	999.0	999.0	999.0	999.0	999.0	999.0
99.00	0.	.100E+33													
999.000	99.000	99.000	99.000	99.000	999.0	999.0	999.0	999.0	999.0	999.0	999.0	9.000	0	0	999.0
999.0	999.0	999.0	999.00	999.00	999.00	999.00	999.00	999.00	999.00	999.00	999.00	999.00	0.	.100E+33	.100E+33
3	.100E+33														
99.0	999.0	999.0	999.0	9.000	0	0	0	999.0	999.0	999.0	999.0	999.0	999.0	999.0	999.0
00	999.00	999.00	999.00	999.00	0.	.100E+33									
.100E+33															
000	99.000	99.000	99.000	999.0	999.0	999.0	999.0	9.000	0	0	0	999.0	999.0	999.0	999.0
999.0	999.0	999.0	999.00	999.00	999.00	999.00	999.00	999.00	999.00	999.00	999.00	999.00	0.	.100E+33	.100E+33
3	.100E+33														
99.0	999.0	999.0	999.0	9.000	0	0	0	999.0	999.0	999.0	999.0	999.0	999.0	999.0	999.0
9.00	999.00	999.00	0.	.100E+33											
9.000	999.000	999.000	99.000	99.000	99.000	999.0	999.0	999.0	999.0	999.0	999.0	999.0	999.0	9.000	0

TAPE NO. *day = 12/6*

RECORD	2	FILE NO.	1	LENGTH	7800										
1978340	1	31727	9.4	-3.8	.1	10.3	.22	.35	-.34	.88	-.37	1.75	.		
03	512.	.110E-03	.310E-04	.130E-04	.785E-05	.206E-05	.137E-05	.640E-06	.554E-06	-5.038	9.010	-			
4.426	.011	.091	-.996	-24.2	347.1	.8	90.3	73.5	.719	1978340	60000	1	31787	8.8	-
4.4	-1.0	10.3	1.22	1.65	.99	2.67	1.18	3.39	.03	466.	.153E-03	.310E-04	.130E-04		
787E-05	.199E-05	.137E-05	.640E-06	.555E-06	-5.040	9.018	-4.420	.011	.091	-.996	-24.1	347.			
1	.8	90.3	73.5	.719	1978340	120000	1	31847	8.9	-4.0	-2.3	10.3	1.28	1.98	.37
3.79	.40	1.00	.04	466.	.275E-03	.317E-04	.130E-04	.790E-05	.206E-05	.137E-05	.640E-06	.5			
55E-06	-5.042	9.027	-4.414	.011	.091	-.996	-24.1	347.1	.8	90.3	73.5	.719	1978340	1	
80000	1	31907	9.6	-.4	-1.4	10.2	.27	.09	.28	8.26	2.48	2.31	.05	465.	.27
5E-03	.317E-04	.135E-04	.789E-05	.206E-05	.137E-05	.640E-06	.555E-06	-5.044	9.035	-4.408	.011				
.091	-.996	-24.0	347.0	.8	90.3	73.5	.719	1978340	240000	1	31967	9.8	1.8	-.1	1
0.2	.28	-.51	.22	2.85	.44	1.51	.06	466.	.120E-03	.307E-04	.135E-04	.786E-05	.206		
E-05	.137E-05	.640E-06	.556E-06	-5.046	9.044	-4.402	.011	.091	-.996	-24.0	347.0	.8	90.		
3	73.5	.719	1978340	300000	1	32027	9.9	1.7	.5	10.1	.12	-.20	-.00	1.24	.1
2	.40	.06	513.	.206E-03	.312E-04	.135E-04	.780E-05	.199E-05	.137E-05	.640E-06	.556E-06	-5.0			
48	9.052	-4.396	.011	.091	-.996	-24.0	347.0	.8	90.3	73.5	.719	1978340	360000	1	3
2087	9.9	2.1	.7	10.2	.08	-.10	-.11	.48	.23	.79	.06	512.	.206E-03	.309E-	
04	.135E-04	.780E-05	.199E-05	.136E-05	.690E-06	.556E-06	-5.050	9.061	-4.390	.011	.091	-.9			
96	-23.9	347.0	.8	90.3	73.5	.719	1978340	420000	1	32147	10.0	1.7	-.2	10.3	.09
-.17	-.18	.88	.82	1.32	.04	466.	.181E-03	.309E-04	.130E-04	.783E-05	.199E-05	.136E-0			
5	.112E-05	.559E-06	-5.052	9.069	-4.384	.011	.091	-.996	-23.9	347.0	.8	90.3	73.5	.71	
9	1978340	480000	1	32207	10.1	1.0	-1.0	10.2	.05	-.03	.03	.23	-.01	.45	
.04	466.	.181E-3	.314E-04	.130E-04	.780E-05	.199E-05	.136E-05	.112E-05	.560E-06	-5.054	9.078				
-4.378	.011	.092	-.996	-23.8	347.0	.8	90.3	73.5	.719	1978340	540000	1	32267	10.1	
.7	.2	10.2	.04	-.00	-.05	.21	-.36	1.90	.03	466.	.233E-03	.316E-04	.125E-04		
.777E-05	.199E-05	.136E-05	.640E-06	.557E-06	-5.055	9.086	-4.372	.010	.092	-.996	-23.8	347			
.0	.8	90.3	73.5	.719	1978340	600000	1	32327	9.8	.2	1.6	10.0	.10	.09	-.10
.20	-.10	.20	.07	466.	.233E-03	.319E-04	.125E-04	.777E-05	.199E-05	.136E-05	.690E-06	.			
557E-06	-5.057	9.094	-4.366	.010	.092	-.996	-23.7	346.9	.8	90.3	73.5	.719	1978340		
660000	1	32387	9.8	.3	1.9	10.0	.07	.10	-.01	.28	-.01	.05	.07	465.	.2
33E-03	.311E-04	.135E-04	.779E-05	.199E-05	.136E-05	.690E-06	.556E-06	-5.059	9.102	-4.360	.01				
0	.092	-.996	-23.7	346.9	.8	90.3	73.5	.719	1978340	720000	1	32447	10.0	.7	2.1
10.2	.02	.00	-.00	.08	.30	.05	.02	513.	.167E-03	.307E-04	.135E-04	.781E-05	.19		
9E-05	.137E-05	.640E-06	.555E-06	-5.061	9.111	-4.354	.010	.092	-.996	-23.6	346.9	.8	90		
.3	73.5	.719	1978340	780000	1	32507	10.0	.6	2.4	10.3	.04	-.03	-.03	.24	-..
03	.09	.03	513.	.197E-03	.316E-04	.130E-04	.782E-05	.206E-05	.137E-05	.640E-06	.555E-06	-5.			
063	9.119	-4.348	.010	.092	-.996	-23.6	346.9	.8	90.3	73.5	.719	1978340	840000	1	
32567	10.0	.3	2.4	10.3	.05	-.07	-.01	.51	-.13	.15	.05	465.	.197E-03	.312E	
-04	.135E-04	.777E-05	.206E-05	.136E-05	.640E-06	.555E-06	-5.065	9.127	-4.342	.010	.092	-..			
996	-23.6	346.9	.8	90.3	73.5	.719	1978340	900000	1	32627	10.2	.4	2.2	10.4	.03
.01	-.01	.44	-.19	.18	.04	466.	.153E-03	.309E-04	.135E-04	.775E-05	.199E-05	.137E-			

*first data record*

# Pioneer Venus Orbiter Neutral Gas Mass Spectrometer Experiment

HASSO B. NIEMANN, MEMBER, IEEE, J. R. BOOTH, J. E. COOLEY, R. E. HARTLE, W. T. KASPRZAK, N. W. SPENCER, S. H. WAY, D. M. HUNTEN, AND G. R. CARIIGNAN

**Abstract**—The Pioneer Venus Orbiter Neutral Mass Spectrometer (ONMS) is designed to measure the vertical and horizontal density variations of the major neutral constituents in the upper atmosphere of Venus. The mass spectrometer sensor includes a retarding potential ion source, hyperbolic quadrupole rod analyzer, and electron multiplier detector. The supporting electronic system consists of hybrid integrated circuits to reduce weight and power. The ONMS instrument was launched aboard the Pioneer Venus Orbiter on May 20, 1978, and turned on in orbit around Venus on December 4, 1978. It has operated flawlessly for over a Venus year (243 earth days) and has returned data of the composition of the major constituents in the Venus atmosphere between the altitudes of 150 and 350 km.

## INTRODUCTION

THE OBJECTIVE OF the Pioneer Venus Orbiter Neutral Mass Spectrometer (ONMS) is to measure the neutral gas composition in the upper atmosphere of Venus between the altitudes of approximately 150 km to 300 km above the surface of the planet. Particle densities are determined for all major constituents and for some isotopes, with adequate spatial resolution to determine the horizontal and vertical variations of the constituents. Measurements of these variations are important when defining the dynamical, chemical, and thermal state of the upper atmosphere. Preliminary data and their interpretation have been published [1], [2]. In this paper we describe the instrument design and the measurement techniques employed.

## MEASUREMENT TECHNIQUES

A quadrupole mass spectrometer equipped with an electron impact ion source is the sensor employed for the composition measurements. The basic instrument concept is derived from similar instruments used in the upper atmosphere of the earth from orbiting satellites [3]–[5] but incorporates a number of modifications to make it more suitable for the intended purpose. For example, a new retarding potential ion source was developed to allow direct sampling (no surface collisions) of reactive gases in the Venus atmosphere.

Manuscript received September 1, 1979.

H. B. Niemann, J. R. Booth, J. E. Cooley, R. E. Hartle, W. T. Kasprzak, N. W. Spencer, and S. H. Way are with Laboratory for Planetary Atmospheres, NASA/Goddard Space Flight Center, Greenbelt, MD 20771.

D. M. Hunten is with the Lunar and Planetary Laboratory, University of Arizona, Tucson, AZ 85721.

G. R. Carignan is with the Space Physics Research Laboratory, University of Michigan, Ann Arbor, MI 48105.

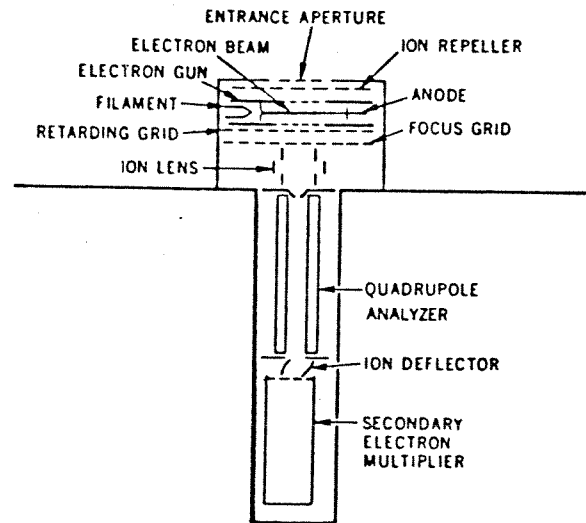


Fig. 1. Schematic cross-sectional view of the functional elements of the ONMS sensor.

A schematic diagram of the sensor is shown in Fig. 1.

The major sensor components are the ion source, the quadrupole analyzer, and a secondary electron multiplier used as an ion detector. The ion source is enclosed, but exposed directly to the ambient atmosphere through a small aperture. An ion repeller grid just inside the aperture is positively biased (approximately 40 V) to reject positive ions. The neutral particles not influenced by the ion repeller potential pass through an ionization region where a fraction is ionized by electron impact either during the first pass through the region or after being reflected once or several times from the inner surfaces. The grids enclosing the ionization region are electrically biased so that all ions produced are drawn through the retarding grid and the focusing grid to the ion lens system where an ion beam is formed by the ion lens system and directed into the quadrupole analyzer field for mass separation. The ion source structure differs considerably from conventional ion source designs, consisting of a combination of an especially structured electron beam gun and grid assembly and a strong focusing ion lens system. The grid assembly also functions as a miniaturized retarding potential analyzer for analysis of the direct streaming neutral particles.

## CLOSED SOURCE OPERATION

The relationship between the ambient particle density of a nonsurface reactive species  $n_0$  and the measured thermalized

particle density in the ionization region  $n_i$  is given by

$$\frac{n_i}{n_0} = \left(\frac{T_0}{T_i}\right)^{1/2} F(s) \quad (1)$$

and

$$F(s) = \exp(-s^2) + (\pi)^{1/2} s [1 + \operatorname{erf}(s)] \quad (2)$$

where  $s$  is the ratio of the normal component of the satellite velocity to the ion source orifice and the most probable thermal velocity of the ambient gas. The kinetic temperature of the ambient gas is  $T_0$  and the gas temperature in the ionization region is  $T_i$ .

The ambient density and temperature are unknown quantities. The vehicle velocity and the angle of attack are obtained from spacecraft data. The kinetic temperature of the gas inside the ionization chamber is essentially equal to the surface temperature of the source electrodes because the gas accommodates to the surface temperature after a few collisions. To eliminate the ambient temperature in the equation it is in principle necessary to make two independent measurements, e.g., at two different angles of attack. In practice, however, at angles of attack smaller than  $60^\circ$  the ambient temperature has only a very weak effect on the density relation, and it does not produce a measurable error in the density determination. The relationship between the particle density in the ion source  $n_i$  and the measured ion current is obtained by laboratory calibration.

The angle of attack dependence of the particle density in the ion source predicted by (1) is shown in Fig. 2. A strong mass dependent enhancement of the source particle density over the ambient particle density occurs which is accurately predictable. The weak angle of attack dependence (cosine function) makes this mode useful for measurements at large angles of attack. It also provides a sensitivity enhancement useful for constituents with low concentration. The contributions of ions coming from direct streaming particles in the focused ion beam is negligible in this mode since surface reflected particles pass the ionization region many times before leaving through the entrance aperture and therefore increase the probability of ionization accordingly.

#### OPEN SOURCE OPERATION

In the open source mode as in the closed source mode, free streaming and surface reflected particles are ionized by the electron beam in the ionization region of the source. The potentials of the electron beam enclosing grids, however, are equal, providing a field free drift space. Since the momentum of the particles is not significantly changed in the ionization process, ionized particles will continue along the path followed prior to ionization. Taking advantage of the large relative kinetic energy of the free streaming particles with respect to the probe, a retarding field caused by a positive potential applied between the retarding grid and the drift space is employed to discriminate between the surface reflected and the free streaming particles. The ions produced from thermalized surface reflected particles are rejected because their kinetic energy is too small to overcome the retarding field. The re-

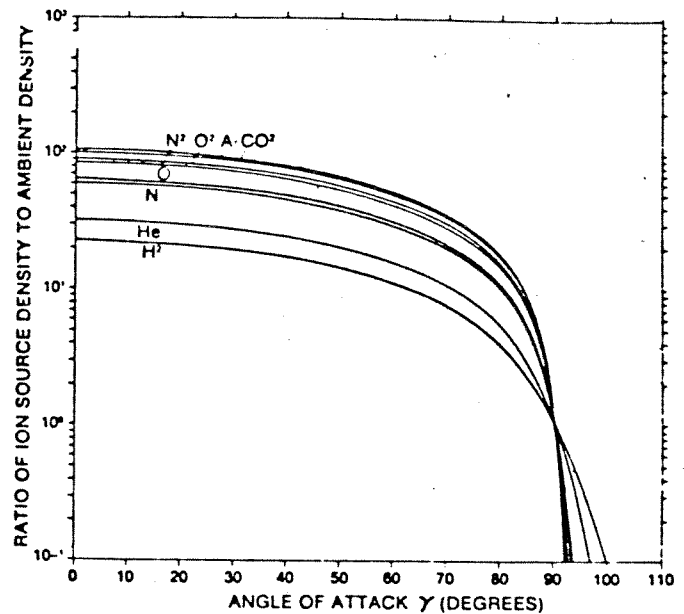


Fig. 2. The dependence of the ion source particle density on angle of attack for the closed source mode. The satellite velocity is 9.8 km/s and the ambient temperature is 300 K.

jected ions will collide with the instrument surfaces and be neutralized. Ions with enough kinetic energy to overcome the retarding field are focused by the ion lens system into the quadrupole mass analyzer for exact mass selection.

The ion current,  $I_i$ , resulting from free streaming particles can be predicted using kinetic theory

$$I_i = \left(\frac{1}{2}\right) n_0 \left[ 1 + \operatorname{erf} \left( \frac{E_\pi^{1/2} - E^{1/2}}{E_0^{1/2}} \right) \right] G \quad (3)$$

where  $E$  is the retarding energy,  $E_\pi$  is the average kinetic energy of the particle relative to the spacecraft motion,  $E_0$  is the thermal energy ( $kT_0$ ) of the ambient particles, and  $G$  is the ion source sensitivity which is determined by the electron beam current, the ionization cross section of the gas to be analyzed, and the transmission factor of the ion optics. The sensitivity is determined either by laboratory calibration using high velocity molecular beams or in flight by comparing measurements made of nonreactive species in both operating modes. The angle of attack dependence is strongly influenced by the efficiency of the ion optics. This is illustrated in Fig. 3(a) where flight data are shown for atomic oxygen measured in the open source mode over several spacecraft spin periods at periapsis. For comparison closed source data obtained for  $\text{CO}_2$  are shown for the same spin periods in Fig. 3(b).

The functional dependence of the ion current on the particle mass and the retarding energy is shown in Fig. 4. The ordinate is normalized to the ambient density, the ionizing electron beam current, and the ionization cross section. A probe velocity of 9.78 km/s normal incidence is assumed. Retarding curves for  $\text{H}_2$ , He, N, O,  $\text{N}_2$ ,  $\text{O}_2$ , Ar, and  $\text{CO}_2$  are shown in the figure. Also shown is a retarding curve (lower left hand corner) of thermal ions of 300 K kinetic temperature.

These curves illustrate that energy discrimination can easily be maintained even for very light constituents. The retarding voltages suitable for the individual masses are indicated in the

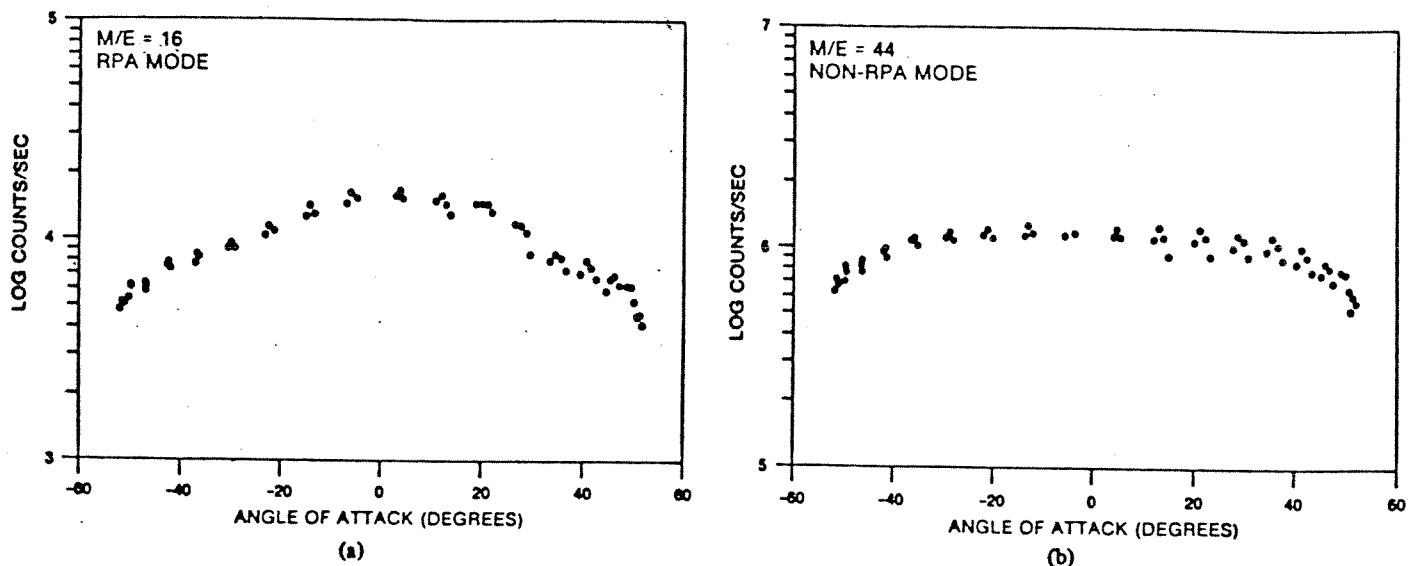


Fig. 3. (a) Atomic oxygen (mass 16) variation in the open source mode with angle of attack obtained at periapsis on orbit 186. (b) Carbon dioxide (mass 44) variation in the closed source mode with angle of attack also obtained at the same time as the data in (a).

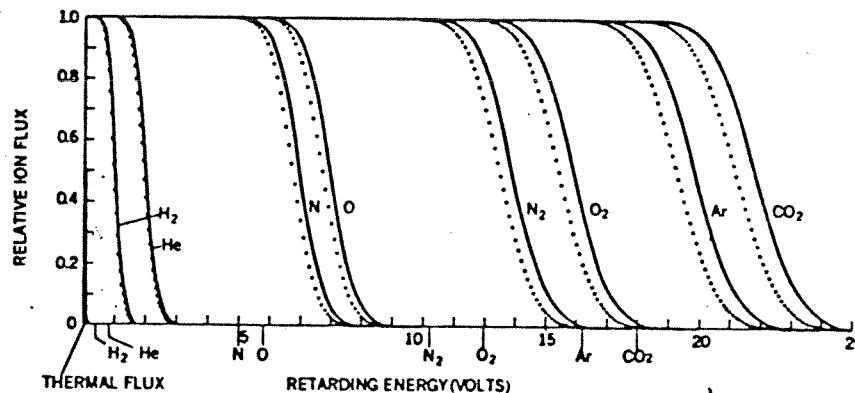


Fig. 4. The dependence of the normalized ion current on the retarding potential. Solid lines are normal incidence, dotted lines are at  $10^\circ$  angle of attack.

figure on the abscissa. They are programmed together with the bias potentials which affect mass selection in the quadrupole mass filter. The dotted curves illustrate the case when the angle of attack is  $10^\circ$ .

#### INSTRUMENT DESCRIPTION

A cross-sectional view of the sensor housing showing the arrangement of the sensor electrodes is given in Fig. 5. An exploded view indicating the mounting of the electronics boards is shown in Fig. 6, and a block diagram of the electronic system is shown in Fig. 7.

The sensor housing is thin walled stainless steel and is bakeable to  $350^\circ\text{C}$  for vacuum cleanup. A small getter pump is provided as part of the mass spectrometer housing which helped to maintain the mass spectrometer below  $10^{-6}$  torr pressure during launch preparation and cruise. The ion source is covered by a metal-ceramic break-off cap which is removed by a pyrotechnic actuator after orbit insertion. The quadrupole mass filter consists of hyperbolically contoured rods 7.5 cm long with a field radius of 0.2 cm. The rod contours are precision ground to an accuracy of 0.0002 cm. The sec-

ondary electron multiplier is a copper beryllium 14 dynode box and grid design. The electronics is packaged around the cylindrical spectrometer tube on a concentric structure fabricated from magnesium. All low power electronic components, about 80 percent of the total, are packaged in hybrid form to save weight and space. The average power consumption of the instrument is 12 W. The instrument is mounted on the spacecraft instrument platform via a wedge shaped crate with its axis pointing  $27^\circ$  off the spacecraft spin axis. This aligns the instrument axis directly with the ram direction once every spin period near periapsis. The weight of the instrument is 3.8 kg including 0.4 kg for the break-off cap assembly which was ejected after orbit insertion.

The ion source is equipped with two electron beam guns to provide redundancy in case of filament burnout. The energy of the ionizing electrons can be switched by ground command to two levels—70 eV and 27 eV. This is needed to aid in the identification of complex mass spectra by observing the fractionated mass peaks at both energy levels.

The mass peaks produced by the precision hyperbolic quadrupole rod assembly have flat tops which permit stepping from

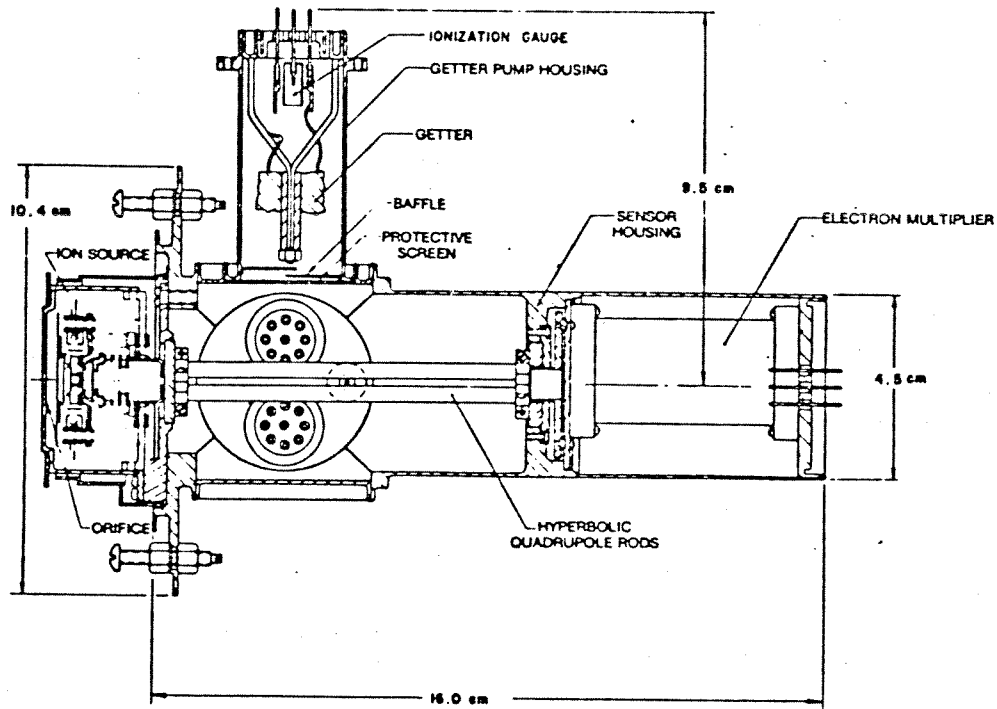


Fig. 5. Cross-sectional drawing of the mass spectrometer sensor.

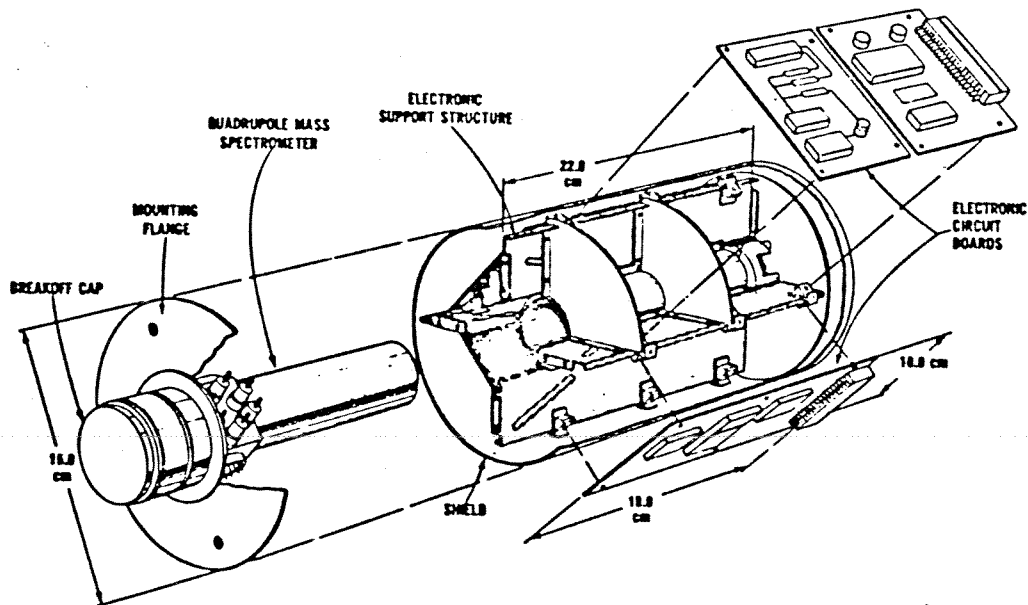


Fig. 6. Exploded view of the instrument showing the mounting of the printed circuit boards and approximate size of the instrument.

mass unit to unit without requiring peak searching. Mass selection in the quadrupole mass spectrometer is achieved through application of proper combinations of ac and dc voltages to the analyzer rods which allows transmission of ions through the analyzer with a specific mass to charge ratio only. Specific masses are selected by stepping the ac and dc voltages. Resolution is determined by the ratio of the ac amplitude to the dc potential. Preselected masses are tested in sequence by stepping the analyzer potential from mass to mass so that no measurement time or telemetry bandwidth is spent on the flanks

and in the valleys between the peaks. The experiment programmer driven by the spacecraft clock furnishes an amplitude command to the RF generator which corresponds to the selected mass. The RF generator is free running and the amplitude stability is achieved by feedback control. The mass to charge ratio (mass number) can be programmed to scan individually any 8 selected mass numbers (0 to 46 amu), to scan sequentially 0 to 46 amu at unit increments (search mode) or to scan sequentially 0 to 46  $\frac{7}{8}$  amu at  $\frac{1}{8}$  amu increments (diagnostic mode). In addition, the RPA mode can

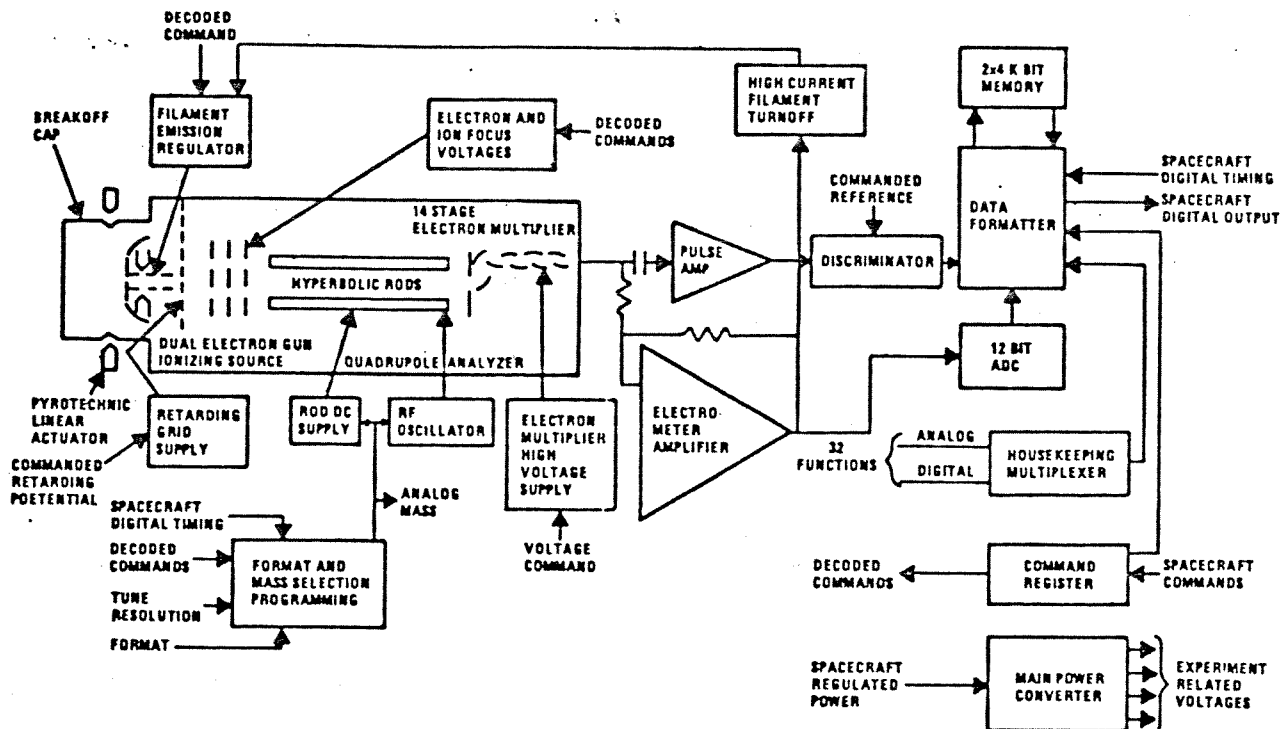


Fig. 7. Block diagram of the electronics system of the Neutral Gas Mass Spectrometer.

be set to retarding, nonretarding, or alternate for each mass number selected. Commandable options exist also to change filaments and electron energy, retarding grid potentials, tuning and resolution in the mass analyzer, secondary electron multiplier high voltage, and discriminator threshold of the pulse counter as well as to set up the various mass and RPA modes described previously.

The ions exiting the analyzer are deflected into the entrance aperture of a secondary electron multiplier by a pair of electrodes. The secondary electron multiplier operates as a charge converter and amplifier and provides a large negative charge pulse at the multiplier anode for each ion impacting the first dynode of the multiplier. The charge pulses at the anode are amplified by a wide-band pulse amplifier and counted. The count rate is proportional to the particle density in the ion source and therefore a measure of the ambient concentration of the analyzed constituent. At high signal levels where the counting system has a significant dead-time, the anode current at the multiplier is used as a measure of the ion current. The dynamic range of the instrument is greater than  $10^6$ .

The basic instrument data are the pulse counter or electrometer output for a given mass and ion source mode. Auxiliary data in the form of monitors of the more important supply voltages, currents etc. complete the telemetry output. The integration period of the pulse counter (and hence the number of samples per second) depends on spacecraft telemetry format (3 possible) and bit rate (12 possible) and is limited to a maximum of 0.172 s. The instrument samples at equally spaced intervals for all spacecraft spin phase angles or only within about  $\pm 45^\circ$  with respect to the occurrence of velocity ram. In the latter case the sampling rate is four times the normal rate and the data are read into a 4 k bit solid state

memory to be transmitted by telemetry at the normal spacecraft rate.

#### CALIBRATION

Preliminary sensor testing was done with a low energy (0-25 eV) ion beam source on a high vacuum system. The source was used to evaluate the angle of attack variation and retarding characteristics in the RPA mode. The ion beam test mode can be successfully used with the sensor filament off and the external ion repeller grids grounded since the ion source uses a nonmagnetically confined electron beam. After mating of the sensor and its flight electronics, operational parameters were finalized and a gas calibration performed over the pressure ranges expected. This established the overall relationship between the thermalized particle density in the ionizing region of the sensor and the electronics telemetry output. Gas calibration pressures for  $\text{CO}_2$ ,  $\text{O}_2$ ,  $\text{N}_2$ , A, and He were generated with an estimated error of  $\pm 2$  percent in the chamber on which the sensor was mounted. Sensitivity values for CO and NO were estimated from ionization cross sections.

The instrument has been in operation in orbit around Venus since December 4, 1978. It has yielded the first detailed data of the neutral gas composition of the upper atmosphere of Venus. The results have shown that the dual approach of retarding potential and closed source operation is an effective measurement technique.

#### ACKNOWLEDGMENT

Success of this experiment is due to the dedication and effort of many people. The authors wish to acknowledge the contributions of R. Abell, R. Aimour, R. Arvey, H. Benton, R. Farmer, R. Lott, J. McChesney, H. Mende, H. Powers, and

J. Richards of GSFC, J. Westberg of CSC, J. Huntington, J. Stafurik, and B. Powell of CSTA, B. Kennedy and J. Maurer of the University of Michigan, and V. Geraci of the General Electric Company.

## REFERENCES

- [1] H. B. Niemann, R. E. Hartle, W. T. Kasprzak, N. W. Spencer, D. M. Hunten, and G. R. Carignan, "Venus upper atmosphere neutral composition: Preliminary results from the Pioneer Venus Orbiter," *Science*, vol. 203, p. 770, 1979.
- [2] H. B. Niemann, R. E. Hartle, A. E. Hedin, W. T. Kasprzak, N. W. Spencer, D. M. Hunten, and G. R. Carignan, "Venus upper atmosphere neutral gas composition: First observations of the diurnal variations," *Science*, vol. 205, p. 54, 1979.
- [3] A. O. Nier, W. E. Potter, D. R. Hickman, and K. Mauersberger, "The open-source neutral-mass spectrometer on Atmosphere Explorer-C, -D, and -E," *Rad. Sci.*, vol. 8, no. 4, Apr. 1973.
- [4] David T. Pelz, Carl A. Reber, Alan E. Hedin, and George R. Carignan, "A neutral-atmosphere composition experiment for the Atmosphere Explorer-C, -D, and -E," *Rad. Sci.*, vol. 8, no. 4, Apr. 1973.
- [5] N. W. Spencer, H. B. Niemann, and G. R. Carignan, "The neutral-atmosphere temperature instrument," *Rad. Sci.*, vol. 8, no. 4, Apr. 1973.

## The Ionotail of Venus: Its Configuration and Evidence for Ion Escape

L. H. BRACE,<sup>1</sup> W. T. KASPRZAK,<sup>1</sup> H. A. TAYLOR,<sup>1</sup> R. F. THEIS,<sup>1</sup> C. T. RUSSELL,<sup>2</sup> A. BARNES,<sup>3</sup>  
J. D. MIHALOV,<sup>3</sup> AND D. M. HUNTEN<sup>4</sup>

The Pioneer Venus Orbiter measurements of the plasma and magnetic environment of the near tail of Venus show that the ionosphere becomes increasingly filamentary with increasing altitude, apparently forming cometlike tail rays that extend several thousand kilometers behind the planet. We call this region the ionotail of Venus. The tail rays are envisioned as plumes of high-beta plasma of ionospheric origin that are surrounded by regions of low-density, low-beta plasma. The ionotail appears to be in quasi-equilibrium, with the plasma pressure in the rays approximately balanced by the magnetic pressure of the region surrounding the rays. The magnetic field in this region is approximately sunaligned as we assume are the tail rays. Magnetic field reversals observed in the tail ray boundaries suggest the presence of strong current sheets there. Unlike the lower ionosphere whose major ion is thermal  $O^+$ , a detailed study of tail ray plasma between 2000 and 2500 km altitude shows that the major ions are superthermal  $O^+$ , with energies in the range of 9-16 eV. The electrons are much cooler, with energies of about 1 eV. A minor, more energetic ion component, having energies exceeding 40 eV is also observed within the tail rays and occasionally between the rays as well. These Pioneer Venus Orbiter measurements reveal an ionotail that is highly dynamic, a region in which solar wind induced magnetic fields configure the ionospheric structures and accelerate the ions beyond the planetary escape velocity. We estimate a total planetary  $O^+$  escape rate of  $5 \times 10^{25}$  ions/s, and we infer an  $H^+$  escape rate of about half that value, about a factor of 2 below the hydrogen escape rate due to  $H^+$  charge exchange with the hydrogen exosphere of Venus.

### INTRODUCTION

In 1979 and 1980 the Pioneer Venus Orbiter (PVO) measurements of the electron density ( $N_e$ ) by the orbiter electron temperature probe (OETP) revealed clouds of ionospheric electrons above the Venus ionosphere, apparently imbedded in the flow of magnetosheath plasma past the flanks of the planet, *Brace et al.* [1982a]. These authors offered two possible explanations for the clouds. They were either detached plasma that had been removed from the ionosphere by solar wind interactions further upstream, or they were attached plasma clouds that were stretched out into long streamers by their interaction with the tailward magnetosheath flow. The existence of such clouds of ionospheric material within the magnetosheath or the mantle suggested the possibility of a bulk removal process which could be causing the escape of planetary ions en masse. The PVO cloud observations were believed significant because they provided the opportunity to examine the more general phenomenon of solar wind interaction with isolated cold plasma clouds, perhaps providing measurements that would be useful in attempts to understand the processes responsible for the formation, acceleration and dissipation of cometary tail rays [*Russell et al.*, 1982].

Unfortunately the low latitude and altitude of periapsis in 1979 and 1980 allowed the plasma clouds to be encountered only in certain high-latitude "cloud zones" where the PVO trajectory crossed into or out of the ionosphere. Thus it was uncertain whether clouds existed only at high latitudes in the vicinity of the terminator or whether they might be present across the entire nightside. Only later, when periapsis was allowed to rise, in response to solar gravitational pertur-

bations, has it been possible to examine the global distribution of the plasma clouds. The goal of this paper is to describe the configuration and morphology of these features up to about 3000 km downstream and to estimate the planetary ion escape rate that may be associated with the dissipation and removal of the ionospheric plasma contained in them.

### OBSERVATIONS

During the past 7 earth years periapsis has risen from its initial height of about 150 km to about 2300 km, while at the same time moving from its initial latitude of  $17^\circ N$  to the equator. The orbital inclination has remained approximately fixed at  $75^\circ$  retrograde and the orbital period has been maintained at 24 hours. With the orbit plane remaining nearly fixed in inertial space, the annual movement of Venus about the sun has swept periapsis repeatedly through all local times, each year providing in situ observations at progressively higher altitudes [*Brace and Colin*, 1984] as illustrated in Figure 1. This upward spiral of periapsis has allowed the plasma instruments to map out the local time and latitude variations of the downstream ionosphere at ten different altitudes between about 150 and 2300 km. We will call this downstream region the ionotail, the region in which the ionosphere merges with the magnetotail. We first provide a statistical look at the morphology of  $N_e$  in the ionotail and, then take a detailed look at the measurements from several PVO instruments obtained during two of these downstream crossings through the ionotail.

#### *Morphology of the Ionotail*

Figure 2 illustrates the changing structure of the nightside  $N_e$  with increasing periapsis altitude as observed by the OETP [*Krehbiel et al.*, 1980]. Each panel shows three  $N_e$  snapshots taken during north to south transits within 2 hours of midnight. Although these represent only about 10% of the transits that are available for analysis, they have been selected to illustrate typical characteristics of the ionotail. The dark vertical bars along the bottom of each panel represent the region where the spacecraft was in the optical umbra of Venus, thus

<sup>1</sup>Goddard Space Flight Center, Greenbelt, Maryland.

<sup>2</sup>University of California at Los Angeles.

<sup>3</sup>Ames Research Center, Moffett Field, California.

<sup>4</sup>University of Arizona, Tucson.

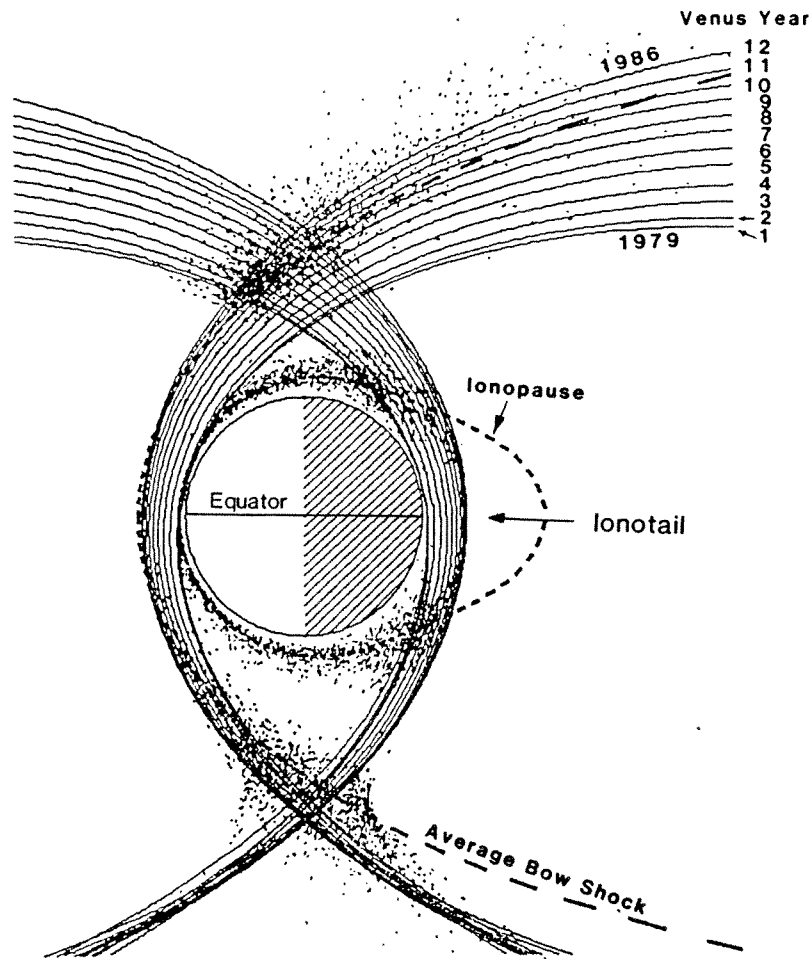


Fig. 1. The upward evolution of the PVO periapsis between 1979 (PVO year 1) and 1986 (year 12), illustrated by projecting the noon and midnight orbit tracks against a scatter plot of the bow shock and ionopause crossing locations measured by the OETP during this interval and rotated into the plane of this figure, which can be viewed as the Y-Z plane. This steady rise of periapsis through the near tail of Venus has allowed the ionotail to be explored at successively higher altitudes.

illustrating the scale size of the ionotail structure relative to the planet. The orbit numbers are given at the left, and at the right the multiplying factor used to minimize overlap of the profiles.

From Figure 2 one sees that the ionosphere becomes increasingly structured and variable above 1000 km, often exhibiting large-scale structures we will call tail rays, with smaller scale filaments superposed. The rays have dimensions of the order of  $1-3 \times 10^3$  km, decreasing in width at higher altitudes, while the filaments are of the order of tens of kilometers across. The downstream extent of these features is unknown since the orbit crosses them almost horizontally. However, they are seen over such a large altitude range that they most certainly must extend tailward at least several thousand kilometers downstream. On occasion, however, downstream passages may show densities less than  $1 \text{ cm}^{-3}$  throughout the umbra, the effective limit of the  $N_e$  measurements.

To examine typical ionotail structure in more detail, Figure 3 shows six transits from the January 1984 period when the periapsis altitude was between 1900 and 1940 km. Although the  $N_e$  structure encountered on these orbits differs greatly from day to day, there is also a degree of similarity. With some imagination, in each orbit one can see raylike structures in the form of three or more broad regions of enhanced  $N_e$  with countless smaller filaments superposed. A central tail ray

is commonly found near the equator with major tail rays on either side (north and south).

As shown in Figure 2, many of the profiles at both lower and higher altitudes exhibit similar patterns of tail rays. This lends confidence to the interpretation of these enhancements as elongated clouds or rays of ionospheric plasma that stretch out behind Venus. Although in situ measurements do not permit the three-dimensional structure of the ionotail to be captured, we envision it having a configuration more or less like the artist's conception shown in Figure 4. This figure is adapted from the earlier sketch by *Brace et al.* [1983] based on the early PVO data base which did not yet include measurements in the ionotail. To better illustrate the typical ionotail structure, the ionosphere is expanded by a factor of 2 or 3 relative to the planet and the bowshock, as are the sample orbit tracks. Our current picture of the nightside is that the tail rays and troughs map downward along the magnetic field into the ionosphere and the holes described by *Brace et al.* [1982b] based on the lower altitude PVO data from 1979-1980.

Clearly, Figure 4 should not be taken too seriously, however. It merely represents an attempt to couple the morphology of the lower ionosphere with that of the ionotail such that they reflect typical structures and scale sizes that are observed. For example, we could not distinguish between attached and

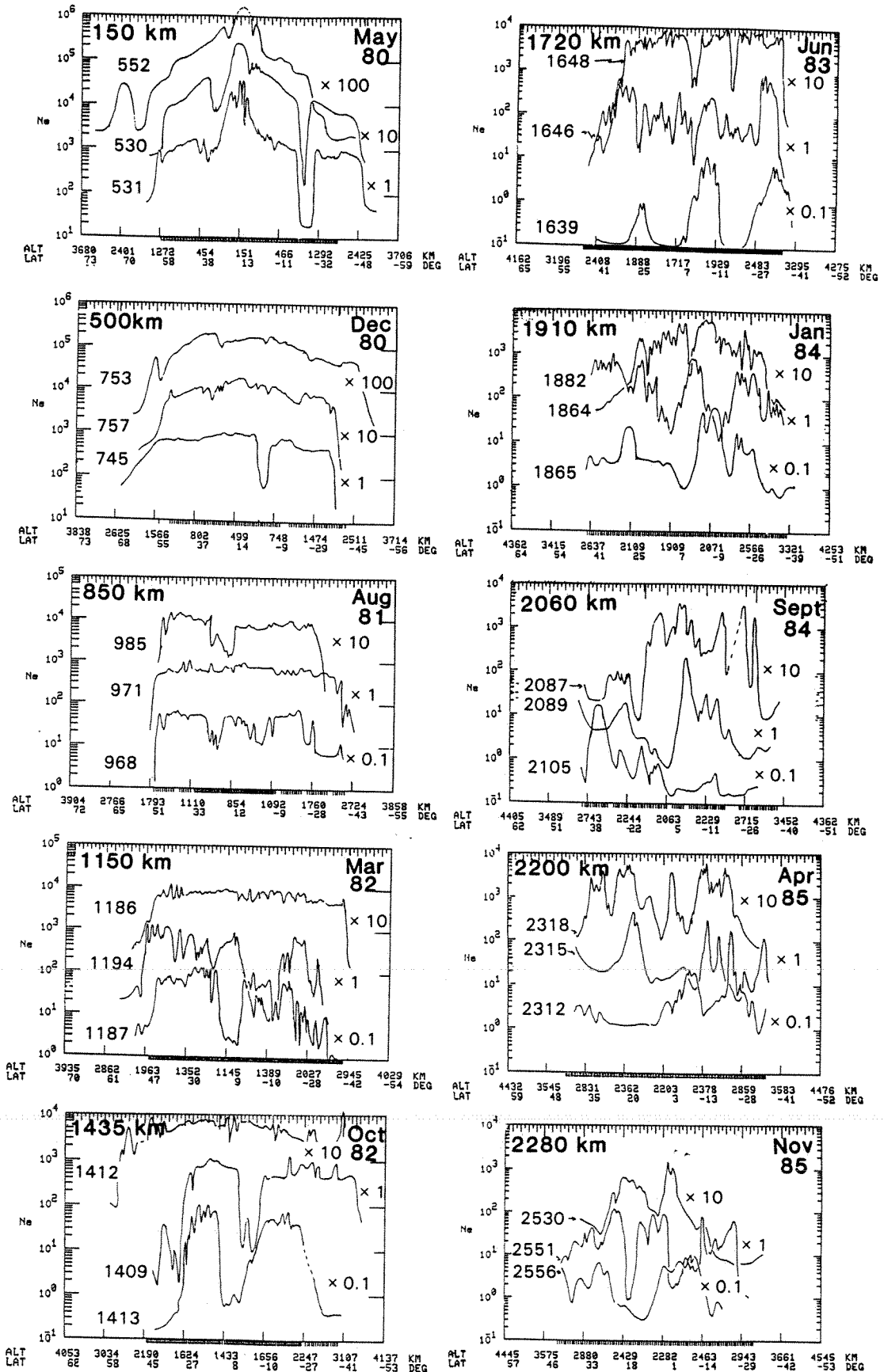


Fig. 2. Groups of three typical  $N_e$  profiles selected from ionotail passages of PVO at successively higher altitudes (periapsis altitude listed at upper left) between May 1980 and November 1985. Orbit numbers are listed at the left and multiplying factors at the right used to reduce overlap. Tail rays and filamentary structure have become more evident since early 1982 when PVO crossings of the umbra (vertical bars) rose above 1000 km.

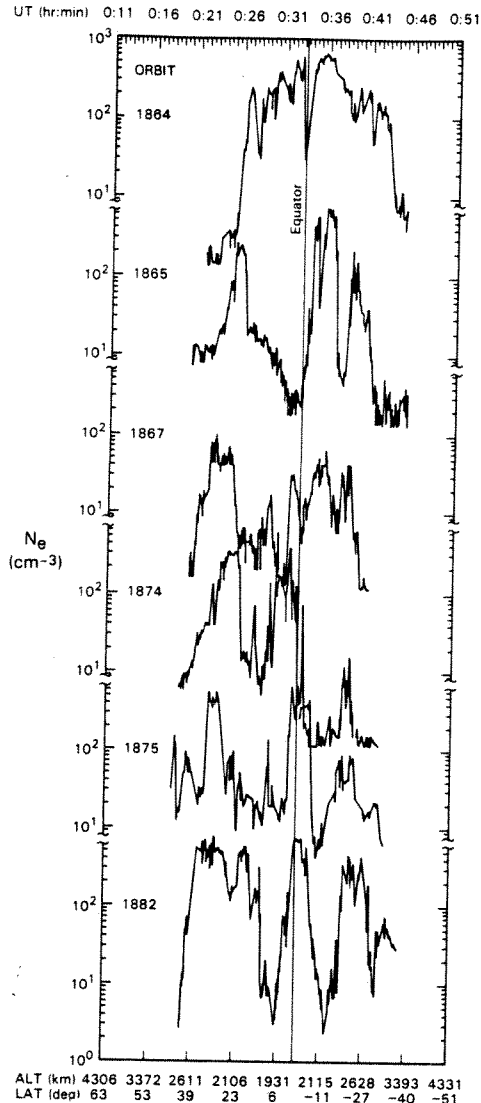


Fig. 3. A more detailed view of 6  $N_e$  profiles through the near-midnight sector of the ionotail at 2000–3000 km altitude, selected from the 30–40 ionotail passages typically available during each Venus year. The ionotail has a tendency to form a central tail ray, often with rays on either side, to the north and south. The filaments may appear superposed on the rays or in the surrounding troughs.

detached clouds, tail rays and filaments. Even if that were possible the ionotail is so highly dynamic that no single drawing could adequately describe the region. Furthermore, periapsis has taken 7 years to spiral out to its present altitude, and it is not known whether the morphological features of Figure 4 remain unchanged between 1979 and 1985, a period of declining solar activity. Continuing operations of PVO through the coming period of rising solar activity may help answer this question.

#### Detailed Look at the Ionotail

The measurements of other PVO instruments provide important insight into the tail ray formation and dissipation processes. In this section the ion mass spectrometer (OIMS) of Taylor *et al.* [1980a, b], the neutral mass spectrometer (ONMS) of Niemann *et al.* [1980], the magnetometer (OMAG) of Russell *et al.* [1980] and the plasma analyzer (OPA) described by Intriligator *et al.* [1980] are combined

with the OETP measurements to take a more detailed look at the ionotail.

The OMAG data allow us to examine the orientation of the ionotail magnetic fields and to detect the presence of currents. The OIMS can determine the densities of the thermal ionospheric ions and, with somewhat less accuracy, superthermal ions which have energies in the range of 9–16 eV which we will call  $O_{st}^+$ . More energetic ions can be detected but, in general, their concentrations and masses cannot be identified precisely. The ONMS, when operating with its filament off, measures fast ions whose energies exceed the 40 V retarding potential of an outer grid that is intended to exclude ionospheric ions [Kasprzak *et al.*, 1986]. Ions above perhaps 200 eV are not focussed by the ONMS analyzer. In this paper we will use only the major ion component and call it  $O_f^+$ . The OPA in its low-energy mode can provide information on the velocity of low energy ions in the ionotail ( $E < 250$  eV). The OETP measures the total electron density ( $N_e$ ) and temperature ( $T_e$ ). Most of the PVO instruments were not designed specifically to measure the diverse and rapidly changing plasma conditions of the ionotail, and the low data transmission rate of PVO introduces limitations in spatial resolution so we can expect increased measurement uncertainties in some regions. Used together, however, these data provide the basis for some preliminary conclusions about the nature of the ionotail and the importance of ion escape as a component of the total planetary escape rate.

Figures 5 and 6 show the PVO measurements from orbits 1875 and 1868, respectively, passages that were selected from the nighttime series of January 1984. From the top down, these figures show the three components of the magnetic field ( $B_x$ ,  $B_y$ ,  $B_z$ ) and the total magnetic field strength  $|B|$ , the total plasma density,  $N_e$ , the superthermal oxygen ion density,  $O_{st}^+$ , the fast atomic oxygen ions,  $O_f^+$ , and the electron temperature,  $T_e$ . The plasma pressure,  $P_p$ , magnetic pressure,  $P_B$ , and total pressure  $P_T$  shown in the bottom panel are discussed later.

Although many other examples of ionotail structure have been examined in similar detail, orbits 1868 and 1875 exhibit most of the salient features that are observed. Orbit 1868 is less typical than orbit 1875 but is shown to illustrate a type of behavior that is perhaps diagnostic of ionotail processes. The magnetic fields are less well organized than those found on orbit 1875, although both orbits exhibit primarily radial or tailward fields between the tail rays. Both orbits exhibit tail rays with densities in the range of 50–500  $cm^{-3}$  separated or surrounded by troughs having densities in the range of 1–10  $cm^{-3}$ . The denser rays are associated with an abrupt reversal of  $B_x$  that is taken as a signature of current flow in the ray. The largest currents actually flow in the skirts or flanks of the rays (e.g., 0035 UT in orbit 1875), but smaller currents also flow inside the ray. The magnetic field tends to be strong, steady, and x-directed in the troughs but is smaller within the tail rays themselves, particularly in the denser rays.  $T_e$  is several times higher in the troughs than in the rays, where  $T_e$  is similar to that found in the underlying ionosphere [Theis *et al.*, 1984].

Perhaps the most important characteristic of the ionotail at these altitudes is that there are very few thermal ions left. The ions in both the rays and the troughs are almost exclusively hot superthermal oxygen whose density agrees remarkably well with  $N_e$ . Superthermal  $H^+$ , if present, would not be observed owing to details of the OIMS design. Ions having ener-

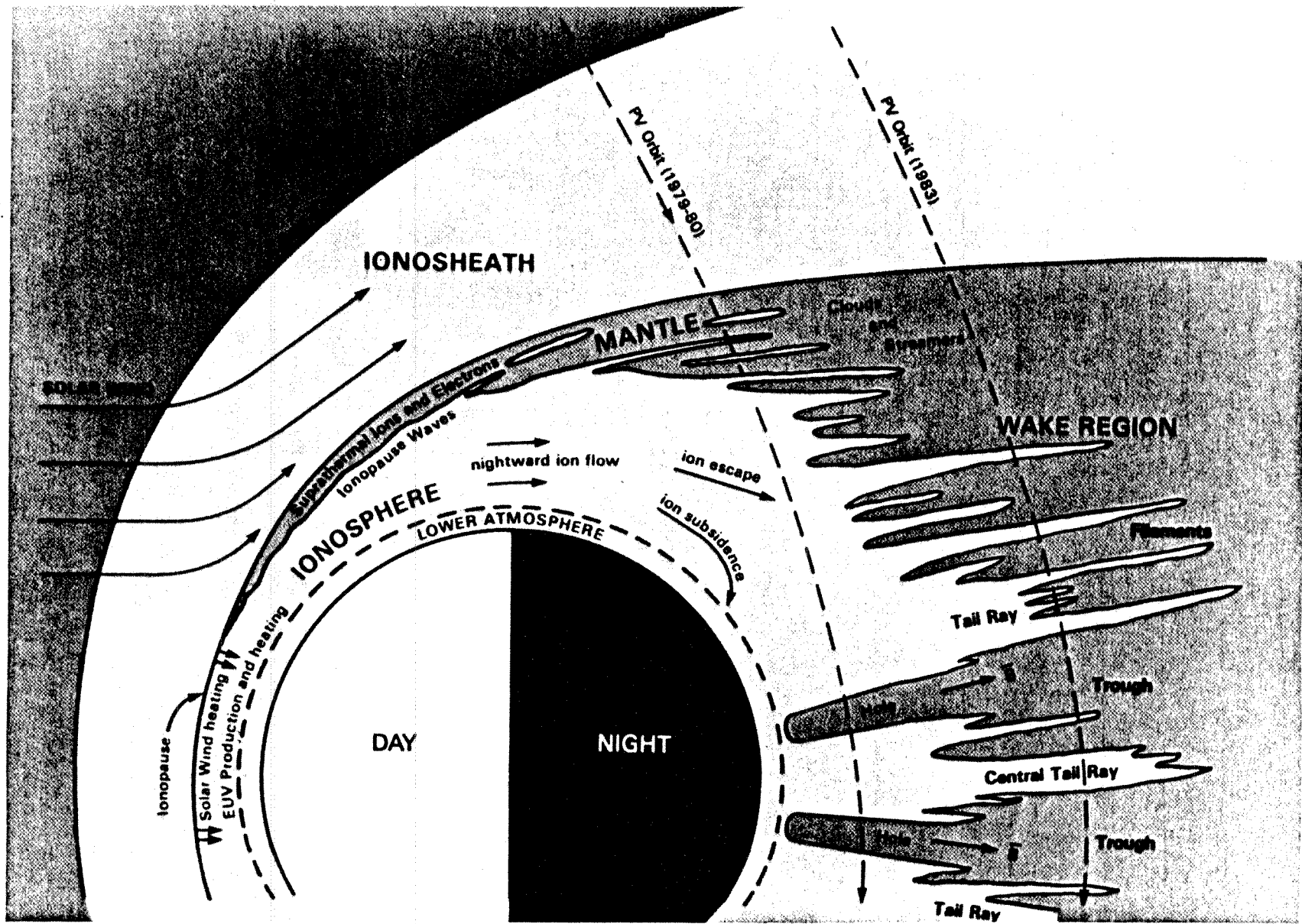


Fig. 4. A sketch illustrating the typical structure of the Venus ionotail based on hundreds of PVO crossings such as those shown in Figures 2 and 3. This drawing was adapted from an earlier sketch by *Brace et al.* [1983] who had available only low altitude measurements in the ionosphere. The scale of both the ionosphere and the sample orbits are expanded by a factor of 2 or 3 relative to the planet to allow annotation.

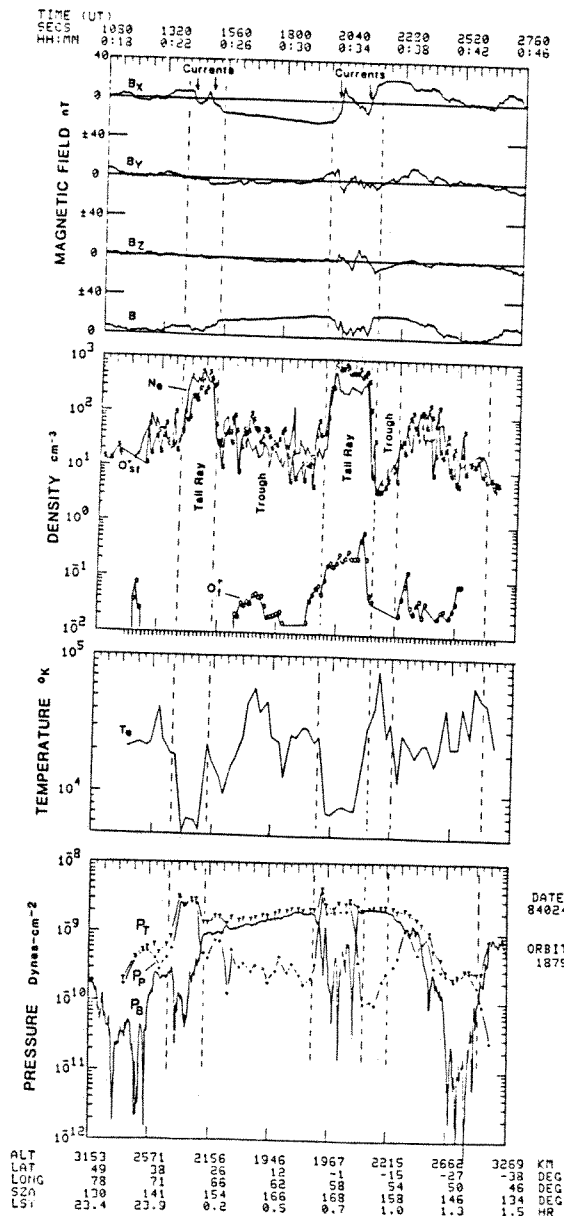


Fig. 5. The combined PVO measurements obtained during an ionotail passage on January 24, 1984. Two large tail rays and a third weak one are evident in the  $N_e$  and  $T_e$  measurements of the OETP. Superthermal ions,  $O_{st}^+$ , observed by OIMS, agree well with  $N_e$ . Smaller densities of fast ionospheric ions,  $O_i^+$ , were observed in one of the tail rays by the ONMS which measures ions with energies exceeding 40 eV.  $T_e$  is elevated in the troughs surrounding the rays. The total magnetic field,  $B$ , is lower in the rays and is strong, steady and primarily tailward,  $B_x$ , in the troughs surrounding the rays. The plasma pressure,  $P_p$ , and the magnetic pressure,  $P_b$ , are approximately in balance at the boundaries of the central ray (00.32–00.36 UT) and strong currents flow there.

gies less than about 9 eV would appear to the OIMS as cold ions, but few if any were observed in these orbits. An examination of many orbits in this series shows that the superthermals predominate in the ionotail at these altitudes, with cold ionospheric ions a minor constituent, if present at all.

Although not specifically designed for detecting ions with energies greater than a few electron volts, the OIMS senses the presence of superthermal ions by virtue of tracking the spectral shift of the appearance potential of  $O^+$  ions. Within the ambient ionosphere, the  $O^+$  ion is detected at an acceleration

potential determined according to the mass of the ion and adjusted for the effect of the spacecraft velocity in producing an effective additional kinetic energy of these ions. Cold ionospheric  $O^+$  ions appear at this prescribed acceleration potential. As the spacecraft enters a region of plasma in which the oxygen ions have energies in excess of the expected value, these ions will be detected at a lower accelerating potential, corresponding to lower mass numbers. For example, near the ionopause the ion velocities begin to increase, the relative kinetic energy of the ions increases, and the ion currents nor-

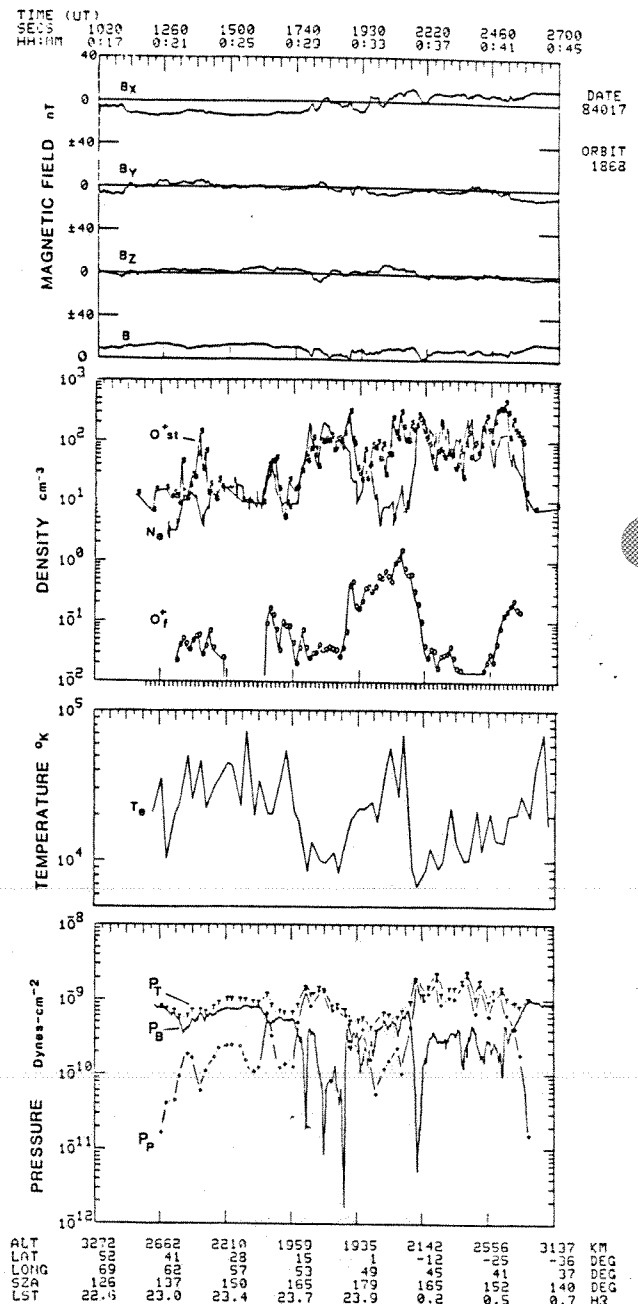


Fig. 6. A less typical ionotail crossing in which the  $O_{st}^+$  component ( $>40$  eV) is enhanced between the tail rays, rather than in the troughs, and  $O_{st}^+$  does not agree with the total density represented by  $N_e$ . Currents evident in  $B_x$  are less well defined but still appear at some of the tail ray boundaries defined by  $N_e$ . The total static pressure  $P_t$  is less uniform across the ionotail than the more typical case shown in Figure 5. This may represent a more disturbed ionotail in which dynamic pressures are acting on the plasma.

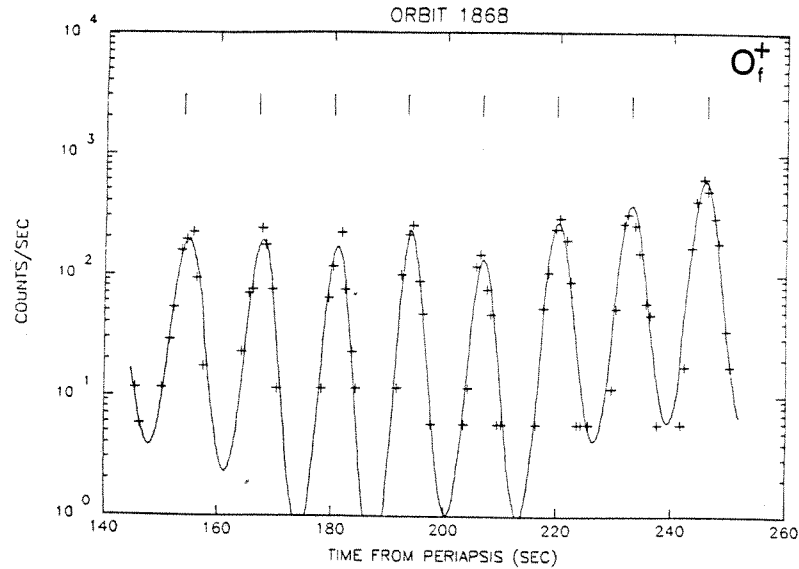


Fig. 7. Spin modulated ONMS signal for  $O_f^+$  ( $>40$  eV) obtained while crossing the fast oxygen ion enhancement within the trough between 0033–0037 UT on orbit 1868 (Figure 6). The solid curve represents a sinusoidal fit to the measurements (pluses). The  $O_f^+$  flux peaks within a few degrees of the solar direction (vertical tick marks), thus showing that the ion flow is tailward. Similar outward flows are seen on most other ionotail passages that have been analyzed in this fashion.

mally detected in the  $O^+$  “window” may be observed to decrease anomalously, in association with a corresponding increase in ion current at the next lower ion mass window, that assigned to  $N^+$ . This displacement results in an apparent increase in the nitrogen ion density, whereas in fact, the dominant  $O^+$  ions have simply shifted into the  $N^+$  position, as illustrated in Figure 4 of Taylor *et al.* [1979]. The excess kinetic energy of the detected oxygen ions is inferred from the differences in acceleration potentials of the mass windows, and for the shift of  $O^+$  into  $N^+$  this additional energy may range from a few volts up to the order of about 16 eV. As the kinetic energies of entering particles increase further and further, the ability of the OIMS to impart resonant velocities to the ions is exceeded and normal mass detection is no longer possible. Thus more energetic particles, whether ambient ions with elevated velocities or superthermal particles of some other origin, may enter the spectrometer and without being coherently resolved according to mass, stimulate currents at the ion collector.

Within the ionosphere, the evidence that ambient oxygen ions are producing the superthermal response is determined from observing the gradual shift of the dominant oxygen ions into the nitrogen ion channel. Thus, if the dominant ion current is detected in the nitrogen window and appears rather coherent, we assume the plasma to be  $O^+$  of ionospheric origin. Conversely, if incoherent highly variable ion currents were observed in many mass windows, this would indicate energies of the order of 100 eV or more. These could be either highly energized ionospheric ions or hot ions from the ionosheath. These more energetic ions are not seen in the ionotail, however.

Several factors contribute to uncertainty in determining the magnitude of the superthermal ion energy. These include the fact that the OIMS does not sense all components of entering particle velocities, nor is it calibrated for response efficiency of superthermal ion detection as a function of angle of attack of the sensor orifice relative to the spacecraft velocity vector. Also, laboratory calibrations for the efficiency of detection of

artificially shifted ions are somewhat uncertain. Consequently, the energy range of the  $O^+$  when it appears in the  $N^+$  window can only be roughly estimated, as we have done, and uncertainties of at least a few volts, high or low, are easily possible. Moreover, the high variability often encountered in the ionotail likely includes variations in the energies which we do not consider.

Another sampling characteristic of OIMS provides a clue to the pitch angle distribution of  $O_{st}^+$ , but a variety of experimental uncertainties make an accurate determination impossible at this time. The instrument accepts ions that approach from angles less than about  $40^\circ$  of the analyzer axis, which is parallel to the spacecraft spin axis, with both pointed directly southward at all times. The spacecraft velocity of 8.5 km/s and a spacecraft potential of one or two volts negative tends to further widen the acceptance angle. The nature of the PVO trajectory near periapsis is such that stationary ions will approach the analyzer with small angles of attack. The superthermal ions which dominate the ionotail express their thermal motion as gyration about the magnetic field, and any bulk motion they may have must be primarily parallel to  $\bar{B}$ . Assuming a purely tailward field, OIMS samples pitch angles between about  $50^\circ$  and  $130^\circ$ , since these lie within  $40^\circ$  of the analyzer axis. OIMS is then less sensitive to the parallel component of velocity in regions where  $B_x$  dominates. The general agreement between  $O_{st}^+$  and  $N_e$  suggests that not many of the superthermals are missed by OIMS; i.e., they must have a flat enough pitch angle distribution to bring most of them into the acceptance cone. A purely isotropic pitch angle distribution also is consistent with the general agreement in  $N_e$  and  $O_{st}^+$ , but so is a high temperature drifting Maxwellian distribution. A tailward flow of cold  $O^+$  would not be consistent with the measurements, since they would fall outside the acceptance angle of the OIMS in a tailward field.

The  $O_f^+$  ions, measured by ONMS, are a minor constituent of the tail rays. Occasionally, they may be found between the rays as in orbit 1868. Orbit 1875 shows the more typical close correlation observed between  $O_f^+$  and  $O_{st}^+$ . We should

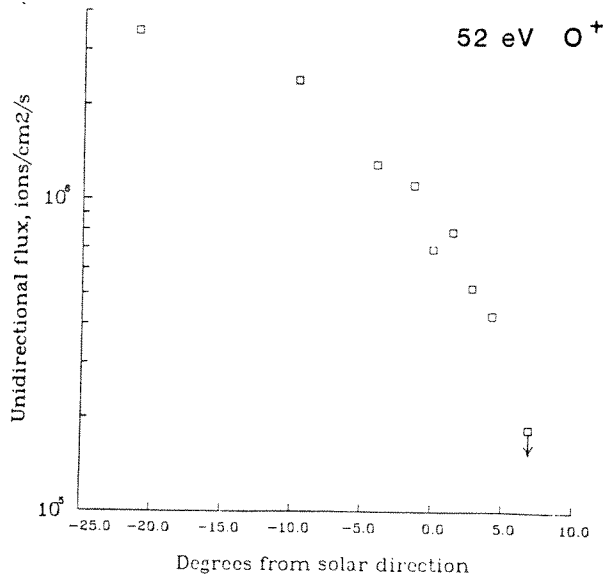


Fig. 8. Fifty-two electron volt  $O^+$  flux observed during a portion of one PVO spin cycle when the OPA instrument happened to be in a low-energy step while entering a tail ray at 00:39:11 UT on orbit 1882 (see Figure 3, the tail ray at the right).

note that the fast ions ( $>40$  eV) are not limited to  $O^+$ . All of the ions measurable by ONMS ( $O^+$ ,  $N^+$ ,  $O_2^+$ ,  $NO^+$ ,  $H_e^+$ ) may be present [Kasprzak, 1986]. The instrument was not designed to cover masses below 2, so no  $H^+$  could have been seen, although it is very likely present as it is observed as a major constituent of the ionosphere at lower altitudes [Taylor et al., 1980a, b].

An additional characteristic of ONMS is its ability to detect the direction of bulk motion of the  $O_f^+$  component. Its orifice is offset about  $26^\circ$  from the spacecraft spin axis, a feature designed to allow the sensor axis to sweep close to the spacecraft velocity vector once per spin. Stationary ions would produce a maximum influx into the spectrometer at that spin angle. Tailward bulk motion of  $O_f^+$  parallel to a tailward  $B$  field would shift the spin phase at which this maximum ion flux occurs. This shift is usually observable in the  $O_f^+$  spin modulated signal thus indicating that the  $>40$  eV ions typically have an outward or tailward component of velocity [Kasprzak et al., 1986]. Orbit 1868 at 0033–0037 UT provided an excellent example of a strong outward flow, as illustrated in Figure 7. The vertical tick marks represent the sun vector, the expected location of the maximum flux if  $O_f^+$  if the flow were purely tailward. The deviation from this antisolar flow is less than  $11^\circ$  in these seven spin cycles (approximately 84 s). A survey of many orbits shows that nearly all have significant  $O_f^+$  densities associated with tail rays, and many of these that can be fitted accurately for flow velocity exhibit generally tailward flow.

The OPA was designed and used primarily for solar wind measurement, but recently it has been used extensively in its low-energy step mode to look for superthermal ions in the near tail. The instrument inlet is mounted so as to sweep through the sun vector once per spin, which on the nightside allows it to look for ions emerging from the ionosphere. In orbit 1882 at 0038:11 UT, as it entered a tail ray while in its 52-V step, ions were observed coming generally upward with the angular distribution shown in Figure 8. The ions also had a northerly component that caused them to strike the target with a polar angle between  $23^\circ$  and  $69^\circ$ . Part of this northerly

motion comes from the spacecraft's 8.5 km/s southward velocity, but some of it may have been caused by a real equatorward component. Assuming that the ions were  $O^+$ , an energy of 52 eV corresponds to a velocity of about 25.5 km/s. These ions are in the same range of energies as observed by the ONMS, but ONMS was not in an appropriate command mode in this orbit to measure  $O_f^+$ . Unfortunately, the OPA spends little time sampling at these low energies, and the tail rays are not present everywhere, so it has not yet been possible to gain a clear picture of the occurrence frequency of these fluxes and their correlation with tail rays, but they do tend to confirm the general tailward ion flow observed regularly by the ONMS.

From the above observations we cannot uniquely describe the typical energy or velocity distribution of the ionotail ions at 2000–3000 km altitude. It seems clear that they are primarily  $O^+$  ions that have been accelerated to energies somewhere above about 9 eV, the energy required to put them above the response of the OIMS for cold thermal ions. The much smaller densities of  $O_f^+$  show that the majority have energies less than 40 eV. The approximate agreement between  $N_e$  and  $O_{st}^+$  suggests that most of the ions also fall below about 16 eV, the OIMS upper limit for unambiguous tracking of the superthermal  $O^+$  ions. But since the absolute accuracy of the OIMS conversion from ion flux to superthermal ion density is not yet well defined, it is conceivable that significant fluxes of superthermal  $O^+$  may exist at energies between 16 eV and 40 eV, where we have no firm information. In addition, superthermal  $H^+$  may be present but not detected by the OIMS. This would contribute to the total density, measured as  $N_e$ , thereby reducing the amount of  $O_{st}^+$  that could be present. Further analysis of the measurement accuracies may reduce the uncertainties involved here, but the absence of thermal ions and the existence of ions at energies above that required to escape leads us to suspect that there must be a substantial bulk flow of plasma down the tail.

This bulk plasma flow in the ionotail must be influenced by the magnetic field there. The field is large and primarily radial in the troughs surrounding the tail rays but much weaker and more variable within the rays. Figures 5 and 6 also show calculated magnetic pressures,  $P_B$ , and static plasma pressures,  $P_p$ , for the two orbits, where  $P_B = B^2/8\pi$  and  $P_p = kN_e[(T_e + T_i)/2]$ . We use the measured values also shown in Figures 5 and 6 and assume a superthermal ion temperature of 13 eV, the middle of the OIMS energy range for detection of these ions. From these calculations it is clear that the plasma pressure dominates in the denser rays and the magnetic pressure dominates in the troughs and the weaker rays. Currents flow in the edges of the rays approximately at the point where the magnetic and plasma pressures are equal. The possible significance of this will be discussed later.

#### Summary of the Observations

The primary characteristics of the Venus ionotail are summarized as follows:

1. The nightside ionosphere becomes increasingly raylike and filamentary with distance downstream. Like cometary tail rays, a central ray is a common feature, with one or more rays often arranged symmetrically on either side.
2. At altitudes in the range of 2000–2500 km, which we have examined in some detail, most of the ions are superthermal  $O^+$  with energies in the range of 9–16 eV. Virtually no cold thermal ions remain at these altitudes. Superthermal

$H^+$  is probably also present, but the PVO instruments could not detect them if present.

3. A minor, but more energetic ion component ( $E > 40$  eV) is observed in the ionotail, usually well correlated with the 9–16 eV superthermals and determined to be flowing tailward on most occasions. Ions at intermediate energies are not observable, but the approximate agreement between the superthermal ion density and the electron density is consistent with the absence of thermal ions and the low density of ions with energies greater than 40 eV. The electron temperature in the tail rays is typically less than 1 eV, not unlike that found in the underlying ionosphere.  $T_e$  is several times higher outside the rays.

4. A strong and steady tailward magnetic field dominates the trough region that surrounds the tail rays. The magnetic field is weaker in the rays and  $B_z$  reversals reveal the flow of strong currents in the edges of the rays. An approximate pressure balance exists in the ionotail, with the static plasma pressure of rays balanced by the magnetic pressure of the surrounding trough regions.

#### DISCUSSION AND INTERPRETATION

The PVO observations reported here provide a glimpse of the plasma conditions in the ionotail of Venus, the region where the ionosphere merges with the magnetotail. Although we have focussed thus far only on the plasma and magnetic conditions between 2000 and 2500 km downstream, we plan future work to examine in more detail the plasma and magnetic conditions in the ionotail at both lower and higher altitudes.

From Figures 2, 3 and 4 it is clear that we can now view the ionotail to consist of a highly dynamic system of rays and filaments of ionospheric plasma that typically stretch out several thousands of kilometers behind Venus. The orbit to orbit differences evident in Figures 2 and 3 illustrate the dynamic nature of the tail rays. Even the instrumental "snapshots" taken during a single passage may be aliased marginally by the bulk transport of the rays as they move in response to  $J \times B$  forces. Like cometary tail rays, the Venus tail rays may form at the flanks and drift toward the axis to accumulate in a central tail ray, a feature that is evident in many passages through the middle of the ionotail. The convergence of magnetosheath flow into the tail provides the force for such behavior [Mihalov et al., 1980] perhaps through the mantle plasma [Spenner et al., 1980], and viscous forces may also be involved [Perez-de-Tejada, 1980].

Other interpretations of the tail ray signatures of Figures 2, 3, 5 and 6 have been suggested to us, in particular, that the appearance of multiple rays could really be produced by a single tail ray flapping north and south at sufficiently high speed to encounter the spacecraft several times during each transit of the Venus wake. This seems highly unlikely because of the large flapping angle that would be required to move a single tail ray through the observed range of latitudes. This explanation also does not explain the predominance of a central tail ray. Furthermore, the OIMS would not measure the tail rays that overtake the spacecraft from the north, since the spacecraft shields this southward looking instrument from such ions. Tail flapping at the required velocities also would cause large discrepancies between the  $O_{st}^+$  and  $N_e$  tail ray profiles roughly half of the time, an effect that is not observed.

The approximate balance across the tail rays between the magnetic pressure and the plasma pressure suggests that the

tail rays form and move about under the control of the magnetic field which bounds them. The magnetic field in turn is configured and compressed by the magnetosheath flow and the plasma pressure of the mantle. This is perhaps analogous to the way in which the magnetic field on the dayside conveys the dynamic pressure of the solar wind to the ionosphere and thereby determines the ionopause altitude [Elphic et al., 1980; Brace et al., 1979]. If this picture is correct, we might expect to find a close correlation between the dynamic pressure of the solar wind, the mantle plasma pressure, the magnetic field strength in the ionotail, and the configuration of the ionotail itself. However, too few cases have been examined thus far to draw any firm conclusions about such a relationship.

In view of the complex structure of the ionotail, one is faced with the side issue of how to define the ionopause on the nightside of Venus. In spite of the fact that the tail rays contain primarily superthermal ions, the ions are of ionospheric origin and are usually separated by a steep  $N_e$  gradient from surrounding regions of high  $T_e$  and high magnetic pressure. This steep gradient continues to provide the most readily identified marker of the ionopause location, and we are forced to view the nightside ionopause a very complex and dynamic surface indeed.

#### Planetary Escape Flux

One of the goals of this work was to refine an earlier upper limit on the planetary ion escape rate [Brace et al., 1982a] by taking advantage of the more recent downstream PVO coverage of the ionotail and by involving the ion and neutral mass spectrometer information on the velocity of ionotail ions. The fact that essentially all of the ions observed by the OIMS and the ONMS at these altitudes have energies exceeding the escape velocity, and that the ionospheric ion  $O^+$  is by far the most abundant ion, leads us to conclude that indeed atmospheric material is escaping from the ionotail. Although  $H^+$  having similar superthermal energies cannot be measured by the OIMS, and  $H^+$  cannot be measured at all by the ONMS, it is likely that this ion is also present in the ionotail as it is a major thermal ion observed at lower altitudes, particularly on the dawnside of midnight [Taylor et al., 1980a, b]. We conclude from the general agreement between  $N_e$  and  $O_{st}^+$  that most of the ionotail ions are  $O^+$ , however, uncertainties in the conversion of OIMS currents to  $O_{st}^+$  density do not preclude a superthermal  $H^+$  population of the same order. We also conclude from this agreement, and from the low density of  $O_{st}^+$  ( $> 40$  eV), that most of the superthermals at this altitude (2000–3000 km) lie within the energy range of 9–16 eV.

Since most of the ionotail ions have velocities in the range of 9 to 16 eV, we can estimate the planetary escape rate,  $F_e$ , using our knowledge of the globally averaged  $N_e$  for the nightside ionosphere at the altitude of the observations shown in Figure 3, using the equation

$$F_e = A_c N_e v_{st}$$

where  $A_c$  is cross-sectional area of the Venus disk,  $N_e$  is average ion (electron) density across the nightside at 2000 km, and  $v_{st}$  is average velocity of the superthermals. The average  $N_e$  over the entire umbra of Venus for the orbits between 1837 and 1901, based on OETP measurements, is  $39 \text{ cm}^{-3}$ , although peak values in the tail rays are typically well over  $1 \times 10^2 \text{ cm}^{-3}$ . From the OIMS measurements we adopt an average energy of 13 eV for the superthermal  $O^+$ , corresponding to a velocity of 12.5 km/s, about 4 km/s greater than the

escape velocity at 2000 km. The resulting escape rate is  $5 \times 10^{25}$  ions/s. This represents a global mean flux of  $1 \times 10^7$   $\text{cm}^{-2} \text{s}^{-1}$ .

Two factors could upset this estimate, but we regard them as improbable. A dc electric field might exist somewhere down the tail that would reflect the superthermals and thus prevent their escape. Or the pitch angle distribution of the ions could be so flat that some of the ions do not have enough tailward velocity to escape. But, if this were so, how did they get to the altitude of 2000 km in the first place? Did they have just enough parallel velocity to reach the PVO altitude and then return to Venus? Since these possibilities seem unlikely, we assume that the ions are escaping, heated and accelerated tailward in some fashion by the magnetic field as it emerges from the nightside ionosphere.

McComas *et al.* [1986] have employed the OMAG far tail measurements to deduce the X-directed ion velocities of the magnetotail. From the calculated *JXB* forces, the plasma velocities and the MHD momentum equation, they estimated the plasma acceleration, density and temperature in the Venus tail. They also found an upper bound on the downtail mass flux of  $\sim 1 \times 10^{26}$  amu/s or  $6 \times 10^{24}$   $\text{O}^+$ /s. If all of the tail material is of planetary origin, this would also represent an upper bound for the planetary escape rate, nearly an order of magnitude smaller than the present results from the near tail.

The question arises whether such fluxes would not have been observed further downstream by the OPA instrument during apoapsis passages through the magnetotail. Mihalov and Barnes [1982] examined the OPA data from several orbits during the first swing through the tail early in 1979. They found that the  $\text{O}^+$  flux at around  $11 R_V$  downstream was always below  $10^7/\text{cm}^2 \text{s}$ , a factor of 2 or more below the average escape flux calculated here for January 1984 conditions.

The reasons for this apparent discrepancy are not immediately obvious, but a couple of factors come to mind. First, the escape rate may be variable with solar activity, but that would appear to have the wrong sign, since the OPA far tail measurements were made at solar maximum when solar wind interactions with the ionosphere might be expected to produce even larger ion pick up rates. Second, the Mihalov and Barnes [1982]  $\text{O}^+$  escape fluxes could only be measured during periods of unusually low solar wind speed because of the 300 km/s instrumental limit for detection of  $\text{O}^+$ . The acceleration process may be highly nonlinear with solar wind speed, or pressure, so that the low escape flux reported by Mihalov and Barnes may not be typical. Slavin *et al.* [1984] have noted that this instrumental characteristic may also be responsible for the apparent lack of 0–8 keV ions in the downstream plasma sheet.

A related factor which may contribute to the inability of the OPA to see most of the escaping  $\text{O}^+$  may be the slingshot effect of the magnetic field lines as they pull out of the ionosphere. If the feet of these field lines are frozen in the solar wind, which by this time has moved far downstream, the loops which have been hung up in the ionosphere have a lot of catching up to do. Once released, the field would exert *JXB* forces on the ions to accelerate them beyond the solar wind velocity in the magnetotail, making the  $\text{O}^+$  component even less likely to fall into the velocity range of the OPA for mass 16 ions.

#### *Momentum Available in the Solar Wind*

Although the nightward flow of ions across the terminator, driven by solar EUV energy, provides initial ion velocities of

1–5 km/s, most of the momentum required to produce ion escape down the tail must come from the solar wind via the IMF. If we assume that momentum can be extracted from the solar wind over an area only as large as the solid planet itself, about 25% of the momentum flux of the solar wind would be required to accelerate the ionotail ions up to the solar wind speed. However, this would ignore the fact that the IMF is frozen into the solar wind and can draw momentum from a much larger area than the cross section of the planet itself. If we adopt instead an effective cross section equal to the area inward of the bow shock in the terminator plane, we find that only about 4% of the average solar wind momentum is needed to produce an escape rate of  $5 \times 10^{25}$  ions/s of  $\text{O}^+$ . However, even larger effective cross sections may be applicable, since the feet of the field lines that are involved in ion acceleration may be far downstream in the solar wind. Therefore we conclude that the solar wind has more than adequate momentum to produce the observed ion escape rates from the ionotail.

#### *Acceleration and Heating Processes*

The mechanism of ion scavenging from the ionotail is not clear at this time, and it is not our primary goal here to elucidate it in any detail. However, from the magnetic signatures associated with the tail rays, it would seem that the process involves the convection of interplanetary magnetic fields through the Venus environment. These fields are known to penetrate the dayside ionosphere during times of high solar wind pressure [Luhmann *et al.*, 1981a] and are convected nightward, either within or below the ionosphere, to emerge in the magnetotail and eventually return to the solar wind. Some of the magnetic flux emerges from the ionospheric holes that penetrate deep into the nightside ionosphere [Brace *et al.*, 1982b; Luhmann *et al.*, 1981b]. This component involves a strong, largely radial magnetic field which we continue to observe in the troughs further downstream. Additional nightside magnetic flux is provided by convection over the top of the ionosphere followed by convergence into the tail.

It is possible that ion acceleration occurs not only in the lower ionosphere (<1000 km) but all along the edges of the tail rays and as far downstream as they extend, until the rays have been completely dissipated. The strong currents observed in the ray boundaries are then simply products of the acceleration process. As we have seen, the edges of the tail rays mark the transition from a high beta to a low beta plasma. It is here that the magnetic field, which has been hung up, finally emerges from the dense nightside ionosphere. In doing so the magnetic field pulls off and heats the outer layers of tail ray ions and deposits them in the troughs where further acceleration by the departing field causes them to escape quickly tailward along the magnetic field. The low density of the troughs may be maintained in this fashion.

Troughs such as those shown in Figure 5 contain a plasma having high electron temperatures, and very small fluxes of superthermal ions which appear in the 9–16 eV range of the OIMS and >40 eV in the ONMS data. This plasma may contain ions and electrons that have been removed from the ionosphere as well as mantle plasma whose origin may be the ionopause further upstream [Spenser *et al.*, 1980]. Less commonly, as illustrated in Figure 6, the  $\text{O}_f^+$  ions may be present primarily in the trough, although not found in the adjacent tail rays themselves. Occasions like this may represent periods of trough movement or trough formation in which enhanced acceleration of ions occurring at lower altitudes was creating the trough at the time of the PVO passage.

This scenario of ionotail formation is an extension of the picture envisioned by *Brace et al.* [1982b] in speculating on the origin of the ionospheric holes. As evident in Figure 4, our current view is that the tail rays and troughs observed here at 2000–2500 km are the high altitude counterparts of similar features in the lower ionosphere. *Cravens et al.* [1982] drew attention to the low-altitude phenomena of disappearing ionospheres which occur during periods of solar wind disturbance and exhibited many of the same characteristics that are seen routinely at the higher altitudes examined in this paper. However, a more extensive analysis of the PVO data at the intervening altitudes is needed to fully explore this connection between the nightside ionosphere and the ionotail.

#### *Implications of Ion Escape for the Nightside Ionosphere*

A Venus escape flux of  $5 \times 10^{25}$  ions/s, while considerably less than the upper limit of  $7 \times 10^{26}$  ions/s estimated by *Brace et al.* [1982a], is still a very interesting value. This total escape flux is approximately 25% of transterminator flow required to form the nightside ionosphere [*Knudsen et al.*, 1980; *Spenner et al.*, 1981]. Given the uncertainties in such calculations, the remaining transterminator flux appears sufficient to produce the average nightside ionosphere densities, with some help from energetic electrons [*Spenner et al.*, 1981].

*Cravens et al.* [1982] attributed much of the variability of the nightside lower ionosphere to solar wind induced changes in the height of the ionopause near the terminator which in turn change the size of the ion reservoir available to supply ions to the nightside. It seems from the results presented here that an additional, and probably related, source of variability may arise from changes in the ion escape flux down the tail in response to changing solar wind and IMF conditions. The profiles of Figures 2 and 3 illustrate some of this variability in  $N_e$ . A few of the orbits not included in this sequence exhibit even greater dynamic range in  $N_e$ , some with the ionotail almost completely missing. This disappearance does not mean that the escape rate is low at these times, just that PVO may have crossed the ionotail following a large ion escape event which removed the ionotail, or that the ions had a velocity too high on that occasion to be detected by the PVO instruments. The causes for this orbit to orbit, or even minute to minute, variability have not yet been identified, but a more complete study of solar wind and IMF conditions associated with escape events may provide important clues.

Of equal interest to the escape of  $O^+$  is that of  $H^+$ . Since this ion, as mentioned above, cannot be measured directly when it is superthermal, we must resort to indirect arguments. It seems likely that the ionotail is escaping as plasma, rather than as individual ions; if so, all the ions move at the same speed and the flux of each is proportional to its density. Acceleration by an electric field, a less likely alternative, would give equal energies rather than equal speeds. Measurements in the underlying nightside ionosphere [*Taylor et al.*, 1980a, b] indicate that the number density of  $H^+$  is about the same as that of  $O^+$  on the dawn side, while  $H^+$  is much less prevalent on the evening side. The average  $H^+/O^+$  ratio is therefore 0.5, and we shall assume the same value for all altitudes and latitudes. The escape rate and global-mean flux of  $H^+$  are then around  $2.5 \times 10^{25} \text{ s}^{-1}$  and  $5 \times 10^6 \text{ cm}^{-2} \text{ s}^{-1}$  or about half that of  $O^+$ . Previous work on other hydrogen escape processes has found the dominant mechanism to be charge exchange between hot protons and exospheric H atoms, and the mean flux is estimated to be  $1.2 \times 10^7 \text{ cm}^{-2} \text{ s}^{-1}$  [*Hodges and Tinsley*, 1981; *Kumar et al.*, 1983]. The rate of the process

discussed here seems therefore to be somewhat smaller but comparable.

*Acknowledgments.* This work was supported by funds from the NASA Pioneer Project at Ames Research Center, Moffett Field, California.

The Editor thanks B. E. Goldstein and D. J. McComas for their assistance in evaluating this paper.

#### REFERENCES

- Brace, L. H., and L. Colin, Pioneer Venus—Evolving coverage of the near-Venus environment, *Eos Trans. AGU*, 65(25), 401, 1984.
- Brace, L. H., R. F. Theis, A. F. Nagy, T. M. Donahue, M. B. McElroy, and A. Pedersen, Electron temperatures and densities in the Venus ionosphere: Pioneer Venus Orbiter electron temperature probe results, *Science*, 203, 763–765, 1979.
- Brace, L. H., R. F. Theis, and W. R. Hoegy, Plasma clouds above the ionopause of Venus and their implications, *Planet. Space Sci.*, 30, 29–37, 1982a.
- Brace, L. H., R. F. Theis, H. G. Mayr, S. A. Curtis, and J. G. Luhmann, Holes in the nightside ionosphere of Venus, *J. Geophys. Res.*, 87, 199–211, 1982b.
- Brace, L. H., T. I. Gombosi, A. J. Kliore, W. C. Knudsen, A. F. Nagy, and H. A. Taylor, Jr., The ionosphere of Venus: Observations and their interpretations, in *Venus*, edited by D. M. Hunter, L. Colin, T. M. Donahue, and V. I. Moroz, chap. 23, pp. 779–840, University of Arizona Press, Tucson, Ariz., 1983.
- Cravens, T. E., L. H. Brace, H. A. Taylor, C. T. Russell, W. L. Knudsen, K. L. Miller, A. Barnes, J. D. Mihalov, F. L. Scarf, S. J. Wuenon, and A. F. Nagy, Disappearing ionospheres on the nightside of Venus, *Icarus*, 51, 271–282, 1982.
- Elphic, R. C., C. T. Russell, J. A. Slavin, and L. H. Brace, Observations of the dayside ionopause and ionosphere of Venus, *J. Geophys. Res.*, 85, 7679–7696, 1980.
- Hodges, R. R., and B. A. Tinsley, Charge exchange and the Venus ionosphere as a source of the hot exospheric hydrogen, *J. Geophys. Res.*, 86, 7649–7656, 1981.
- Intriligator, D. S., J. H. Wolfe, and J. D. Mihalov, The PVO plasma analyzer experiment, *IEEE Trans. Geosci. Remote Sens.*, GE-18, 39–43, 1980.
- Kasprzak, W. T., H. B. Niemann, and P. Mahaffy, Observations of energetic ions on the nightside of Venus, *J. Geophys. Res.*, 92, 291–298, 1987.
- Knudsen, W. C., K. Spenner, K. Miller, and V. Novac, Transport of ionospheric  $O^+$  ions across the Venus terminator and implications, *J. Geophys. Res.*, 85(A13), 7803–7810, 1980.
- Krehbiel, J. P., L. H. Brace, R. F. Theis, J. R. Cutler, W. H. Dinkus, and R. B. Kaplan, PVO electron temperature probe, *IEEE Trans. Geosci. Remote Sens.*, GE-18, 49–53, 1980.
- Kumar, S., D. M. Hunten, and J. B. Poilack, Nonthermal escape of hydrogen and deuterium from Venus and implications for loss of water, *Icarus*, 55, 369–389, 1983.
- Luhmann, J. G., R. C. Elphic, and L. H. Brace, Large-scale current systems in the dayside Venus ionosphere, *J. Geophys. Res.*, 86, 3509–3514, 1981a.
- Luhmann, J. G., R. C. Elphic, C. T. Russell, J. A. Slavin, and J. D. Mihalov, Observations of large-scale steady magnetic fields in the nightside Venus ionosphere and near wake, *Geophys. Res. Lett.*, 8, 517–520, 1981b.
- McComas, D. J., H. E. Spence, C. T. Russell, and M. A. Saunders, The average magnetic field draping and consistent plasma properties of the Venus magnetotail, *J. Geophys. Res.*, 91, 7939–7953, 1986.
- Mihalov, J. D., and A. Barnes, The distant interplanetary wake of Venus: Plasma observations from Pioneer Venus, *J. Geophys. Res.*, 87, 9045–9053, 1982.
- Mihalov, J. D., J. H. Wolfe, and D. S. Intriligator, Pioneer Venus observations of the solar wind–Venus interaction, *J. Geophys. Res.*, 85, 7613–7624, 1980.
- Niemann, H. B., J. R. Booth, J. E. Cooley, R. E. Hartle, W. T. Kasprzak, N. W. Spencer, S. H. Way, D. M. Hunten, and G. R. Carignan, PVO neutral gas mass spectrometer experiment, *IEEE Trans. Geosci. Remote Sens.*, GE-18, 60–64, 1980.
- Perez-de-Tejada, H., Evidence for a viscous boundary layer at the venus ionopause from preliminary Pioneer Venus results, *J. Geophys. Res.*, 85, 7709–7714, 1980.
- Russell, C. T., R. C. Snare, J. D. Means, and R. C. Elphic, PVO

- fluxgate magnetometer, *IEEE Trans. Geosci. Remote Sens.*, *GE-18*, 32-35, 1980.
- Russell, C. T., J. G. Luhmann, R. C. Elphic, and M. Neugebauer, Solar wind interactions with comets: Lessons from Venus, in *Comets: Bases, Ices, Grains and Plasma*, edited by L. Willkening, pp. 561-587, University of Arizona, Tucson, Ariz., 1982.
- Slavin, J. A., E. J. Smith, and D. S. Intriligator, A comparative study of distant magnetotail structure at Venus and earth, *Geophys. Res. Lett.*, *11*, 1074-1077, 1984.
- Spenser, K., W. C. Knudsen, K. L. Miller, V. Novak, C. T. Russell, and R. C. Elphic, Observations of the Venus mantle: The boundary between the solar wind and the ionosphere, *J. Geophys. Res.*, *85*, 7655-7663, 1980.
- Spenser, K., V. Novak, W. C. Knudsen, K. L. Miller, R. C. Whitten, and P. E. Michelson, On the maintenance of the nightside ionosphere: Electron precipitation and plasma transport, *J. Geophys. Res.*, *86*, 9170-9178, 1981.
- Taylor, H. A., H. C. Brinton, S. J. Bauer, R. E. Hartle, P. A. Cloutier, F. C. Michel, R. E. Daniell, T. M. Donahue, and R. C. Maehl, Ionosphere of Venus: First observations of the effects of dynamics on the dayside composition, *Science*, *203*, 755-757, 1979.
- Taylor, H. A., H. C. Brinton, T. C. G. Wayne, B. H. Blackwell, and G. R. Cordier, Bennett ion mass spectrometers on the PV bus an orbiter, *IEEE Trans. Geosci. Remote Sens.*, *GE-18*, 44-48, 1980a.
- Taylor, H. A., Jr., H. C. Brinton, S. J. Bauer, R. E. Hartle, P. A. Cloutier, and R. E. Daniell, Jr., Global observations of the composition and dynamics of the ionosphere of Venus: Implications for the solar wind interaction, *J. Geophys. Res.*, *85*, 7765-7777, 1980b.
- Theis, R. F., L. H. Brace, R. C. Elphic, and H. G. Mayr, New empirical model of the application to transterminator flow, *J. Geophys. Res.*, *89*, 1477-1488, 1984.
- 
- A. Barnes and J. D. Mihalov, Ames Research Center, Moffett Field, CA 94035.
- L. H. Brace, W. T. Kasprzak, H. A. Taylor, and R. F. Theis, Goddard Space Flight Center, Code 614, Greenbelt, MD 20771.
- D. M. Hunten, University of Arizona, Tucson, AZ 85721.
- C. T. Russell, University of California at Los Angeles, Los Angeles, CA 90024.

(Received June 30, 1986;  
revised September 17, 1986;  
accepted September 29, 1986.)

DSC # 637  
B37506  
78-051A-11

## Observations of Energetic Ions on the Nightside of Venus

W. T. KASPRZAK AND H. B. NIEMANN

*Laboratory for Atmospheres, NASA Goddard Space Flight Center, Greenbelt, Maryland*

P. MAHAFFY

*Science Applications Research, Lanham, Maryland*

Ions with energy greater than 40 eV have been measured on the nightside of Venus by the Pioneer Venus orbiter neutral mass spectrometer (ONMS). For periapsis altitudes beyond 1500 km they are confined to solar zenith angles greater than 120°. The nightside energetic ion composition at 2000 km resembles the nightside thermal ion composition occurring at 1000 km with the dominant species being O<sup>+</sup>. Postflight laboratory calibrations performed on the ONMS backup unit have been used to estimate the energetic O<sup>+</sup> ambient flux and density. The direction from which the energetic ions appear to be coming can be determined because the ONMS is mounted at an angle with respect to the spin axis of the spacecraft. Both tailward and antitailward components of the apparent ion flow are exhibited when projected into the ecliptic plane. The major component of the apparent ion flow is observed perpendicular to the ecliptic plane.

### INTRODUCTION

Ions with energy greater than 40 eV have been observed by the Pioneer Venus orbiter neutral mass spectrometer (ONMS) and reported by Kasprzak *et al.* [1982]. The energetic ion species most frequently seen occur at a mass/charge ratio of 16 and are due to accelerated O<sup>+</sup> whose source is the ionosphere. Energetic ions have been detected in both the dayside and nightside sectors of Venus. In the dayside sector they usually occur near the ionopause of Venus, as suggested by comparison with electron density data from the orbiter electron temperature probe (OETP), and are also associated with superthermal ions of a lower energy range detected by the orbiter ion mass spectrometer (OIMS) [Kasprzak *et al.*, 1982]. The nightside energetic ions appear to be part of the more erratic plasma structure seen by both the OETP and OIMS instruments.

The ONMS instrument [Niemann *et al.*, 1980] is a quadrupole mass spectrometer primarily designed for measurement of the neutral gas composition in the Venus thermosphere. In the neutral measurement mode an electron beam, created by a hot filament, ionizes the incoming neutral gas. Two grids in front of the ionization region, at -6 V and +40 V relative to the spacecraft potential, reject ambient electrons and ions, respectively. Ions with greater than 40 eV energy were first detected while operating in the neutral mode. The instrument can operate in the thermal ion mode, with the filament off and the ion repeller at spacecraft ground, or in the energetic ion mode, with the filament off and the ion repeller at 40 V. The ions exiting the ion source enter a quadrupole mass analyzer where specific mass/charge ratios are selected and are subsequently detected by a secondary electron multiplier operating in pulse counting mode.

Since the initial description of the energetic ion results in the work by Kasprzak *et al.* [1982], additional data have been acquired from later orbits of the spacecraft. Laboratory data have been used to refine the flux estimate of these particles

and their possible energy. New instrument operating modes have been implemented to increase the sensitivity of the instrument for energetic ions and to search for characteristic properties.

### DISTRIBUTION AND COMPOSITION

The energetic ion measurements described by Kasprzak *et al.* [1982] covered the first 700 orbits when the orbiter periapsis was maintained at low altitude for neutral density and lower ionosphere measurements. The measurement time was confined to about one hour centered at periapsis and is a small fraction of the 24-hour orbital period. The energetic ions were primarily observed at the ionopause, particularly on the dayside. After orbit 600, periapsis was no longer maintained at low altitude and rose in response to solar gravitational perturbations [Brace and Colin, 1984]. Because of the increase in periapsis altitude the neutral atmosphere was no longer sampled, and the ONMS instrument was configured to measure thermal and energetic ions. As periapsis rose above the ionopause, measurements of energetic ions on the dayside dwindled and by orbit 1450 (periapsis altitude greater than 1500 km) were no longer observed. Figure 1 shows locations where energetic O<sup>+</sup> ions were observed for orbit numbers beyond 1450. The ions occur only on the nightside at solar zenith angles greater than about 120° (corresponding approximately to the geometrical shadow of Venus). A comparison with Figure 3 of Kasprzak *et al.* [1982] shows the extent to which the rise in the periapsis altitude has limited the observation of energetic ions in the nightside region. The nightside ions are observed more or less irrespectively of the altitude of periapsis and are restricted only by the limitations of the orbit coverage.

The energetic ion species most frequently observed is O<sup>+</sup>, but it is not the only species observed. Typical energetic ion mode composition data obtained in orbit 1878 are shown in Figure 2. The pulse counter output of the instrument is plotted versus time for several mass to charge ratios. The programmed mass mode [Niemann *et al.*, 1980] was used with measurements at mass numbers 4, 14, 16, 28, 30, 32, and 44. The data are spin modulated, and this results in a wide scatter band. The dominant species at mass 16 is O<sup>+</sup> since it is the main constituent of the ionosphere. There are significant

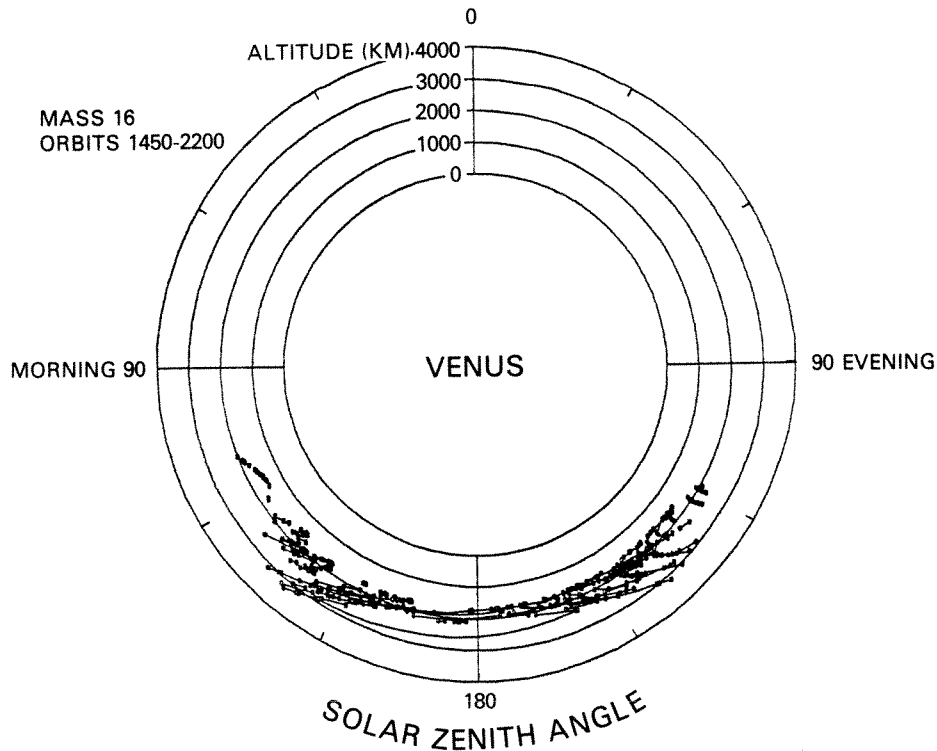


Fig. 1. The location in solar zenith angle and altitude of the ONMS signatures for energetic  $O^+$  in the orbit range 1450–2200. Line segments connect beginning and ending points of a data section in an orbit where energetic ions are observed. The sun is located at the top of the diagram at a solar zenith of  $0^\circ$ .

counts at other masses (4, 14, 28, 30, 32), and these represent the ionospheric species ( $He^+$ ,  $N^+$ ,  $N_2^+/CO^+$ ,  $NO^+$ ,  $O_2^+$ ) which are also known to be present in the thermal nightside ionosphere. The average thermal ion composition at 1000 km in the solar zenith angle range  $150^\circ$ – $180^\circ$  presented by Taylor *et al.* [1985] shows  $O^+$ ,  $N^+$ ,  $He^+$ , and ( $O_2^+$ ,  $N_2^+/CO^+$ ,  $NO^+$ ) as species in descending order of relative concentration, and this order appears in the energetic ion composition at 2000 km. Mass 44 ( $CO_2^+$ ) is not seen in the energetic ions, but this may be due to its low concentration and the decrease in instrument transmission with increasing mass number. Other species such as  $C^+$  also exist as energetic ions but were not measured in this orbit because they were not included in the programmed mass sequence. Hydrogen mass peaks cannot be resolved by the instrument.

#### ONMS ENERGETIC ION DATA ANALYSIS

Laboratory studies have made it possible to refine the estimate given by Kasprzak *et al.* [1982] for the conversion of instrument signal output to ambient ion flux. The backup flight unit for the ONMS was configured to match the sensitivity and peak shape of the in situ orbiting instrument.  $O^+$  ions were generated from a  $CO_2$  plasma discharge, extracted, and velocity filtered to obtain an ion beam with a small energy spread. The ion path was angled slightly before impinging on the sensor orifice so as to reduce the effect of radiation and metastable neutral species generated in the discharge. The beam width was sufficient to cover the 1.27-cm-diameter entrance orifice and raster scanned across the orifice in order to reduce the effects of beam nonuniformity and slight drifts that would normally occur. The transmission of the instrument with the ion repeller set at 40 V was determined from the current impinging on the sensor orifice, as measured

by a retractable plate, and the pulse counter output of the instrument. The ion energy was determined by sweeping the retarding potential grid while maintaining the ion repeller grid and other associated entrance grids at ground potential. The results for  $O^+$  over a range of 40–200 eV show that maximum transmission occurs at 50 eV with a flux of  $4 \times 10^7$  particles  $cm^{-2} s^{-1}$  corresponding to  $1 \times 10^4$  counts  $s^{-1}$ . The transmission drops to zero below 40 eV and tails to a constant 15% of the maximum transmission value above 100 eV. The flux at 50 eV is only a factor of 2 higher than the lower limit given by Kasprzak *et al.* [1982] which assumed that the ion lens system of the quadrupole does not focus the ions and that the appropriate area of collection is the nozzle orifice, the smallest geometrical constriction in the ion source. The transmission decreases with increasing mass number, and for  $A^+$  ions (mass/charge ratio of 40) it is about a factor of 2.5 below that for  $O^+$  at 50 eV.

In order to deduce reasonable estimates of the energetic ion flux and number density it is necessary to specify the approximate ion energy, which in turn implies some gross knowledge of the ion velocity distribution. One feature that can be checked indirectly is whether the bulk of the ions seen by the ONMS in the energetic ion mode have energies greater than 40 eV. The width of the mass 16 peak due to  $O^+$  is a function of the incident ion energy. Figure 3a shows the results of a laboratory simulation using a variable energy ion beam and the ONMS flight backup unit with the ion repeller set at 40 V. As the incident ion beam energy is increased from 43.2 V to 208.2 V, the peak width increases. In Figures 3b and 3c, data are presented from two orbits where the instrument was commanded to a  $\frac{1}{2}$ -amu mass scan while in the energetic ion mode so that the peak width could be determined. Only a few scans were obtained, but the data are consistent with an incident ion

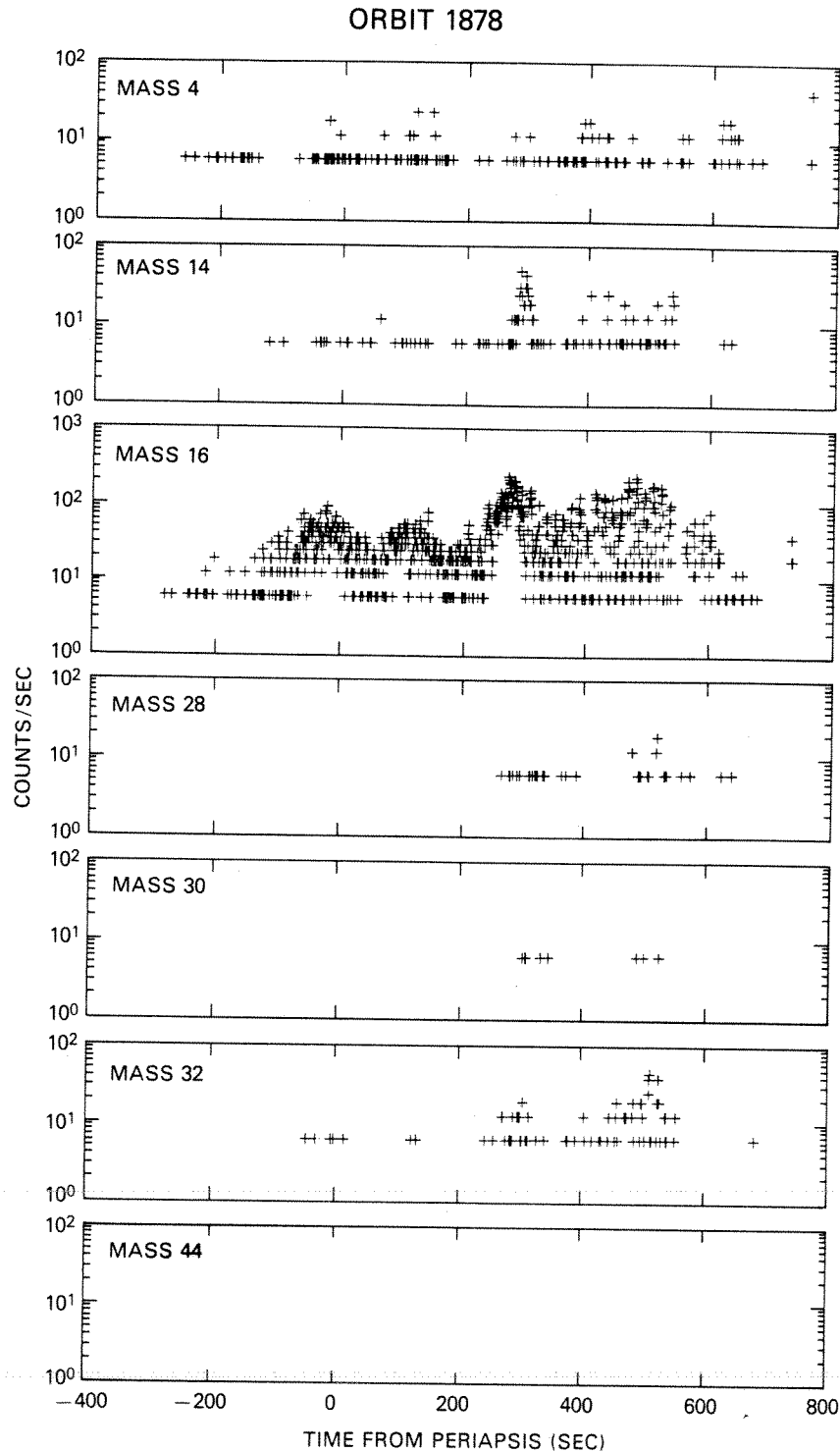


Fig. 2. Energetic ion mode composition data (in pulse counts per second) plotted as a function of time from periapsis for orbit 1878 (day 27, year 1984) and a range of mass numbers. Periapsis occurred at 0031:52 UT at an altitude of 1929 km, Venus latitude of  $8.1^\circ$  N, solar zenith angle of  $165^\circ$ , and 0055:12 local solar time.

energy very near that of the ion repeller grid, namely 40 V, and not with some substantially larger energy. The fine structure observed in the peak shape is due to fluctuations in the incident ion flux. Another method of measuring the peak width is to use the mass peak 15/16 ratio obtained while in 1-amu mass sweep. The orbit range 942–1896 was covered in this survey, and the results are similar to those obtained from the  $\frac{1}{8}$ -amu scan. This suggests that there is a distribution simi-

lar to that of a Maxwellian for  $O^+$  whose center is below 40 eV and whose high-energy tail is being observed by the ONMS instrument. Bulk velocities of  $O^+$  up to 8 km/s (5 eV) have been observed [Knudsen *et al.*, 1980] near the terminator in the ionosphere. Superthermal ion measurements by the OIMS [Taylor *et al.*, 1980] for disturbed nightside conditions in the dusk region indicate up to 10 km/s flow within the main body of the ionosphere and higher values (up to 20 km/s)

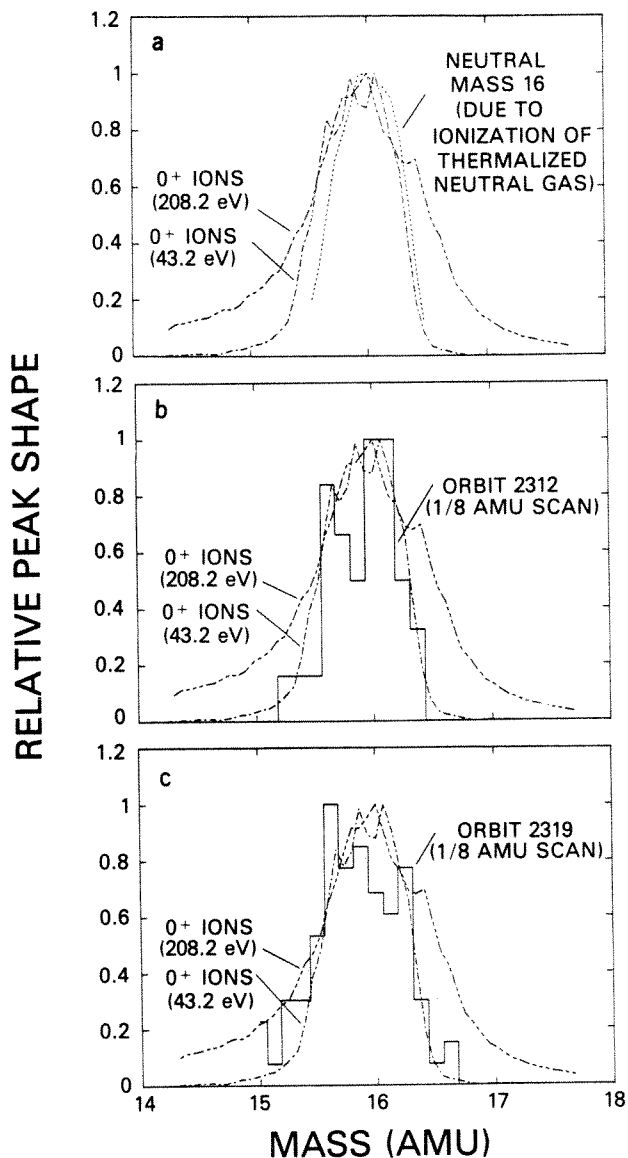


Fig. 3. (a) The variation of the mass 16 peak width due to  $O^+$  as a function of incident ion energy with the ion repeller set at 40 V from laboratory measurements using the flight backup mass spectrometer. All curves have been normalized to peak amplitude of 1. The angle of attack is  $0^\circ$ . The normal peak width due to ionization of thermalized neutral gas is also shown. (b) The incident ion energy curves from Figure 3a are repeated, and the data for orbit 2312 (day 94, year 1985) obtained while the instrument was in  $\frac{1}{8}$ -amu sweep are shown. The time of the data is 2236:52 UT. (c) Similar to Figure 3b but for orbit 2319 (day 101, year 1985). The time of the data is 2236:45 UT.

outside the ionosphere. Results of superthermal  $O^+$  measurements by the OIMS for the nightside series of orbits in the range 1850–1900 near 2000 km altitude [Brace *et al.*, 1987] imply bulk speeds with an average energy of 13 eV (or 13 km/s). These values are all smaller than 40 eV (or 22 km/s) and are consistent with the ONMS results.

The convolution of a decreasing (or at least constant) ion velocity distribution with increasing energy above 40 eV and an instrument transmission which is zero at 40 eV, maximum at 50 eV, and decreasing to a constant value above 100 eV produces a preferred energy range where ONMS will detect ions. The maximum contribution to the signal detected by the ONMS would most likely come from ions with an energy near 45 eV. This assumes an average nightside spacecraft potential

of  $-5$  V which would accelerate the ions to about 50 eV (maximum instrument transmission) before they reach the sensor orifice. Assuming that the nightside energetic ions measured by the ONMS have an energy near 45 eV allows both the flux and number density of the particles of that energy to be reasonably estimated.

The detector output signal from the ONMS instrument is spin modulated because the instrument is mounted  $26.6^\circ$  away from the spin axis (see Figure 4). The spin axis of the spacecraft is almost perpendicular to the ecliptic plane, pointing toward the south pole, and the spin period is nominally 12 s. If there is a directional flow of the ions that is not along the spin axis, then the signal detected by the ONMS would be spin modulated provided that the ions have the required energy (greater than 40 eV) in the spacecraft reference frame. The apparent direction of the ion flow in the ecliptic plane is determined by the position of the instrument axis at signal

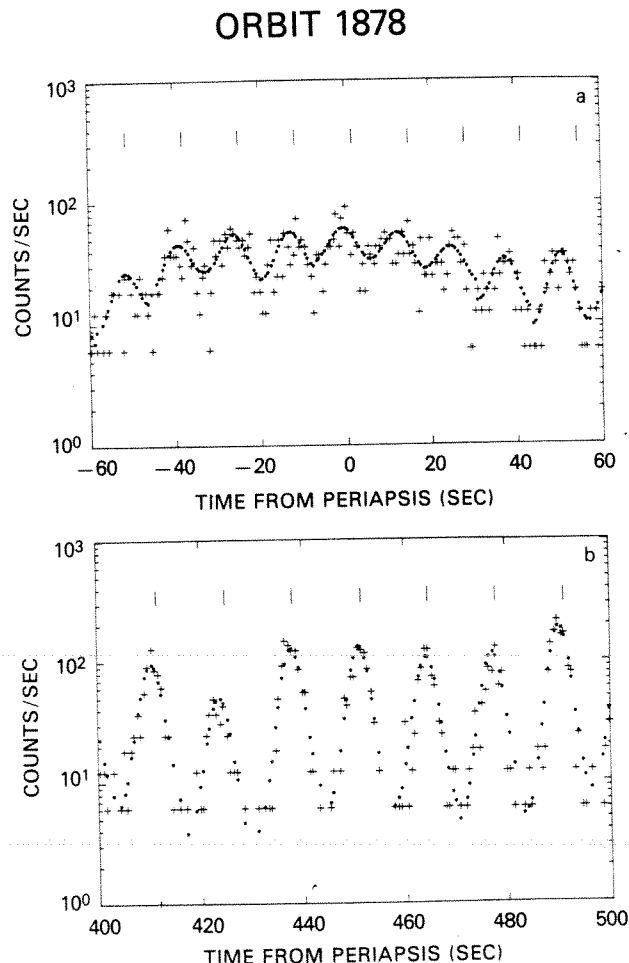


Fig. 4. Example of the spin-modulated pulse counter signal for mass 16, orbit 1878, plotted as a function of time from periapsis. The pluses denote data points, and the circles represent the calculated signal used in deriving the estimated ambient energetic ion density. The vertical lines represent the time at which the axis of the ONMS projected into the ecliptic plane would point toward the sun. The maximum signal points in the pulse counter data represent the time of "ram" or closest approach of the ONMS to the drift velocity vector of the ions. (a) Periapsis time  $-60$  to  $60$  s. The pulse counter data have a small spin modulation, and fluctuations in the incident ion flux are evident in the detected signal. (b) Periapsis time 400 to 500 s. The spin modulation is well defined with a large amplitude compared to the data displayed in Figure 4a.

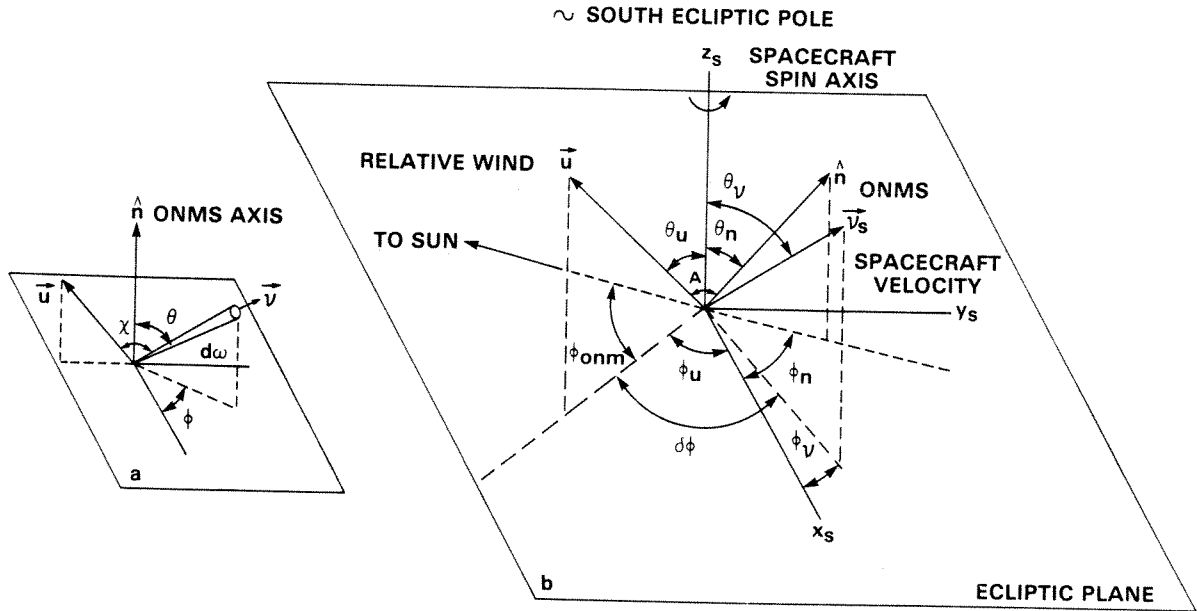


Fig. 5. The geometry associated with equations (1)–(3). (a) The flux due to a molecular velocity  $v$  in a solid angle  $d\omega$  at a zenith angle  $\theta$  and azimuthal angle  $\phi$  with respect to the axis of ONMS;  $u$  is the relative velocity of ONMS, and  $\chi$  the angle between  $u$  and  $v$ . (b) The various vectors in the spacecraft reference frame: the spacecraft velocity  $v_s$  ( $\theta_v, \phi_v$ ), the axis of ONMS  $\hat{n}$  ( $\theta_n, \phi_n$ ), and the relative velocity  $u$  ( $\theta_u, \phi_u$ );  $\phi_{om}$  is the azimuthal angle in the ecliptic plane of the maximum signal point (minimum angle attack).

maximum when the relative velocity angle of attack is a minimum. The azimuthal angle is primarily determined by the direction of ion flow and not the spacecraft velocity because of the much larger energy involved.

Laboratory data on the angular response of the ONMS in the (thermal) ion or energetic ion mode are limited. Data in the ion mode for  $N_2^+$  at 22 eV energy indicates that at half amplitude the acceptance cone half angle is about  $5^\circ$ . This is much smaller than the geometrical acceptance cone based on line of sight to the ion source of about  $38^\circ$ . The narrow acceptance angle suggests that the transmission is primarily along the instrument axis.

Some insight into the form of the angular response of an instrument with a narrow acceptance angle can be obtained from kinetic theory calculations of the flux in a solid angle incident on a surface [e.g., Nocilla, 1963; Hughes and De Leeuw, 1965; Hueser and Fowler, 1972; Melfi and Brock, 1973]. In those derivations the ambient particle distribution is assumed to be Maxwellian (with bulk velocity  $v_0 = 0$ ), and the surface is assumed to be moving with velocity  $v_s$ ; when the ambient gas is also moving, the relative velocity,  $u$ , with respect to the surface becomes  $u = v_0 - v_s$ . Placing the  $z$  direction along the instrument axis and converting to spherical coordinates (Figure 5a), the differential flux  $dF$  is

$$dF = \frac{n_a v_m}{\pi^{3/2}} \{ \exp[-S_u^2 \sin^2(\chi)] \} \cos(\theta) T(\theta) \cdot g_3[r_c, S_u \cos(\chi)] d\omega dA \quad (1)$$

where

- $n_a$  ambient density;
- $v_m = (2kT/m)^{1/2}$ ;
- $T$  temperature;
- $m$  molecular mass;
- $k$  Boltzmann's constant;
- $S_u = u/v_m$ ;

- $\theta$  zenith angle with respect to the  $z$  axis;
- $T(\theta)$  instrument transmission;
- $\chi$  angle between the relative velocity  $u$  and the molecular velocity  $v$ ;
- $r_c = (2e\phi_R/m)^{1/2}/v_m \cos(\theta)$ ;
- $\phi_R$  retarding potential;
- $dA$  differential area;
- $d\omega$  differential solid angle;

$$g_3(x, u) = \int_x^\infty v^3 e^{-(v-u)^2} dv = \frac{1}{2}(\pi)^{1/2} u(u^2 + \frac{3}{2}) \cdot [1 + \operatorname{erf}(u-x)] + \frac{1}{2}(1+x^2+u^2+ux)e^{-(u-x)^2}$$

The presence of a retarding potential  $\phi_R$  modifies the lower limit of integral  $g_3$ . The instrument transmission is assumed to be cylindrically symmetric and not a function of the particle speed. It can be considered to be a delta function in  $\theta$  (i.e., transmission only along the instrument axis). Simplification after integration can be accomplished since  $r_c > S_u \cos(\theta)$  (the spacecraft speed is 10 km/s, near-midnight ion temperatures for  $O^+$  extrapolated to 2000 km are about  $10^4 K$  [Miller et al., 1980], and for  $\phi_R = 45$  V, the ratio  $r_c/S_u \cos(\theta) > 2$  with  $S_u \sim 3$ ). The result is approximately

$$\text{flux} \sim n_a u A_0 f(A) h(A) \quad (2)$$

where

- $A_0$  orifice area;
- $f(A) = \cos(A)[3 + 2B \cos^2(A)]e^{-B \sin^2(A)}$ ;
- $h(A) = \frac{1}{2} \{ 1 + \operatorname{erf}[(B)^{1/2} \cos(A) - r_c] \}$ ;
- $B = S_u^2$ ;
- $\cos(A) = \cos(\theta_u) \cos(\theta_n) + \sin(\theta_n) \sin(\theta_u) \cos(\phi_u - \phi_n)$ ;
- $\theta$  zenith angle;
- $\phi$  azimuthal angle.

In equation (2) the coordinate system has been rotated to place the  $z$  direction along the spacecraft spin axis (see Figure 5b). The angular position of the axis of ONMS is  $(\theta_n, \phi_n)$ , the

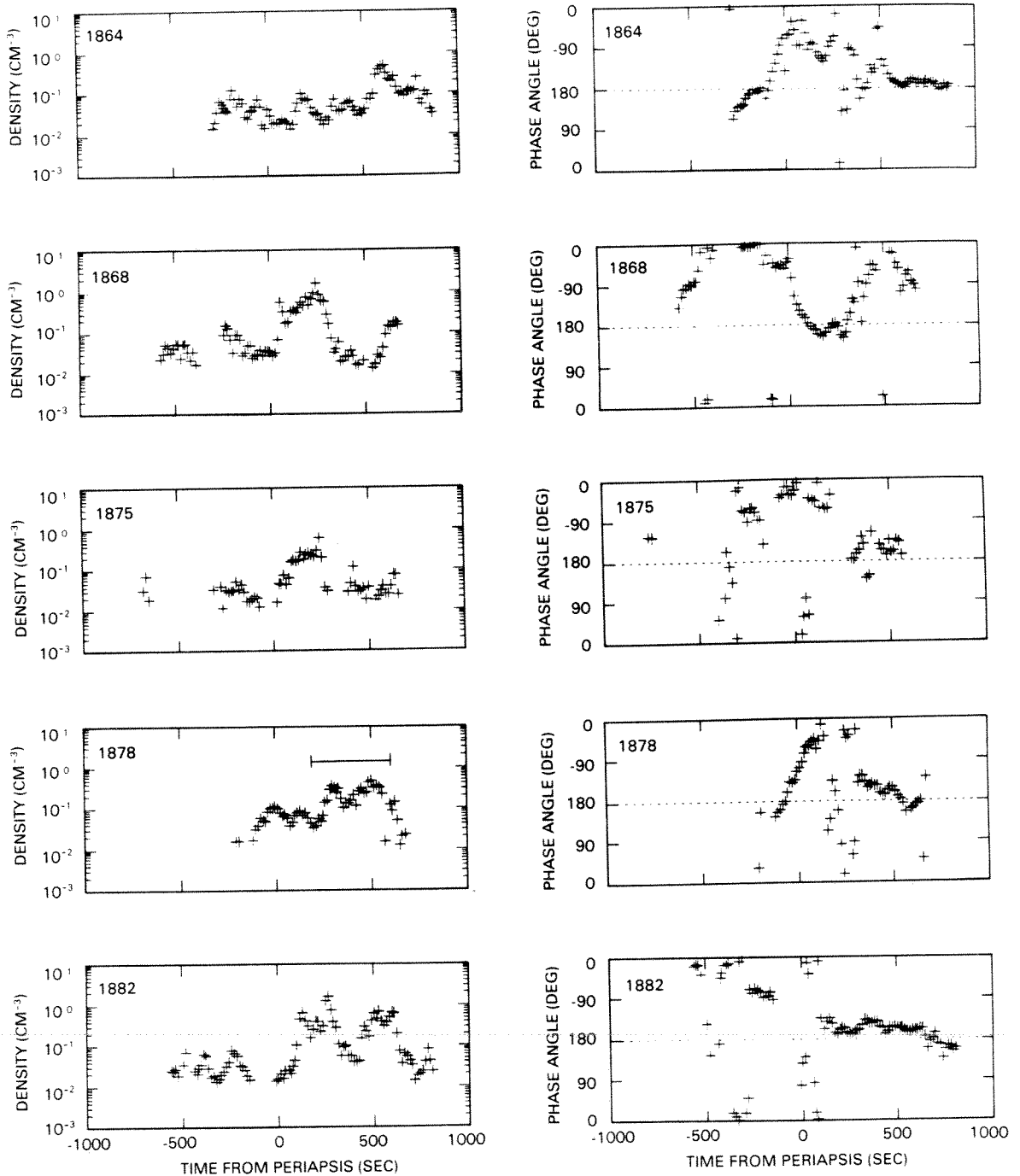


Fig. 6. The ONMS estimated density (particles per cubic centimeter) for energetic  $O^+$  and the ONMS phase angle for several orbits near midnight. The ONMS phase angle is the azimuthal angle of the apparent ion flow with respect to the sun at the time of signal maximum as viewed in the ecliptic plane. For a midnight orbit,  $180^\circ$  corresponds to an apparent tailward ion flow. Local solar time at periapsis is 2324, 2348, 0036, 0055:12, and 0118 for orbits 1864, 1868, 1875, 1878, and 1882, respectively. The horizontal bar marks the density enhancement mentioned in the text for orbit 1878.

direction of the relative velocity  $\mathbf{u}$  is  $(\theta_u, \phi_u)$ , and the direction of the spacecraft velocity  $\mathbf{v}_s$  is  $(\theta_v, \phi_v)$ .

The instrument response is taken to be

$$\text{signal} = SFf(A)/f(0) \quad (3)$$

where

signal instrument output, counts  $s^{-1}$ ;  
 $F$  ambient flux, particles  $cm^{-2} s^{-1}$ ;  
 $S$  sensitivity, counts particle $^{-1} cm^{-2}$ , equal to  $(10^4 \text{ counts } s^{-1})/(4 \times 10^7 \text{ particles } cm^{-2} s^{-1})$ ;  
 $f(0) = 3 + 2B$ .

The factor  $F$  is the estimated ambient flux at 45 eV, and the sensitivity  $S$  is based on laboratory data, as described previously, assuming an effective ion energy of 45 eV. The angular response has been taken to be  $f(A)$ , using (2) as a guide, and has been normalized to its value at  $0^\circ$  angle of attack  $f(0)$ , so as to reproduce the laboratory results. Both laboratory and flight data fit the functional form  $f(A)$  with  $B$  as a parameter. The factor  $f(A)/f(0)$  should be viewed as a semi-empirical function designed to remove the angular dependence of the incident ion flux. The magnitude of  $\mathbf{u}$  and the ion temperature  $T$  are unknown, as is the direction  $\theta_u$ . For practical purposes,  $\theta_u$  was taken to be equal to the spacecraft veloci-

ty vector  $\theta_v$ . The azimuthal angle  $\phi_u = \phi_v + \delta\phi$  was set to that derived from the spacecraft velocity but with an additional offset angle  $\delta\phi$  (spin phase angle difference), to allow the signal maximum to occur at the correct position in the azimuthal sweep due to the spinning spacecraft. The assumption  $\theta_u = \theta_v$  (or equally well  $\theta_u = \theta_n$ ) is a necessary compromise. The correlation between the unknown flux  $F$  and the zenith angle of the relative drift velocity  $\theta_u$  is extremely high, and it has not been possible to independently determine  $\theta_u$ . It might be thought that the spin modulation amplitude should reflect only the temperature  $T$ . However, both  $T$  and  $\theta_u$  affect the spin modulation in a similar manner. A retarding potential sweep technique [Hanson and Heelis, 1975] can separate  $u \cos(A)$  and  $T$ . Although the ONMS has such a sweep, it was not designed to cover the high-energy range encountered in this application.

In order to determine the ambient flux, 36 s (3 spin periods) of data are fit in a least squares sense with  $F$ , the constant  $B$ , and the spin phase angle difference  $\delta\phi$  as parameters. Only the center 12 s of data are converted to an estimated flux. The estimated ambient  $O^+$  density is determined by dividing the flux by the speed corresponding to 45 eV ( $2.33 \times 10^6$  cm/s). Variations in  $B$  partially compensate for a lack of knowledge about the angle between the spacecraft spin axis and the ion velocity vector. For this reason,  $B$  is not considered a reliable measure of the temperature  $T$ . However, an estimate of the possible ion temperature implied by  $B$  can be made assuming that the bulk speed of the  $O^+$  distribution is near 13 eV [Brace et al., 1987]. Interpreting  $B$  strictly as a reflection of the ion temperature  $T$  yields a value that ranges from low  $10^4$  K to low  $10^6$  K. The ion temperature estimated from Miller et al. [1980] is about  $10^4$  K near midnight extrapolated to 2000 km. The azimuthal angle of the apparent ion flow  $u$  relative to the sun,  $\phi_{onms}$ , is determined from the spin phase angle  $\delta\phi$  (Figure 5b) and is called the ONMS phase angle. This is the direction of the total relative velocity as measured in the spacecraft reference frame. It is very nearly the direction of the apparent ion flow since the correction to the azimuthal angle due to the spacecraft velocity is less than  $10^\circ$  for a 45-eV  $O^+$  ion.

An example of the fit of the function described by (3) to the data is shown in Figure 4 for orbit 1878. The spin-modulated pulse counter data and the calculated function are plotted as a function of time for two different time periods. The pulse counter data from  $-60$  to  $60$  s (Figure 4a) have a discernible offset and a small spin amplitude. The times of signal "ram" (signal maximum) show a component of the ion flow in the ecliptic plane that is almost antisunward initially and moving further away from that direction as time increases. Since periapsis for this orbit is near midnight, it also indicates apparent tailward ion flow. The spin modulation is not well defined by the data because of the large fluctuations in the incident ion flux. The effect of the fluctuations is to cause an apparent broadening of the peak near signal maximum over a substantial portion of the spin cycle. In order to fit such a broad peak the calculated spin amplitude must be reduced, and as a result the function does not fit the minima nearly as well as it fits the data in Figure 4b. The data from 400 to 500 s (Figure 4b) have a well-defined spin modulation with a larger amplitude. The time of signal "ram" shows an almost antisunward (i.e., tailward) apparent ion flow component in the ecliptic plane. The ONMS estimated average density derived from the fit is shown in Figure 6 along with the corresponding ONMS phase angles. The phase angles form

two systematic patterns from  $-100$  to  $100$  and from  $300$  to  $650$  s with more erratic behavior elsewhere.

## DISCUSSION

The largest magnitude  $O^+$  density enhancement in orbit 1878 (marked by the horizontal bar in Figure 6) is associated with ONMS phase angles indicating apparent tailward ion flow. Other orbits in Figure 6 also show regions where there is an apparent tailward ion flow in the ecliptic plane (i.e., phase angles greater than  $90^\circ$  with respect to the sun). In some cases this apparent tailward flow is associated with major  $O^+$  density enhancements (e.g., orbit 1882), and in other cases the reverse is true (e.g., orbit 1875).

The ONMS measurements filter the energetic ion motion in both energy and direction. The narrow acceptance angle of the ONMS restricts the observations to a wedge-shaped cone and the instrument transmission to a narrow energy band. Because of the orientation of the instrument with respect to the spin axis (and hence with respect to the south ecliptic pole) the major component of the observed energetic ion flow is perpendicular to the ecliptic plane in the south to north direction. A smaller component is present in the ecliptic plane. For a 45-eV  $O^+$  ion observed in the spacecraft reference frame, about 6–8 km/s of that motion is due to the spacecraft itself with the remainder about 14 km/s along the spin axis and 7 km/s in the ecliptic plane. Because the ONMS cannot cover a wide range of pitch angles because of its sampling geometry and only a small energy range, it is not clear whether the ONMS phase angles observed are representative of the ion motion in general.

Mihalov and Barnes [1982] have observed ions in the magnetotail region of Venus, some 8–12 Venus radii behind the planet, with an energy to charge ratio in excess of 4 keV. The ions are identified as  $O^+$ , and the estimated flux is less than  $10^7$  ions  $cm^{-2} s^{-1}$ . The maximum energetic  $O^+$  flux observed by the ONMS between 1900 and 2500 km is less than  $4 \times 10^6$  ions  $cm^{-2} s^{-1}$ . This is consistent with the magnetotail estimate, ignoring any possible solar cycle variation between the two measurements. The average  $O^+$  flux for ions exceeding 40 eV observed by the ONMS, disregarding direction, is about  $4 \times 10^4$  ions  $cm^{-2} s^{-1}$  for the orbit range 1847–1896.

*Acknowledgments.* The authors wish to thank the referees for their useful comments in evaluating this paper.

The Editor thanks R. E. Daniell and another referee for their assistance in evaluating this paper.

## REFERENCES

- Brace, L. H., and L. Colin, Pioneer Venus: Evolving coverage of the near-Venus environment, *Eos Trans. AGU*, 65, 401–402, 1984.
- Brace, L. H., W. T. Kasprzak, H. A. Taylor, R. F. Theis, C. T. Russell, A. Barnes, J. D. Mihalov, and D. M. Hunten, The ionotail of Venus: Its configuration and evidence for ion escape, *J. Geophys. Res.*, 92, 15–26, 1987.
- Hanson, W. B., and R. A. Heelis, Techniques for measuring bulk gas-motions from satellites, *Space Sci. Instrum.*, 1, 493–524, 1975.
- Hueser, J. E., and P. Fowler, Thermospheric temperature measurement technique, *J. Vac. Sci. Technol.*, 9, 467–470, 1972.
- Hughes, P. C., and J. H. De Leeuw, Theory for the free molecule impact probe at an angle of attack, in *4th International Symposium on Rarefied Gas Dynamics*, pp. 653–676, Academic, Orlando, Fla., 1965.
- Kasprzak, W. T., H. A. Taylor, L. H. Brace, H. B. Niemann, and F. L. Scarf, Observations of energetic ions near the Venus ionopause, *Planet. Space Sci.*, 30, 1107–1115, 1982.
- Knudsen, W. C., K. Spenner, K. L. Miller, and V. Novak, Transport of ionospheric  $O^+$  ions across the Venus terminator and implications, *J. Geophys. Res.*, 85, 7803–7810, 1980.
- Melfi, L. T., and F. J. Brock, Molecular beam techniques applied to

- mass spectrometric thermospheric density measurements, *Rev. Sci. Instrum.*, **44**, 1524-1527, 1973.
- Mihalov, J. D., and A. Barnes, The distant interplanetary wake of Venus: Plasma observations from Pioneer Venus, *J. Geophys. Res.*, **87**, 9045-9053, 1982.
- Miller, K. L., W. C. Knudsen, K. Spenser, R. C. Whitten, and V. Novak, Solar zenith angle dependence of ionospheric ion and electron temperatures and density on Venus, *J. Geophys. Res.*, **85**, 7759-7764, 1980.
- Niemann, H. B., J. R. Booth, J. E. Cooley, R. E. Hartle, W. T. Kasprzak, N. W. Spencer, S. H. Way, D. M. Hunten, and G. R. Carignan, Pioneer Venus orbiter neutral gas mass spectrometer experiment, *IEEE Trans. Geosci. Remote Sens.*, *GE-18*, 60-65, 1980.
- Nocilla, S., The surface re-emission law in free molecule flow, in *3rd International Symposium on Rarefied Gas Dynamics*, pp. 327-346, Academic, Orlando, Fla., 1963.
- Taylor, H. A., H. C. Brinton, S. J. Bauer, and R. E. Hartle, Global observations of the composition and dynamics of the ionosphere of Venus: Implications for the solar wind interaction, *J. Geophys. Res.*, **85**, 7765-7777, 1980.
- Taylor, H. A., H. G. Mayr, H. B. Niemann, and J. Larson, Empirical model of the composition of the Venus ionosphere: Repeatable characteristics and key features not modeled, *Adv. Space Res.*, **5**, 157-163, 1985.
- 
- W. T. Kasprzak, NASA Goddard Space Flight Center, Code 615.1, Greenbelt, MD 20771.
- P. Mahaffy, Science Applications Research, 4400 Forbes Boulevard, Lanham, MD 20706.
- H. B. Niemann, NASA Goddard Space Flight Center, Code 615, Greenbelt, MD 20771.

(Received June 24, 1986;  
revised September 29, 1986;  
accepted September 19, 1986.)

# MASS 16

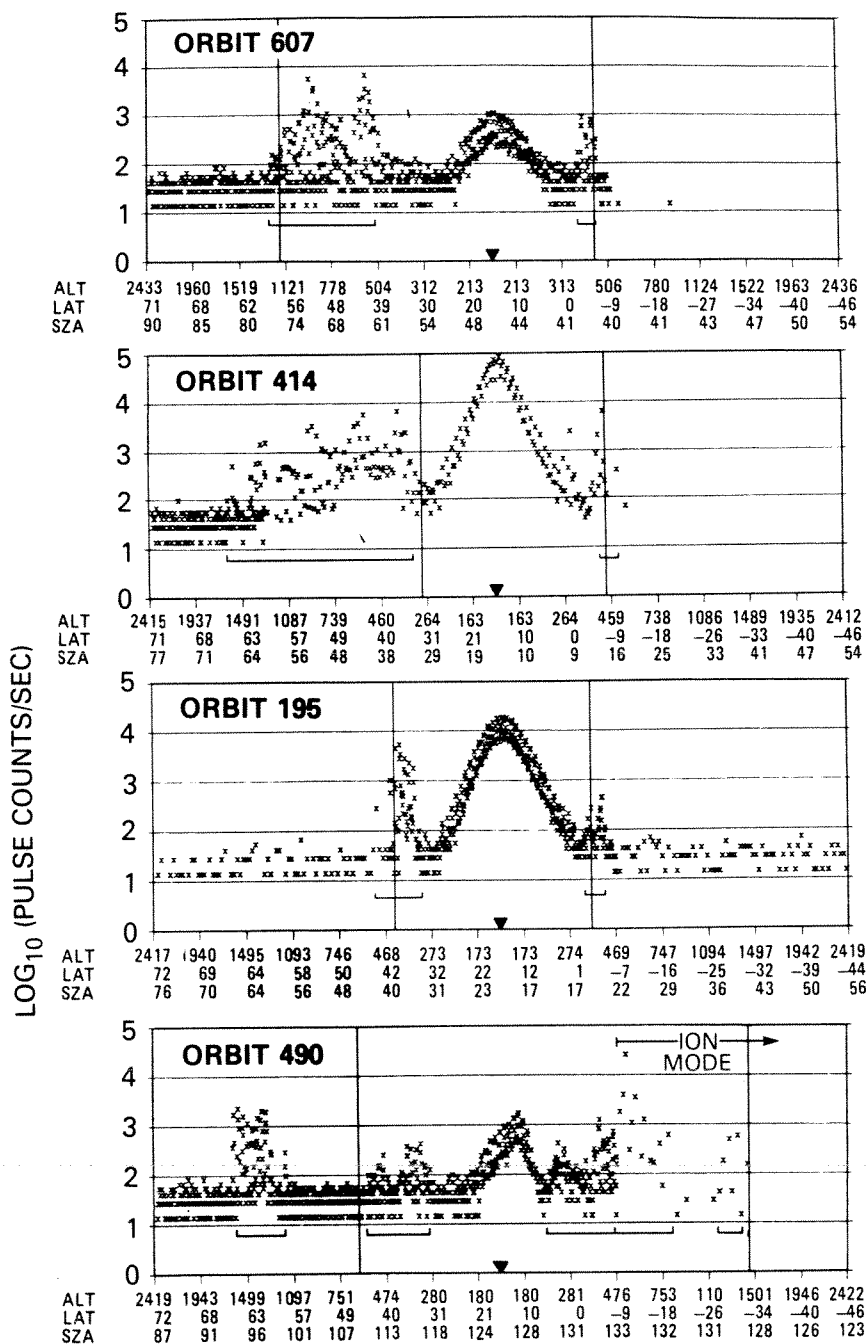


FIG. 2.

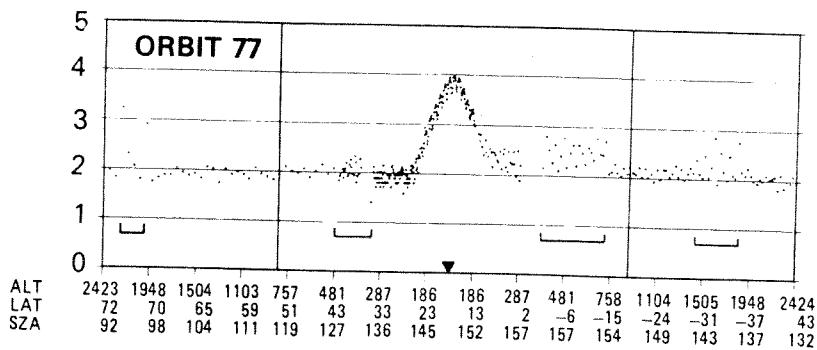


FIG. 2. EXAMPLES OF ONMS ENERGETIC ION DATA (MASS 16) PLOTTED AS A FUNCTION OF TIME. All orbits encompass 15 minutes on either side of periapsis (marked by down triangle). The labels have the same meaning as in Fig. 1. Note the diversity in altitude extent and the number of energetic ion sections. The vertical lines represent the OETP ionopause and the horizontal brackets denote the energetic ion sections. The local solar time of periapsis is 8.9<sup>h</sup>, 1.2<sup>h</sup>, 12.8<sup>h</sup>, 20.4<sup>h</sup> and 0.3<sup>h</sup> for orbits 607, 414, 195, 490 and 77 respectively. Only NON-RPA mode data was available for orbit 77 and it is plotted with a different symbol.

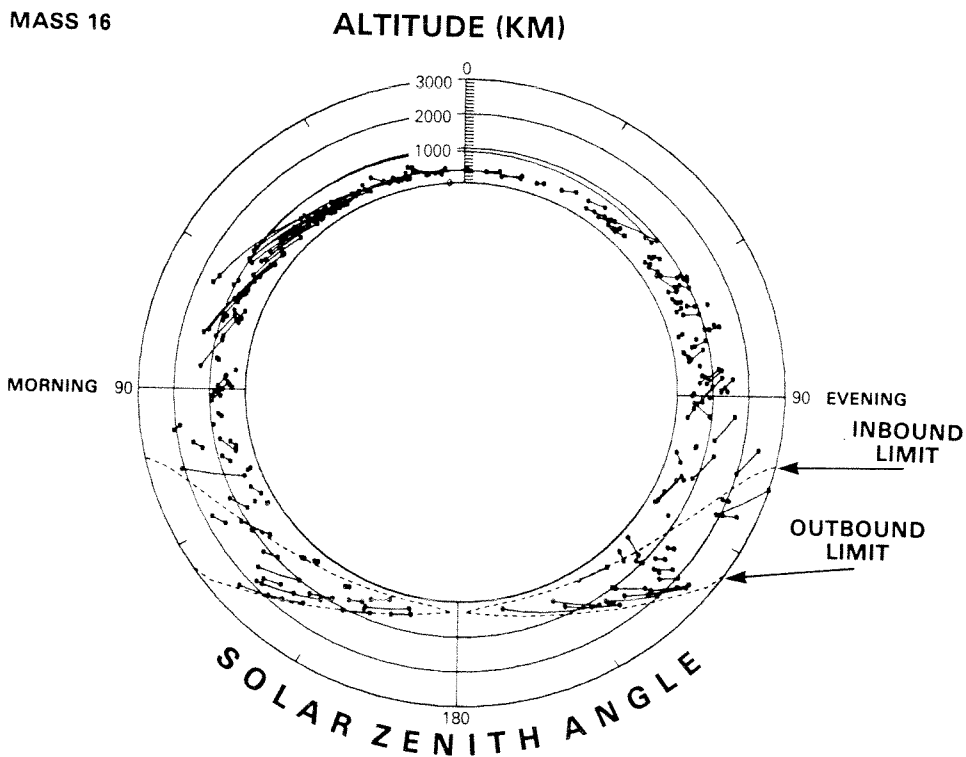


FIG. 3. THE LOCATION IN SOLAR ZENITH ANGLE AND ALTITUDE OF THE ONMS ENERGETIC ION SIGNATURES FOR MASS 16. Line segments connect beginning and ending points of an energetic ion section for a given orbit and leg (inbound or outbound) of the pass. The inbound and outbound limits indicate the maximum altitude-solar zenith angle combinations that are possible due to orbit constraints.

wave measurements, including a discussion of the coupling between the solar wind and thermal ions, has been presented by Taylor *et al.* (1981). Figure 4 shows a plot of data from orbit 403 for superthermal ions (OIMS), energetic ions (ONMS), electron density (OETP) and plasma wave (OEPD) measurements. OIMS shows the superthermal ion signature of  $\text{CO}^+$ ,  $\text{N}_2^+$  and  $\text{CO}_2^+$  as an energy shifted signal at the lower mass numbers 24 and 40, which are normally vacant of thermal ionospheric ions. Measurements of the bulk flow velocity of  $\text{O}^+$  by OIMS indicate thermal speed ions (at most  $1 \text{ km s}^{-1}$ ) implying that ONMS is observing an energetic tail of the ion distribution. The correspondence in location of the energetic and superthermal ion signatures is typical of other comparisons made. It is clear that both instruments are seeing a high energy ion component signature at the same time although not necessarily detected in the same species. The OETP data for this orbit shows the shocked solar wind electron density remaining at a rather constant level until the position of the ionopause is reached at which time ONMS and OIMS show the signature of energetic/superthermal ions. The energetic ion region is marked by wave-like plasma structures in the electron density data. Plasma wave measurements by the electric field detector (OEPD) show some irregular field enhancement corresponding to portions of the superthermal and energetic ion signatures, followed by a sharp attenuation of the 730 and 100 Hz channels within the upper ionopause which is typical of daytime orbits.

Brace *et al.* (1982) have identified a number of characteristic ionospheric structures that are indicative of solar wind-ionospheric interactions including plasma clouds/streamers and wave-like plasmas in the dayside ionosphere. The wave-like signatures are interpreted to be ionopause surface waves which are being encountered by the spacecraft as it skims the ionopause surface in a nearly tangent fashion. The plasma clouds are interpreted as being ionospheric plasma swept up by the tailward ionosheath flow. A comparison of OETP plasma cloud positions with the occurrence of ONMS energetic ions shows a coincidence of about 10%. The plasma within the clouds is like that of the upper ionosphere in both density and temperature and a small percentage of the clouds are accompanied by energetic ions which would seem to indicate that their origin is in the upper ionosphere near the ionopause.

Figure 5 shows orbit 490 data. Plasma clouds are evident in both the inbound and outbound legs of

the pass and they are associated with energetic/superthermal ions. The coincidence between the electron density data and the energetic ion data is striking. Measurements by OPA (Orbiter Plasma Analyzer) indicate that ions (interpreted to be  $\text{O}^+$ ) with approximately 100 eV energy were observed flowing northward and in the antisolar direction from about 40043 to 40092 seconds (Cravens *et al.*, 1982). As Fig. 5 shows, this corresponds to a plasma cloud that was observed with accompanying energetic and superthermal ions.

Superthermal ions are also seen at periapsis. The neutral O data is very asymmetric indicating strong density gradients in the thermosphere. Plasma wave measurements show unusual activity in 3 of the 4 channels at periapsis. The electron density data shows an eroded ionosphere that suggests significant loss of ionospheric plasma was occurring at the time of this orbit. OPA measurements show a larger than average solar wind proton peak speed for orbit 490 (Mihalov *et al.*, 1980) indicating a deeper penetration of the solar wind into the "normal" ionosphere and thermosphere. The solar wind dynamic pressure for orbit 490 was about 10 times larger than that for the more "normal" nightside orbit 491 and apparently this is one of the contributing factors in the disappearance of the ionosphere seen in orbit 490 (Cravens *et al.*, 1982). Associated with this process was the formation of plasma clouds/streamers with a high energy component.

The presence of energetic ions at the ionopause is evidence that it is the site for acceleration of ionospheric plasma by the shocked solar wind. Some small fraction of the plasma clouds/streamers are also formed with a high energy component. The direction of the energetic ion  $\text{O}^+$  flow is presumably the same as that of the main  $\text{O}^+$  flow which is basically anti-sunward at the terminators (Knudsen *et al.*, 1980).

There are several possible mechanisms which might produce energetic ions from a relatively cool ionosphere at the ionopause. Damping of whistler mode turbulence, as suggested by the strong attenuation of 100 Hz waves in the transition through the ionopause, can transfer energy from the shocked solar wind to ionospheric electrons in the region of the ionopause (Scarf *et al.*, 1980). This process heats only the electrons. Electromagnetic and electrostatic instabilities can accelerate ions born in the solar wind (Hartle and Wu, 1973). However, the ions are not localized at the ionopause and would be generated over an area that is comparable to the extent of the neutral

ORBIT 403

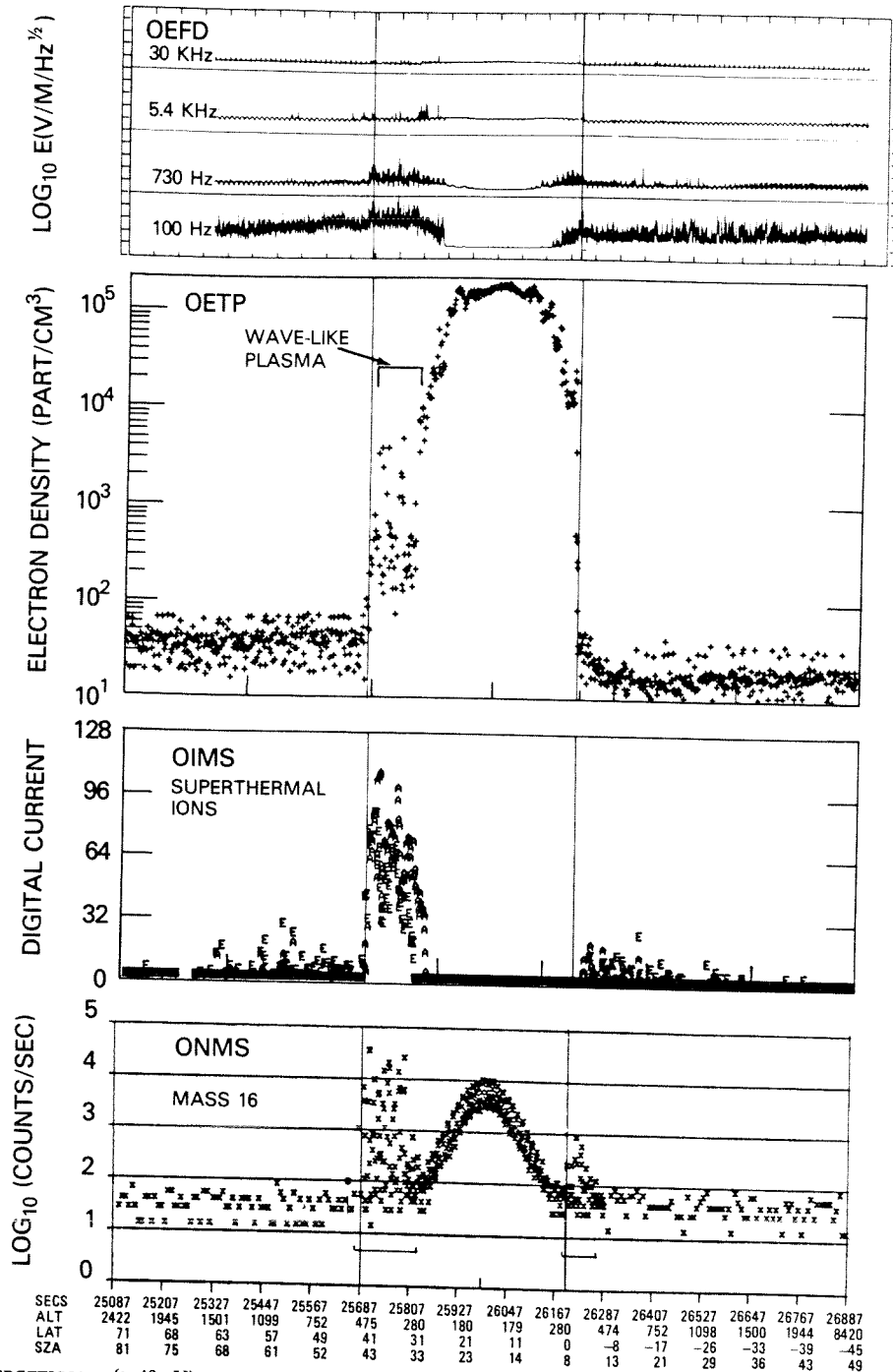


FIG. 4. ENERGETIC IONS (>40 eV) AT MASS 16 DETECTED BY ONMS (HORIZONTAL BRACKETS) AND SUPERTHERMAL (20-30 eV) IONS OBSERVED BY IMOS (A = MASS 24, E = MASS 40).

The correspondence between the two observations in the location of the signatures is typical of comparisons made on other orbits. An inbound superthermal ion peak near 25440 s observed by OIMS is apparently not seen by ONMS due to differences in angle of attack. The OIMS instrument accepts ions moving parallel to the spacecraft spin axis and ONMS looks 27° off axis (the spin axis points toward the South celestial pole). On the inbound leg OETP electron density shows a wave-like plasma at the ionopause. Near the ionopause plasma wave measurements by OEFD show attenuation of the 100 and 730 Hz signals. The plot labels have the same meaning as in Fig. 1.

exosphere which provides the source of the newly born ions.

Brace *et al.* (1980) has speculated on a scenario for plasma pickup involving impulsive removal of ionospheric plasma as a result of solar wind pressure discontinuities. Wavelike irregularities generated at the ionopause, perhaps by Kelvin-Helmholtz instabilities, allows the ionosheath magnetic field to penetrate the ionosphere removing the plasma in the form of clouds/streamers that are carried downstream by the ionosheath flow leaving an eroded ionosphere. Curtis *et al.* (1981) has proposed a specific mechanism in which the acceleration of ions is accomplished by an electric field parallel to the local magnetic field at the ionopause. Shear in the large scale (i.e. much greater than the ion gyroradius) ionosheath flow parallel to the ionopause generates MHD waves at the ionopause that are seen as wavelike irregularities in the electron density. The origin of the electric field is the conversion of the Kelvin-Helmholtz driven MHD surface wave to a shear Alfvén wave with an electric field component parallel to the local magnetic field. This parallel electric field accelerates the ionospheric ions to energies like that observed by ONMS over a region size comparable to the ion gyroradius. The accelerated ions basically follow the draped magnetic field around the planet in an anti-sunward direction. This process can account for the localized production of energetic ions at the ionopause, the observed flow pattern at the terminator and also the formation of plasma clouds/streamers via a Rayleigh-Taylor instability driven by the shear Alfvén wave's magnetic field (S. A. Curtis, private communication).

*Acknowledgements*—The authors want to thank the referee for his helpful comments. We also would like to acknowledge the competent support received from the Laboratory for Planetary Atmospheres and in particular the very useful discussions with S. A. Curtis on the generation of energetic ions from a relatively cool ionosphere.

#### REFERENCES

- Brace, L. H., Taylor, H. A., Jr., Cloutier, P. A., Daniell, R. E., Jr. and Nagy, A. F. (1979). On the configuration of the nightside Venus ionopause. *Geophys. Res. Lett.* **6**, 345.
- Brace, L. H., Theis, R. F., Hoegy, W. R., Wolfe, J. H., Mihalov, J. D., Russell, C. T., Elphic, R. C. and Nagy, A. F. (1980). The dynamic behavior of the Venus ionosphere in response to the solar wind interactions. *J. geophys. Res.* **85**, 7663.
- Brace, L. H., Theis, R. F. and Hoegy, W. R. (1982). Plasma clouds above the ionopause of Venus and their implications. *Planet. Space Sci.* **30**, 29.
- Cravens, T. E., Brace, L. H., Taylor, H. A., Jr., Russell, C. T., Knudsen, W. L., Miller, K. L., Barnes, A., Mihalov, J. D., Scarf, F. L., Quenon, S. J. and Nagy, A. F. (1982). Disappearing ionospheres on the nightside of Venus. *ICARUS* (in press).
- Curtis, S. A., Brace, L. H. and Kasprzak, W. T. (1981). Acceleration of Plasma at the Dayside Venus Ionopause. Paper presented at An International Conference on the Venus Environment, NASA/Ames Research Center, November 1-8, 1981.
- Hartle, R. E. and Wu, C. S. (1973). Effects of electrostatic instabilities on planetary and interstellar ions in the solar wind. *J. geophys. Res.* **78**, 5802.
- Hedin, A. E., Niemann, H. B., Kasprzak, W. T. and Sieff, A. (1982). Global empirical model of the Venus thermosphere. *J. geophys. Res.* (in press).
- Kasprzak, W. T., Hedin, A. E., Niemann, H. B. and Spencer, N. W. (1980). Atomic nitrogen in the upper atmosphere of Venus. *Geophys. Res. Lett.* **7**, 106.
- Knudsen, W. C., Spenner, K., Miller, K. L. and Novak, V. (1980). Transport of ionospheric O<sup>+</sup> ions across the Venus terminator and implications. *J. geophys. Res.* **85**, 7803.
- Mihalov, J. D., Wolfe, J. H. and Intriligator, D. S. (1980). Pioneer Venus plasma observations of the solar wind-Venus interaction. *J. geophys. Res.* **85**, 7613.
- Niemann, H. B., Hartle, R. E., Kasprzak, W. T., Spencer, N. W., Hunten, D. M. and Carignan, G. R. (1979a). Venus upper atmosphere neutral composition: Preliminary results from the Pioneer Venus Orbiter. *Science* **203**, 770.
- Niemann, H. B., Hartle, R. E., Hedin, A. E., Kasprzak, W. R., Spencer, N. W., Hunten, D. M. and Carignan, G. R. (1979b). Venus upper atmosphere neutral gas composition: First observations of the diurnal variations. *Science* **205**, 54.
- Niemann, H. B., Booth, J. R., Cooley, J. E., Hartle, R. E., Kasprzak, W. T., Spencer, N. W., Way, S. H., Hunten, D. M. and Carignan, G. R. (1980a). Pioneer Venus Orbiter neutral gas mass spectrometer experiment. *IEEE Trans. Geosci. Remote Sensing* **GE-18**, 60.
- Niemann, H. B., Kasprzak, W. T., Hedin, A. E., Hunten, D. M. and Spencer, N. W. (1980b). Mass spectrometric measurements of the neutral gas composition of the thermosphere and exosphere of Venus. *J. geophys. Res.* **85**, 7817.
- Scarf, F. L., Taylor, W. W. L., Russell, C. T. and Elphic, R. C. (1980). Pioneer Venus plasma wave observations: The solar wind-Venus interaction. *J. geophys. Res.* **85**, 7599.
- Taylor, H. A., Jr., Brinton, H. C., Bauer, S. J., Hartle, R. E., Cloutier, P. A. and Daniell, R. E., Jr. (1980). Global observations of the composition and dynamics of the ionosphere of Venus: Implications for the solar wind interaction. *J. geophys. Res.* **85**, 7765.
- Taylor, H. A., Daniell, R. E., Hartle, R. E., Brinton, H. C., Bauer, S. J. and Scarf, F. L. (1981). Dynamic variations observed in thermal and superthermal ion distributions in the dayside ionosphere of Venus. *Adv. Space Res.* **1**, 247.

## ORBIT 490

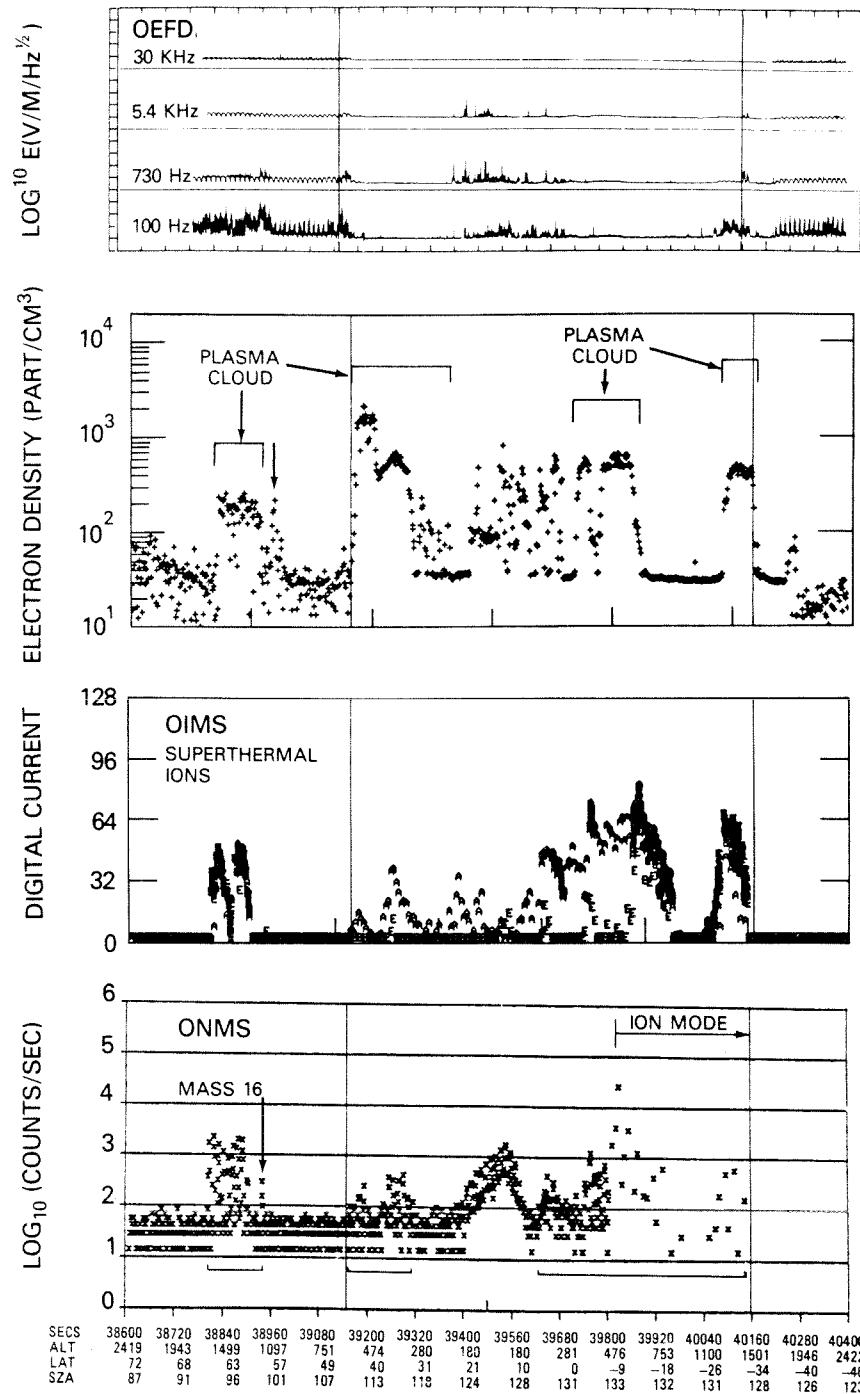


FIG. 5. COMPARISON OF ENERGETIC/SUPER-THERMAL ION DATA AND OETP ELECTRON DENSITY DATA FROM ORBIT 490. The plot labels have the same meaning as in Fig. 1. Plasma clouds as observed by OETP are accompanied by energetic/superthermal ions. Note the very narrow time event, marked by down arrow, in both the ONMS and OETP data. This particular orbit is very perturbed. Even at periaapsis the neutral data is disturbed; the electron density shows an eroded ionosphere, there is plasma wave activity and superthermal ions are detected.

mass 16. Because the ONMS instrument is canted  $27^\circ$  relative to the spacecraft spin axis, the signature is also spin modulated. The signals at the various mass numbers presumably represent  $\text{He}^+(4)$ ,  $\text{N}^+(14)$ ,  $\text{O}^+(16)$ ,  $\text{CO}^+(28)$  and  $\text{N}_2^+(28)$ ,  $\text{NO}^+(30)$ ,  $\text{O}_2^+(32)$  and  $\text{CO}_2^+(44)$ . The composition of the energetic ions resembles the composition of the thermal ionosphere (Taylor, 1980) rather than the solar wind and indicates its probable origin.

The energetic ion signature was detected on orbit 1 and occurs in approximately 13% of the 700 orbits examined. It can occur on the inbound and/or the outbound leg of the pass and may even occur several distinct times in either leg of the pass. Most of the orbits examined characteristically show that the energetic ion signature occurs at or very near the ionopause which is the boundary between the shocked solar wind and the Venus ionosphere.

Energetic ions are uniquely identified during neutral mode operation when the ion repeller is at +40 eV relative to the spacecraft potential present at the entrance aperture. The ion repeller was designed to reject thermal ionospheric ions. For example, thermal  $\text{O}^+$  ions in the spacecraft rest frame have an energy of about 8 eV for a spacecraft speed of  $10 \text{ km s}^{-1}$ . The spacecraft potential, as determined by OETP, is normally a volt or two negative in the ionosphere. Outside the ionosphere the potential is a few volts positive in sunlight and a few volts negative in darkness. The ONMS instrument can detect  $\text{O}^+$  ions while in neutral mode configuration only if they have energies in excess of 40 eV or about  $20 \text{ km s}^{-1}$  in the spacecraft rest frame. Measurements by the Orbiter Ion Mass Spectrometer (OIMS) at the same time typically show substantial concentrations of thermal  $\text{O}^+$  with drift velocities of at most a few  $\text{km s}^{-1}$ . Measurements from the Retarding Potential Analyzer (ORPA) also typically indicate bulk  $\text{O}^+$  velocities of a few  $\text{km s}^{-1}$  at or below the ionopause (Knudsen, 1980). Thus it appears that two portions of the  $\text{O}^+$  population are being sampled. The OIMS and ORPA instruments sample the bulk of  $\text{O}^+$  near thermal energies and drifting at most a few  $\text{km s}^{-1}$ , while the ONMS instrument detects an energetic component moving with velocities greater than  $20 \text{ km s}^{-1}$  in the spacecraft rest frame.

Although the signal level of the energetic ions shown in Figure 1 is comparable to that generated by the detection of the neutral atmosphere constituents, the sensitivity of the instrument for energetic ions is significantly less than for the

neutrals. An estimate of the energetic ion flux can be made by assuming: (a) the ion lens system of the quadrupole does not focus the ions (lower limit); or (b) that the flux represents all of the thermal ions (upper limit). Based on these assumptions the ion flux corresponding to  $1 \times 10^4$  pulse counts  $\text{s}^{-1}$  is probably greater than  $2 \times 10^7$  and probably less than  $3 \times 10^8$  ions/ $\text{cm}^2 \text{ s}^{-1}$  as measured in the spacecraft rest frame. For the lower limit the appropriate particle density is less than  $10 \text{ cm}^{-3}$ .

Figure 2 shows further examples of ONMS energetic ions for both day and night illustrating the variety of signatures that have been encountered. Again note the coincidence of the ionopause location and the energetic ion sites. Orbit 490 is interesting because it is also a highly perturbed orbit at periaapsis in both the neutral atmosphere and the ionosphere. This orbit shows several energetic ion signatures. At 5 minutes after periaapsis ONMS was commanded to the ion mode and the data rate was changed. The signature is still visible in the ion mode which supports the contention that its origin is due to ion and not neutral particles.

The distribution of the energetic  $\text{O}^+$  ions in solar zenith angle and altitude is shown in Fig. 3 assuming cylindrical symmetry about the Sun-Venus line. Other ion masses show a similar solar zenith angle distribution. On most of the orbits examined, the energetic ions occur at or near the ionopause and with a varying altitude extent. In the daytime the inbound (high latitude) leg is favored over the outbound (lower latitude) leg similar to the behavior of superthermal ions described by Taylor *et al.* (1981). At night, however, the reverse is true. Most of the data at low solar zenith angles comes from the third diurnal cycle where the periaapsis altitude was high enough to cross the ionopause near the subsolar point. Most of the nighttime energetic ion data is from first diurnal cycle. The maximum altitude of the energetic ions increases with increasing solar zenith angle following the higher altitude ionopause (Brace *et al.*, 1979). At night the energetic ion data are scattered in altitude reflecting a more erratic nighttime ionopause (Brace *et al.*, 1980). The inbound and outbound limits (dashed lines) represent altitude and solar zenith angle combinations not accessible due to orbit constraints.

Superthermal ions have been observed by the Orbiter Ion Mass Spectrometer (OIMS) near the ionopause (Taylor *et al.*, 1980). A correlation between the superthermal ions and OEFD plasma

DSC # 631

B43066

78-051A-11

## OBSERVATIONS OF ENERGETIC IONS NEAR THE VENUS IONOPAUSE

W. T. KASPRZAK, H. A. TAYLOR, L. H. BRACE and H. B. NIEMANN

NASA/Goddard Space Flight Center, Laboratory for Planetary Atmospheres, Greenbelt, MD 20771, U.S.A.

and

F. L. SCARF

Space Sciences Department, TRW Defense, Space and Systems Group, Redondo Beach, CA 90278, U.S.A.

(Received in final form 7 April 1982)

**Abstract**—Ions (primarily  $O^+$ ) with spacecraft rest frame energies  $>40$  eV have been observed by the Pioneer Venus Neutral Mass Spectrometer. The signature occurs in about 13% of the 700 orbits examined, primarily near the ionopause and at all solar zenith angles. The energetic ions coincide in location with superthermal ions observed by the Ion Mass Spectrometer and more rarely occur in some of the plasma clouds observed by the Electron Temperature Probe. These observations in conjunction with measurements by the Plasma Wave Instrument near the ionopause suggest that the ions are accelerated out of ionospheric plasma by the shocked solar wind through plasma wave-particle interactions.

### INTRODUCTION

The Pioneer Venus Orbiter Neutral Mass Spectrometer (ONMS) was designed to determine the neutral gas composition of the upper atmosphere of Venus. The quadrupole mass spectrometer has been described by Niemann *et al.* (1980a); the diurnal variation of the neutral composition by Niemann *et al.* (1979a, 1979b, 1980b), Kasprzak *et al.* (1980) and Hedin *et al.* (1982). The ONMS instrument has unexpectedly also detected energetic (i.e. superthermal) ions while operating in its neutral mode.

Evidence for ions of superthermal energy detected by the Orbiter Ion Mass Spectrometer (OIMS) has been presented by Taylor *et al.* (1980, 1981). The Orbiter Plasma Analyzer (OPA) has acquired data downstream in the Venus' ionosheath which is consistent with  $O^+$ , scavenged from the ionosphere, travelling at the solar wind speed (Mihalov *et al.*, 1980).

### DATA AND RESULTS

In the ONMS instrument, a hot filament provides electrons for ionization of incoming neutral gas. A grid in front of the ionization region is biased so as to reject ambient electrons of less than 6 eV and an ion repeller rejects ionospheric ions of less than 40 eV relative to the spacecraft potential. The ONMS instrument can also be operated as an ion mass spectrometer. In this mode the filament is turned off and the 40 eV ion

repeller is set to spacecraft ground. There is also a retarding potential analysis (RPA) mode in which a retarding potential is applied to the ions leaving the ionization region prior to entering the mass analyzer. The RPA mode is used to discriminate between direct beaming and thermalized neutral particles in order to measure surface reactive species such as atomic oxygen.

Figure 1 is an example of RPA data acquired by ONMS during a periapsis pass while in neutral mode operation. The two vertical lines are a measurement of the position of the ionopause by the Orbiter Electron Density Probe (OETP) instrument. The pulse counter output in counts  $s^{-1}$  is plotted as a function of universal time for a selection of mass numbers. Near periapsis the signal is primarily due to the incoming neutral atmosphere gas flowing at  $10$  km  $s^{-1}$  in the spacecraft reference frame. At very high altitudes the signal is dominated by instrument surface outgassing as a result of the absorption of gases during periapsis passage. Beyond the detectable neutral atmosphere an unexpected signal was observed which is believed to be due to ions having energies in excess of 40 eV, the ion repeller grid bias potential. This signal is most easily seen in RPA mode data where the thermal gas background is about an order of magnitude lower than in the NON-RPA mode. For this reason RPA mode data has been used wherever possible in analysis of the ONMS results presented in this paper.

The energetic ion signature is seen primarily at

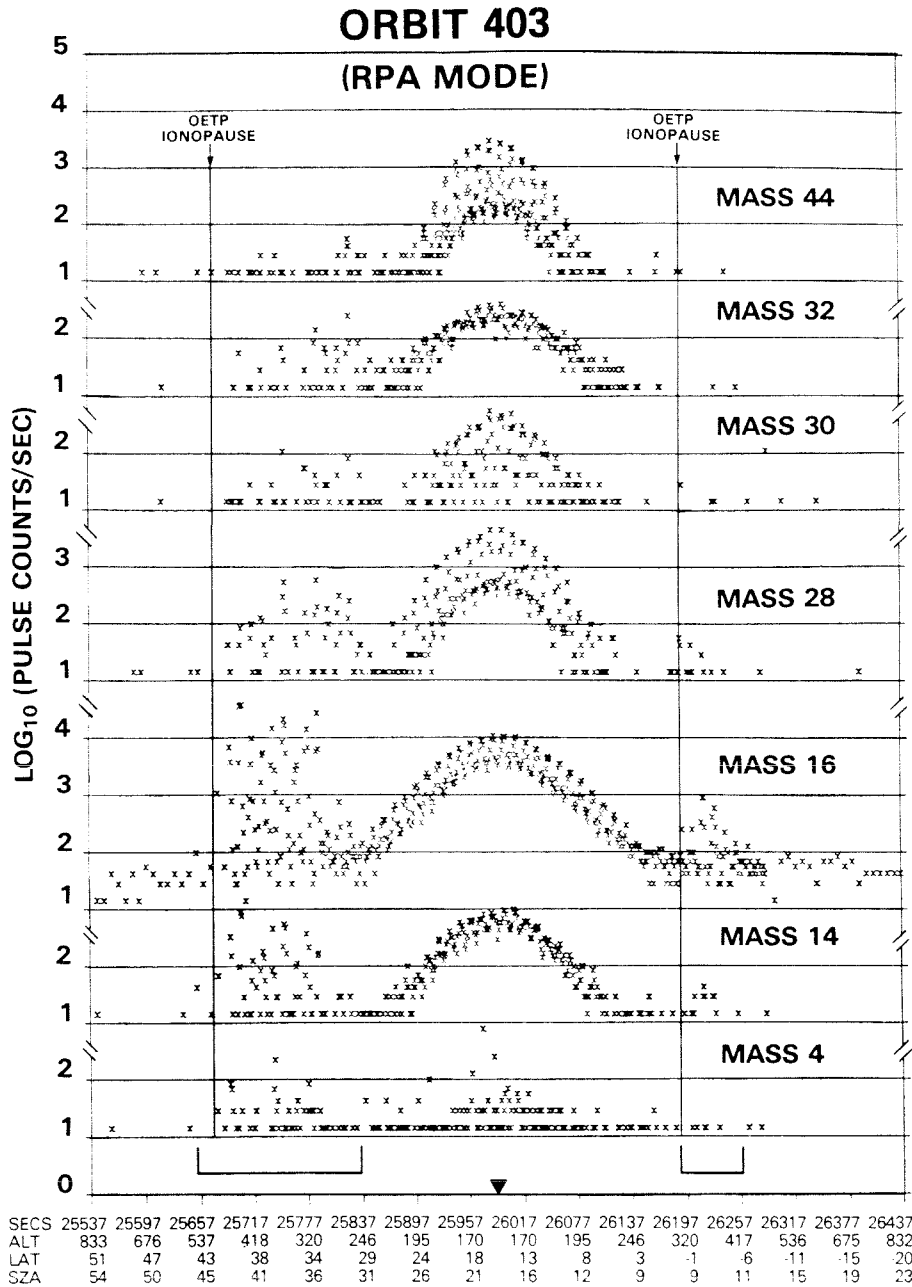


FIG. 1. ONMS RPA MODE PULSE COUNTS  $s^{-1}$  FOR A RANGE OF MASS NUMBERS PLOTTED AS A FUNCTION OF TIME FOR ORBIT 403.

The normal neutral data near periapsis (downward triangle) merges with the instrumental gas background at high altitude and energetic ions (horizontal brackets) are detected well beyond the sensible neutral atmosphere. The small time scale variations are due to the 12 s spin modulation of the data. Mass 16 has the most predominant signal. The vertical lines show the ionopause position as determined from OETP data. A characteristic of the energetic ion signal is that it occurs at or very near the ionopause. Plot labels: SECS = U.T.(s), ALT = altitude (km), LAT = latitude (degrees), SZA = solar zenith angle (degrees). The local solar time of periapsis is 11.0<sup>h</sup>.

DSC #651  
ONMS -1

Superseded  
by 1989 doc !!  
01-OCT-1987

78-051A-11D

NSSDC DOCUMENTATION FOR  
PIONEER VENUS ORBITER NEUTRAL MASS SPECTROMETER

ENERGETIC ION DATA

I. The Orbiter Neutral Mass Spectrometer (ONMS)

The instrument was primarily designed to determine the composition of the neutral exosphere/thermosphere of Venus. However, it has also detected energetic or fast ions whose energy exceeds 40 eV in the spacecraft frame of reference. These ions were observed in early orbits at an altitude higher than that required for measuring the neutral density at periapsis. Once the periapsis altitude had risen above the point where sensible neutral density measurements could be made the instrument was configured specifically to detect energetic ions.

The ONMS instrument has been described in "Pioneer Venus Orbiter Neutral Gas Mass Spectrometer Experiment," IEEE Transactions on Geoscience and Remote Sensing, GE-18 (1), 1980. A summary of the early results for energetic ions has been described in "Observations of Energetic Ions near the Venus Ionopause," Planet. Sp. Sci., 30, 1107-1115, 1982. The method used to reduce the energetic ion data to a flux and density has been described in "Observations of Energetic Ions on the Nightside of Venus," J. Geophys. Res., 92, 291-298, 1987. The data has been used as part of a study of the iontail of Venus in "The Iontail of Venus: Its Configuration and Evidence for Ion Escape," J. Geophys. Res., 92, 15-26, 1987. The papers are reproduced here for convenient reference.

II. Reduction to flux and number density

Reference to the basic data reduction has been given in Section I. Because of the paucity of data at other mass numbers only mass 16 (atomic oxygen) has been reduced to a flux and number density. As part of the reduction process the angle in the ecliptic plane of the apparent ion flow has also been deduced. An approximate correction has been applied to the angle and flux in order to remove the space-craft velocity. In order to fit the data a minimum of 30 points were required in 36 seconds. In addition the maximum to minimum count ratio was required to be a factor of 3 or greater in order to insure that there was a definitive spin modulation. For those masses not fit by this process (all masses except 16 [atomic oxygen]) or those data that did not satisfy the above criteria a separate plot of the maximum count rate per 12 seconds was included in the microfiche data

set. A rough conversion of  $4 \times 10^7 \text{ cm}^{-2} \text{ s}^{-1} / 10^4 \text{ counts s}^{-1}$  can be used to convert to a flux and a speed of  $2.33 \times 10^6 \text{ cm s}^{-1}$  can be used to convert to number density. The minimum count rate is 1 per integration period, depending on the bit rate and format of the telemetry data, or about 6 to 12 counts/s. A constant spacecraft potential of  $-5 \text{ v}$  has been assumed in assigning the effective energy of the ions to 45 eV. The ion species regularly monitored include:  $\text{He}^+$ ,  $\text{N}^+$ ,  $\text{O}^+$ ,  $\text{N}_2^+/\text{CO}^+$  and  $\text{CO}_2^+$ .

In general for orbit numbers 1 to 645 data were taken from RPA mode since the gas background with the filament on was considerably less than in non-RPA mode. For orbit numbers above 923 the instrument was deliberately configured with the filament off and non-RPA mode data was used. For mass 16 the RPA voltage is about +3.8 volts.

### III. Summary data.

All orbits have been processed where data exists or can be visually determined to exist. For orbits 1 to 645 a visual examination of the neutral mode data is required in order to identify the regions of energetic ions. For orbits beyond 923 no visual examination was needed. The ONMS instrument was not on for all orbits nor were energetic ions seen on all those orbits in which it was in operation. The flux values are estimated for an energy in the spacecraft reference frame of 45 eV. The density represents only that portion of the total density which is in this same energy range. It is computed from the flux by dividing it by a speed corresponding to 45 eV.

The data values are constructed for UT times supplied by the Pioneer Venus Project.

## IV. Summary data tape.

The summary data tape was constructed in accordance with the recommendations of the Pioneer Venus archiving committee. A copy of that format is included for reference. The data tape has the following characteristics:

MEDIUM:	MAGNETIC TAPE
FORMAT:	ASCII
DENSITY:	1600 BPI
TRACKS:	9
PHYSICAL BLOCKSIZE:	4400 BYTES
LOGICAL RECORD SIZE:	78 BYTES
RECORDS/PHYSICAL BLOCK:	50
PHYSICAL RECORD TYPE:	FIXED BLOCK
TAPE LABEL:	UNLABELED
DENSITY:	1600 BPI
FORMAT:	ASCII
COMPUTER USED:	PDP 11/70

The orbits on the tape have been arranged sequentially. The format of the tape is briefly:

## RECORD 1:

DESCRIPTION: number of variables and 4 character variable names

FORMAT: (I3,<N> (1X,A4)) where N=number of variables

## RECORD 2:

DESCRIPTION: FORTRAN format of succeeding data records

FORMAT: (<M>A1) where M=number of bytes per logical record

## RECORD 3:

DESCRIPTION: fill data definition for each data field

FORMAT: format contained in record 2

## RECORD 4...:

DESCRIPTION: summary data

FORMAT: format contained in record 2

The variables listed in RECORD 1 have the following meaning:

<u>VARIABLE</u>	<u>COMMENT</u>
DO+	Density of energetic atomic oxygen in $\text{cm}^{-3}$
FO+	Flux of energetic atomic oxygen in $\text{cm}^{-2} \text{ s}^{-1}$
FANG	Angle of the ion flow in the ecliptic plane with respect to the sun in degrees
VALT	Altitude above the mean surface of Venus in km
VLAT	Venus latitude in degrees
VLST	Venus local solar time in hr
VSZA	Venus solar zenith angle in degrees

## V. Description of microfiche plots.

Each orbit processed consists of 5 plots.

<u>PAGE</u>	<u>COMMENT</u>
1	Header page identifying the spacecraft and instrument, orbit number, UT date and time of periapsis, and the principal investigator telephone and address .
2	Maximum pulse counts/sec for a selected set of mass numbers plotted versus time from periapsis; the data are multiplied by a factor in order to put them on a common vertical axis (the multipliers are indicated by the numbers following the X on the left hand side of the plot).
3	The 12 second average density for atomic oxygen plotted versus periapsis time.
4	The 12 second average flux for atomic oxygen plotted versus periapsis time.
5	The angle of the atomic oxygen flow vector in the ecliptic plane.

Positional parameters for the data are available on the summary tape.

An example of a plot set has been included for reference.

## VI. Energetic ion event list

A list of start and stop times for sections of the orbit where energetic ions have been observed has been included for orbits 1 to 706. Also included in the list are several location parameters for the spacecraft corresponding to these times.